Universidad Autónoma
de Madrid

Theoretical and observational aspects of the variation of fundamental constants of Nature

Franco D. Albareti

A dissertation submitted in partial fulfillment
of the requirements for the degree of

Doctor of Philosophy in Theoretical Physics

Supervised by

Prof. Antonio L. Maroto and Prof. Francisco Prada

Instituto de
Física
Teórica
UAM-CSIC

Instituto de Física Teórica
November 2018

A mis padres, Alfredo y Lidia,
por su cálida compañía.

Acknowledgements

First of all, I would like to thank my supervisors, Prof. Antonio L. Maroto and Prof. Francisco Prada. Thanks to Prof. Maroto; for insightful discussions, for being always willing to check the computations in very detail and for encouraging me to continue on doing them until the end. Thanks to Prof. Prada; for engaging me on many different research projects, and for his continuous support and motivation during the first years of this thesis. A word of gratitude also goes to my tutor, Prof. Carlos Muñoz.

I am also very grateful with Dr. Johan Comparat, for his advice and useful help with my first encounter with data analysis (and for sharing some cups of coffee, too). I also want to thank Prof. Anatoly Klypin for our brief but fruitful research collaboration.

This PhD thesis was financially supported by a 'la Caixa'-Severo Ochoa International fellowship granted by the Institute of Theoretical Physics UAM+CSIC (IFT), to whom I am deeply thankful for this opportunity.

No estaría escribiendo esta tesis, sino fuera por el constante apoyo de mi familia. Gracias a mis padres, Lidia y Alfredo, por ser mis compañeros cuando lo necesitaba, y por confiar en mí. A mis hermanos, Gianni y Paola, a los que tanto quiero y extraño. Y a Laura, por su cariño y su dulce paciencia, con la que comparto tantos buenos recuerdos.

Gracias a mis compañeros de doctorado en el IFT, en especial a Donald, Sergio, Dagoberto e Iñaki. Por supuesto, a mis compañeros de despacho, Ginevra y Sergio. Un especial abrazo para los excelentes anfitriones de la Universidad Complutense de Madrid; Santos, Héctor, Jose, Miguel y muchos más (incluyendo a algún profe también).

Por último, me gustaría terminar mencionando a mis amigos, a los de toda la vida. Demasiados para nombrarlos a todos, pero sin duda han aportado su granito de arena a esta tesis.

Contents

PhD Thesis

"Theoretical and observational aspects of the variation of fundamental constants of Nature"

Abstract

The fundamental constants of Nature play a crucial role in our understanding of the Universe. They represent the limits of our knowledge of the laws of Physics but at the same time encode new phenomena yet to be discovered. In recent years, an enormous observational effort has been devoted to study the possible variation in space and time of some of these fundamental constants. Such a discovery would have deep consequences in our current models for physical interactions, and in particular for the theoretical framework behind gravitation. Astrophysics and Cosmology provide us with a great window to look for any variation, with space and time scales ranging from the Solar System to the whole observable Universe and its origin. On the other side, theoretical models to accommodate variation of fundamental constants are also being actively explored.

This thesis is divided into an observational analysis and a theoretical study. First, we present the most precise observational constraint to date for the cosmological variation of the fine structure constant using emission lines present in quasar spectra up to redshift $z = 1$. From the Sloan Digital Sky Survey Quasar Catalog (Data Release 12), we build a sample of 13 175 quasar spectra showing the [O III] doublet ($\lambda\lambda$ 4960, 5008 Å). Then, by measuring the separation between both lines we obtain the following relative constraint on the time variation of the fine structure constant $\Delta\alpha/\alpha = (0.9 \pm 1.8) \times 10^{-5}$. We also impose limits on its variation in redshift bins ($\Delta z \approx 0.06$) over the last 7.9 Gyr at the 10^{-4} level. Several sources of systematics are analyzed including sky contamination and line blendings.

In the second part, we explore a theoretical mechanism producing expectations values of scalar fields to depend on the gravitational potential. To have varying expectation values is one of the usual ways to accommodate variation of fundamental constants. We develop a formalism that enables us to compute the complete one-loop quantum corrections to the effective potential and energy momentum tensor of scalar fields arising in the presence of gravity. This formalism provides the local part, usually computed with the well-known DeWitt-Schwinger expansion, but it would also allow to obtain the non-local contributions. Assuming weak and slowly varying gravitational fields, we obtain a complete set of mode solutions for the Klein-Gordon equation in perturbed Friedmann-Robertson-Walker geometries at leading order in the adiabatic approximation. Then, we compute the corresponding expectation values of a self-interacting scalar field as a mode summation in different quantum states and apply dimensional regularization to obtain the final contributions. Although there is no effect due to metric perturbation in vacuum states, there are thermal corrections that could modify the expectation value of scalar fields.

Resumen

Las constantes fundamentales de la Naturaleza desempeñan un papel crucial en la comprensión del Universo. Representan los límites de nuestro conocimiento de las leyes de la física, y al mismo tiempo podrían esconder nuevos fenómenos que están aún por descubrir. En los últimos años, se ha realizado un enorme esfuerzo observacional dirigido a estudiar la variación espacial y temporal de algunas de estas constantes fundamentales. Un descubrimiento en este sentido tendría profundas consecuencias en los modelos actuales que describen las interacciones físicas, y en particular afectaría al marco teórico en el que se sustenta la gravitación. La Astrofísica y la Cosmología nos brindan una gran oportunidad para buscar estas variaciones en un rango muy amplio de escalas espaciales y temporales, abarcando desde el Sistema Solar hasta la totalidad del Universo observable, incluyendo su origen. Por otro lado, los modelos teóricos que permiten acomodar la variación de constantes fundamentales también se están desarrollando de forma activa.

La presente tesis se compone de un análisis observacional y un estudio teórico. Primero, presentamos la cota observacional más precisa hasta la fecha a la variación cosmológica de la constante de estructura fina utilizando líneas de emisión en espectros de cuásares con redshift $z \lesssim 1$. A partir del catálogo de cuásares elaborado por el Sloan Digital Sky Survey (Data Release 12), construimos una muestra de 13 175 espectros de cuásares que presentan el doblete [O III] ($\lambda\lambda$ 4960, 5008 Å) en emisión. Posteriormente, midiendo la separación entre ambas líneas obtenemos la siguiente cota relativa a la variación temporal de la constante de estructura fina $\Delta\alpha/\alpha = (0.9 \pm 1.8) \times 10^{-5}$. Además imponemos cotas a diferentes desplazamientos al rojo ($\Delta z \approx 0.06$) a lo largo de los últimos 7.9 Ga, alcanzando una precisión relativa de 10^{-4}. Por último, analizamos varias fuentes de errores sistemáticos, como por ejemplo la contaminación del cielo y la superposición de diferentes líneas.

En la segunda parte, estudiamos un mecanismo teórico en el que es posible obtener valores esperados de campos escalares que dependen del potencial gravitatorio. Esta es una de las formas habituales para producir una variación de constantes fundamentales. Desarrollamos un formalismo que permite calcular las correcciones cuánticas a un loop al potencial efectivo y al tensor energía-momento de campos escalares que surgen en presencia de gravedad. Este formalismo proporciona la parte local, que generalmente se calcula a partir de la conocida expansión de DeWitt-Schwinger, pero también permitiría obtener las contribuciones no locales. Para este cálculo asumimos que los campos gravitatorios son débiles y que varían lentamente, así obtenemos un conjunto completo de modos hasta el primer orden adiabático dominante para la ecuación de Klein-Gordon en geometrías Friedmann-Robertson-Walker perturbadas. Finalmente, calculamos los valores esperados de un campo escalar con autointeracciones como una suma de modos en diferentes estados cuánticos

y aplicamos regularización dimensional para obtener las contribuciones finitas. Aunque no hay ningún efecto debido a la perturbación métrica en los estados de vacío, hay correcciones térmicas que podrían modificar el valor esperado de los campos escalares.

Notation

In this thesis, the following symbols are used:

c	speed of light
h ($\hbar$)	Planck constant (reduced Planck constant)
G	Newton gravitational constant
α	the fine structure constant
α_s	coupling constant for the strong interactions
m_e	mass of the electron
m_p	mass of the proton
m_n	mass of the neutron
$\mu = \frac{m_p}{m_e}$	proton-to-electron mass ratio
e	electron charge (absolute value)
g_p	proton gyromagnetic factor
R_∞	Rydberg constant
H_0	Hubble constant
z	redshift

Introduction

The fundamental constants of Nature have been defined as any parameter involved in a given theory whose numerical value cannot be computed with our present knowledge of Physics (Weinberg, 1983).[1] As a consequence of our ignorance about their ultimate origin, it is natural to consider whether observations could challenge the main property by which they are defined.

After some historical picture, we discuss the role played by constants in the conceptual structure of Physics. A revision of the Copernican Principle when applied to the variation of physical constants is commented. Next, the distinction between dimensionful and dimensionless constants brings in the actual definition of physical dimension and considerations about the process of measurement. Then, a well known classification of fundamental constants is presented in order to come across with a list of the fundamental constants of Nature. Finally, theoretical models able to accommodate a possible variation of fundamental constants are briefly reviewed.

Historical background

The beginning of this branch of physics is usually attributed to Dirac (1937, 1938), who argued in favour of a variation of the fundamental constants of Nature with his Large Number Hypothesis. Dirac's idea is based on the unlikely fact that the most fundamental constants in the Universe have a certain fixed numerical value which cannot be explained with our current understanding of physics, for instance the value of the fine structure constant α being approximately 1/137. It is more likely to think that their present values are the result of a dynamical process which had left the value of the fundamental constants as they are today. Then, they should be considered as characterizing the state of the Universe.

In particular, Dirac argued that the dimensionless ratio between the electromagnetic force and the gravitational force is of the same order of magnitude as the age of the Universe measured in classical atomic units,[2] i.e.

$$\frac{e^2}{G\, m_p\, m_e} \sim \frac{1/H_0}{e^2/m_e c^3} \sim 10^{40}\,. \tag{1}$$

[1] *"(...) constants whose value we cannot calculate with precision in terms of more fundamental constants, not just because the calculation is too complicated (as for the viscosity of water or the mass of the proton) but because we do not know of anything more fundamental."*

[2] Or as the size of the observable Universe (c/H_0) expressed in terms of the classical radius of the electron ($e^2/m_e c^2$).

For him, this fact suggests that these dimensionless numbers are somehow related. Since the age of the Universe is not a constant, the electromagnetic/gravitational ratio is expected to vary in time in the same way. This would imply that the strength of the gravitational interaction is decreasing in time with respect to the electromagnetic one. This led him to propose a time variation of the Newton constant G. He also noticed that the number of protons in the Universe is of the same order of magnitude as the square of the age of the Universe measured in atomic units, therefore suggesting a continuous creation of particles (Dirac, 1974).[3]

Teller (1948) refuted Dirac's hypothesis about a decreasing Newton constant G arguing that such variation would have led to a steep increase in the Earth's surface temperature in the past contradicting paleontological evidence (Barrow, 2005; Uzan, 2003).

Later works by Dicke (1961) and Carter (1974, 1983) explained the numerical coincidences found by Dirac in terms of the anthropic principle, i.e. the presence of an observer in the Universe places constraints on the relation between those numbers. Since then, several bounds for fundamental constants have been derived based on anthropic arguments (Hogan, 2000). For instance, quite stringent constraints for the strong ($< 0.5\%$) and electromagnetic ($< 4\%$) forces are obtained due to the fine tuning of certain nuclear reactions in order to produce the observed abundances of atomic elements, in particular Carbon and Oxygen[4] (Rozental and Estrin, 1988; Oberhummer et al., 2000).

One of the first theoretical model to include a variation of fundamental constants was proposed by Jordan (1937), and later studied in detail by Fierz (1956), and Brans and Dicke (1961). This model, known as Brans-Dicke theory, describes a scalar field coupled to the gravitational field (a coupling with the electromagnetic field was explicitly discarded by Fierz in order to prevent spacetime dependence of atomic spectra). This model represents a particular example of a general class of relativistic field theories known as scalar-tensor theories (Faraoni, 2004). These theories provide alternative ways to explain the accelerated expansion of the Universe besides accommodating variation of fundamental constants in a natural way. Later on, further theoretical developments, including higher dimensional and string inspired theories, provided several scenarios where a variation of fundamental constants is expected on general grounds.

Besides the real physical content in Dirac's arguments, his early concerns about the fundamental constants of Nature emphasized the importance of testing the attribute explicitly given by their own name. A new horizon to look for unexpected physics was uncovered.[5]

[3]Note that the first relation established by Dirac (a) together with the Friedmann equation (b) imply the connection between the number of protons and the age of the Universe if the remaining cosmological fluids (including curvature) are at most of the same order as the dust contribution

$$\left.\begin{array}{ll} \text{(a)} & \dfrac{e^2}{G\,m_p\,m_e} \sim \dfrac{m_e\,c^3}{H_0\,e^2} \\ \text{(b)} & H_0^2 \sim G\,\rho_0 \sim G\dfrac{N\,m_p}{(c/H_0)^3} \end{array}\right\} \Rightarrow N \sim \left(\frac{m_e\,c^3}{H_0\,e^2}\right)^2 \sim 10^{80}, \tag{2}$$

where N is the number of protons in the observable Universe (Eddington number). This is an alternative anthropic explanation of Dirac's second relation from a cosmological perspective in contrast to the astrophysical one given by Dicke (1957) based on the lifetime of main-sequence stars.

[4]The involved nuclear process is the $3\alpha \rightarrow {}^{12}\mathrm{C}$ reaction taking place inside helium-burning red giant stars.

[5]We refer to Uzan (2003, 2011) for a more detailed historical perspective of the topic.

Constants in Physics

The role played by the fundamental constants of Nature in the logical or conceptual structure of Physics well deserves some discussion (or may be not, see Tisza (1963)).

Theoretical physics studies the fundamental laws of Nature by building mathematical models that describe the physical world.[6] Following the scientific method, it is through observations and experiments that we are able to carry out this task. The different existing models to describe physical phenomena are not completely independent from one another. In fact, it turns out that it is possible to accommodate many different models under the same set of basic principles. These basic principles, known as theoretical frameworks, provide a logical and mathematical structure in order to study the consequences and predictions of a wide variety of models.

For example, let us consider Newton's equation, the first theoretical framework developed in Physics. Through the appropriate mathematical tools, it describes the dynamics of any object using as a starting point straight paths traveled with constant velocity. Any observed deviation from such behavior is parameterized by including a term in Newton equation, known as a force. Forces are not an absolute concept, instead they are tied up with the chosen starting description for the evolution of a system. Within this framework, particular models are only expected to propose a certain function of some variables of the system, dubbed "force", in order to explain observations. In this way, we get to know Newtonian gravitation, electro and magnetostatics; all of them different models for interactions that follow the same logical structure, Newton's equation. In the same way, non-relativistic quantum mechanics relies on the interacting part of the Hamiltonian to play the same role. In this sense, theoretical frameworks in general could be considered as useful and simple mathematical parameterizations that encapsulate a wide variety of physical interactions.

Once our mathematical abstractions, namely theoretical frameworks with specific models, are built and providing accurate predictions, one may wonder about the fingerprint left by Nature in our construction. This question is an epistemological one and any attempt to give a naive answer is well outside the scope of this discussion. However, there is a clear distinction among the set of principles defining a theoretical framework or model. Some of them are completely necessary in order to obtain correct predictions, but they do not affect the conceptual or logical structure at all. These principles are the ones which fix the value of the free parameters involved in our model according to the outcomes of the experiments. In this way, these parameters settle down a scale (which indeed could be dimensionless) that connects pure numbers with physical phenomena. These free parameters are the fundamental constants of Nature and they are good candidates to be considered as evident links between experiments and our models since they are eventually responsible for correct quantitative predictions.

The fact that this connection is manifested through numerical constants may not be an accidental

[6] A somehow reverse, but very interesting, point of view is expressed in Tegmark (1998), where a classification scheme of the physical world is proposed on the basis of being completely mathematical or not. The second possibility is discarded because of the lost of predictive power (very much related with religious beliefs). In our opinion, even the principle of causality and the logical self-consistency of the physical world is an experimental fact. To identify Nature with mathematical models could be a quite restrictive limitation.

one, but a logical consequence of our philosophical conception of aesthetics. This conception is partially based on the Occam's razor principle and leads us to consider a theory to be more powerful compared to another one if the former needs less input from experiment than the later (once the model is already established of course). Then, the aim of theoretical physics can be thought of as the effort to find mathematical models whose defining principles are minimally connected with the physical world. A good starting point for this minimal connection could be a set of numerical constants.

Let us consider an analogy with linear algebra. Given a linear operator, it is not straightforward to describe its action over every element of the vector space. However, if the operator is diagonalizable, we can find its eigenvalues and a basis of eigenvectors over which the action of the linear operator is very simple. To know how the linear operator acts over any element, we only have to express the element in terms of this basis. Following this analogy, our description of the complex phenomena taking place in Nature could be thought of as a search for a "basis" of mathematical models and its eigenvalues, i.e. the fundamental constants of Nature, that simplify the task. In this scenario, a varying fundamental constant means a not appropriate selection of our basis.

This analogy also works for some epistemological concerns arising in Theoretical Physics. Nature well could be non-diagonalizable or a non-linear operator, in the sense of being impossible to describe the full physical phenomena according to the same set of principles.[7] Only linear approximations of the operator or "boxes" could be diagonalized. This could be the case for gravitation and quantum phenomena.

From a practical point of view, theoretical physics has developed two major frameworks to describe the physical world, Special Relativity[8] and Quantum Mechanics. Each of them have an associated fundamental constant of Nature, namely the speed of light c and Planck constant h, respectively; which are very deep rooted on their foundations. The speed of light establishes a scale for causal relationships, while the Planck constant sets the level of intrinsic uncertainty and the threshold of determinism. Both frameworks have demonstrated by their own to be extremely useful and precise when applied to the description of experiments and even more powerful when combined into quantum field theory.

Within these theoretical frameworks, two models have been constructed in order to explain the electromagnetism, the weak and strong nuclear interactions and gravity which are up-to-know the only interactions observed in Nature (besides the Yukawa coupling of the Higgs field with fermions). One of them is General Relativity[9] that explains gravitational interactions. The other one is the Standard Model of Particle Physics[10] that describes all the constituents of matter and their interactions, except gravitation. Both models involve several constants which are measured from experiments. For the moment, let us delay the discussion of a complete list of current fundamental constants to a following section.

[7] Nature could be unintelligible, at least in a tiny amount.

[8] In this work, Special Relativity is understood as the theoretical framework identifying space and time with a 4-dimensional manifold with lorentzian metric properties.

[9] Wald (1984).

[10] Halzen and Martin (1984).

The Copernican Principle

A variation of a fundamental constant stands for a space or time variation or both. When the laws of Physics are considered to be spacetime dependent, the Copernican Principle is often mentioned. This principle states that our place in the Universe is not special, and hence the fundamental laws of physics are the same in every location of space and every instant of time. This idea fits within the Newtonian conception[11] of space and time as absolute entities which are independent of the physical phenomena.

From a naive perspective it seems that this principle is not compatible with a variation of the fundamental constants of Nature but this is subject to interpretation. For instance, let us consider that the laws of electromagnetism, Maxwell's equations, are the same in every point of spacetime but the coupling constant of this interaction with charged particles, the fine structure constant α, varies according to a well defined law, for example depending on the gravitational potential. In this case, the law for the variation of α would not violate the Copernican Principle since the variation obeys a fundamental law that apply to every location of spacetime, and it is explained by a different value for the gravitational potential in different locations. This example is well suited in the framework of General Relativity where space and time are not absolute but a unified dynamical entity, spacetime, that evolves according to its energy and momentum content.

Spacetime properties affect the propagation of particles and it could also affect the interactions between them by an effective modification of the coupling constants. Since the properties of spacetime are not homogeneous nor isotropic, a spacetime dependence of the fundamental constants of Nature is expected on general grounds. This consideration suggests to soften the implications of the Copernican Principle over the fundamental constants of Nature, and therefore to be aware that a variation of the later does not necessary come together with a violation of this principle.

On the other hand, the variation of fundamental constants is not to be confused with the running of constants with energy in quantum field theory[12]. The actual value of the fundamental constants are defined in terms of its conversion into reality. Then, in order to measure with accuracy any constant, the specific circumstances under which the experiment should be carried out have to be precisely defined. Energy (momentum transfer, indeed) is a fundamental variable in order to describe any particle physics experiment and it turns out that it modifies the values of some constants, for instance the coupling strengths, according to quantum field theory predictions. It is important to note that while the dependence with energy is predicted by the theory, the particular numerical value at a certain energy is not, and hence it has the properties for being considered a constant of Nature.

[11] *"Absolute, true, and mathematical time, of itself, and from its own nature, flows equably without relation to anything external (...). Absolute space, in its own nature, without relation to anything external, remains always similar and immovable"*, Newton et al. (1729).

[12] Itzykson and Zuber (2012).

Dimensionless/ful constants

An important distinction among the fundamental constants of Nature is that some of them are dimensionless while others do have dimensions. Physical dimension is a concept first used by Joseph Fourier in 1822 in his famous treatise "The Analytical Theory of Heat"[13] where he highlights the importance of dimensional homogeneity in physical equations.[14] However, physical dimensions do not have an absolute and independent meaning but they are identified according to our subjective perception of the external world. In fact, our current theoretical understanding of Physics has reduced the number of physical dimensions considered in Newtonian Physics, for instance length and time are considered to have the same dimension in Special Relativity.

Another example of the relative character of a physical dimension is the following. Electric charge is generally considered to have dimension and there is a unit associated with it (the Coulomb in the SI system). On the other side, color or hypercharge are not considered to have dimensions and there are no units associated with them. However, the theory of gauge interactions tells us that there is no conceptual difference between them, all of them are gauge charges. The reason underlying this asymmetry on assigning them a dimension or not could be identified with the fact that color and hypercharge do not manifest as macroscopic quantities, because of color confinement and massive mediators of the weak interaction; and there has not been a practical need to define a new dimension.

A further logical consequence of this argument based on the relative meaning of dimension is that dimensionless quantities are not either an absolute concept. This challenges the more fundamental status usually attributed to them for being independent of human constructs like units. However, this statement relies on the identification of some physical magnitudes as having the same dimension (therefore relying on a particular theoretical framework) and on using the same unit to measure them, and eventually to compute our dimensionless constant. An example that illustrates this idea is the dimensionful/less speed of light.

Hopefully, these three examples have helped to convince the reader that physical dimension is not an absolute concept, neither a necessary one from a purely theoretical point of view.

However, dimensions are important in physics. The reason why it is so is their connection with measurements. The process of measurement basically consists in a comparison between what we want to measure and a standard for that measurement, known as unit. A set of standards for different physical magnitudes/dimensions is known as a system of units. From what the following pragmatic definition of dimension is derived: two physical magnitudes that can be compared have the same dimension.[15]

This definition encompasses the experimental side of a dimension when the comparison could be done through measurements, but it also has some useful extensions on the theoretical side. For instance, the coupling constants of the gauge interactions have the same dimension because they can be compared in a meaningful way within the gauge interaction formalism. However, to compare

[13] Fourier (2009).

[14] The formal statement of this idea is known as the Buckingham Pi theorem (Buckingham, 1914).

[15] It is clear that the problem of defining what is a physical dimension has been moved to the meaning of comparison.

the fine structure constant α and the Yukawa couplings of the Higgs field with fermions may not be appropriate since one of them is a gauge coupling while the other is not, then according to the previous definition they would not have the same dimension.

Back to the topic of measurements; given a system of units, physical quantities can be expressed as the number of times k that a given standard S of that magnitude is contained in the measurement. Therefore, the variation of a physical constant may result from the variation of the quantity itself, manifested by a variation of k, or by a variation of our standard S (Uzan, 2003). Then, in order to fully understand the theoretical implications of a variation of constants, it is mandatory to know how a standard or unit is defined.

According to Metrology,[16] there are three methods to bring a unit of measurement into reality which are defined in the International Vocabulary of Metrology (Köhler, 2010):

- a physical realisation of the unit from its definition,
- a highly-reproducible measurement as a reproduction of the definition,
- the use of a material object as the measurement method.

The SI system of units defines seven standards for practical purposes, which are in fact interdependent. Let us focus on only three magnitudes, namely time, length and mass. Their standards, namely second, meter and kilogram, are defined[17] as the duration of 9192631770 periods of the radiation corresponding to the transition between the two hyperfine levels of the ground state of the caesium-133 atom, the length travelled by light in vacuum during a time interval of 1/299792458 of a second, and the mass of the international prototype kilogram, respectively. Each of these definitions falls into one of the previous categories, in fact the second is defined in terms of a physical realization, the meter in terms of a highly-reproducible measurement and the kilogram by using a material object.

In this system of units, a spacetime dependence of the speed of light and/or the standard of time, the second, would modify the standard of length. This implies that, for instance, if a previously calibrated 1-meter ruler is observed to increase when measured in meters, we cannot unambiguously conclude that it is the ruler or the speed of light or the frequency of the caesium transition what is actually varying. In the same way, the definition of the second involves details of the electromagnetic interaction between the electrons and nuclei, in particular the fine structure constant α and the masses of electrons and nucleons (in fact, it only involves some combinations of these parameters). Therefore, any variation of these constants would show up in any time interval measured in seconds. The definition of the kilogram is much more complex in this sense, since the mass attributed to the international prototype kilogram is mainly dependent on the mass of the proton m_p and the neutron m_n, which at the same time are a result of the collective interactions of its constituents, the quarks, through the strong interaction.

In general, it is not straightforward to accept that the physics involved in the definition of a particular system of units is spacetime independent. In fact, it is necessary to assume even much

[16] Metrology is the science of measurement, it is concerned with the definition of units of measurements, its realization in practice and applying chains of traceability.

[17] www.bipm.org/utils/common/pdf/si_brochure_8_en.pdf

more than that since measurements are not performed using the actual definition of the units but using calibrated apparatus. These devices possibly work under different physical principles than the ones appearing in the definition of the standards. Therefore, assuming the constancy of a physical standard in space and time for a real measurement implies the constancy of several laws of physics, may be even the one that we want to check.

It should be clear by now that from a single measurement it is not possible to disentangle the actual variation of a physical magnitude from a possible variation of our standards of measurements, and hence of the physics involved in their definition and/or in our measuring devices. Therefore, from an observational point of view it is sensible to consider only the variation of dimensionless quantities. In this way, it is guaranteed that the actual measured variation, if any, is independent of the foundations of our system of units and of our measuring instruments, while it only depends on the physics involved in the observed phenomena and on the assumed theoretical framework.

The idea expressed above does not imply that the ultimate origin of a variation could not be found in a varying dimensionful constant. It does not even imply that asking for the variation of dimensionful constants is confusing or operationally not well defined (see Duff, 2015, for an opposite view). It only highlights the mixture between the physics involved in the definition of our units and the physics under study when measuring variation of dimensionful constants. In particular, to use a specific set of units where c, h and/or G are equal to unity does not imply anything about those fundamental constants, because units are human constructs and they are arbitrary.[18] On the other side, the fact that the speed of light c enters in the definition of the meter does not mean that we are not able to measure a variation of c, it only means that we have to use another unit. It is even not necessary to find a standard of length that is independent of the speed of light, but one having a different functional dependence on c than the meter has.

Which constants are fundamental?

From the actual definition of the fundamental constants of Nature referred to at the beginning of this introduction, it is obvious that they are very related with our knowledge of the physical world. As theoretical progress is made, some constants could be explained in terms of even more fundamental constants by new and more powerful models, or new constants may appear and old ones disappear due to a change of paradigm in our theoretical frameworks. Therefore, the list of fundamental constants is not close neither definitive.

Physics is full of constants, but not all of them seem to have the same status. The question arises about which criteria could be used to classify them. One of such classification established by Levy-Leblond (1977) considers the following categories:

- Class A: Constants which are specific of a particular object.
- Class B: Constants which describe a particular phenomenon.
- Class C: Constants which are universal.

[18] For instance, to use units where $G = 1$ to measure a variation of Newton constant G does not imply anything about the variation of G, they just do not seem to be an appropriate set of units to measure a variation of Newton constant.

These categories can be rephrased as a constant either belonging to a general theoretical framework (Class C), appearing in the description of a particular physical interaction (Class B), or describing the characteristic of the different entities involved in the interactions (Class A).

This classification also depends on our current theoretical understanding of physics. For instance, the character of a constant could change, the speed of light being a good historical example (Uzan, 2003) since it was first considered a Class A constant, describing a property of light, then it was realized that it was also present in Maxwell's equations thus describing the electromagnetic interaction, and nowadays it is considered a Class C constant since it imposes limits on causality.

The possible theoretical implications of the variation of a fundamental constant could be quite different depending on the category of that constant. The variation of a Class C constant would entail the modification of a complete theoretical framework and of the models built within that framework. Instead, any variation of the constants falling under the Class B category would imply a modification of the details of the interactions, which could be fitted without changing the theoretical framework. Finally, from the perspective of fundamental physics, a variation of a Class A constant, those that describe specific objects, can be interpreted as a variation of the interactions of that object with external entities. This may force us to consider interactions that are unique for some objects, for instance the Yukawa couplings of the Higgs field with fermions.

Moreover, in relation with microscopic Class A constants, the postulates of quantum mechanics constrain us to assume any elementary particle to be identical among themselves given the experimental evidence in favor of quantum statistical mechanics. The charges of elementary particles, understood as the properties defining the specific transformation rules under the action of an element of the gauge groups, should be considered identical among particles of the same kind and fixed. For example, it does not make sense to consider the variation of the electron charge e within the framework of quantum mechanics, but it does to consider the variation of the strength of the electromagnetic interaction described by the coupling constant of the gauge group α. For the same reason, it does not make sense to look for a variation of hypercharge or color, but it does for the corresponding gauge couplings.

Let us mention here that there are several theories implementing a varying electron charge e, varying speed of light c or varying Planck constant h (see, for instance, Magueijo et al., 2002, and references therein). In fact these models could be mapped into one another by a suitable redefinition of units (Barrow and Magueijo, 1998). However, although these models start by imposing an effective variation of these constants, the underlying physical mechanism is a new scalar field coupled to different terms of the action/Lagrangian. Referring them to as varying e, c or h, despite of being usual in the literature, could be misleading (see Ellis and Uzan, 2005; Ellis, 2007, for a similar remark in the case of varying speed of light theories).

A truly variation of e, c or h would result for instance in a violation of the Pauli Exclusion Principle, a breakdown of the local Lorentz invariance, and a reformulation of the wave-particle duality, respectively. These phenomena would entail a full revision of Physics and the mathematical tools we are used to; starting for instance with the identification of physical entities as representations of symmetry groups, spacetime as a manifold or even the use of fields. In this sense, c and h have been referred to as kinematical variables in an attempt to recognize their profound meaning in our

current theoretical frameworks. On the other side, from the point of view of current knowledge, the measured electron charge e has nothing to do with the electron itself but with the strength of the electromagnetic interactions, namely the fine structure constant α. Varying α theories although they are also usually implemented with scalar field couplings could not be interpreted as having such deep consequences in our mathematical formulation of Physics like the violation of the Pauli Exclusion Principle. Further details about these theories will be given in a following section.

Considering this hierarchical classification of fundamental constant and the constraints imposed by Special Relativity and Quantum Mechanics, it is natural to look first for a variation of Class B constants, namely coupling constants of interactions, in order to advance in this field without changing a complete theoretical framework, a much more formidable task. Furthermore, trying to find variations on Class C constants without a proper generalized theoretical paradigm could lead to wrong conclusions since we lack of the appropriate tools to interpret our experiments. Moreover, there are no contradictions in the interpretation of experiments that suggest a modification of our theoretical frameworks.

It should be noted that although it is almost accepted that the speed of light and Planck constant are universal constants and therefore belong to the Class C category, it is still a subject of debate whether Newton constant should also be considered a Class C constant (Uzan, 2011). There is a famous representation of different physical models and its range of applicability as a cube, where each axis stands for h (Quantum Mechanics), $1/c$ (Special Relativity) and G (Newton gravity) (Okun, 1991). Then, the coordinate planes represent their combination. This construction suggests that these three constants have the same logical status in our understanding of Nature. However, from a purely conceptual perspective, theoretical frameworks (Special Relativity and Quantum Mechanics) and models (Newtonian and Einstein gravity) are mixed in this cube, therefore the axis are not on the same footing.

It has also been argued that while the speed of light establishes a relation between space and time, and Planck constant makes a connection between energy and frequency (or time), Newton constant establishes a connection between matter and spacetime curvature (Ellis and Uzan, 2005). However, the electroweak or strong gauge couplings indeed can be interpreted as establishing a connection between the gauge charge and the curvature of the corresponding internal space. The fact that spacetime and mass have macroscopic effects, making our senses participant in the discussion, does not entitled them for a higher logical status. The property of these constants being "concept synthesizer", a role that still remains even when they have been set to unity, only expresses that the these constants are related with wide theoretical frameworks while others only appear in specific interactions. The presence of G in a list of universal constants of Nature has likely more to do with the absence of a satisfactory quantum theory of Gravity than with its fundamental status in our current theoretical frameworks. Although it does provide us with a useful scale, dubbed as Planck mass, its ultimate role, either hiding a Class C or Class B fundamental constant, is yet to be discovered.

There is also an interesting discussion about the number of fundamental dimensionful constants in Physics in Duff et al. (2002), where arguments in favor of three, two and zero fundamental dimensionful constants are given. In a previous section we have developed the idea that physical

dimensions are not an absolute concept, they depend on our perception of the external world as well as on the considered theoretical framework. In our opinion, both ideas are well illustrated in that discussion for being mainly responsible for the disagreement among the authors.

A list of constants

According to the previous discussion, given the two theoretical frameworks available, Special Relativity and Quantum Mechanics, its associated constants, the speed of light c and the Planck constant h, are considered universal constants of Nature (Class C).

Within these two theoretical frameworks, two models, General Relativity and the Standard Model of Particle Physics, describe the whole physical interactions that we are aware of, except for some evidence of new physics for which we lack of an accepted theory/model yet, for instance the fact that the neutrinos are massive or the observed dark matter and dark energy in galactic and cosmological scales. The Standard Model respects the principles of Quantum Mechanics and Special Relativity since it is built on top of the foundations of Quantum Field Theory (QFT), a framework that encompasses Quantum Mechanics and Special Relativity.[19] In contrast, General Relativity is a classical theory which does not take into account Quantum Mechanics.

The free parameters involved in these two models are 20: the Newton constant G, 6 Yukawa couplings for quarks and other 3 for leptons, 2 parameters for the Higgs potential, 4 parameters for the Cabibbo-Kobayashi-Maskawa matrix, 3 coupling constants for the gauge groups describing the electroweak and strong interactions, and a phase for the QCD vacuum. From this list, a new one could be built with a unique dimensionful parameter, for example the Planck mass $m_{\rm P}$ ($=\sqrt{\hbar c/G}$) and 19 dimensionless combinations.

Nevertheless, this list is not very useful from the ground of observations. The complexity in looking for a variation in some of them, for instance in the Yukawa coupling for quarks, is well beyond the available observational methods. The experimental efforts in order to seek for a spacetime variation of fundamental constants have been focused in the Newton constant G, the proton-to-electron mass ratio μ and the electromagnetic α and strong α_s gauge couplings. However, there have also been attempts to constrain variations of the speed of light c, the Planck constant h and the electron charge e.

Finally, it has been historically considered that microphysics is more fundamental than macrophysics since the later could be explained by an effective average of micro degrees of freedom. However, the discovery of the accelerated expansion of the Universe has revealed a new constant of cosmological origin, the cosmological constant, for which no microscopic explanation is available. Many experiments, including galaxy lensing and clustering (Abbott et al., 2018) and the Cosmic Microwave Background (Planck Collaboration et al., 2016), have tested the equation of state of this new cosmological fluid, yet no departure from the theoretical equation of state corresponding to a constant has been observed. The cosmological constant still remains as a macroscopic fundamental constant.

[19] However, the formulation on curved backgrounds of QFT is not free of ambiguities and it is still a subject of research. A more detailed discussion about this topic will be given at the beginning of Part II.

Theoretical models

As discussed in the historical section, the first theories accommodating a variation of fundamental constants were formulated in terms of a scalar field interaction. This scalar field being coupled to the spacetime curvature would mimic a variation of the Newton constant in the particular case of Brans-Dicke theory. Variation of other coupling constants could also be achieved by these means, i.e. by coupling scalar fields to the kinetic terms of the gauge fields (see for instance Magueijo, 2003). In a similar way, models involving not only scalar, but vector or tensor interactions, could be thought of. In the same line, modified gravity theories ($f(R)$, bimetric theories, Horava-Lifschitz gravity, ...) are capable of producing varying fundamental constants (Clifton et al., 2012).

On the other side, higher-dimensional theories (Kaluza-Klein, Randall-Sundrum, ...) or string theory (Maeda, 1988) involve fundamental constants in the higher dimensional level, but the effective 4-dimensional constants may encode the dynamics of scalar fields and/or scales, i.e. curvature or other geometrical properties, related with the higher dimensions. Therefore, the variation of a 4-dimensional constant could be easily accommodated.

Another possibility could be that the dynamics of spacetime itself modified the details of the interactions giving rise to a variation in the coupling constants. This scenario has the advantage of not postulating any new interaction, either scalar or of a different nature.

General Relativity, the theory that explains the dynamics of spacetime, has been stayed with us for a long time, more than a century ago. Furthermore, quantum field theory, the model that combines the postulates of Quantum Mechanics and Special Relativity is also very well known and it has collected an amazing success with Quantum Electrodynamics. Then, it may seem straightforward to postulate a spacetime variation of the coupling constants of the interactions.

However, we lack for the right tool, namely a quantum theory of gravity, to give a complete theoretical answer to this hypothesis about the spacetime variation of fundamental constant. Nevertheless, we have an effective theory to deal with this topic given the different scales involved in the gravitational and quantum interactions, known as Quantum Field Theory in curved spacetimes. In fact, it is well known since the eighties (Birrell and Davies, 1984) that expectation values of fields in curved backgrounds have a contribution proportional to the curvature. Therefore, an expectation value like the one of the Higgs field is predicted to vary in space and time according to the curvature of spacetime, and consequently, the masses of the fermions would be affected by this effect and would also acquire a spacetime variation. However, the relative size of these contributions is given by the curvature divided by the square of the mass of the field which, in the case of the Higgs field, is negligible during the most part of the history of the Universe. We continue this discussion in Part II.

Thesis overview

This thesis is presented as a compendium of three publications derived from two branches of research centered around the variation of the fundamental constants of Nature. The first one was focused on the observational side of the topic. Thanks to the Institute of Theoretical Physics (IFT) membership, throughout the funding support of the MultiDark Consolider Project, to the Sloan Digital Sky Survey (SDSS-III/IV), we benefited from early access to observational data and the collaboration expertise to obtain a competitive cosmological constraint upto redshift $z = 1$ for the relative variation of the fine structure constant. For this result, we used more than 13 000 optical quasar spectra from the SDSS-III/BOSS[20] Data Release 12. This scientific project ended up producing one publication which is presented in this thesis after a brief introduction to some of the astrophysical methods to constraint the fine structure constant. We also attach a scientific proposal 'APOGEE-Q' written for the Ancillary Science Projects within the SDSS-IV/APOGEE-2 Survey to take infrared spectra from high redshift $2.0 < z < 2.4$ quasars using the APOGEE spectrograph. This proposal was approved by the scientific committee of APOGEE-2, but the program finally did not pass through the observation phase because of low S/N ratio in the preliminary spectra.

The aim of the second part of the thesis was to consider a straightforward mechanism to obtain a spacetime variation of fundamental constants without introducing new interactions nor extending the current paradigm of Particle Physics. Within the effective framework of Quantum Field Theory (QFT) in curved spacetimes, non-homogeneous effects could arise as quantum corrections to the dynamics of physical fields due to the spacetime properties. In order to explain this statement, we discuss the basics of QFT in curved spacetimes before presenting the two publications concerning this part. In the first one, we computed the one-loop quantum contribution to the effective potential and energy-momentum tensor of a scalar field in vacuum in perturbed flat Friedmann-Robertson-Walker and static spacetimes. In the second one, we calculate the effects of a thermal bath on these contributions and study low and high temperature regimes.

Finally, this thesis ends presenting general conclusions about both research topics.

[20]The SDSS-III project consists of four different surveys: BOSS, SEGUE-2, APOGUEE and MARVELS. The SDSS-IV project is divided into the APOGEE-2, eBOSS and MaNGA surveys. See www.sdss.org.

Authorship Papers

Paper I: MNRAS 452, 4153-4168 (2015).

"Constraint on the time variation of the fine-structure constant with the SDSS-III/BOSS DR12 quasar sample"

Franco D. Albareti, Johan Comparat, Carlos M. Gutiérrez, Francisco Prada, Isabelle Pâris, David Schlegel, Martín López-Corredoira, Donald P. Schneider, Arturo Manchado, D. A. García-Hernández, Patrick Petitjean and Jian Ge.

In this paper, I did the full analysis of the quasar spectra from SDSS-III/BOSS DR12 and SDSS-II DR7 in order to obtain a cosmological constraint for the fine structure constant. This analysis included continuum subtraction, identification of emission lines (in particular, [O III] and [Ne III] doublets), precise determination of their wavelength through different fitting procedures, and simulations for testing our methodology. Several samples were considered, and a detailed study about systematic effects, for instance sky contamination and line blendings, was performed. I wrote the full paper.

Paper II: Physical Review D 95, 044030 (2017).

"Gravitational perturbations of the Higgs field"

Franco D. Albareti, Antonio L. Maroto and Francisco Prada.

I was responsible for the detailed calculation of the one-loop quantum contribution to the effective potential of the Higgs field in perturbed flat FRW spacetimes. For this aim, new computational methods were developed including dimensional regularization techniques for non-standard integrands. The same techniques also allowed us to compute the quantum corrections to the energy-momentum tensor of a scalar field. I wrote a major part of this paper.

Paper III: Physical Review D 97, 125017 (2018).

"Finite-temperature corrections to the energy-momentum tensor at one loop in static spacetimes"

Franco D. Albareti, Antonio L. Maroto and Francisco Prada.

In this work, I did the full computations of the thermal one-loop contribution to the effective potential of a scalar field in static spacetimes. Approximation techniques were used to obtain closed analytical expressions in the ultrarelativistic and non-relativistic regimes. This analysis was also applied to the energy momentum tensor of scalar fields in thermal states. I wrote a major part of this paper.

Co-authored Publications

As a member of the SDSS Collaboration, I coauthored the following publications:

- *The Eleventh and Twelfth Data Releases of the Sloan Digital Sky Survey: Final Data from SDSS-III*, SDSS Collaboration (+ Franco D. Albareti) et al., ApJS 219 1, 12 (2015).
- *The SDSS-IV extended Baryon Oscillation Spectroscopic Survey: Overview and Early Data*, Kyle Dawson (+ Franco D. Albareti) et al., AJ 151, 44 (2016).
- *The Thirteenth Data Release of the Sloan Digital Sky Survey: First Spectroscopic Data from the SDSS-IV Survey Mapping Nearby Galaxies at Apache Point Observatory*, SDSS Collaboration (+ Franco D. Albareti) et al., ApJS 233 2, 25 (2017).
- *The Sloan Digital Sky Survey Quasar Catalog: twelfth data release*, Isabelle Pâris (+ Franco D. Albareti) et al., A&A 597, A79 (2017).
- *Sloan Digital Sky Survey IV: Mapping the Milky Way, Nearby Galaxies and the Distant Universe*, Michael R. Blanton (+ Franco D. Albareti) et al., AJ 154, 28 (2017).

Besides, I contributed to the following paper

- *Density distribution of the cosmological matter field*, Anatoly Klypin, Francisco Prada, Juan Betancort-Rijo and Franco D. Albareti, MNRAS 481, 4588-4601 (2018).

Part I
Observational methods

Whether fundamental constants do vary in time or space or both, the answer is to be found in observations. In the following, a brief overview of the different methodologies employed to constrain fundamental constants in different regimes is given. Then, we focus on the astrophysical methods to constrain the fine structure constant in order to provide the reader with a preliminary context before reading Paper I.

Overview of methodologies

Observations looking for a spacetime variation of fundamental constants have been mainly focused in four fundamental constants:

- proton-to-electron mass ratio μ,
- Newton constant G,
- the fine structure constant α
- the strong gauge coupling α_s

The last three fall into the Class B category of fundamental constants from the point of view of our current models of Nature. The proton-to-electron mass ratio is a relative measurement of Class B constants (Yukawa couplings of fermions with the Higgs field) mixed with the Higgs vacuum expectation value and hidden under the complex dynamics of the strong interaction.

The experimental methods to test the variation of fundamental constants are usually divided into atomic, nuclear and gravitational ones (Uzan, 2003).

Atomic methods mainly involve measurements from atomic clocks, quasar absorption spectra and the Cosmic Microwave Background (CMB). They are based on comparing wavelengths or frequencies corresponding to different atomic transitions. In particular, they play an important role in constraining the variation of the fine structure constant since the electromagnetic force is the dominant interaction responsible for the atomic structure. However, they can also be used to put constraints on the proton-to-electron mass ratio and the gyromagnetic factor of the proton.

Nuclear methods are related with alpha and beta decay, Big Bang Nucleosynthesis and the Oklo reactor. The observables are abundances, lifetimes and cross-sections of different nuclear species.

When using nuclear methods, one cannot disentangle the effects of the electromagnetic and strong interactions in a clean manner. Further assumptions are necessary, for instance a model for their respective contribution to the nucleus mass.

Finally, gravitational methods include from tests of the universality of free fall to stellar and galactic evolution. They usually compare a gravitational time scale with other one that is independent of the gravitational interaction.

The constraints obtained from atomic methods have the advantage of being quite model independent in comparison with nuclear methods, where it is not possible to isolate the effects of electromagnetic, strong and weak interactions.

Besides, these methods can be further divided into truly experimental, where a better control of the systematics is possible, or observational which allow for huge time and/or space scales to look for a variation. Along this line, it is important to note that the compatibility of these measurements is not straightforward and it should be kept in mind that every constraint on the variation of a fundamental constant is obtained as a result of several assumptions, for instance assumptions about the sample, the theoretical model, the variation of other involved fundamental constants, etc.

In the remaining, we will focus on the astrophysical methods based on the observation of optical spectra from quasars to set constraints on the fine structure constant α. We refer to excellent reviews such as Uzan (2003, 2011); García-Berro et al. (2007) for the methodologies and experimental constraints imposed on the remaining constants and for non-astrophysical constraints on α. On the other side, for a recent review of spectroscopic measurements of α, μ and g_p we refer to Martins (2017).

Constraining α with quasar optical spectra

Astrophysical observations to test the variation of fundamental constants mostly rely on atomic methods, which are based on the comparison between wavelengths corresponding to different transitions. In the nonrelativistic approximation, all the transition energies have the same α-dependence, which cannot be disentangled from a Doppler shift of the lines due to the peculiar velocity of the astronomical object or the cosmological expansion. Therefore, one has to consider the relativistic spectrum. The first to point out this fact was Savedoff (1956). The fine and hyperfine structure together with molecular transitions allow to test the variation of α, μ and the proton gyromagnetic factor g_p.

Following Dzuba et al. (1999a), the α-dependence of the transition frequencies could be parameterized as

$$\omega = \omega_0 + q_1 \left[\left(\frac{\alpha}{\alpha_0} \right)^2 - 1 \right] + q_2 \left[\left(\frac{\alpha}{\alpha_0} \right)^4 - 1 \right], \tag{3}$$

where ω is the transition frequency in the rest-frame of the observed astrophysical object, ω_0 is the transition frequency measured in the laboratory, α is the value of the fine structure constant when and where the transition happens, α_0 is the value of the fine structure constant involved in the

laboratory measurements of the frequencies, and q_1 and q_2 include relativistic corrections, many-body effects and spin-orbit interactions. The relativistic and many-body corrections are computed using a relativistic Hartree-Fock (or Dirac-Hartree-Fock) method and many-body perturbation theory (Dzuba et al., 1996), while the spin-orbit effects are derived from experimental data. The coefficient q_1 dominates since it is usually an order of magnitude larger than the coefficient q_2. Several methods have been developed in order to take advantage of the different values of q_1 and q_2 for a number of atomic elements (see Dzuba et al., 1999b, and Berengut et al., 2011, for a list of these coefficients).

Let us describe the principal methods used in the literature.

Alkali doublet method

This was the first method used to constrain the time variation of the fine structure constant. It is based on the fact that the fine structure doublet splitting obeys

$$\Delta\nu \propto \frac{\alpha^2 Z^4 R_\infty}{2 n^3}, \tag{4}$$

where Z is the atomic number, R_∞ is the Rydberg constant and n is the principal quantum number. From the last expression it can be deduced that

$$\frac{\Delta\alpha}{\alpha} = \frac{c_r}{2}\left[\frac{(\lambda_2-\lambda_1)/(\lambda_1+\lambda_2)|_z}{(\lambda_2-\lambda_1)/(\lambda_1+\lambda_2)|_0} - 1\right], \tag{5}$$

where $c_r \approx 1$ takes into account relativistic corrections.[21]

This method is mainly used on quasar absorption spectra and it has been applied to several species including C IV, Mg II, Al III, Si II and Si IV (Potekhin and Varshalovich, 1994; Murphy et al., 2001b; Martínez Fiorenzano et al., 2003).

One of the most stringent constraints using this method was obtained by Chand et al. (2005). They apply the alkali doublet method on 15 Si IV absorption systems observed with the UVES spectrograph at the ESO-VLT to obtain

$$\frac{\Delta\alpha}{\alpha} = (0.15 \pm 0.43) \times 10^{-5} \tag{7}$$

over a redshift range of $1.59 \leq z \leq 2.92$.

[21] In fact, c_r can be related with the previously defined q_1 and q_2 coefficients, i.e.

$$c_r = \frac{\delta q_1 + \delta q_2}{\delta q_1 + 2\,\delta q_2}, \tag{6}$$

where δq stands for the difference between the q coefficients for the doublet transitions (Uzan, 2011).

Many multiplet method

This is a generalization of the alkali doublet method where as the name suggests, several multiplets are used, not only doublets. It was proposed by Dzuba et al. (1999c).

Depending on the value of the q_1 and q_2 coefficients for different transitions, it happens to be that some atoms are fairly insensitive to a variation of the fine structure constant, while others are more suitable to detect a variation of α. This allows to use some species as "anchors" in order to compare with other transitions. In this way an order of magnitude increase in accuracy is achieved ($\sim 10^{-6}$). This idea was carried out by Webb et al. (1999) where they compare, in a sample of quasars, the shifts in several Fe II multiplets, which are very sensitive to a variation in α, with a Mg II doublet which acts as anchor. There are two implicit assumptions made when applying this method. The first one is ionization and chemical homogeneity among the several ions employed. The second one concerns the isotopic abundance of Mg II being close to the terrestrial value.

This method attracted much attention because of the claim of a variation of the fine structure constant made by Webb et al. (1999). Since then, several analysis were performed using more observations from Keck/HIRES (Murphy et al., 2001a; Webb et al., 2001; Murphy et al., 2003) and VLT/UVES (Chand et al., 2004; Srianand et al., 2004) where a non-zero and a null variation were found respectively. It was suggested that a possible explanation could be a spatially varying fine structure constant due to the fact that Keck and VLT data do not correspond to the same hemisphere. Indeed, a dipole model was fitted at the 4σ confidence level to the spatial variation of α (Webb et al., 2011; King et al., 2012). Recently, systematic errors have been found on the Keck, VLT and Subaru telescopes. In particular, they show long-range distortions in the wavelength range of quasar spectra (Evans et al., 2014; Whitmore and Murphy, 2015). When these distortions are corrected, no evidence for a variation of α is found (Evans et al., 2014; Murphy et al., 2016; Kotuš et al., 2017). Nevertheless, this methodology is still active and providing new constraints using spectra from quasars in different locations of the sky and taken with different telescopes (e.g. Murphy and Cooksey 2017).

Single ion differential measurement

This method is a modification of the many multiplet method and it was proposed by Levshakov et al. (2005). It only considers transitions from a single ion in high-resolution spectra taken in individual exposures. In this way, it avoids the assumption of chemical and ionization homogeneity and the non-zero offsets between different exposures. In particular, the selected ion is Fe II which provides transitions with positive and negative q-coefficients therefore enhancing the effect produced by a variation of the fine structure constant. In fact, the level of precision achieved is similar to the many-multiplet method ($\sim 10^{-6}$).

This method was applied to quasar spectra taken with the VLT/UVES spectrograph (Levshakov et al., 2006, 2007) and also spectra from the HARPS instrument (Chand et al., 2006). The constraints are compatible with no variation of α.

Emission spectra

All of the methods described above use absorption lines instead of emission ones. The main reason is that emission lines in quasars are usually broader than absorption ones and show more complex structure. They are originated in different regions of quasars, therefore they show superimposed profiles, typically a narrow and a broader one. As a consequence, the individual error of each measurement is larger than in absorption spectra, but it is possible to achieve comparable precision using larger samples.

Emission lines were used very early by Bahcall and Salpeter (1965) and Bahcall et al. (1967) to put constraints on the variation of the fine structure constant. In particular, the [O III] doublet ($\lambda\lambda$ 4960, 5008 Å) was first proposed by Bahcall and Schmidt (1967) as a good candidate in order to look for a variation in α with emission lines. At that time they were able to constrain a possible variation of the fine structure constant at the level of 10^{-3}. More recently, Bahcall et al. (2004) analyzed the [O III] doublet from a sample of 165 quasars from the Sloan Digital Sky Survey (SDSS, York et al. 2000) achieving a relative precision of 10^{-4}. Later on, the method was applied by Grupe et al. (2005) to several optical emission lines ([Ne III], [Ne IV], [O III], [O I], [S II]) all at once in order to increase the accuracy. Following works (Rahmani et al., 2014; Gutiérrez and López-Corredoira, 2010) took advantage of the increase in the number of quasar spectra observed by the SDSS getting an order of magnitude improvement in the errors (10^{-5}).

Following this line of research, Paper I presents the most competitive constraint to date on the variation of the fine structure constant using the [O III] doublet detected on emission in more than 13 000 quasars spectra from the SDSS between redshift 0.02 and 0.8.

Paper I

"Constraint on the time variation of the fine-structure constant with the SDSS-III/BOSS DR12 quasar sample"

Monthly Notices of the Royal Astronomical Society, Volume 452, Issue 4, 4153-4168.

Authors: Franco D. Albareti, Johan Comparat, Carlos M. Gutiérrez, Francisco Prada, Isabelle Pâris, David Schlegel, Martín López-Corredoira, Donald P. Schneider, Arturo Manchado, D. A. García-Hernández, Patrick Petitjean and Jian Ge.

Motivation

Since the claim in 1999 of a variation of the fine structure constant at redshift $z \sim 1.3$ measured through quasar absorption spectra, the field has attracted much attention from the scientific community. Different observational procedures have been designed in order to confirm or discard that claim. Among the astrophysical methods, a major part of them relies on absorption spectra instead of emission ones. Emission lines present a more complex structure which translates into greater uncertainty in the measurements. However, large statistical samples help us to reduce those errors. In the light of the huge amount of quasar spectra observed by SDSS-II and especially by SDSS-III, in this paper we analyse the largest sample of quasars considered to date up to redshift $z = 1$, which show [O III] emission lines, to set a constraint on the variation of the fine structure constant at the $\sim 10^{-5}$ level.

Monthly Notices of the ROYAL ASTRONOMICAL SOCIETY
MNRAS **452,** 4153–4168 (2015) doi:10.1093/mnras/stv1406

Constraint on the time variation of the fine-structure constant with the SDSS-III/BOSS DR12 quasar sample

Franco D. Albareti,[1★†] Johan Comparat,[1] Carlos M. Gutiérrez,[2,3] Francisco Prada,[1,4,5] Isabelle Pâris,[6] David Schlegel,[7] Martín López-Corredoira,[2,3] Donald P. Schneider,[8,9] Arturo Manchado,[2,3,10] D. A. García-Hernández,[2,3] Patrick Petitjean[11] and Jian Ge[12]

[1]*Instituto de Física Teórica (UAM/CSIC), Universidad Autónoma de Madrid, Cantoblanco, E-28049 Madrid, Spain*
[2]*Instituto de Astrofísica de Canarias (IAC), La Laguna, E-38205 Tenerife, Spain*
[3]*Departamento de Astrofísica, Universidad de La Laguna, La Laguna, E-38206 Tenerife, Spain*
[4]*Campus of International Excellence UAM+CSIC, Cantoblanco, E-28049 Madrid, Spain*
[5]*Instituto de Astrofísica de Andalucía (CSIC), Glorieta de la Astronomía, E-18080 Granada, Spain*
[6]*INAF, Osservatorio Astronomico di Trieste, Via G. B. Tiepolo 11, I-34131 Trieste, Italy*
[7]*Lawrence Berkeley National Laboratory, 1 Cyclotron Road, Berkeley, CA 94720, USA*
[8]*Department of Astronomy and Astrophysics, The Pennsylvania State University, University Park, PA 16802, USA*
[9]*Institute for Gravitation and the Cosmos, The Pennsylvania State University, University Park, PA 16802, USA*
[10]*CSIC, Spain*
[11]*Institut d'Astrophysique de Paris, CNRS-UPMC, UMR7095, 98bis bd Arago, F-75014 Paris, France*
[12]*Department of Astronomy, University of Florida, Gainesville, FL 32611-2055, USA*

Accepted 2015 June 23. Received 2015 June 23; in original form 2015 January 13

ABSTRACT

From the Sloan Digital Sky Survey (SDSS) Data Release 12, which covers the full Baryonic Oscillation Spectroscopic Survey (BOSS) footprint, we investigate the possible variation of the fine-structure constant over cosmological time-scales. We analyse the largest quasar sample considered so far in the literature, which contains 13 175 spectra (10 363 from SDSS-III/BOSS DR12 + 2812 from SDSS-II DR7) with redshift $z < 1$. We apply the emission-line method on the [O III] doublet ($\lambda\lambda$ 4960, 5008 Å) and obtain $\Delta\alpha/\alpha = (0.9 \pm 1.8) \times 10^{-5}$ for the relative variation of the fine-structure constant. We also investigate the possible sources of systematics: misidentification of the lines, sky OH lines, H β and broad line contamination, Gaussian and Voigt fitting profiles, optimal wavelength range for the Gaussian fits, chosen polynomial order for the continuum spectrum, signal-to-noise ratio and good quality of the fits. The uncertainty of the measurement is dominated by the sky subtraction. The results presented in this work, being systematics limited, have sufficient statistics to constrain robustly the variation of the fine-structure constant in redshift bins ($\Delta z \approx 0.06$) over the last 7.9 Gyr. In addition, we study the [Ne III] doublet ($\lambda\lambda$ 3869, 3968 Å) present in 462 quasar spectra and discuss the systematic effects on using these emission lines to constrain the fine-structure constant variation. Better constraints on $\Delta\alpha/\alpha$ ($< 10^{-6}$) using the emission-line method would be possible with high-resolution spectroscopy and large galaxy/qso surveys.

Key words: line: profiles – surveys – quasars: emission lines – cosmology: observations – large-scale structure of Universe.

1 INTRODUCTION

Since Dirac's philosophical argument (Dirac 1937) against the fixed value of fundamental constants of Nature, several experiments have been performed to constrain possible variations on dimensionless constants of physical theories. Fundamental constants of physics could be thought of as parameters which enter in our description of Nature but they cannot be predicted with our current theories and should be measured. Dirac's idea is based on the unlikely fact that the most fundamental constants of the Universe have a certain fixed value (at a given energy) with no apparent relation with the real world. It is more likely that their present values are the result of

★'la Caixa'-Severo Ochoa Scholar.
†E-mail: franco.albareti@uam.es

Table 1. Summary of the results obtained by recent works based on the [O III] emission-line method for the possible variation of the fine-structure constant.

Reference	Quasar spectra	SDSS release	$z_{\rm min}$	$z_{\rm max}$	Time ago (Gyr)[a]	$\Delta\alpha/\alpha$ ($\times10^{-5}$)
Bahcall, Steinhardt & Schlegel (2004)	42	EDR (Stoughton et al. 2002)	0.16	0.80	7.0	7 ± 14
Gutiérrez & López-Corredoira (2010)	1568	DR6 (Adelman-McCarthy et al. 2008)	0.00	0.80	7.0	2.4 ± 2.5
Rahmani, Maheshwari & Srianand (2014)	2347	DR7 (Abazajian et al. 2009)	0.02	0.74	6.7	-2.1 ± 1.6
This work (2015)	13 175	DR12 (Alam et al. 2015)	0.04	1.00	7.9	0.9 ± 1.8[b]

Notes. [a] For a ΛCDM cosmology with $H_0 = 67.8\ {\rm km\,s^{-1}\,Mpc^{-1}}$, $\Omega_{\rm m} = 0.31$ and $\Omega_\Lambda = 0.69$ from *Planck*+*WMAP*-9+BAO (Planck Collaboration et al. 2014).
[b] Note: Since we have a larger sample than Gutiérrez & López-Corredoira (2010), we expect a factor ≈ 2.5 of improvement in the error just from purely statistical reasons. In Figs 9 and 10, it is shown that the error is dominated by the sky subtraction algorithm, which suggests that the performed analysis have reached the maximum precision with the available data.

a dynamical process, which had yielded the fundamental constants as they are measured today. Therefore, they should be considered as characterizing the state of the Universe (Uzan 2003). There are many current theoretical frameworks which allow for such variation of the fundamental constants, for instance, string theory (Maeda 1988), modified gravity and theories with extra dimensions (e.g. Clifton et al. 2012). Moreover, the experimental bounds on their variation have become a stringent test for those theoretical models (Thompson 2012; Leal, Martins & Ventura 2014). The most studied fundamental constants are the fine-structure constant α, the Newton gravitational constant G and the electron-to-proton mass ratio μ (Uzan 2003, 2011; García-Berro, Isern & Kubyshin 2007).

The fine-structure constant governs the electromagnetic coupling between photons and charged particles $\alpha = e^2/(\hbar c)$. The current constraint on its relative variation $\Delta\alpha/\alpha$, over geological timescales, is $|\Delta\alpha/\alpha| < 7 \times 10^{-8}$ up to $z \approx 0.15$ (2 Gyr ago); obtained from the Oklo phenomenon (e.g. Petrov et al. 2006). It has also been reported $|\Delta\alpha/\alpha| < 3 \times 10^{-7}$ up to $z \approx 0.45$ (4–5 Gyr ago) from meteorites (Olive et al. 2002); which also excludes possible variations on the scales of the Solar system. On the other hand, there are also constraints, $|\Delta\alpha/\alpha| \lesssim 10^{-2}$, based on the cosmic microwave background (CMB; Landau & Scóccola 2010; Planck Collaboration et al. 2014) at $z \approx 1100$ and from big bang nucleosynthesis, the latter being model-dependent. By measuring fine-structure multiplets at different redshift in the absorption or emission spectra of galaxies and quasars, located at different directions in the sky, one can measure an estimate of the variation of α with time or space over cosmological scales.

The first measurements on the variation of α from astronomical observations reached an accuracy of $\Delta\alpha/\alpha \approx 10^{-2}$–$10^{-3}$ (Savedoff 1956; Bahcall & Salpeter 1965; Bahcall & Schmidt 1967; Bahcall, Sargent & Schmidt 1967). Since then, the methodology and understanding of systematics has dramatically improved. Current measurements of absorption multiplets along the line of sight of three quasars around redshift 1.5, observed with spectral resolving power $R \approx 60\,000$ at UVES/ESO-VLT, reached the $\approx 5 \times 10^{-6}$ level (Evans et al. 2014). Using emission lines, an accuracy of $\approx 2 \times 10^{-5}$ was achieved analysing 1500–2300 quasar spectra at $z \approx 0.6$ (Gutiérrez & López-Corredoira 2010; Rahmani et al. 2014), taken with the Sloan Digital Sky Survey (SDSS) $R \approx 2000$ spectrograph.

The measurements on absorption features on a quasar spectrum are currently limited by the precision in the absolute wavelength calibration of the spectra, i.e. 50–200 m s^{-1} using spectra with $R \approx 60\,000$ (Molaro et al. 2013; Evans et al. 2014; Whitmore & Murphy 2015). Furthermore, the so-called many-multiplet (MM) method used in Evans et al. (2014), although more precise, remains controversial as several assumptions are made, the most important one being ionization and chemical homogeneity. These assumptions may induce systematic biases on the value of α.

In this article, we use the method based on the [O III] emission lines, first proposed by Bahcall & Salpeter (1965), which is less affected by systematics. In particular, there is no need for assuming ionization and chemical homogeneity, since the studied lines have the same profile (the transitions originate at the same upper energy level). Furthermore, the emission-line method suffers of much less spectral distortion, since the measurements of $\Delta\alpha/\alpha$ are done on a spectral window ∼100 Å as compared to ∼1000 Å when the MM method is used. With a large ensemble of quasars and/or using high-resolution spectroscopy, the uncertainty can be reduced significantly, and will compete with the absorption method when using high-resolution spectroscopy.

The beginning of the SDSS survey opened a new era of precision, allowing us to use big samples of quasars; thus, reducing the statistical uncertainty of the measurement of $\Delta\alpha/\alpha$ (see Table 1). Here, we extend these works by using the SDSS-III/BOSS Data Relase 12 (SDSS-DR12; Alam et al. 2015), which covers the full Baryonic Oscillation Spectroscopic Survey (BOSS) survey footprint with an area coverage of 10 000 deg^2. In contrast to these previous investigations, we use spectra obtained with the current BOSS spectrograph (Smee et al. 2013) instead of the previous SDSS-I/II instrument, making our BOSS sample totally independent from previous works. Moreover, the spectral range of the BOSS spectrograph allows an extension of the redshift interval for the [O III] doublet from $z = 0.8$ to $z = 1$. The number of quasar spectra is increased by a factor of 5 with respect to SDSS-DR7. All these spectra have been visually inspected and classified as quasars by the BOSS collaboration, and their products are provided in the SDSS-III/BOSS Data Release 12 Quasar catalogue (DR12Q; see Pâris et al., in preparation). For the final constraint on $\Delta\alpha/\alpha$, we combine in this work the BOSS sample with the previously studied SDSS-II DR7 quasar sample.

There are several emission doublets, in addition to [O III] (λλ 4960, 5008 Å), that can be used to measure $\Delta\alpha/\alpha$ as noted by Bahcall et al. (2004), and first used by Grupe, Pradhan & Frank (2005). Gutiérrez & López-Corredoira (2010) analysed different doublets and found that the [Ne III] (λλ 3869, 3968 Å) and [Si II] (λλ 6719, 6733 Å) doublets appear in quasar spectra with sufficient frequency to have a meaningful sample. Results for [Si II] are consistent with no variation of the fine-structure constant, although the uncertainty is an order of magnitude bigger than for [O III] , and this doublet can only be used at low redshift <0.4 for optical spectra. However, they obtained a positive variation of the fine-structure constant, $\Delta\alpha/\alpha = (34 \pm 1) \times 10^{-4}$, when the [Ne III] lines are used. No explanation was found for this positive variation. In this work, we also analyse the [Ne III] lines to check whether the same effect is present in our BOSS quasar sample.

There are investigations which use Si IV absorption lines (λλ 1394, 1403 Å) to obtain a precision of 4×10^{-6} (Chand et al. 2005). This method also avoids the assumption of ionization and

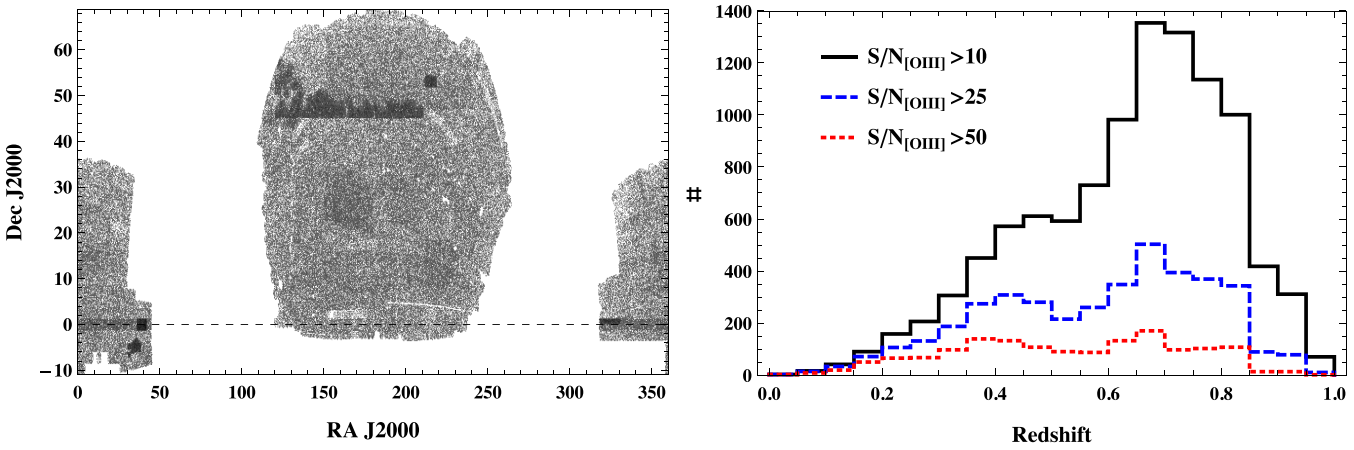

Figure 1. Left-hand panel: sky distribution of the full SDSS-III/BOSS DR12Q quasars (297 301) in J2000 equatorial coordinates. Right-hand panel: number of quasars with [O III] emission lines in our fiducial sample (10 363 quasars) in $\Delta z = 0.05$ bins. $S/N_{[O\,III]\,5008} > 10$ (10 363 quasars), black solid line; $S/N_{[O\,III]\,5008} > 25$ (4015 quasars), blue dashed line; and $S/N_{[O\,III]\,5008} > 50$ (1498 quasars), red dotted line.

chemical homogeneity. However, since the separation between both lines is only ≈9 Å, the wavelength precision needed in the laboratory for the separation between both lines is five times higher than using [O III] lines. Nevertheless, these constraints apply to the redshift interval $1.59 < z < 2.92$, which does not overlap with our range, thus they are complementary to the ones reported in this research.

Finally, in the light of the upcoming large galaxy surveys, like eBOSS and DESI, that will provide millions of high-redshift galaxy spectra, we also discuss using galaxies instead of quasars to set constraints on the fine-structure constant.

The paper is organized as follows. First, in Section 2, we describe the data set used for our analysis. Next, in Section 3, the methodology is presented, the emission-line method is explained, and the code and simulations to analyse the spectra are described. In Section 4, we study several samples to check for systematics. Then, our results are presented in Section 5. Finally, we provide in Section 6 a summary of the main conclusions achieved with this research project.

2 SAMPLE DESCRIPTION

All the spectra used in this investigation were downloaded from the SDSS Database. This survey (York et al. 2000), which began taking observations in 1998, consists of a massive collection of optical images and spectra from astronomical objects including stars, galaxies and quasars. For this purpose, there is a dedicated 2.5-m wide-angle optical telescope at Apache Point Observatory in New Mexico (USA; for more details, see Gunn et al. 2006). The third phase of this project (SDSS-III; Eisenstein et al. 2011) includes BOSS (Dawson et al. 2013) among its four main surveys. The data analysed in this research were provided by BOSS, and it is used for measuring $\Delta\alpha/\alpha$ for the first time. The SDSS-III/BOSS pipeline (Bolton et al. 2012) classifies the objects as quasars with a χ^2 minimization procedure to fit the observed spectrum to multiple galaxy and quasar spectrum templates for all allowed redshifts. Then, a visually-inspected quasar catalogue is built from these objects. Our fiducial sample is obtained from the DR12Q catalogue version (Pâris et al., in preparation).

The wavelength coverage of the SDSS-III/BOSS spectrograph is 3600–10 400 Å and that of the SDSS-II spectrograph is 3800–9200 Å. The BOSS sample is homogeneous since all the spectra have been obtained with the same instrument, and it is independent from previous investigations. The wider coverage of the new spectra allows consideration of higher redshifts (up to $z = 1$ for [O III] doublet) than in the previous SDSS-II analysis based on the same method (see Table 1). The BOSS spectrograph has two channels (blue and red) whose wavelength coverage is 3600–6350 Å and 5650–10 400 Å, respectively. The resolving power ranges from 1560 at 3700 Å to 2270 at 6000 Å (blue channel) and from 1850 at 6000 Å to 2650 at 9000 Å (red channel). For our sample, the [O III] lines fall in the red channel for >96 per cent of the quasars. The number of pixels of each spectrum is about 4600 for the BOSS spectra and 3800 for the SDSS-I/II spectra. The pixel spacing is uniform in log-wavelengths ($\Delta \log \lambda = 10^{-4}$ dex). More complete information about the SDSS-I/II and BOSS spectrographs can be found in Smee et al. (2013).

2.1 Data selection

The SDSS-III/BOSS DR12Q catalogue contains 297 301 objects. Fig. 1 (left-hand panel) shows the quasar distribution in the sky. We summarize below the main selection criteria in order to define our fiducial sample from this catalogue.

(i) Redshift <1. This limitation is imposed by the wavelength range of the BOSS optical spectrograph and the position of the [O III] lines. This criterion decreases the sample down to 45 802 quasars.

(ii) $S/N_{[O\,III]\,5008} > 10$. We impose a mild constraint on the signal-to-noise ratio (S/N) of the stronger [O III] line (5008 Å) in order to preserve a large number of spectra. Constraints on the expected width and amplitudes of the lines help in avoiding misidentifications of the [O III] doublet (see Section 4). This selection reduces the sample from 45 802 to 13 023 objects.

(iii) Non-converging fits. Since we analyse spectra with low S/N, there are some cases where the Gaussian fit to the lines does not converge. 1244 spectra are discarded, leaving us with 11 779 spectra.

(iv) Sky emission lines. Strong atmospheric lines, for instance the O I 5578 Å line, are poorly or not completely removed by the SDSS sky subtraction algorithm. This may lead to a wrong identification of the [O III] lines and to include low $S/N_{[O\,III]}$ spectra (Gutiérrez

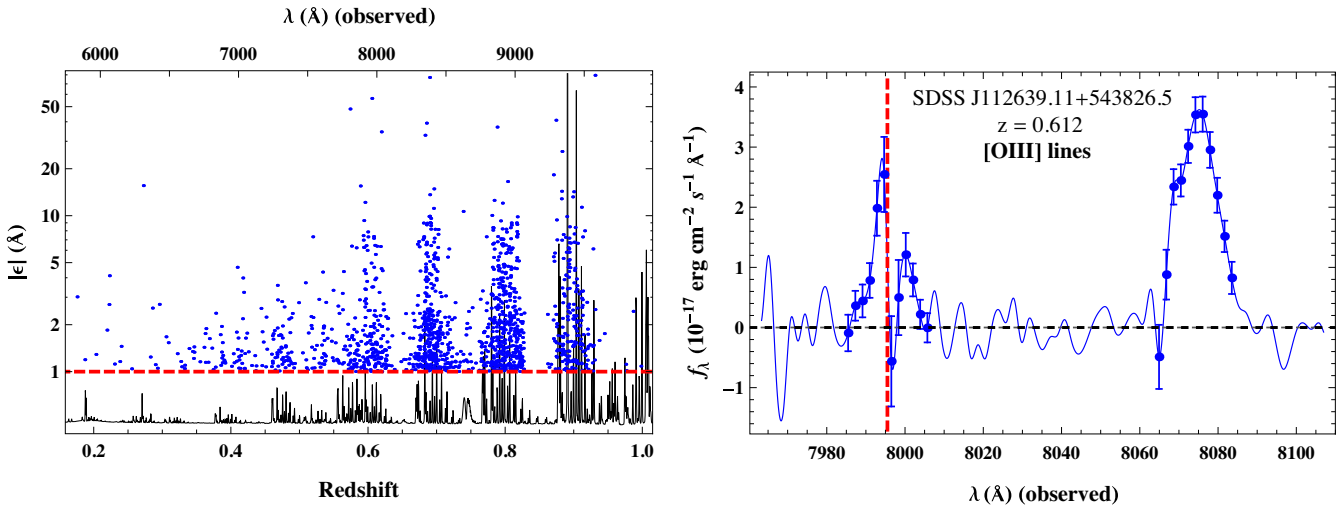

Figure 2. Left-hand panel: data points (1416) for which $|\epsilon| = |\delta\lambda_z/(1+z) - \delta\lambda_0|$, namely the absolute value of the difference between the measured line separation at redshift z in rest frame and the local one, is bigger than 1 Å plotted as a function of redshift (and the wavelength observed for [O III] 4960). We compare with a typical sky spectrum: the [O III] positions for these spectra correlate with the sky emission lines. Hence, these high values of $|\epsilon|$ are due to bad sky subtractions and/or low S/N. These spectra are removed. Right-hand panel: a spectrum removed from the sample because of the sky emission-line criteria. For this quasar, we get $\epsilon = 1.2 \pm 0.6$ Å. The weak [O III] line is affected by the subtraction of the 7995 Å OH sky emission line, indicated by the vertical red dashed line.

& López-Corredoira 2010). Both effects will produce outliers. We use the SDSS sky mask for Lyα forest studies which contains 872 lines (see Delubac et al. 2015 for more details) to remove spectra whose [O III] lines lie within a particular distance from the strongest sky lines. Even though we vary the distance [O III] – sky lines, use different set of sky lines (according to their intensity), or evaluate other conditions (S/N, fit errors, etc.) to remove affected spectra; we usually eliminate 3–5 good spectra for each bad spectra eliminated. Thus, these tests decrease significantly the number of quasars while not being very effective: typically 50 per cent of the outliers are not removed. Thus, we decided to eliminate all spectra for which the separation between both lines differ by more than 1 Å from the local value (see the last paragraph in Section 3.3). Fig. 2 (left-hand panel) shows that the distribution of these outliers is correlated with a typical sky spectrum. From a visual inspection, we observed that these spectra have low S/N, and they are in fact contaminated by sky emission line subtraction (see right-hand panel of Fig. 2). This effect causes us to discard 1416 spectra (12 per cent of the previous 11 779 quasars). Finally, we have 10 363 quasar spectra (our 'fiducial sample').

The presence of broad H β emission line (4861 Å) near the weak [O III] line 4960 Å could produce a blueshift in the determination of the [O III] line position. This could mimic a positive variation on the fine-structure constant. Therefore, a constraint on the strength and/or width of the H β emission line has been imposed on previous investigations (Bahcall et al. 2004; Gutiérrez & López-Corredoira 2010; Rahmani et al. 2014). However, we do not restrict any characteristic of the H β line in our fiducial sample. We obtain a weighted mean for $\Delta\alpha/\alpha$ using as weights the uncertainty in $\Delta\alpha/\alpha$ computed with the standard errors for the position of the lines derived from the Gaussian fits. The contamination of H β is automatically taken into account. For instance, a broad H β line near the [O III] 4960 line means a bad Gaussian fit. Thus, we obtain larger errors in the position of the line centroids and, consequently, in $\Delta\alpha/\alpha$. In Section 4, we analyse several samples where the $S/N_{H\beta}$ is constrained to check that the H β contamination has little weight on the final constraint value.

An electronic table is published along with the paper which contains all the information of each spectrum from our fiducial sample of 10 363 quasars (see Appendix A).

The distribution of the selected quasars in redshift according to their selected $S/N_{[O\,III]\ 5008}$ is plotted in Fig. 1 (right-hand panel). Fig. 3 (left-hand panel) displays a composite image built with all the spectra from our fiducial sample sorted by redshift. The right-hand panel shows the [O III] doublet in rest frame.

3 METHODOLOGY

3.1 Measurement method

To first order, the difference between the energy levels of an atom is proportional to α^2. Transitions between energy levels of the same atom at a given ionization level, with the same principal quantum number and different total angular momentum J, have an energy difference proportional to α^4. These groups of transitions are called fine-structure multiplets. Savedoff (1956) first realized that the fine structure of these energy levels could be used to break the degeneracy between the redshift effect and a possible variation of α.

The value of the fine-structure constant can be measured through the separation between absorption or emission multiplets in the spectra of distant quasars (Uzan 2003) as

$$\frac{\Delta\alpha}{\alpha}(z) \equiv \frac{1}{2}\left\{\frac{[(\lambda_2-\lambda_1)/(\lambda_2+\lambda_1)]_z}{[(\lambda_2-\lambda_1)/(\lambda_2+\lambda_1)]_0} - 1\right\}, \quad (1)$$

where $\lambda_{1,2}$ ($\lambda_2 > \lambda_1$) are the wavelengths of the transitions and subscript 0 and z stand for their value at redshift zero (theoretical/laboratory values) and at redshift z, respectively. For illustrative purposes, expression (1) can be approximated by

$$\frac{\Delta\alpha}{\alpha} \approx \frac{\epsilon}{2\,\delta\lambda_0}, \quad (2)$$

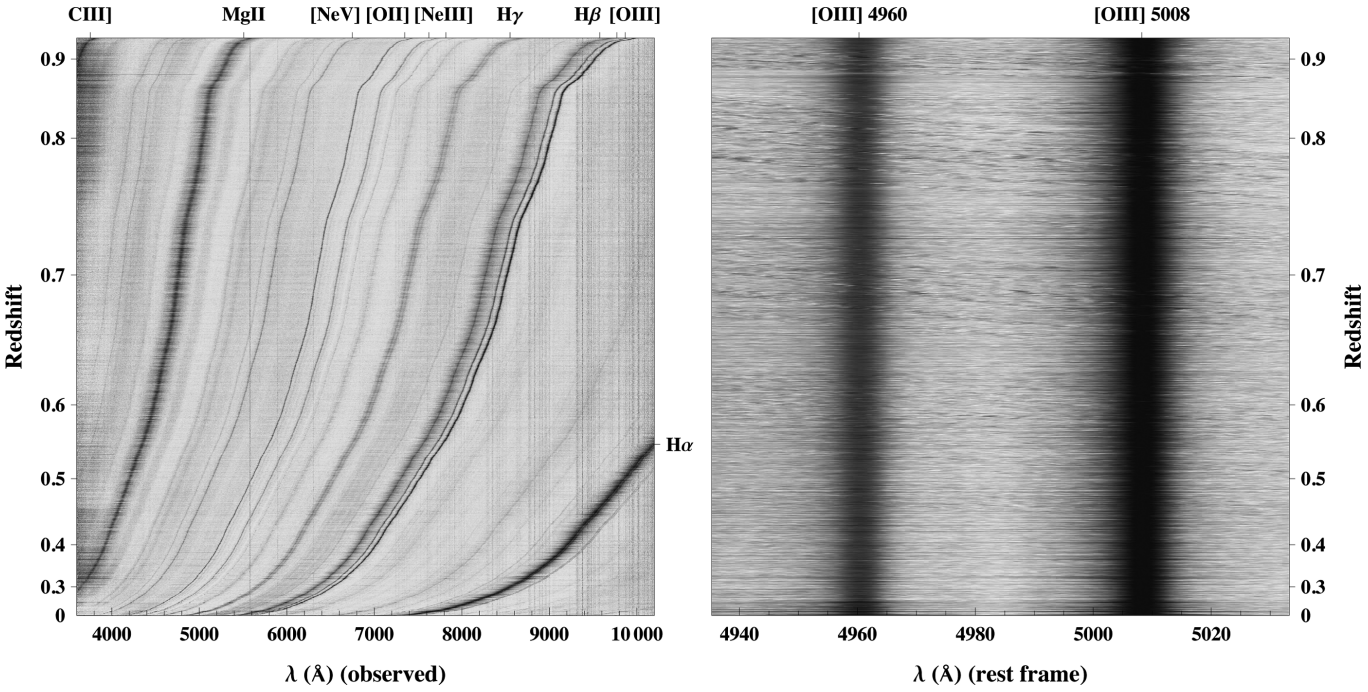

Figure 3. Composite image with our fiducial sample of 10 363 BOSS quasar spectra sorted by redshift. Left-hand panel: the whole range of wavelengths is shown. From right to left, the strongest emission lines are H α 6565 Å; [O III] $\lambda\lambda$ 4960, 5008 Å; H β 4861 Å; H γ 4341 Å; [Ne III] $\lambda\lambda$ 3869, 3968 Å; [O II] 3730 Å; [Ne V] 3426 Å; Mg II 2796 Å and C III] 1906 Å. The narrow straight line at 5579 Å is the strong [O I] atmospheric line. Right-hand panel: wavelength interval centred at the [O III] doublet in rest frame.

where $\delta\lambda_0 = [\lambda_2 - \lambda_1]_0$ is the local $z = 0$ separation between both wavelengths, and $\epsilon = \delta\lambda_z/(1+z) - \delta\lambda_0$ is the difference between the measured line separation at redshift z in rest frame and the local one. Thus, in principle, the larger the difference between the pair of lines, the better the precision for measuring $\Delta\alpha/\alpha$.

Concerning emission lines, the most suitable pair of lines is the [O III] doublet, which is often present in quasar spectra with relatively high-S/N. The vacuum values for the [O III] doublet wavelengths are

$$\lambda_1^{[\mathrm{O\,III}]} = 4960.295 \text{ Å} \qquad \lambda_2^{[\mathrm{O\,III}]} = 5008.240 \text{ Å} \tag{3}$$

$$\delta\lambda_0^{[\mathrm{O\,III}]} = 47.945 \text{ Å}, \tag{4}$$

which are published in the NIST Atomic Spectra Database.[1] These transitions are forbidden (they correspond to magnetic dipole and electric quadrupole transitions), and they are not observed in the laboratory. The wavelength experimental values are obtained indirectly by first computing the energy levels from observed wavelengths using a theta-pinch discharge (Pettersson 1982). The wavelength separation has directly been measured in the infrared from H II regions using a balloon-borne telescope and Michelson interferometer (Moorwood et al. 1980). Both measurements of the wavelength separation, indirectly with the theta-pinch discharge and directly with the Michelson interferometer, are in good agreement, being the Michelson interferometer more accurate with an error $<5 \times 10^{-4}$ Å.

From equation (2), a determination of ϵ with a precision of 1 Å allows for an uncertainty of 10^{-2} in $\Delta\alpha/\alpha$ when using the [O III] doublet. The precision from the NIST atomic data allows for a determination of $\Delta\alpha/\alpha$ up to 10^{-5}, which is a bit less than the uncertainty in our result. One could perform a blind analysis in order to search for a possible variation on α, where the absolute wavelength values are not required, if one had a large enough sample distributed in redshift. However, the precision on the absolute wavelengths limits the usefulness of high-resolution spectroscopy until better measurements of the [O III] lines (or just their separation) are available.

[1] http://physics.nist.gov/PhysRefData/ASD/lines_form.html

3.2 Implementation

The code developed for the analysis of the quasar spectra follows the one described in Gutiérrez & López-Corredoira (2010), although there are some modifications and more information has been extracted from the analysis. We describe the main characteristics of our code below.

3.2.1 Wavelength sampling

We consider only the experimental data together with their errors as processed by the SDSS pipeline to obtain the constraint on the possible variation of α. We do not resample the wavelength range by using an interpolation method. Since the pixel spacing is uniform in log-wavelengths, a given range of wavelengths in rest frame (λ_-, λ_+) has the same number of pixels N, i.e.

$$N \propto \int_{\lambda_-(1+z)}^{\lambda_+(1+z)} \mathrm{d}\,(\log\lambda) = \log\frac{\lambda_+(1+z)}{\lambda_-(1+z)} = \log\frac{\lambda_+}{\lambda_-}, \tag{5}$$

and is independent of the redshift of the object. All the wavelength intervals with the same width in rest frame will have the same number of experimental points.

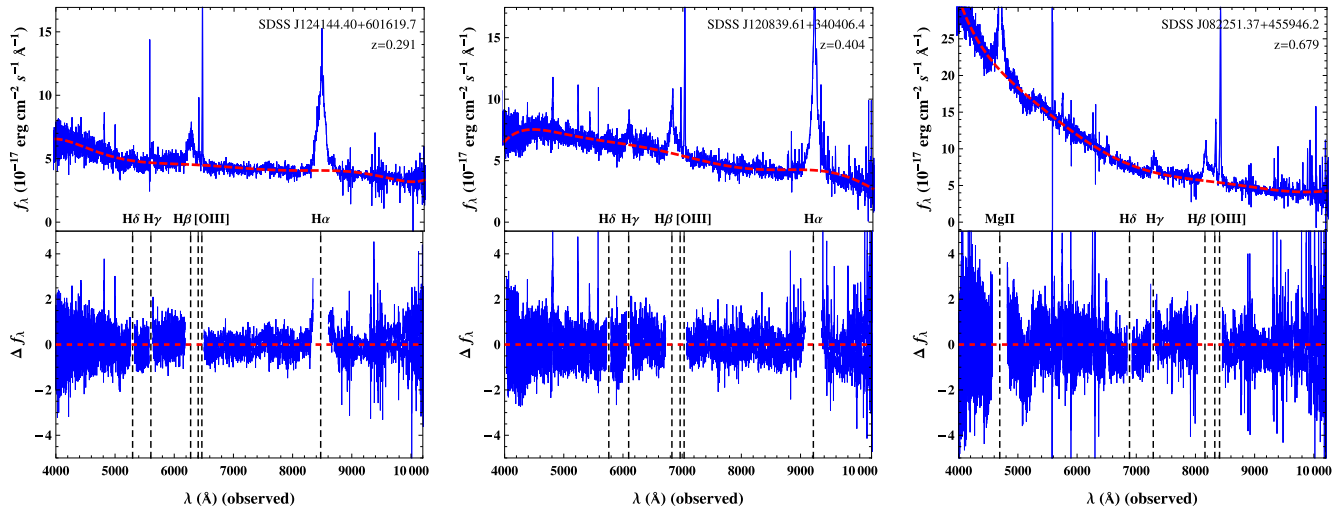

Figure 4. Seventh-order polynomial fits (red) to the continuum spectrum with their residuals for three typical quasar spectra at different redshift. The gaps in the residuals are the masked regions corresponding to (from right to left) H α, the [O III] doublet, H β, H γ, H δ and Mg II (black dashed lines).

3.2.2 *Fit of the continuum spectrum*

First, we fit a seventh-order polynomial to subtract the continuum spectrum while masking regions where strong and wide emission lines are present (H α, H β, H γ, H δ, Mg II and the [O III] doublet). Our method differs from Gutiérrez & López-Corredoira (2010) in that they use a cubic local spline to fit the continuum masking strong emission lines. The chosen order of the polynomial provides enough degrees of freedom to reproduce different continuum features. In Section 3, we test how our measurement for $\Delta\alpha/\alpha$ is affected by changing the polynomial order. Hundreds of continuum spectra fits were checked by eye. The residuals from the fits are smaller than the errors on the flux densities. Fig. 4 shows three different spectra with their continuum fit and residuals.

3.2.3 *Signal-to-noise ratio*

We follow Gutiérrez & López-Corredoira (2010) for the determination of S/N. Hence, we compute the standard deviation of the flux between $5040\,(1+z)$ and $5100\,(1+z)$ Å (where z is the redshift of the quasar) where there are no strong emission or absorption lines. Then, we search for the maximum of the [O III] 5008 line, and determine $\mathrm{S/N}_{[\mathrm{O\,III}]\ 5008}$ as the ratio between the maximum of the line and the previously computed standard deviation. Although for a more reliable determination of the S/N, it is better to use a Gaussian fit to the line. This procedure avoids possible issues related when fitting data with very low S/N. This S/N is used in the criterion ii (Section 2) to build our fiducial sample.

3.2.4 *Measurement of the emission-line wavelengths*

To measure the wavelengths of the [O III] doublet, our fitting code needs as input an accurate estimate of the redshift of the quasar, at least with an error $\Delta z < 3\times10^{-3}$. This allows a search for the emission lines in a 15 Å window around the expected location of the [O III] lines. The SDSS pipeline provides a determination of the redshift based on a χ^2 fit to different templates; we refer to Bolton et al. (2012) for more details. These redshift estimates have errors between 10^{-4} and 10^{-5}, which are sufficient for our purposes. Moreover, there is also a visual redshift estimation which can be found in the quasar catalogue DR12Q (Paris et al., in preparation). The difference between both redshift estimates (if any) is usually $|z_{\mathrm{vis}} - z_{\mathrm{pipe}}| \approx 5\times10^{-4}$. We decided to adopt the visual redshifts.

The centroid positions of the [O III] emission lines are determined by four different methods.

(i) Gaussian profile method.
First, we search for the maximum flux value in an $\sim15\,(1+z)$ Å window around the expected position of the line (according to the redshift provided by the DR12Q catalogue). This procedure automatically erases any bias produced by the redshift value. Then, we make an initial Gaussian fit around the position of the maximum flux value using a fixed width of $\sim10\,(1+z)$ Å. From this first fit, we obtain a new position for the line centroid and a Gaussian width. These values are used as initial parameters for the final fit of the lines; namely, the wavelength range considered to perform the final fit is centred around the position of the line centroid, and it is four times the Gaussian width of the lines. This approach means that we consider pixels up to 2σ away from the centre of the line. Hence, some lines are fitted using ∼4–5 pixels, while others with ∼15–20 pixels depending on the line width. The fit takes into account the flux errors for each pixel, i.e. we use the *ivar* column found in each spectrum as weights for the fit. Our final centroid measurement for each considered line corresponds to the centroid of the Gaussian fit done in the last step of the adopted procedure. We also derive an error for $\Delta\alpha/\alpha$ using the standard errors for the centre position of the Gaussians. This is our main method for measuring α.

(ii) Voigt profile method.
Following the same procedure than when using a Gaussian profile, we make the fit with a Voigt profile instead of a Gaussian. More precisely, we use a pseudo-Voigt profile which is a linear combination of a Gaussian and a Lorentzian profile. Then, we have one more parameter, i.e. the amplitude of the Lorentzian function, while its width and its position are the same as those for the Gaussian profile. In Fig. 5, we depict the [O III] and [Ne III] lines for the same quasar spectrum to illustrate the Gaussian and Voigt fitting methods.

(iii) Integration method.
Here, the centroids of the lines are obtained by integrating around 1σ from the position of the fitted Gaussian profile. This technique provides indications of whether there is H β contamination. However, due to the mid-resolution of the spectra $R\approx2000$, this method is not very accurate.

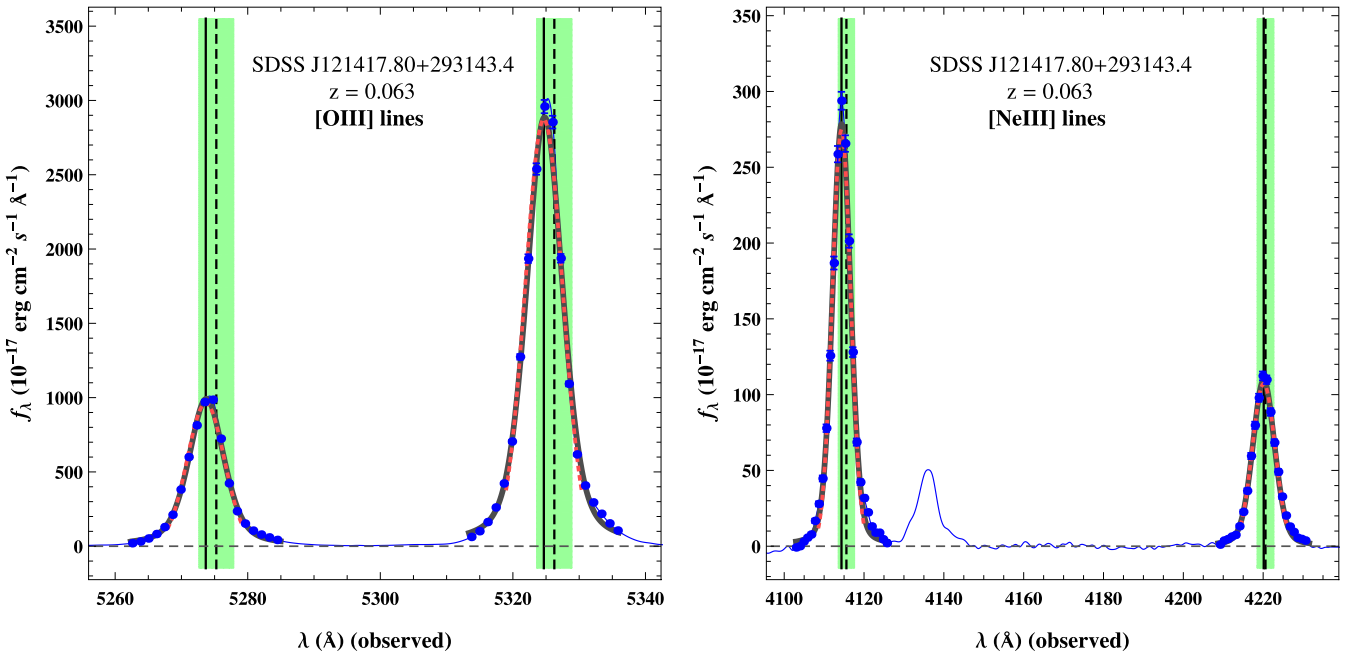

Figure 5. [O III] (left-hand panel) and [Ne III] (right-hand panel) lines for SDSS-J121417.80+293143.4, at redshift $z = 0.063$. The measured $\Delta\alpha/\alpha$ for this quasar is $\Delta\alpha/\alpha^{\rm Gauss}_{\rm [O\,III]} = (2.3 \pm 7.6) \times 10^{-4}$, $\Delta\alpha/\alpha^{\rm Voigt}_{\rm [O\,III]} = (3.3 \pm 12.6) \times 10^{-4}$ and $\Delta\alpha/\alpha^{\rm Gauss}_{\rm [Ne\,III]} = (39 \pm 8) \times 10^{-4}$, $\Delta\alpha/\alpha^{\rm Voigt}_{\rm [Ne\,III]} = (37 \pm 9) \times 10^{-4}$. The measured $\Delta\alpha/\alpha$ for [Ne III] is not consistent with zero regardless of the profile; see Fig. 14 and last paragraph of Section 4 for discussion. Each panel shows the flux density for each pixel with their respective error bars (solid symbols), together with the Gaussian fit (dotted red curve) and the pseudo-Voigt profile (thick grey curve) to each of the lines. The fitting procedure (described in the text) only takes into account the experimental data (solid symbols) weighted by their error bars. Notice how the deviation of the line centroid position derived from our Gaussian fit (vertical solid line) with respect to the expected position of the line (vertical dashed line) according to the visual redshift provided by the DR12Q catalogue are well correlated for the same pair of [O III] and [Ne III] lines, and for the different set of lines. The green shaded vertical areas highlight the uncertainty for the expected position of the lines due to the quasar redshift error ($\approx 5 \times 10^{-4}$). Also shown is a fourth-order spline interpolation to the spectrum after subtracting the continuum (thin solid line). The [Ne III] lines are weaker by one order of magnitude than the [O III] lines, which is usually the case for all the spectra showing both pair of lines. The weak line near the stronger [Ne III] line is blended with He I (3889.75 Å) and H ζ (3890.16 Å).

(iv) Modified Bahcall method.
In Bahcall et al. (2004) the authors used a different approach to compute the line positions. They performed a third-order spline interpolation to the stronger [O III] 5008 line, then fitted this interpolation to the weaker 4960 line by adjusting the amplitude and separation of the profile. We have modified this method by using a Gaussian fit to the stronger line rather than a third-order spline.

Although we have described four different methods, the main results for $\Delta\alpha/\alpha$ presented in this work are based on the Gaussian fitting method, while the other three are used only for comparison (see Section 4).

Finally, our final result for $\Delta\alpha/\alpha$ and its error is obtained in the same way as in Chand et al. (2005), namely we compute a weighted mean and a weighted standard deviation, where the errors for $\Delta\alpha/\alpha$ of each spectrum are used as weights.

3.3 Simulated spectra

In order to test the robustness and accuracy of our methodology, we generate realizations of quasar spectra using as noise a normal distribution centred at the flux value, and taking the error in each pixel as the standard deviation. From our fiducial sample (10 363 quasars), we simulate 100 realizations for each spectrum (> a million in total). This number of realizations provides reasonable statistics to derive an error from the standard deviation of the measurements on the realizations of each real spectrum, while the computation time remains reasonable ($\sim$ 2 d) using a standard-size computer. The estimated error derived from the simulations $\Delta(\Delta\alpha/\alpha)_{\rm sim}$ includes

$$\Delta(\Delta\alpha/\alpha)^2_{\rm sim} = \Delta(\Delta\alpha/\alpha)^2_{\rm fit} + \Delta(\Delta\alpha/\alpha)^2_{\rm continuum} + \Delta(\Delta\alpha/\alpha)^2_{\rm code}, \quad (6)$$

where $\Delta(\Delta\alpha/\alpha)_{\rm fit}$ is the error derived from the Gaussian fits, which is our error estimate for each real spectrum; $\Delta(\Delta\alpha/\alpha)_{\rm continuum}$ is the error from different continuum subtraction due to the Gaussian noise, and $\Delta(\Delta\alpha/\alpha)_{\rm code}$ is the systematic error of our code. Then, we expect $\Delta(\Delta\alpha/\alpha)_{\rm sim} > \Delta(\Delta\alpha/\alpha)_{\rm fit}$ and their difference will be an indication of the continuum and systematic errors.

Fig. 6 (left-hand panel) shows the correlation between the error in $\Delta\alpha/\alpha$ from the Gaussian fits of each real spectrum and the standard deviation for $\Delta\alpha/\alpha$ of its 100 realizations. The standard deviations from the simulations are within a factor of 0.5–2 of the standard errors from the fits for 97 per cent (84 per cent) of the cases when both quantities are $<5 \times 10^{-3}$ ($<50 \times 10^{-3}$). This shows that our code and the continuum subtraction do not introduce noticeable systematic errors compared to the Gaussian fitting. However, there is a set of spectra (9 per cent of the total) for which the simulations provide much larger errors $\Delta(\Delta\alpha/\alpha) > 0.1$. Fig. 6 (right-hand panel) shows the errors from the simulations as a function of redshift for our fiducial sample. Red crosses stand for spectra whose Gaussian fit error $\Delta(\Delta\alpha/\alpha)_{\rm fit} > 5 \times 10^{-3}$ (24 per cent). The errors are distributed in two clouds of points. For the cloud with $\Delta(\Delta\alpha/\alpha)_{\rm sim} \sim 1$, the virtual realizations of each spectrum seem to differ significantly from the real spectrum. Since we use the error in each pixel to build the realizations, the relative error is large for these spectra, which is an

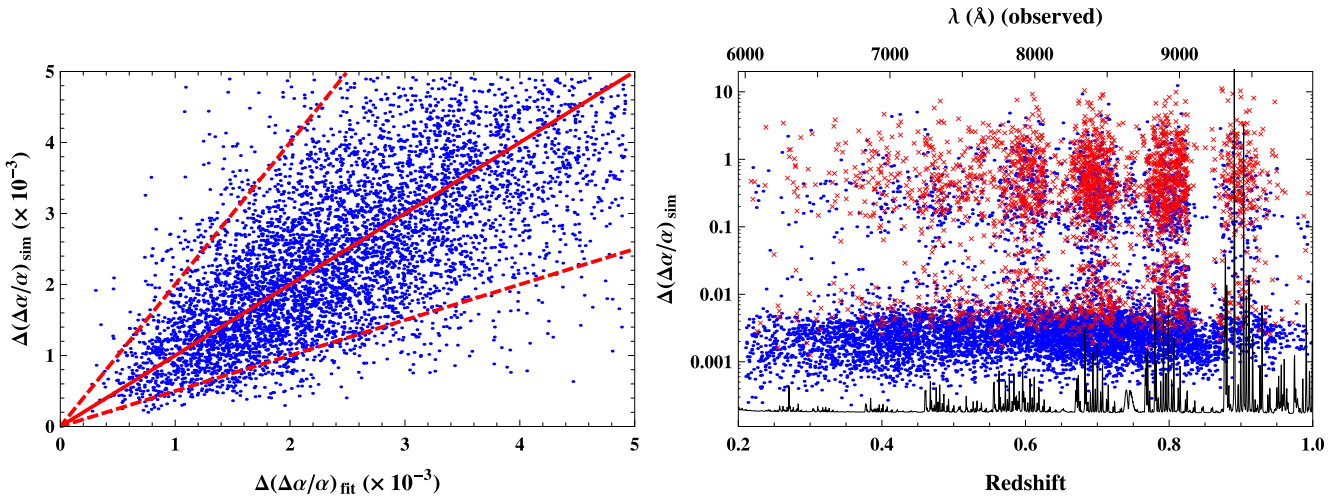

Figure 6. Left-hand panel: errors for $\Delta\alpha/\alpha$ obtained from the simulations (standard deviation of the $\Delta\alpha/\alpha$ measurements on 100 realizations of each real spectrum) and standard errors from the Gaussian fits for our fiducial sample. The solid line represents a one-to-one correspondence, while the dashed lines have slopes of 2 and 0.5. Only the simulation and fit errors smaller than $<5 \times 10^{-3}$ are shown. Right-hand panel: errors estimated from the simulations as a function of redshift. Spectra with $\Delta(\Delta\alpha/\alpha)_{\rm fit} > 5 \times 10^{-3}$ are shown as red crosses (24 per cent of the total). There is a clear division between two different set of spectra which correlates with the sky emission lines (see discussion in the main text).

indication of a low S/N ratio or large absolute errors in the pixels, for instance in wavelength regions with sky emission lines. In fact, the cloud with bigger errors mimics the sky spectrum. Note also the strong correlation between this cloud of points and the spectra with large Gaussian fitting errors (red crosses). The other set of points with $\Delta(\Delta\alpha/\alpha)_{\rm sim} \sim 10^{-3}$ are close to our error estimation on the measurement of $\Delta\alpha/\alpha$ based on the Gaussian fits.

As a further proof, we also simulate realizations of the 1416 dropped spectra because of sky emission lines (criterion iv, see Section 2). We found that more than 80 per cent of the spectra have $\Delta(\Delta\alpha/\alpha)_{\rm sim} > 0.1$. This confirms that these spectra have very low S/N and/or large pixels error due to the proximity of the lines to strong sky emission lines.

3.4 Gaussian versus Voigt fitting profiles

The results obtained when using Voigt profiles instead of Gaussian ones are compared in Fig. 7. The Voigt and Gaussian measurements are 1σ-compatible for the 93.5 per cent of the cases (98.3 per cent at 2σ). Regarding the errors, there is no clear improvement when using either of both methods. However, Voigt profiles have one more parameter and restrict the number of degrees of freedom. Due to the spectral mid-resolution and the fact that the [O III] lines are very narrow, there are often only a few pixels to fit, which frequently lead to non-convergent fits. This reduces the quasar sample in ≈1000 quasars. Further discussion about both profiles can be found in Section 4.

4 SYSTEMATICS

In this section, we examine the possible unnoticed systematic errors by analysing different quasar samples. Table 2 summarizes all the samples considered together with their mean redshifts and the measured value for $\Delta\alpha/\alpha$.

We consider the following sources of systematic errors.

(i) Misidentification of the lines. The expected line widths and amplitudes are useful to avoid misidentification of the

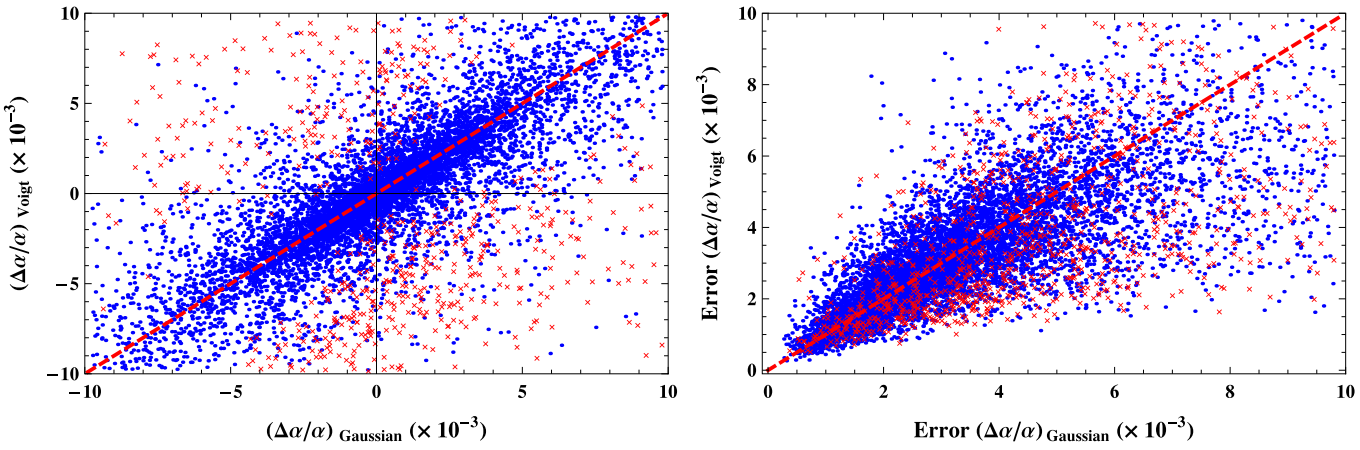

Figure 7. Left-hand panel: measurements of $\Delta\alpha/\alpha$ using Gaussian and Voigt fitting profiles. Non-compatible measurements at 1σ are shown as red crosses (6.5 per cent of the total). Right-hand panel: errors from the Gaussian and Voigt fitting. Non-compatible measurements at 1σ are shown as red crosses.

Table 2. Results for $\Delta\alpha/\alpha$ considering several samples with different constraints. The number of quasar spectra, the mean and standard deviation of the redshift and the value for $\Delta\alpha/\alpha$ are shown.

$\sigma_{4960/5008} - 1$	No. of quasar spectra	Redshift	$\Delta\alpha/\alpha$ ($\times 10^{-5}$)
<50 per cent	10 028	0.56 ± 0.21	1.6 ± 2.3
<25 per cent	8877	0.56 ± 0.21	1.9 ± 2.3
<10 per cent	5846	0.56 ± 0.21	1.7 ± 2.5
<5 per cent	3458	0.54 ± 0.22	−0.9 ± 3.0
$[F_\lambda \times \sigma]_{5008/4960}$	No. of quasar spectra	Redshift	$\Delta\alpha/\alpha$ ($\times 10^{-5}$)
2.98 ± 0.50	8327	0.56 ± 0.21	1.8 ± 2.4
2.98 ± 0.25	5761	0.55 ± 0.21	−0.4 ± 2.6
2.98 ± 0.10	2658	0.54 ± 0.21	0.0 ± 3.4
2.98 ± 0.05	1411	0.52 ± 0.22	5.2 ± 4.6
Fit width	No. of quasar spectra	Redshift	$\Delta\alpha/\alpha$ ($\times 10^{-5}$)
2σ	10 363	0.56 ± 0.21	1.4 ± 2.3
3σ	10 252	0.59 ± 0.20	5.5 ± 2.5
4σ	9978	0.59 ± 0.20	7.1 ± 2.7
5σ	9726	0.59 ± 0.20	5.3 ± 2.6
$S/N_{H\beta/[Oiii]4960}$	No. of quasar spectra	Redshift	$\Delta\alpha/\alpha$ ($\times 10^{-5}$)
<5	10 338	0.57 ± 0.21	1.4 ± 2.3
<2	9831	0.57 ± 0.21	0.6 ± 2.3
<1	8162	0.57 ± 0.21	0.1 ± 2.5
<0.5	5831	0.58 ± 0.21	−0.7 ± 2.8
Pol. order (cont.)	No. of quasar spectra	Redshift	$\Delta\alpha/\alpha$ ($\times 10^{-5}$)
3	10 528	0.57 ± 0.21	1.0 ± 2.3
5	10 550	0.57 ± 0.21	1.3 ± 2.3
7	10 363	0.56 ± 0.21	1.4 ± 2.3
9	10 471	0.56 ± 0.21	−1.1 ± 2.3
R^2 (both fits)	No. of quasar spectra	Redshift	$\Delta\alpha/\alpha$ ($\times 10^{-5}$)
>0.9	9254	0.56 ± 0.21	1.5 ± 2.4
>0.97	6045	0.56 ± 0.21	2.8 ± 2.7
>0.99	2301	0.54 ± 0.21	2.0 ± 3.5
>0.995	845	0.51 ± 0.22	−0.4 ± 4.8
[O III] 5008 (km s^{-1})	No. of quasar spectra	Redshift	$\Delta\alpha/\alpha$ ($\times 10^{-5}$)
<1000	10 353	0.56 ± 0.21	1.4 ± 2.3
<500	8990	0.56 ± 0.21	0.2 ± 2.4
<300	2798	0.52 ± 0.22	−6.8 ± 3.9
<200	150	0.52 ± 0.24	21 ± 18
Method	No. of quasar spectra	Redshift	$\Delta\alpha/\alpha$ ($\times 10^{-5}$)
Gaussian (weighted)	4537	0.58 ± 0.20	−0.4 ± 2.8
Gaussian	4537	0.58 ± 0.20	1.2 ± 4.5
Integration	4537	0.58 ± 0.20	3.6 ± 4.8
Modified Bahcall	4537	0.58 ± 0.20	0.8 ± 4.4
Median	4537	0.58 ± 0.20	1.8 ± 1.4
Gauss versus Voigt	No. of quasar spectra	Redshift	$\Delta\alpha/\alpha$ ($\times 10^{-5}$)
Gaussian profiles	8485	0.55 ± 0.19	0.4 ± 2.5
Voigt profiles	8485	0.55 ± 0.19	−1.1 ± 2.8
Mixed profiles	8485	0.55 ± 0.19	1.3 ± 2.4

[O III] emission lines. (a) Line widths: since both lines originate on the same upper energy level, their width must coincide. We check that this is the case by considering quasars whose [O III] line widths are the same within a relative fraction. For more than half of our fiducial sample, the [O III] line widths differ by less than 10 per cent (see Table 2). (b) Amplitude ratio: atomic physics states that the amplitude ratio between the [O III] 5008 and [O III] 4960 lines is 2.98 (Storey & Zeippen 2000, as quoted in Section 5, we obtain $2.96 \pm 0.02_{\rm syst}$). Thus, we consider different samples where this ratio differs by less than a certain amount from 2.98 (see Table 2). All the samples considered in this test yield results for $\Delta\alpha/\alpha$ compatible with zero. Fig. 8 displays the Gaussian widths and fluxes of both [O III] emission lines for our fiducial sample.

(ii) Windows for the Gaussian fits. We use a wavelength range of 2σ around each [O III] line in order to obtain the final Gaussian fit to the line profiles. We study how our results depend on this choice. By considering a larger wavelength interval, the results are more affected by the H β contamination and possible asymmetries on the line wings. The differences in the number of spectra for these samples [which are obtained by applying the selection criteria (i)–(iv) discussed in Section 2.1] arise because of the criteria concerning the non-converging fits and the sky emission lines described in Section 2.

(iii) H β contamination. We analyse samples where the ratio between $S/N_{H\beta}$ and $S/N_{[O\,III]\ 4960}$ is constrained. Despite the fact that the value for $\Delta\alpha/\alpha$ decreases as we place more stringent constraints on H β, it is always consistent with no variation in α within the errors. This analysis demonstrates that the strength and/or width of the H β line do not affect substantially the result for $\Delta\alpha/\alpha$ when a weighted mean is adopted.

(iv) Continuum subtraction. We use a seventh-order polynomial to subtract the continuum spectrum. We examine if the polynomial order has important effects on our measurements. Our values for $\Delta\alpha/\alpha$ and their errors are only slightly affected by the chosen polynomial order.

(v) Goodness of Gaussian fits. We quantify the quality of the Gaussian fits by the R^2 coefficient. All the considered samples show values for $\Delta\alpha/\alpha$ consistent with no variation in α.

(vi) Broad lines. We also study samples where the width of both lines is less than a certain value (in km s^{-1}). These samples are consistent with no variation of α. Samples built from narrow lines <300 km s^{-1} may be more affected by misidentification of [O III] lines as sky lines.

(vii) Different methods for measuring the [O III] line position. We compare the results obtained by the methods to measure the position of the [O III] lines described in Section 3.2.4. Since not all the methods provide an error for the measurement, we cannot calculate a weighted mean, and it is necessary to select a more restricted sample. Then, we consider a sample where the difference between the widths of the lines is less than 25 per cent, the amplitude ratio is constrained to differ from the theoretical value 2.98 (Storey & Zeippen 2000) by less than 0.5, and the $S/N_{H\beta}$ is smaller than half the $S/N_{[O\,III]\ 4960}$.

(viii) Gaussian versus Voigt profiles. We compare the results for 8485 quasars from our fiducial sample after dropping 1878 spectra with non-converging Voigt fits (this reduction increases the statistical error). We also compute a 'mixed' value for $\Delta\alpha/\alpha$ where for each spectrum we use the value for the variation of the fine-structure constant with smaller error, either $(\Delta\alpha/\alpha)_{\rm Gauss}$ or $(\Delta\alpha/\alpha)_{\rm Voigt}$.

We have also analysed the standard deviation and errors of the results for $\Delta\alpha/\alpha$ as a function of redshift (Fig. 9). Even though we have imposed a constraint on our initial sample based on the sky emission lines, the standard deviation and errors still correlate with the sky. In particular, for the correlation with the moving standard deviation, this means that the precision in our measurement of $\Delta\alpha/\alpha$ along the whole redshift interval is limited by the sky subtraction algorithm.

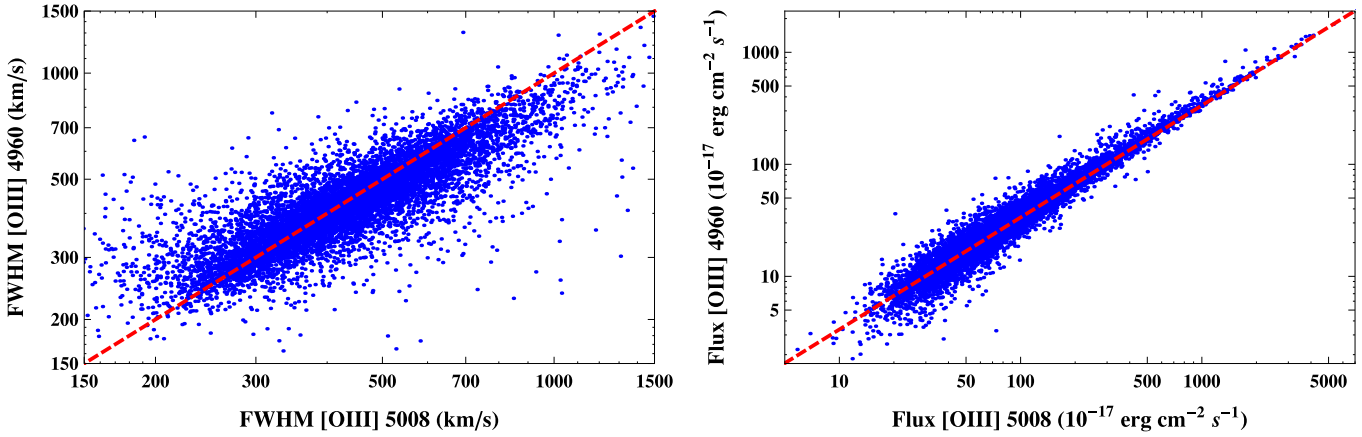

Figure 8. Left-hand panel: Gaussian widths (in km s^{-1}) for both [O III] lines. Both lines originate on the same upper energy level, then their widths must coincide (red dashed line). Right-hand panel: fluxes for both [O III] lines. The theoretical flux ratio is 2.98 (red dashed line). The entire fiducial quasar sample is shown.

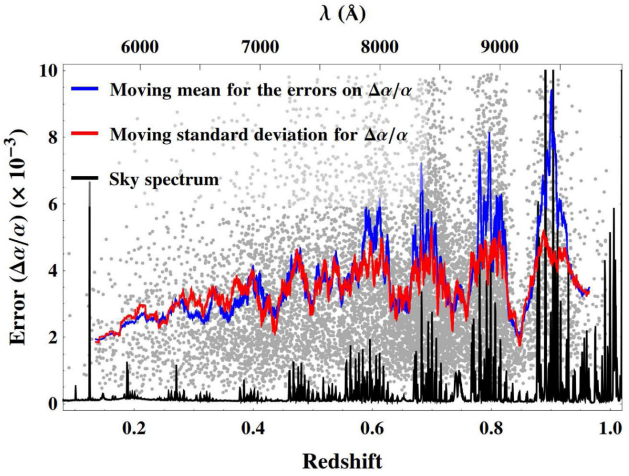

Figure 9. Errors for $\Delta\alpha/\alpha$ derived from the Gaussian fits (grey points) for our fiducial sample, moving mean of the these errors (blue line) using overlapping bins (100 spectra per bin, $\Delta z \approx 0.025$), moving standard deviation of $\Delta\alpha/\alpha$ measurements using the same bins (red line) and a typical sky spectrum.

5 RESULTS

5.1 [O III] lines

We used a total of 10 363 quasar spectra, drawn from the SDSS-III/BOSS DR12Q catalogue, after applying the selection criteria (i)–(iv) (see Section 2), to measure the possible variation of the fine-structure constant. The following measurement is obtained:

$$\frac{\Delta\alpha}{\alpha} = (1.4 \pm 2.3) \times 10^{-5}\,.$$

This value is consistent with the previous results reported in different investigations based on the same method: Bahcall et al. (2004), Gutiérrez & López-Corredoira (2010), and Rahmani et al. (2014). The redshift dependence of the measurements is shown in Fig. 10 (left-hand panel), where several bins have been made taking into account the redshift intervals affected by the sky (shaded zones). In the right-hand panel, we show the results obtained from the simulations described in Section 3, using the same redshifts intervals for the bins. The main differences between the real results and the simulations are in the regions where there are strong sky lines (shaded regions), while being in agreement in the remaining zones. Detailed information about each bin for the real data can be found in Table 3.

Our results are little affected by the specific constraints imposed in our sample as discussed in Section 4. For instance, we vary the width for the Gaussian fits, the contamination of Hβ, the polynomial order used to fit the continuum spectrum, the quality of the Gaussian fits and test different methods to measure $\Delta\alpha/\alpha$. The most important effect found is that by considering broader widths for the Gaussian fits, the results are more affected by the contamination from Hβ and possible asymmetries in the line wings. We have also checked for possible misidentifications of the [O III] emission lines using their expected widths and amplitude ratio.

Table 4 contains the results for $\Delta\alpha/\alpha$ when the lower bound on the $S/N_{[O\,III]\ 5008}$ is increased. All the results remain consistent with no variation of the fine-structure constant. In Fig. 11, the measured $\Delta\alpha/\alpha$ for our fiducial sample as a function of the $S/N_{[O\,III]\ 5008}$ are plotted together with their errors.

The distribution of BOSS quasars in the sky (see Fig. 1, left-hand panel) suggests to divide the sample into two, one for the North galactic cap and one for the South galactic cap. Table 5 describes the results for each galactic hemisphere, and no statistical meaningful difference is found. In order to look for a spatial variation, we also carried out a more precise analysis by fitting a dipole. First, we fixed the direction on the sky of the dipole and performed a linear fit ($\Delta\alpha/\alpha(\theta) = a\cos\theta + b$) of the measurements of the variation of the fine-structure constant as a function of $\cos\theta$, where θ is the angle between the dipole axis and a quasar in the sky. Different fits were done for the dipole axis lying in a grid in RA and Dec. ($\sim 1^\circ \times 1^\circ$). However, there is not statistical significance to determine the dipole axis with a meaningful error, i.e. smaller than the whole sky. There has been a claim on a significant deviation of α from being a constant as a function of space (King et al. 2012), with a dipole amplitude $0.97^{+0.22}_{-0.20} \times 10^{-5}$ in the direction RA $= 17.3 \pm 1.0$ h and Dec. $= -61^\circ \pm 10^\circ$. Fixing the dipole in that direction, we get $(-4.3 \pm 3.4) \times 10^{-5}$ for the dipole amplitude and $(0.8 \pm 2.3) \times 10^{-5}$ for the monopole term, which are not precise enough to compare with that work.

We are inclined to parametrize the possible time variation of α with redshift z. This is justified since any possible variation on α must be dominated by the local geometry of space–time (at least

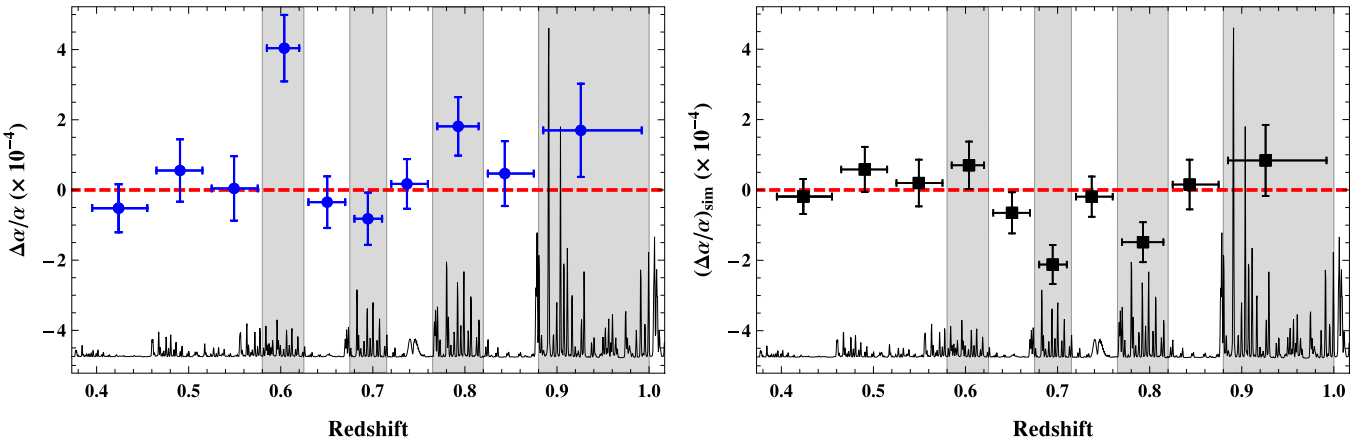

Figure 10. Left-hand panel: $\Delta\alpha/\alpha$ versus redshift (real data). Details about each bin are listed in Table 3. Right-hand panel: $(\Delta\alpha/\alpha)_{\rm sim}$ versus redshift (simulations). A typical sky spectrum and shadowed regions where the sky contamination is expected to be large, are shown as reference.

Table 3. Detailed information about the bins in Fig. 10.

Redshift interval	No. of quasar spectra	Redshift	$\Delta\alpha/\alpha$ ($\times 10^{-5}$)
0.390–0.460	817	0.42 ± 0.02	−5.2 ± 6.8
0.460–0.520	723	0.49 ± 0.02	5.5 ± 8.9
0.520–0.580	757	0.55 ± 0.02	0.4 ± 9.2
0.580–0.625	843	0.60 ± 0.01	40.4 ± 9.4
0.625–0.675	988	0.65 ± 0.01	−3.5 ± 7.4
0.675–0.715	1299	0.69 ± 0.01	−8.2 ± 7.4
0.715–0.765	1117	0.74 ± 0.01	1.7 ± 7.1
0.765–0.820	1444	0.79 ± 0.02	18.1 ± 8.3
0.820–0.880	644	0.84 ± 0.02	4.7 ± 9.2
0.880–1.000	580	0.93 ± 0.03	17.0 ± 13.3

Table 4. Results for several samples with different constraints on the $S/N_{[O\,III]\ 5008}$. For each sample, the number of quasar spectra, the mean redshift, together with its standard deviation and the value for $\Delta\alpha/\alpha$ are shown.

$S/N_{[O\,III]\ 5008}$	No. of quasar spectra	Redshift	$\Delta\alpha/\alpha$ ($\times 10^{-5}$)
>10	10 363	0.56 ± 0.21	1.4 ± 2.3
>20	5270	0.53 ± 0.21	−0.5 ± 2.5
>50	1498	0.47 ± 0.20	−3.4 ± 3.1
>100	451	0.41 ± 0.19	−2.0 ± 3.6
>500	12	0.24 ± 0.19	6 ± 12

if we consider the dynamics of the Universe as the main reason for such variation). Therefore, one is led to consider the possible variation of α as a function of redshift ($z = 1/a(t) - 1$) or the Ricci scalar ($R(t) = 6H(t)^2[1 - q(t)]$), where $a(t)$ is the scale factor, $H(t)$ the *Hubble* parameter and $q(t)$ is the deceleration parameter. Since the Ricci scalar is not known for each quasar, it is straightforward to consider a possible variation with redshift. In contrast, for a time parametrized model of the variation of α the analysis depends on the particular cosmology considered. Since there is no significant clear dependence, we use a linear model in redshift. Then, for

$$\Delta\alpha/\alpha = a\,z + b, \tag{7}$$

we obtain

$$a = (0.7 \pm 2.1) \times 10^{-4}\,; \qquad b = (0.7 \pm 1.4) \times 10^{-4}\,; \tag{8}$$

which do not show any dependence of $\Delta\alpha/\alpha$ with redshift.

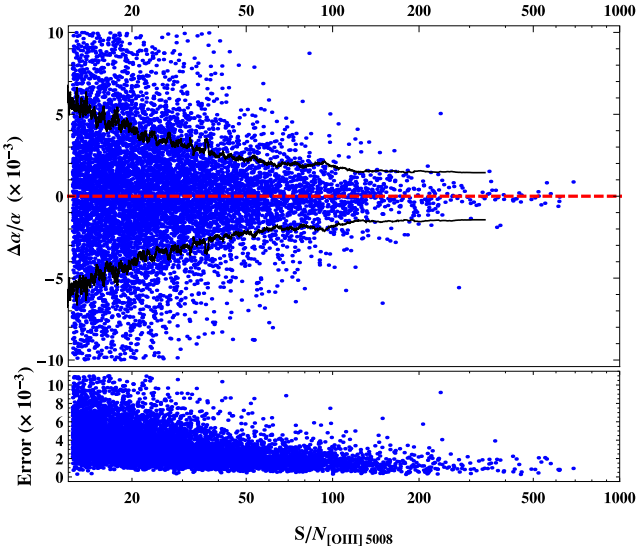

Figure 11. $\Delta\alpha/\alpha$ versus $S/N_{[O\,III]\ 5008}$ (top panel) with the moving standard deviation (black lines) using overlapping bins (100 spectra per bin) and the error on $\Delta\alpha/\alpha$ (bottom panel) in linear-log scale for our fiducial sample. The deviation of $\Delta\alpha/\alpha$ from zero and its error steadily decreases as the S/N increases.

Table 5. Results for the North and South galactic hemispheres.

Galactic hemisphere	No. of quasar spectra	Redshift	$\Delta\alpha/\alpha$ ($\times 10^{-5}$)
North	8069	0.56 ± 0.21	2.6 ± 2.6
South	2294	0.59 ± 0.20	−3.1 ± 4.9

From this sample, we also obtain a value for the line ratio $[F_\lambda \times \sigma]_{5008}/[F_\lambda \times \sigma]_{4960} = 2.96 \pm 0.02_{\rm syst}$, where F_λ is the maximum flux density of the line, and σ is the Gaussian width. The value reported is a weighted mean where the $S/N_{[O\,III]\ 5008}$ is used as weights. The quoted systematic error is computed from the analysis of samples with different polynomial orders for the continuum fit and different widths for the line fitting (see Table 6), since this quantity is more affected by these two parameters. The value we obtain is in agreement with the best current theoretical value, i.e. 2.98 (Storey & Zeippen 2000).

Table 6. Results for the line ratio when polynomials of different orders are used to subtract the continuum and different range for the Gaussian fits are used. For each sample, the number of quasar spectra, the mean redshift together with its standard deviation and the value for $[F_\lambda \times \sigma]_{5008}/[F_\lambda \times \sigma]_{4960}$ are shown.

Polynomial order	No. of quasar spectra	Redshift	$[F_\lambda \times \sigma]_{5008/4960}$
3	10 528	0.57 ± 0.21	2.96
5	10 550	0.57 ± 0.21	2.94
7	10 363	0.56 ± 0.21	2.96
9	10 471	0.56 ± 0.21	2.98
Fit width	**No. of quasar spectra**	**Redshift**	$[F_\lambda \times \sigma]_{5008/4960}$
2σ	10 363	0.56 ± 0.21	2.96
3σ	10 252	0.59 ± 0.20	2.92
4σ	9978	0.59 ± 0.20	2.98
5σ	9726	0.56 ± 0.21	2.98

Table 7. Results for SDSS-II/DR7 and BOSS (SDSS-III/DR12) samples. For each sample, the number of quasar spectra, the mean redshift, together with its standard deviation and value for $\Delta\alpha/\alpha$ are shown.

Sample	No. of quasar spectra	Redshift	$\Delta\alpha/\alpha\ (\times 10^{-5})$
DR7	2853	0.38 ± 0.15	0.5 ± 2.8
DR7 (SDSS cont.)	3009	0.38 ± 0.15	−0.4 ± 2.7
BOSS (DR12)	10 363	0.56 ± 0.21	1.4 ± 2.3
BOSS + DR7	13 175	0.51 ± 0.21	0.9 ± 1.8

Finally, we have also considered quasar spectra from the SDSS-II/DR7, which were observed using the previous spectrograph instead of the upgraded BOSS spectrograph (see Section 2). From the DR7 quasar catalogue (Schneider et al. 2010), which contains 105 783 quasars, we select a sample of 2853 quasars up to redshift $z = 0.8$ using the same criteria described in Section 2. This number is similar to the quasar spectra considered by Rahmani et al. (2014, Table 1) . We re-analyse this sample using the methodology presented in this work, and we find $\Delta\alpha/\alpha = (0.5 \pm 2.8) \times 10^{-5}$. By combining this DR7 sample with our fiducial BOSS (DR12) quasar sample (after eliminating 41 spectra which were re-observed by BOSS), we obtain our final sample which contains a total of 13 175 quasars. The value obtained for this combined sample is reported as a final result of this investigation:

$$\frac{\Delta\alpha}{\alpha} = (0.9 \pm 1.8) \times 10^{-5}\,.$$

Table 7 shows the results for DR7, DR7 using the continuum fit provided by the SDSS pipeline,[2] BOSS (DR12) and the combined BOSS+DR7. It can be seen that the mean redshift for the DR7 sample is lower than that for BOSS. Note that there is also a big difference on the mean $S/N_{[O\,III]\ 5008}$ of both samples: $S/N^{DR7}_{[O\,III]\ 5008} = 60$ and $S/N^{BOSS}_{[O\,III]\ 5008} = 33$, which also explains why the statistical errors for $\Delta\alpha/\alpha$ do not reflect the expected reduction due to the increase in the number of quasars of our BOSS sample. Table 8 shows the results of $\Delta\alpha/\alpha$ using the combined sample in the same redshift bins considered for our fiducial sample. Fig. 12 shows the difference of the values obtained for $\Delta\alpha/\alpha$ for the 41 re-observed quasars. Both BOSS and DR7 measurements are in perfect agreement within the error bars. This test is a good check for the reliability of our code and the consistency of the SDSS spectra obtained with different spectrographs.

[2] The SDSS pipeline provides a continuum fit for the DR7 spectra. The good agreement between the value for $\Delta\alpha/\alpha$ obtained with the SDSS continuum fit and our continuum fit is a good test for our code.

Table 8. Values of $\Delta\alpha/\alpha$ using the combined sample BOSS+DR7 for the same redshift bins as in Table 3.

Redshift interval	No. of quasar spectra	Redshift	$\Delta\alpha/\alpha\ (\times 10^{-5})$
0.390–0.460	1279	0.42 ± 0.02	−2.5 ± 4.8
0.460–0.520	1076	0.49 ± 0.02	7.2 ± 6.4
0.520–0.580	1071	0.55 ± 0.02	1.1 ± 7.1
0.580–0.625	1025	0.60 ± 0.01	30.8 ± 8.1
0.625–0.675	1191	0.65 ± 0.01	−5.1 ± 6.5
0.675–0.715	1424	0.69 ± 0.01	−6.2 ± 7.0
0.715–0.765	1220	0.74 ± 0.01	1.4 ± 6.8
0.765–0.820	1519	0.79 ± 0.02	15.0 ± 8.1
0.820–0.880	644	0.84 ± 0.02	4.7 ± 9.2
0.880–1.000	580	0.93 ± 0.03	17.0 ± 13.3

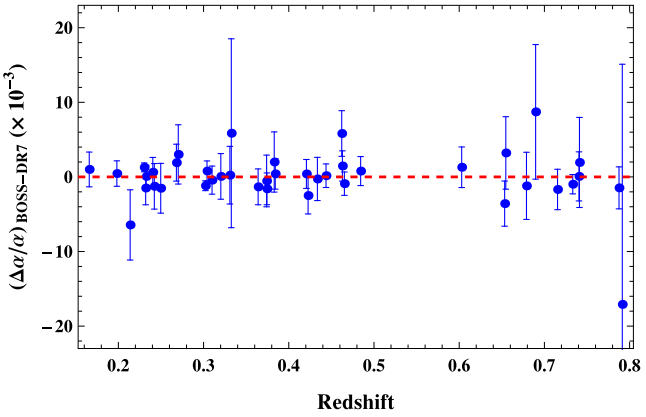

Figure 12. Difference between $(\Delta\alpha/\alpha)_{BOSS}$ and $(\Delta\alpha/\alpha)_{DR7}$ measurements for the 41 quasars observed by SDSS-I/II that were re-observed by BOSS. Both values for $\Delta\alpha/\alpha$ are consistent.

There are massive galaxy surveys to be carried out during the next decade. For instance, eBOSS and DESI will take spectra from millions of galaxies. Therefore, it is interesting to give an estimation of the accuracy that will be obtained when using galaxy spectra instead of quasars. For this, we have analysed the galaxy spectra collected by the DEEP2 survey (Newman et al. 2013) taken with resolving power ≈6000. From this sample, we found 4056 galaxies with strong [OIII] lines. Naively, one would expect that the error on $\Delta\alpha/\alpha$ should be

$$\Delta\,(\Delta\alpha/\alpha)_{\rm galaxies,DEEP2} \approx f_{\rm sample} \times f_{\rm inst} \times f_{\rm object} \times \Delta\,(\Delta\alpha/\alpha)_{\rm quasars,BOSS}\,, \quad (9)$$

where $f_{\rm sample}(=\sqrt{10\,363/4056})$ takes into account the different number of objects in each sample, $f_{\rm inst}(\approx 2000/6000)$ stands for the different resolution of the spectra and $f_{\rm object}$ is an extra factor due to the different characteristics of quasar and galaxy emission lines which affect the uncertainty of the line positions. This last factor is proportional to the line widths and inversely proportional to the line fluxes:

$$f_{\rm object} \approx \frac{\rm FWHM_{galaxies}}{\rm FWHM_{quasars}} \times \left(\frac{\rm Flux_{galaxies}}{\rm Flux_{quasars}}\right)^{-1}\,. \quad (10)$$

These numbers for the [O III] 5008 line are approximately $\rm FWHM_{galaxies} \approx 120$ km s^{-1}, $\rm FWHM_{quasars} \approx 420$ km s^{-1},

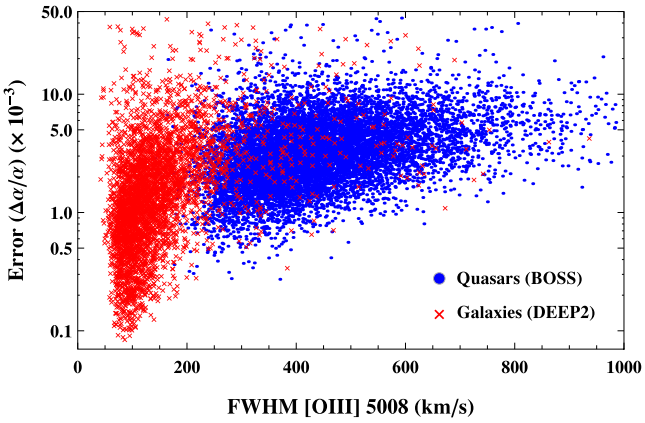

Figure 13. Errors on $\Delta\alpha/\alpha$ as a function of the FWHM of [O III] 5008 for our fiducial BOSS quasar sample (blue points) and for the DEEP2 galaxy sample (red crosses).

$\mathrm{Flux}_{\mathrm{galaxies}} \approx 70$ and $\mathrm{Flux}_{\mathrm{quasars}} \approx 210$ in units of 10^{-17} erg cm^{-2} s^{-1}, obtained from the DEEP2 sample and from our fiducial sample. Thus, the expected error is 1.1×10^{-5}, where we have considered the error of our fiducial sample $\Delta(\Delta\alpha/\alpha)_{\mathrm{quasars,\ BOSS}} = 2.3 \times 10^{-5}$. Applying the same criteria described in Section 2 to the DEEP2 galaxy sample, we get $\Delta\alpha/\alpha = (-0.9 \pm 1.6) \times 10^{-5}$. Thus, the upcoming future galaxy surveys will be quite competitive for constraining the variation of the fine-structure constant at low redshift $z < 2$. Fig. 13 shows the error on $\Delta\alpha/\alpha$ for the DEEP2 and BOSS samples.

5.2 [Ne III] lines

We also measure from 462 quasar spectra with [Ne III] emission lines the following constraint on the fine-structure constant:

$$\Delta\alpha/\alpha_{[\mathrm{Ne\,III}]} = (34 \pm 1) \times 10^{-4}\,, \tag{11}$$

to be compared with

$$\Delta\alpha/\alpha_{[\mathrm{Ne\,III}]} = (36 \pm 1) \times 10^{-4} \tag{12}$$

obtained by Gutiérrez & López-Corredoira (2010). The analysis of the [Ne III] lines reveals the same systematic effect previously observed, namely a clear tendency for a positive variation of α. Fig. 14 compares the results obtained for $\Delta\alpha/\alpha$ for spectra where both [O III] and [Ne III] lines are present. To account for this effect, a shift $\sim$0.6 Å on the theoretical or observed values of the wavelengths for the [Ne III] lines is necessary. There are experimental (Bowen 1955) and indirect (Kramida & Nave 2006) values for the wavelengths of the [Ne III] lines which are in agreement with errors $\approx 3 \times 10^{-2}$ Å. We use the NIST values for the [Ne III] lines

$$\lambda_1^{[\mathrm{Ne\,III}]} = 3869.86 \text{ Å} \qquad \lambda_2^{[\mathrm{Ne\,III}]} = 3968.59 \text{ Å} \tag{13}$$

$$\delta\lambda_0^{[\mathrm{Ne\,III}]} = 98.73 \text{ Å}. \tag{14}$$

The results for the [O III] doublet guarantee the good calibration of the SDSS spectra (and many more independent scientific results based on the SDSS spectra). Thus, we have measured the [Ne III] lines using a high-resolution optical spectrum from the planetary nebula IC 418. The IC 418 optical spectrum (3600–7200 Å) was taken under service time at the Nordic Optical Telescope (NOT; Roque de los Muchachos, La Palma) in 2013 March with the FIES spectrograph. We used FIES in the low-resolution mode

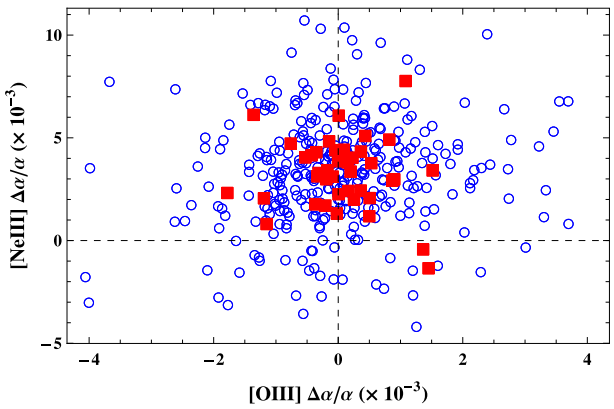

Figure 14. [Ne III] and [O III] measurements for $\Delta\alpha/\alpha$. Empty symbols stand for spectra with $\mathrm{S/N}_{[\mathrm{Ne\,III}]\ 3869} < 35$ and solid squares for spectra with $\mathrm{S/N}_{[\mathrm{Ne\,III}]\ 3869} > 35$. [Ne III] measurements have a clear tendency to a positive variation of α, which is due to a systematic effect affecting the [Ne III] measurement. The same effect has already been noticed by Gutiérrez & López-Corredoira (2010), and it is explained in Section 5.2.

($R \approx 25\,000$) with the 2.5 arsecfibre (centred at the central star of IC 418). Three exposures of 1200 s each were combined into a final IC 418 spectrum, reaching a S/N (in the stellar continuum) of $\sim$60 at 4000 Å and in excess of $\sim$150 at wavelengths longer than 5000 Å (see Díaz-Luis et al. 2015, for more observational details). To measure $\Delta\alpha/\alpha$, we need to know the ratio

$$\mathcal{R} = [(\lambda_2 - \lambda_1)/(\lambda_2 + \lambda_1)]_0\,, \tag{15}$$

which is independent of the peculiar velocity of the planetary nebula. From our data, we obtain

$$\mathcal{R} = (1259561 \pm 4) \times 10^{-8}, \tag{16}$$

compared to the one using NIST values for the wavelengths

$$\mathcal{R}_{\mathrm{NIST}} = 1259560 \times 10^{-8}. \tag{17}$$

The difference between the two values translates into a variation on $\Delta\alpha/\alpha < 10^{-6}$. Thus, the measured wavelength separation for the [Ne III] doublet does not account for the positive variation on α observed using these lines. Fig. 15 (left-hand panel) shows the Gaussian fit to the [Ne III] line profiles present in the IC 418 spectrum.

The IC 418 spectrum shows two different lines near the [Ne III] 3968 Å line (see Fig. 15, right-hand panel). The stronger one is H ϵ 3971 Å, the other one is He I 3965 Å. Hence, we search for a possible blending of the [Ne III] line 3968 with these two lines in our much lower spectral resolution quasar spectra. Fig. 16 (left-hand panel) shows stack quasar spectra with broad [Ne III] emission lines. It can be seen that the weak [Ne III] line is blended.

To quantify the displacement produced by the blending with Hϵ line, we did a Gaussian convolution of the Planetary Nebula spectrum to lower the resolution down to $R \approx 2000$. Since the line intensity ratio of [Ne III] and H ϵ may differ in the quasar narrow emission-line region and the Planetary Nebula, we show in Fig. 16 (right-hand panel) the shift produced by the H ϵ line as a function of the ratio [Ne III] /H ϵ. We get a shift $\sim$0.6 Å when H ϵ/[Ne III] is $\sim$0.5. This explains the systematic found when using [Ne III] lines to measure the variation of the fine-structure constant $\Delta\alpha/\alpha$ in previous studies (Gutiérrez & López-Corredoira 2010; Grupe et al. 2005).

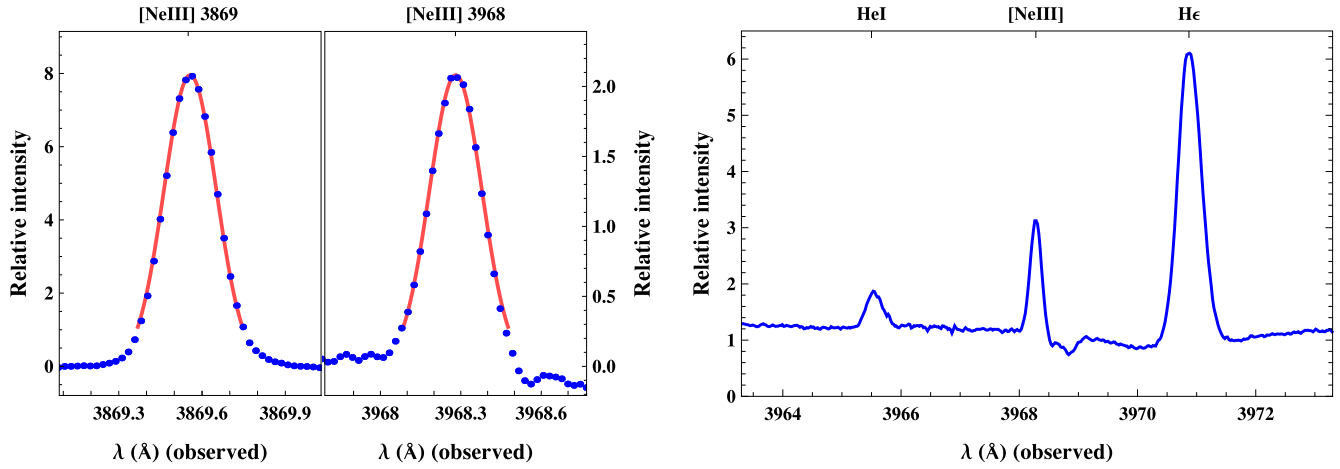

Figure 15. Left-hand panel: [Ne III] 3869 and [Ne III] 3968 together with our Gaussian fits (solid line) from a high-resolution ($R \approx 25\,000$) spectrum of the Planetary Nebula IC 418 obtained with the FIES spectrograph at the NOT telescope. Right-hand panel: IC 418 spectrum centred at [Ne III] 3968 line. The two close lines are H ϵ 3971 Å and He I 3965 Å.

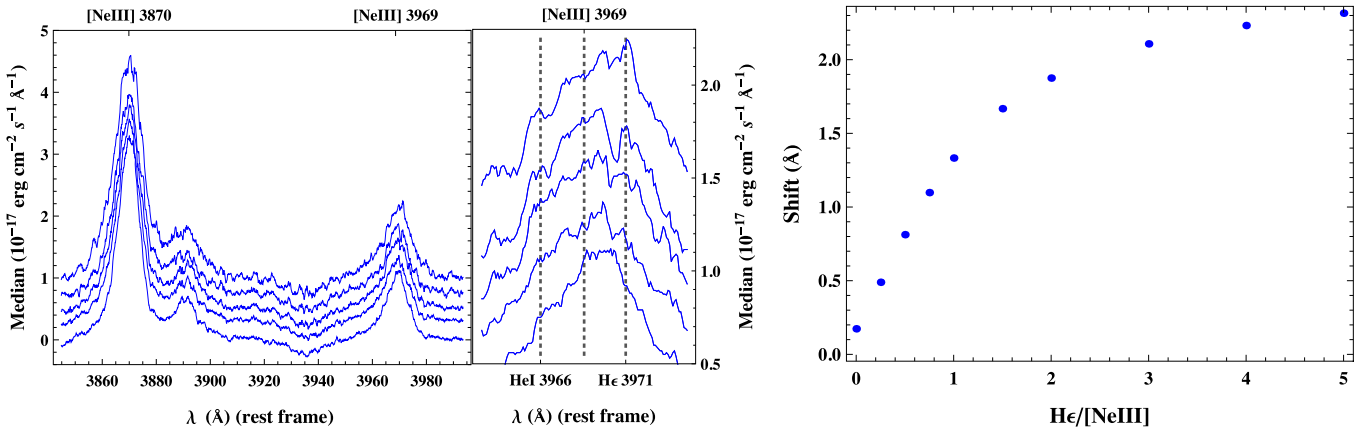

Figure 16. Left-hand panel: median-stacked quasar spectra with broad [Ne III] lines (increasing line width from bottom to top). Both [Ne III] lines are shown ($\lambda\lambda$ 3869, 3968 Å). The weak [Ne III] line is blended with the two lines H ϵ 3971 Å and He I 3965 Å. Right-hand panel: shift produced by the H ϵ line in the [Ne III] 3968 line as a function of the line intensity ratio of both lines as measured from the Planetary Nebula convolved spectrum.

6 SUMMARY

The main conclusions of this work are as follows.

(i) From 45 802 objects at $z < 1$ classified as quasars in the SDSS-III/BOSS DR12 quasar catalogue, we have extracted a sample of 10 363 quasars with [O III] emission lines. Combining this fiducial sample with a sample of 2853 previously studied SDSS-II/DR7 quasars, we got a final sample of 13 175 after eliminating 41 re-observed quasars.

(ii) With this combined sample, we have estimated a value for the possible variation of the fine-structure constant of $\Delta\alpha/\alpha = (0.9 \pm 1.8) \times 10^{-5}$, which represents the most accurate result obtained with this methodology.

(iii) We have also studied how much our results change when analysing the fiducial sample according to different properties (width, amplitude, S/N and R^2 coefficient of the [O III] lines), and when modifying some parameters of the analysis (polynomial order for the continuum subtraction, different methods to determine the line position, e.g. Gaussian/Voigt profiles). We conclude that our results are quite robust, and they are consistent with no variation of the fine-structure constant.

(iv) From over one million simulated realizations of quasar spectra, we conclude that the precision of our emission-line method is dominated by the error from the Gaussian fits. Hence, the error from the continuum subtraction and any possible systematics from our code are small.

(v) The standard deviation of the results as a function of redshift correlates with the sky. This result suggests that our main source of uncertainty is determined by the sky subtraction algorithm.

(vi) We have determined the ratio of the [O III] transition lines to be $2.96 \pm 0.02_{\rm syst}$, which is in good agreement with previous experimental and theoretical values.

(vii) The same systematic effect previously noticed by Gutiérrez & López-Corredoira (2010) has been found on the [Ne III] lines measurement. Incorrect measurement for the separation of the [Ne III] has been excluded as a possible explanation, and a blending of the H ϵ and the [Ne III] 3968 has been identified as the source of this effect.

(viii) The measurement of $\Delta\alpha/\alpha$ using SDSS-III/BOSS spectra has reached the maximum precision unless better sky subtraction algorithms are developed. To obtain better constraints ($<10^{-6}$) using the emission-line method, high-resolution spectroscopy ($R \approx 100\,000$) is mandatory.

(ix) We note that future large galaxies survey like eBOSS or DESI could provide quite stringent constraint for $\Delta\alpha/\alpha$ at low redshift, following our analysis of galaxy spectra taken from the DEEP2 survey.

ACKNOWLEDGEMENTS

FDA, JC and FP acknowledge support from the Spanish MICINNs Consolider-Ingenio 2010 Programme under grant MultiDark CSD2009-00064, MINECO Centro de Excelencia Severo Ochoa Programme under grant SEV-2012-0249 and MINECO grants AYA-2012-31101 and AYA2014-60641-C2-1-P. FDA also acknowledges financial support from 'la Caixa'-Severo Ochoa doctoral fellowship, UAM+CSIC Campus of International Excellence and Instituto de Astrofísica de Canarias for a summer stay where this work began. AM and DAGH acknowledge support provided by the Spanish Ministry of Economy and Competitiveness (MINECO) under grant AYA-2011-27754.

Funding for SDSS-III has been provided by the Alfred P. Sloan Foundation, the Participating Institutions, the National Science Foundation, and the U.S. Department of Energy Office of Science. The SDSS-III web site is http://www.sdss3.org/.

SDSS-III is managed by the Astrophysical Research Consortium for the Participating Institutions of the SDSS-III Collaboration including the University of Arizona, the Brazilian Participation Group, Brookhaven National Laboratory, University of Cambridge, Carnegie Mellon University, University of Florida, the French Participation Group, the German Participation Group, Harvard University, the Instituto de Astrofísica de Canarias, the Michigan State/Notre Dame/JINA Participation Group, Johns Hopkins University, Lawrence Berkeley National Laboratory, Max Planck Institute for Astrophysics, Max Planck Institute for Extraterrestrial Physics, New Mexico State University, New York University, Ohio State University, Pennsylvania State University, University of Portsmouth, Princeton University, the Spanish Participation Group, University of Tokyo, University of Utah, Vanderbilt University, University of Virginia, University of Washington and Yale University.

This article is also partially based on service observations made with the Nordic Optical Telescope operated on the island of La Palma by the Nordic Optical Telescope Scientific Association in the Spanish Observatorio del Roque de Los Muchachos of the Instituto de Astrofísica de Canarias.

REFERENCES

Abazajian K. N. et al., 2009, ApJS, 182, 543
Adelman-McCarthy J. K. et al., 2008, ApJS, 175, 297
Alam S. et al., 2015, ApJS, 219, 12
Bahcall J. N., Salpeter E. E., 1965, ApJ, 142, 1677
Bahcall J. N., Schmidt M., 1967, Phys. Rev. Lett., 19, 1294
Bahcall J. N., Sargent W. L. W., Schmidt M., 1967, ApJ, 149, L11
Bahcall J. N., Steinhardt C. L., Schlegel D., 2004, ApJ, 600, 520
Bolton A. S. et al., 2012, AJ, 144, 144
Bowen I. S., 1955, ApJ, 121, 306
Chand H., Petitjean P., Srianand R., Aracil B., 2005, A&A, 430, 47
Clifton T., Ferreira P. G., Padilla A., Skordis C., 2012, Phys. Rep., 513, 1
Dawson K. S. et al., 2013, AJ, 145, 10
Delubac T. et al., 2015, A&A, 574, A59
Díaz-Luis J. J., García-Hernández D. A., Kameswara Rao N., Manchado A., Cataldo F., 2015, A&A, 573, A97
Dirac P. A. M., 1937, Nature, 139, 323
Eisenstein D. J. et al., 2011, AJ, 142, 72
Evans T. M. et al., 2014, MNRAS, 445, 128
García-Berro E., Isern J., Kubyshin Y. A., 2007, A&AR, 14, 113
Grupe D., Pradhan A. K., Frank S., 2005, AJ, 130, 355
Gunn J. E. et al., 2006, AJ, 131, 2332
Gutiérrez C. M., López-Corredoira M., 2010, ApJ, 713, 46
King J. A., Webb J. K., Murphy M. T., Flambaum V. V., Carswell R. F., Bainbridge M. B., Wilczynska M. R., Koch F. E., 2012, MNRAS, 422, 3370
Kramida A. E., Nave G., 2006, Eur. Phys. J. D, 37, 1
Landau S. J., Scóccola G., 2010, A&A, 517, A62
Leal P. M. M., Martins C. J. A. P., Ventura L. B., 2014, Phys. Rev. D, 90, 027305
Maeda K.-I., 1988, Mod. Phys. Lett. A, 3, 243
Molaro P. et al., 2013, A&A, 555, A68
Moorwood A. F. M., Salinari P., Furniss I., Jennings R. E., King K. J., 1980, A&A, 90, 304
Newman J. A. et al., 2013, ApJS, 208, 5
Olive K. A., Pospelov M., Qian Y.-Z., Coc A., Cassé M., Vangioni-Flam E., 2002, Phys. Rev. D, 66, 045022
Petrov Y. V., Nazarov A. I., Onegin M. S., Petrov V. Y., Sakhnovsky E. G., 2006, Phys. Rev. C, 74, 064610
Pettersson S.-G., 1982, Phys. Scr., 26, 296
Planck Collaboration XVI, 2014, A&A, 571, A16
Rahmani H., Maheshwari N., Srianand R., 2014, MNRAS, 439, L70
Savedoff M. P., 1956, Nature, 178, 688
Schneider D. P. et al., 2010, AJ, 139, 2360
Smee S. A. et al., 2013, AJ, 146, 32
Storey P. J., Zeippen C. J., 2000, MNRAS, 312, 813
Stoughton C. et al., 2002, AJ, 123, 485
Thompson R. I., 2012, MNRAS, 422, 67
Uzan J.-P., 2003, Rev. Mod. Phys., 75, 403
Uzan J.-P., 2011, Living Rev. Relativ., 14, 2
Whitmore J. B., Murphy M. T., 2015, MNRAS, 447, 446
York D. G. et al., 2000, AJ, 120, 1579

SUPPORTING INFORMATION

Additional Supporting Information may be found in the online version of this article:

(http://mnras.oxfordjournals.org/lookup/suppl/doi:10.1093/mnras/stv1406/-/DC1).

Please note: Oxford University Press are not responsible for the content or functionality of any supporting materials supplied by the authors. Any queries (other than missing material) should be directed to the corresponding author for the article.

APPENDIX A

We publish along with this paper an electronic table with the combined SDSS-III/BOSS DR12 and SDSS-II/DR7 sample of 13 175 quasars used in this work. Table A1 describes the information and format of each column.

Table A1. Description of the electronic table with the combined sample (13 175 quasars) published along with the paper.

Column	Name	Format	Description
1	SDSS_NAME	STRING	SDSS-DR12 designation hhmmss.ss+ddmmss.s (J2000)
2	RA	DOUBLE	Right Ascension in decimal degrees (J2000)
3	DEC	DOUBLE	Declination in decimal degrees (J2000)
4	THING_ID	INT32	Thing_ID
5	PLATE	INT32	Spectroscopic plate number
6	MJD	INT32	Spectroscopic MJD (>55000 SDSS-III/BOSS spectra, <55000 SDSS-II spectra)
7	FIBER	INT32	Spectroscopic fibre number
8	Z_VI	DOUBLE	Redshift from visual inspection
9	Z_PIPE	DOUBLE	Redshift from BOSS pipeline
10	ERR_ZPIPE	DOUBLE	Error on BOSS pipeline redshift
11	ALPHA	FLOAT	$\Delta\alpha/\alpha$ from the Gaussian fits
12	ERR_ALPHA	FLOAT	Standard error for $\Delta\alpha/\alpha$ from the Gaussian fits
13	SN_O1	FLOAT	S/N for the [O III] 4960 line
14	SN_O2	FLOAT	S/N for the [O III] 5008 line
15	O1_FIT	FLOAT	Line centroid for the [O III] 4960 line
16	O2_FIT	FLOAT	Line centroid for the [O III] 5008 line
17	ERR_O1	FLOAT	Error on the line centroid for the [O III] 4960 line
18	ERR_O2	FLOAT	Error on the line centroid for the [O III] 5008 line
19	O1_AMPLITUDE	FLOAT	Gaussian amplitude at the centre for the [O III] 4960 line
20	O2_AMPLITUDE	FLOAT	Gaussian amplitude at the centre for the [O III] 5008 line
21	O1_WIDTH	FLOAT	Gaussian width for the [O III] 4960 line
22	O2_WIDTH	FLOAT	Gaussian width for the [O III] 5008 line
23	FILE_NAME	STRING	File name to download from the SDSS server

This paper has been typeset from a TEX/LATEX file prepared by the author.

Observational proposal for the SDSS

"APOGEE Quasar Survey (APOGEE-Q)"

Authors: Franco D. Albareti, Johan Comparat, Francisco Prada, Isabelle Pâris, Andreu Font, David Schlegel, Joseph Hennawi and Jean-Paul Kneib

Motivation

In order to extend at higher redshift the constraint on the variation of the fine structure constant with the same method used in Paper I, we presented the following observational proposal for the APOGEE Ancillary Science Projects within the SDSS-IV Collaboration. Besides, the survey had two other main goals: 1) Calibrate methods based on Mg II and C IV emission lines to determine Super Massive Black Hole masses and 2) Reduce systematic and dispersion errors on the redshift measurements when using broad emission lines (C IV, C III] and [Mg II]). The three goals were to be accomplished by observation of the Hβ line and [O III] doublet falling in the infrared part of the electromagnetic spectrum in high redshift quasars for which an optical spectra was already available from the SDSS-II/SDSS-III. The APOGEE infrared spectrograph and the APOGEE-II survey observational plan represented a good opportunity to carry out these observations.

APOGEE-Q
APOGEE Quasar Survey
Letter of Intent

P.I.: **F. D. Albareti**
Instituto de Física Teórica UAM/CSIC, Cantoblanco, C/ Nicolás Cabrera, 13-15, 28049 Madrid
franco.albareti@uam.es

Co-Is: **J. Comparat** (IFT-UAM/CSIC), **F. Prada** (IFT-UAM/CSIC), **I. Pâris** (INAF/OATS), **A. Font** (LBNL), **D. Schlegel** (LBNL), **JP. Kneib** (EPFL)

February 1, 2015

Science goal

We propose the observation of high redshift quasars ($2.0 < z < 2.4$) with APOGEE-2 to detect [OIII] emission lines $\lambda 4960, 5008$ Å in the near-IR. It is known for a long time that there is a discrepancy between the redshifts measured from different quasar emission lines [1]. Redshifs obtained from broad emission lines, e.g. CIV $\lambda 1550$ Å or CIII] $\lambda 1909$ Å are the most affected with typical blueshifts of 500 km/s with respect to the quasar systemic redshift, e.g. [2]. The broad MgII $\lambda 2800$ Å emission line was thought to be a good tracer of quasar redshifts and was used in the SDSS-III/BOSS quasar catalog [3]. However, different studies have shown that the MgII line is also affected by a systematic shift of the order of ~ 200 km/s [4], and that this effect depends on quasar luminosity [5]. One of the best tracers of quasar systemic redshifts is the [OIII] $\lambda 4960$, 5008 Å doublet [6]. This doublet cannot be observed with the BOSS spectrograph at redshifts larger than 1, where most of our quasars lie. The APOGEE spectrograph wavelength range allows the detection of these prominent lines for quasars with redshifts in the range $2.0 < z < 2.4$ (we count 81,392 out of the total 297,301 quasars taken from DR12Q). A careful study of the emission line redshifts measured from broad emission lines observed in the BOSS spectra (CIV, CIII] and MgII), and [OIII] emission lines in the APOGEE spectra will allow to significantly reduce both systematic and dispersion of errors on redshift measurements, which is crucial for many quasar science studies, including quasar clustering analyses. In addition, we will obtain a competitive constraint ($< 10^{-5}$) on the possible time and/or spatial variation of the fine structure constant at redshift $z \approx 2.2$ using the [OIII] emission line method, thanks to the 10x higher spectral resolution of the APOGEE spectrograph as compared to our previous work using the BOSS quasar DR12 sample [7]. This constraint will be the first at high-z using emission lines and it will compete and test the results from the absorption line method using the VLT/UVES, Keck/HIRES and Subaru/HDS spectrographs, which are highly affected by different systematics [8]. In summary, this Ancillary Science program will provide scientific results from large scale structure to fundamental physics, broadening the scientific scope of the APOGEE-2 survey, while having a minimal impact on the main survey goals as discussed in the observational strategy, below.

Observational strategy

This is a Type-1 proposal, we request fiber placement on specific targets in already-specified APOGEE-2 (or MaNGA-led) survey pointings. From the 81,392 quasars of DR12Q with redshift $2.0 < z < 2.4$ (see Figure 1, left panel), we plan to perform a careful selection of targets based on the properties of the MgII/CIII]/CIV lines (see Figure 1, right panel) to maximize the probability to detect the [OIII] doublet, while taking into account the APOGEE plates. The collision diameter of APOGEE-2N fibers and the problems to observe targets in the center of the field-of-view can easily be taken into account in the target selection process. Therefore, this program has a minimal impact on the main APOGEE survey and it could easily fit to any possible change in the APOGEE targeting plan.

We estimate the [OIII] emission lines to be observed to have a mean flux density $2{\times}10^{-16}$ erg/cm^2/s/A, that extends over 10 pixels. With APOGEE, such a flux would be detected at a signal-to-noise ratio of 5 within a 3-hour exposure. We are interested in APOGEE fields with a large number of visits to increase the S/N of the lines. Because of the galactic extinction effects, quasars are observed outside the galactic plane. Thus, we request ancillary fibers of Halo and

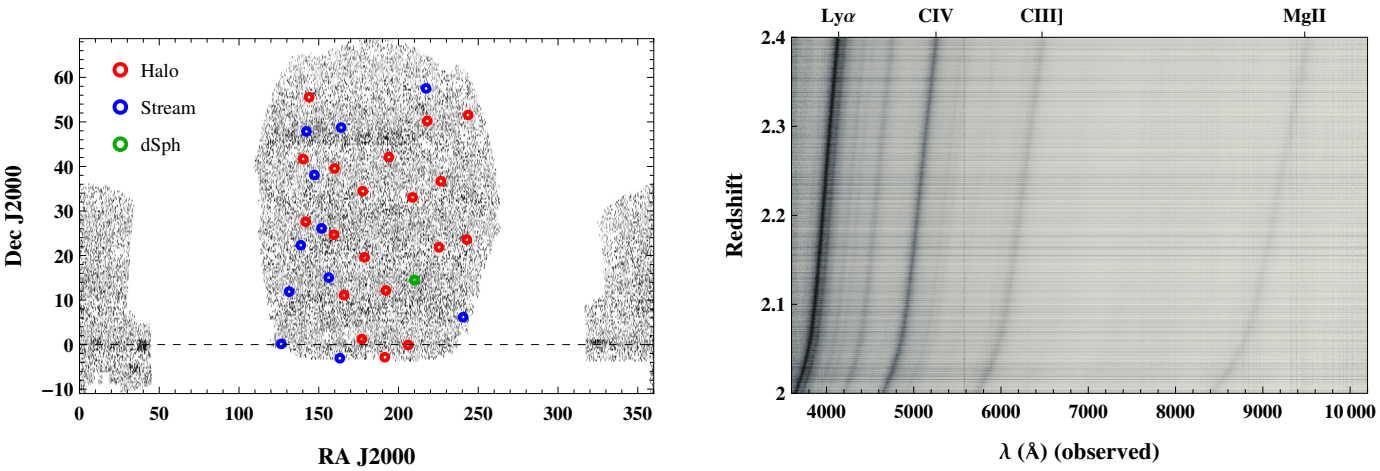

Figure 1: Left panel: Sky distribution of the SDSS-III/BOSS DR12Q quasars with $2.0 < z < 2.4$ (81,392) in J2000 equatorial coordinates and overlapping APOGEE fields of view. Right panel: BOSS spectra of the 81,392 quasars with $2.0 < z < 2.4$ sorted by redshift. These spectra will be used for an effective target selection.

Stream+dSph fields distributed in 105 <RA< 260 and −5 <Dec< 70, which are planned to have >20 visits and they overlap with the quasar sky distribution of the North Galactic Cap (see Figure 1, left panel).

We acknowledge advice about the possible inter-fiber contamination affecting our observation (because of the low flux of our targets, this does not affect the main APOGEE survey).

References.

[**1**] Gaskell, C. M. 1982. A redshift difference between high and low ionization emission-line regions in QSOs - Evidence for radial motions. ApJ 263, 79.
[**2**] Richards et al. 2011. Unification of Luminous Type 1 Quasars through C IV Emission. AJ, 141, 167.
[**3**] Paris et al. 2012. The Sloan Digital Sky Survey quasar catalog: ninth data release. A&A 548, AA66.
[**4**] Font-Ribera et al. 2013. The large-scale quasar-Lyman α forest cross-correlation from BOSS. JCAP, 5, 018.
[**5**] Marziani et al. 2013. Low-ionization Outflows in High Eddington Ratio Quasars. ApJ, 764, 150.
[**6**] Hewett & Wild. 2010. Improved redshifts for SDSS quasar spectra. MNRAS, 405, 2302.
[**7**] F.D. Albareti, J. Comparat et al. 2015. Constraint on the time variation of the fine-structure constant with the SDSS-III/BOSS quasar sample.
[**8**] Evans et al. 2014. The UVES Large Program for testing fundamental physics - III. Constraints on the fine-structure constant from 3 telescopes. MNRAS 445, 128.

APOGEE-2 Ancillary Science Proposal

August 11, 2015

APOGEE-Q
APOGEE Quasar Survey

Type of request: 1

PI

Franco D. Albareti

Instituto de Física Teórica UAM/CSIC
Cantoblanco, C/ Nicolás Cabrera, 13-15, 28049 Madrid
Phone number: +34 91 299 98 71
E-mail: franco.albareti@uam.es

Co-Is

Johan Comparat

Instituto de Física Teórica UAM/CSIC

Francisco Prada

Instituto de Física Teórica UAM/CSIC

Isabelle Pâris

Instituto Nazionali di Astrofisica/Osservatorio Astronomico di Trieste

Andreu Font

Lawrence Berkeley National Laboratory

David Schlegel

Lawrence Berkeley National Laboratory

Joseph Hennawi

Max-Planck-Institut für Astronomie

Jean-Paul Kneib

École Polytechnique Fédérale de Lausanne

All participants are SDSS-IV members

Scientific & Technical Justification

Science case

We propose the observation of ∼1,200 high redshift quasars ($2.0 < z < 2.4$) within the SDSS-IV/APOGEE-2 survey to detect the rest-frame optical Hβ-[OIII] emission lines (Hβ λ4960 Å; [OIII] λ4960, λ5008 Å), which lies in the near-IR H-band ($1.5 - 1.7\,\mu$m) at the quoted redshift. These lines cannot be observed with the BOSS spectrograph (3600-10400 Å) at redshifts larger than 1.

The detection of these lines will enable us to push further the investigations on three hot topics in the field of cosmology. First, we will measure the possible variation of the fine-structure constant at redshift 2.2 with unprecedented accuracy using the [OIII] emission lines. Secondly, we will calibrate different methods for computing the mass of super massive black holes (SMBHs) to test the "anti-hierarchical" scenario for growth of black holes. Last, this sample will enable a robust investigation on the existing redshift systematic discrepancy between Magnesium and Oxygen lines.

This Ancillary Science program will provide self-standing scientific results in the fields of fundamental physics and extra-galactic astrophysics. Furthermore, this program has a minimal impact on the main survey goals.

Variation of the fine structure constant

The fine structure constant governs the electromagnetic coupling between photons and charged particles $\alpha = e^2/\hbar c$. Current constraints on its relative variation $\Delta\alpha/\alpha$ over geological time scales are $|\Delta\alpha/\alpha| < 7 \times 10^{-8}$ up to $z \approx 0.15$ (2 Gyrs ago), obtained from the Oklo phenomenon [2]; and $|\Delta\alpha/\alpha| < 3 \times 10^{-7}$ up to $z \approx 0.45$ (4-5 Gyrs ago) from meteorites [3]; which also excludes possible variations on the scales of the solar system. By measuring fine-structure multiplets at different redshift in the absorption or emission spectra of galaxies, located in different directions of the extragalactic Universe, we can measure an eventual cosmological variation of α with time or space.

The [OIII] emission lines could be used to obtain a competitive constraint, $< 10^{-5}$ with about ∼300 quasars, on the possible time and/or spatial variation of the fine structure constant at redshift $z \approx 2.2$. The [OIII] lines could be centered within a 0.14 Å accuracy in rest-frame with a $S/N_{\lambda 5007} \approx 25$ using the BOSS spectrograph ($R \sim 2,000$), see Albareti et al. (2015), in contrast to the 0.009 Å accuracy level that will be achieved by the APOGEE spectrograph, thanks to its 10× higher spectral resolution and twice higher S/N due to longer exposure times. With a single APOGEE-2 quasar spectrum, we can produce a measurement of the relative variation of the fine structure constant of $\sim 9 \times 10^{-5}$ at $z \approx 2.2$; to be compared with our previous work using the BOSS quasar DR12 sample $\Delta\alpha/\alpha < 2.5 \times 10^{-5}$ at $z \approx 0.6$ obtained from $> 10,000$ quasars [4]. The APOGEE constraint will be the first obtained at high-z using emission lines and it will compete and test the results from the absorption line method using the VLT/UVES, Keck/HIRES and Subaru/HDS spectrographs, which are affected by different systematics [5].

SMBH mass determination

The discovery of tight correlations between the masses of SMBHs and their host galaxy bulges [e.g. 6] resulted in a new industry of studies of black hole growth over cosmic time, and the concomitant evolution of their host galaxies. In the now popular picture of cosmic downsizing or so-called "anti-hierarchical" black hole growth [e.g. 7, 8], the most massive $M \sim 10^9$ $M_\odot$ SMBHs grew at early times (z∼3) during the peak of the luminous quasar activity, whereas at lower redshift (z<1) the less massive $M \sim 10^7$ $M_\odot$ systems are growing at the centers of quasars. As stellar dynamics based black hole masses estimates are impossible for distant objects, the reverberation mapping technique has emerged as a means for measuring black hole masses in more distant quasars [e.g. 9-12].

At low-redshift, these studies have correlated the Hβ line width against black hole mass $M_{\rm BH}$, but Hβ is redshifted out of the optical spectral window at z > 1, forcing reliance on the rest-frame ultraviolet emission lines like MgII λ2798 (1 < z < 2.3) and CIV λ1549 (z > 2.3). These emission lines are associated with larger uncertainties on the derived masses, particularly when using the high ionization CIV line [13, 14], which is believed to have contributions from non-gravitational motions possibly due to accretion disk winds [e.g. 14, 15]. Because so far only ∼ 10 quasars have been reverberation mapped in CIV [9-12], all work based on black hole masses at z > 2.5, such as the Eddington ratio distribution and studies of black hole and host scaling relations, are highly susceptible to a systematic offset in the black hole mass scale due to poor reverberation mapping calibration.

The APOGEE measurements of the Hβ line λ4860 Å in >300 quasars, with known MgII, will greatly enhance today's SMBH calibration sample. We will combine the measurement of the FWHM of Hβ with the continuum luminosity (and hence broad-line region size) to measure black hole masses and therefore further calibrate the MgII and/or CIV determined black holes masses. This will enable us to characterize the Eddington ratio distribution and the black hole mass function for the entire SDSS sample with the systematics due to poorly understood MgII and CIV black hole masses minimized.

Redshift systematics

It is known for a long time that there is a discrepancy between the redshifts measured from different quasar emission lines [16]. Redshifts obtained from broad emission lines, e.g. CIV λ1550 or CIII] λ1909 Å are the most affected with typical blueshifts of 500 km/s with respect to the quasar systemic redshift, e.g. [17]. The broad MgII λ2800 Å emission line was thought to be a good tracer of

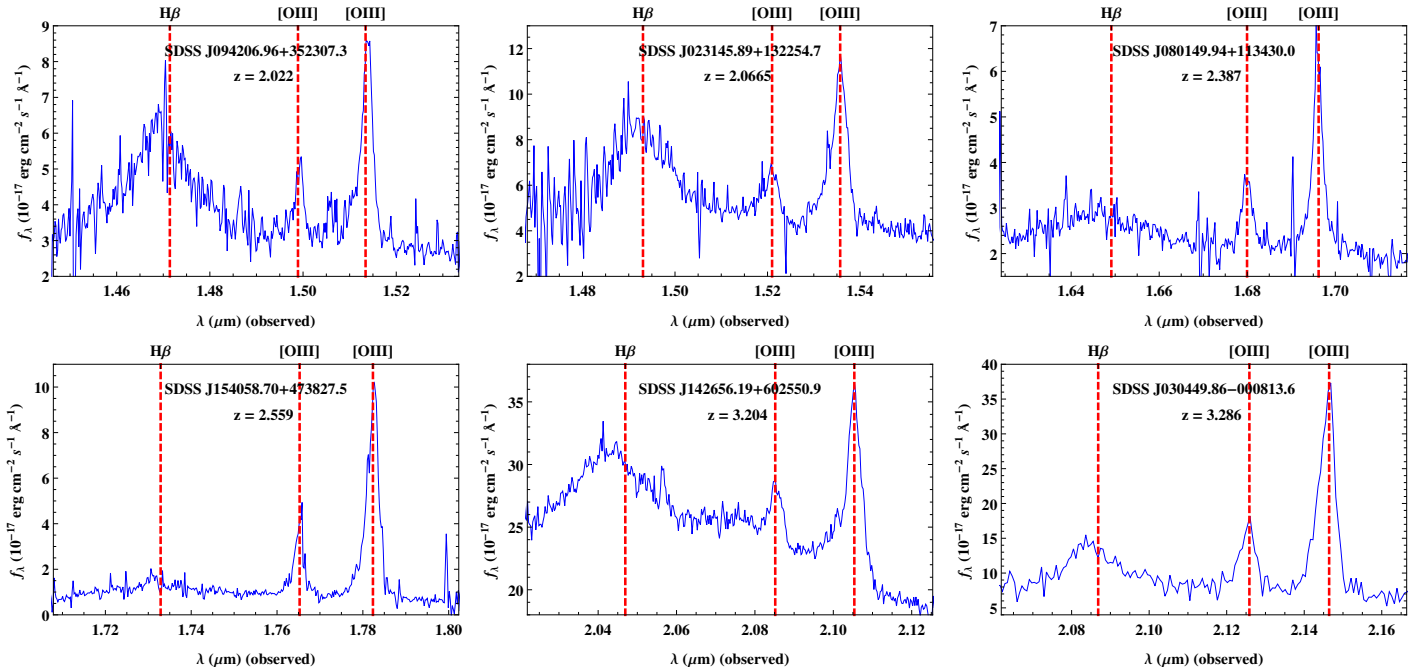

Figure 1: Flux-calibrated IR quasar spectra with Hβ and [OIII] lines taken with the Palomar 200" telescope and the Triplespec instrument ($R \sim 3,000$). These lines are the strongest features that are present in H-band spectra for quasar at redshift $z \sim 2.2$.

quasar redshifts and was used in the SDSS-III/BOSS quasar catalog [18]. However, different studies have shown that the MgII line is also affected by a systematic shift of the order of $\sim$ 200 km/s [19], and that this effect depends on quasar luminosity [20]. One of the best tracers of quasar systemic redshifts is the [OIII] λ4960, λ5008 Å doublet [21], which are strong emission lines, easily detected, and because they are emitted from the narrow-line region, they trace the systemic redshift of the quasar to an accuracy of $z = 44$ km s^{-1} [22, 23]. A careful study of the emission line redshifts measured from broad emission lines observed in the BOSS spectra (CIV, CIII] and MgII), and from [OIII] emission lines in the APOGEE spectra will allow to significantly reduce both systematic and dispersion of errors on the redshift measurements, which is crucial for many quasar science studies, including quasar clustering analyses.

Figure 1 shows flux-calibrated IR spectra with strong Hβ and [OIII] lines.

Feasibility assessment

This is a Type-1 proposal, we request fiber placement on optically observed SDSS-III/BOSS quasars in already-specified APOGEE-2/North survey pointings.

BOSS quasars in the redshift range $2.0 < z < 2.4$ have Vega magnitudes in the H-band >16. Besides, because of the galactic extinction effects, quasars are best to be observed outside the galactic plane. For these reasons, ancillary fibers of `halo`, `halo_stream` and `halo_dsph` fields distributed in $105 <$ RA < 260 and $-5 <$ Dec < 70, which are planned to have ≥ 6 visits and overlap with the BOSS quasar sky distribution of the North Galactic Cap (see Figure 2, left panel) are the best suitable pointings to this ancillary science project. The large number of visits will increase the final S/N of the spectra. From the quasar sample with [OIII] lines analized in [4], we derive a mean flux of 6.0×10^{-17}, 4.2×10^{-17} and 1.5×10^{-17} erg/cm^2/s for Hβ λ4960, [OIII] λ5007 and λ4960 respectively. Their FWHM extend over $\sim$ 200 (Hβ) and $\sim$ 30 ([OIII]) pixels. Converting to Vega H-band magnitudes we get 15.7, 16.1 and 17.3 respectively. Hence, from the typical signal-to-noise ratio per pixel achieved by the APOGEE spectrograph,[1] we estimate the lines to be detected with a $S/N \sim 62$, ~ 45 and ~ 20 respectively if 24 visits are completed. We note that even with 6 visits the lines will be detected at half the S/N quoted above, which is enough to reach for instance a competitive error on $\Delta\alpha/\alpha$, and reach the other scientific goals since a factor 1/2 on the S/N will translate into a factor $\sqrt{2}$ in the error for the position of the lines. Furthermore, the S/N of the continuum will be detected with $S/N > 6$ for quasars with H-band magnitudes H<19, and $S/N > 23$ for magnitudes H<17.

The possible inter-fiber cross-talk does not affect typical APOGEE targets since their H-band magnitudes are brighter than the magnitudes of our quasar targets.

[1] From https://trac.sdss.org/wiki/APOGEE2/AncillaryCall2015.

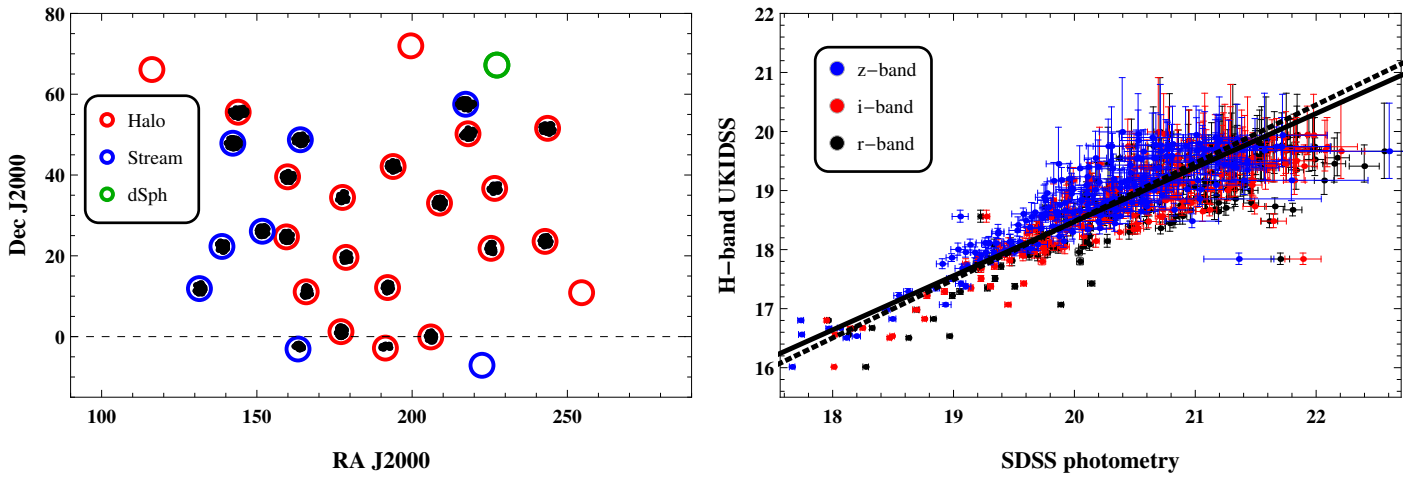

Figure 2: Left panel: SDSS-III/BOSS DR12Q quasars (1,265) with $2.0 < z < 2.4$ in J2000 equatorial coordinates overlapping with the APOGEE-2-North halo, stream and dsph fields. Right panel: UKIDSS H-band magnitudes (Vega) and the SDSS r, i and z band magnitudes of our Sample 1 (215 quasars). The solid line is the weighted linear fit between all quasars with UKIDSS magnitude < 21 (22,420) used to estimate the H-band magnitude for quasars without UKIDSS data, while the dotted line is the same fit using only our Sample 1, shown for comparison.

Data reduction

The APOGEE-2 data reduction and analysis pipeline will provide us 1-D extracted calibrated spectra corrected from airglow emission, telluric absorption, and instrumental response.

The code for the analysis of the Hβ and [OIII] lines is already written. As a first guess, the code uses the redshift of the object which is already known from the BOSS optical spectra.

We will need to implement the code to co-add the spectra from the different visits. The method will be calibrated after the first quasar are observed multiple times. We estimate the implementation to last about a week.

Previous ancillary science programs

JP. K. was the PI of the Sloan Extended QUasar, ELG and LRG Survey (SEQUELS), where J. C., A. F. and D. S. were also involved in. This ancillary science project consisted in a $\sim$ 1000 deg^2 survey to study the physical and clustering properties of galaxies and quasars in the $z > 0.6$ Universe. Three principal classes of targets were observed: i) Luminous Red Galaxies (LRG) identified using SDSS combined with the all-sky WISE survey; ii) Quasars detected in the SDSS and WISE data, as well as using PTF and PanSTARRS variability criteria; iii) Emission Line Galaxies (ELG) identified from U-band and SDSS data. The SEQUELS sample helped in starting the SDSS-IV/eBOSS survey, and enhanced the legacy value of the SDSS and BOSS surveys.

JP. K. was also the PI of "Luminous Blue Galaxies at $0.7 < z < 1.7$, "Do They Reside in Massive Dark Matter Halos?", where J. C. and D. S. where also involved in.

J. C. was the PI of "S3/eBOSS ELG target selection with S3-like or DES-like photometry", where JP. K. was also involved.

Target information

Using the APOGEE-2 field list published in https://trac.sdss.org/wiki/APOGEE2/TargetingPlan and cross-matching with the list of plates updated by G. Zasowski and provided by K. Covey (which includes expected number of visits and starting year), we selected those plates which will be observed by the APOGEE-North spectrograph observed during and after year 3 (August 2016-July 2017), whose type is `halo`, `halo_stream` or `halo_dsph`; and will be visited ≥ 6 times. We are left with 30 fields (20 `halo`, 9 `halo_stream` and 1 `halo_dsph`).

From the 297,301 quasars of DR12Q, 81,392 have a redshift $2.0 < z < 2.4$, and 1,265 are located in the selected fields (within a radius of 1.4 degrees from the center of the field); see Figure 2, left panel. Only 255 have H-band flux measurements from UKIDSS (neither of them have 2MASS H-band magnitude measurements[2]). Using the UKIDSS measurements, we further restrict our targets to have H-band magnitudes < 20. In this way, we are left with 215 targets which are distributed in 6 fields (5 `halo`, 1 `halo_stream`, 0 `halo_dsph`). This defines Sample 1.

[2]The H-band magnitude limit in this survey was 15.1, our sources have H-band magnitudes > 16.

Table 1: Summary of targets.

Field name	Type	Year	Quasars	Fiber hours
GD1-2	halo_stream	3	37	444
GD1-3	halo_stream	4	58	1044
ORPHAN-5	halo_stream	6	80	1920
160+45	halo	4	58	1392
ORPHAN-3	halo_stream	5	73	1752
210+60	halo	4	66	792
180+60	halo	5	47	1128
GD1-4	halo_stream	6	62	1488
ORPHAN-1	halo_stream	4	22	528
240+60	halo	4	40	960
270+60	halo	3	52	312
180+75	halo	3	38	456
240+75	halo	3	47	1128
300+60	halo	3	19	456
300+75	halo	3	48	576
120+75	halo	3	50	600
330+60	halo	5	38	456
060+75	halo	5	51	1224
GD1-5	halo_stream	5	69	1242
090+60	halo	4	51	1224
030+60	halo	3	35	840
060+60	halo	6	29	696
040+45	halo	3	56	672
080+45	halo	3	49	1176

The UKIDSS H-band photometric survey only covers 6 out of the 30 plates with possible quasar targets. To increase the possible number of targets, we studied the correlation between the UKIDSS H-band measurements and the r, i, z-band magnitudes from the SDSS photometry using all quasars (22,420) with UKIDSS H-band magnitude H< 21 and redshift $2.0 < z < 2.4$ (not only the ones overlapping with APOGEE fields of view), and derived a correlation that can be used to estimate H-band magnitudes (see Figure 2, right panel). Thus, constraining the estimated H-band magnitude to be < 20, we define our Sample 2 which contains 960 quasars distributed in 24 fields (17 `halo`, 7 `halo_stream`, 0 `halo_dsph`).

Using both samples, we build a complete sample of 1,175 quasars. In each plate, the targets are given priority ranking according to their H-band magnitudes obtained either from UKIDSS or estimated from the SDSS z-band photometry. 726 of them are expected to be observed during the years 3-4 while the remaining ones 449 are to be observed in the period 5-6. The total fiber hours are 22,506 (12,600 for years 3-4; 9,906 for years 5-6). However, we will reduce this sample, keeping the brightest quasars, according to the number of allocated fiber hours, if any.

Table 1 describes the distribution of quasars per plate. Table 2 contains the brightest 21 targets in the H-band, with H<16.7. Please, find the complete list of targets (1,175) at

https://trac.sdss3.org/attachment/wiki/QSOalphaVar/apogee_q_targets.txt.

References.

[1] Uzan, J.-P. 2003. The fundamental constants and their variation: observational and theoretical status. RvMP 75 403.

[2] Petrov, Yu.V. et al 2006. Natural nuclear reactor Oklo and variation of fundamental constants. PRC 74.

[3] Olive, K. A., Pospelov, M., Qian, Y.-Z., et al. 2002, PRD, 66, 045022.

[4] Albareti, Comparat et al. 2015. Constraint on the time variation of the fine-structure constant with the SDSS-III/BOSS quasar sample.

[5] Evans et al. 2014. The UVES Large Program for testing fundamental physics - III. Constraints on the fine-structure constant from 3 telescopes. MNRAS 445, 128.

[6] Magorrian et al. 1998. The Demography of Massive Dark Objects in Galaxy Centers. AJ, 115, 2285.

[7] Merloni. 2004. The anti-hierarchical growth of supermassive black holes. MNRAS, 353, 1035.

[8] Shankar 2009. The demography of supermassive black holes: Growing monsters at the heart of galaxies. New Astron Rev, 53, 57.

[9] Kaspi et al. 2000. Reverberation Measurements for 17 Quasars and the Size-Mass-Luminosity Relations in Active Galactic Nuclei. ApJ, 533,631.
[10] Kaspi et al. 2005. The Relationship between Luminosity and Broad-Line Region Size in Active Galactic Nuclei. ApJ, 629, 61.
[11] Vestergaard et al. 2006. Determining Central Black Hole Masses in Distant Active Galaxies and Quasars. II. Improved Optical and UV Scaling Relationships. ApJ, 641, 689.
[12] Kaspi et al. 2007. Reverberation Mapping of High-Luminosity Quasars: First Results. ApJ, 659, 997.
[13] Decarli et al. 2008. On the geometry of broad emission region in quasars. MNRAS, 387, 1237.
[14] Decarli et al. 2008. Are the black hole masses in narrow-line Seyfert 1 galaxies actually small?. MNRAS, 386, L15.
[15] Richards et al. 2002. Optical and Radio Properties of Extragalactic Sources Observed by the FIRST Survey and the Sloan Digital Sky Survey. AJ, 124, 1.
[16] Gaskell, C. M. 1982. A redshift difference between high and low ionization emission-line regions in QSOs - Evidence for radial motions. ApJ 263, 79.
[17] Richards et al. 2011. Unification of Luminous Type 1 Quasars through C IV Emission. AJ, 141, 167.
[18] Paris et al. 2012. The Sloan Digital Sky Survey quasar catalog: ninth data release. A&A 548, AA66.
[19] Font-Ribera et al. 2013. The large-scale quasar-Lyman α forest cross-correlation from BOSS. JCAP, 5, 018.
[20] Marziani et al. 2013. Low-ionization Outflows in High Eddington Ratio Quasars. ApJ, 764, 150.
[21] Hewett & Wild. 2010. Improved redshifts for SDSS quasar spectra. MNRAS, 405, 2302.
[22] Vanden Verk et al. 2001. Composite Quasar Spectra from the Sloan Digital Sky Survey. AJ, 122, 549.
[23] Boroson et al. 2005. Blueshifted [O III] Emission: Indications of a Dynamic Narrow-Line Region. AJ, 130, 381.

Table 2: Target description. The 21 brightest targets are shown (H< 16.7). SDSS z-band means that the H-band magnitude is obtained through the correlation observed between UKIDSS H-band and SDSS z-band magnitudes. Proper motion measurements are not needed for the kind of targets we request. A link to the ascii file containing all the targets is provided in the bulk text.

Field name	Type	SDSS ID	RA (J2000)	Dec (J2000)	H-band (Vega)	Source for H-band photometry	Visits	Year	S/N_{min}	Redshift	Priority
210+60	halo	J103641.96+250236.3	10:36:41.96	+25:02:36.3	15.95	SDSS z-band	12	4	10	2.015	1
210+60	halo	J103410.41+233657.7	10:34:10.41	+23:36:57.7	16.71	SDSS z-band	12	4	10	2.353	2
300+60	halo	J124924.86-023339.7	12:49:24.86	-02:33:39.7	16.36	SDSS z-band	24	3	10	2.12	1
300+75	halo	J125150.45+114340.7	12:51:50.45	+11:43:40.7	15.75	SDSS z-band	12	3	10	2.195	1
300+75	halo	J124848.31+114616.6	12:48:48.31	+11:46:16.6	16.67	UKIDSS	12	3	10	2.331	2
060+75	halo	J135417.90+334859.8	13:54:17.90	+33:48:59.8	16.36	SDSS z-band	24	5	10	2.246	1
060+75	halo	J134849.80+324402.2	13:48:49.80	+32:44:02.2	16.56	UKIDSS	24	5	10	2.203	2
090+60	halo	J142500.24+494729.2	14:25:00.24	+49:47:29.2	15.75	SDSS z-band	24	4	10	2.26	1
090+60	halo	J142605.79+500426.6	14:26:05.79	+50:04:26.6	16.17	SDSS z-band	24	4	10	2.239	2
090+60	halo	J142628.01+500248.3	14:26:28.01	+50:02:48.3	16.5	SDSS z-band	24	4	10	2.326	3
030+60	halo	J145822.96+214636.9	14:58:22.96	+21:46:36.9	16.66	SDSS z-band	24	3	10	2.02	1
040+45	halo	J161301.96+245417.1	16:13:01.96	+24:54:17.1	16.65	SDSS z-band	12	3	10	2.334	1
080+45	halo	J162117.08+511213.6	16:21:17.08	+51:12:13.6	16.69	SDSS z-band	24	3	10	2.304	1
240+60	halo	J110206.66+112104.9	11:02:06.66	+11:21:04.9	16.01	UKIDSS	24	4	10	2.35	1
270+60	halo	J115122.14+020426.3	11:51:22.14	+02:04:26.3	16.51	UKIDSS	6	3	10	2.397	1
270+60	halo	J114551.66+012606.5	11:45:51.66	+01:26:06.5	16.66	UKIDSS	6	3	10	2.296	2
330+60	halo	J134145.12-003631.0	13:41:45.12	-00:36:31.0	16.54	UKIDSS	12	5	10	2.183	1
ORPHAN-3	halo_stream	J100343.64+245427.0	10:03:43.64	+24:54:27.0	16.33	SDSS z-band	24	5	10	2.329	1
GD1-4	halo_stream	J105657.54+492957.9	10:56:57.54	+49:29:57.9	16.63	SDSS z-band	24	6	10	2.162	1
GD1-4	halo_stream	J105216.03+485619.1	10:52:16.03	+48:56:19.1	16.69	SDSS z-band	24	6	10	2.233	2
ORPHAN-1	halo_stream	J105811.93-023724.0	10:58:11.93	-02:37:24.0	16.25	SDSS z-band	24	4	10	2.378	1

Part II
QFT in curved spacetimes

Quantum Field Theory (QFT) in curved spacetimes is an effective theory where matter and its non-gravitational interactions are fully quantized. The gravitational field is treated in a classical way. QFT in curved spacetimes works in a very well-defined range of energy scales because of the huge difference in the coupling strength between non-gravitational interactions and gravity. Due to the lack of a full quantum theory of gravity, this framework is useful to deal with quantum fields in the presence of gravitational interactions. Nevertheless, it has also provided us with the first predictions on quantum and gravitational effects, the most notorious one being the Hawking radiation.

Formulation of QFT in curved spacetimes

To extend the formulation of classical field theory from flat to curved spacetimes is straightforward. However, it is highly non-trivial to extend the quantum version. One of the main reasons is that the notion of particles or, in general, of states is not invariant under diffeomorphism, i.e. general coordinate transformations. Therefore, there is no way to define a canonical vacuum state unless the spacetime has some symmetry, for instance a timelike (conformal) Killing vector field. This imposes a quite restrictive and unrealistic limitation on the theory. One can relax this assumption by requiring the spacetime to be only asymptotically stationary. In this way, an asymptotic notion of particles can be defined and creation/annihilation of particles in the presence of gravitational fields be studied, for instance by defining an S-matrix between early ($\langle \text{in}|$) and late ($|\text{out}\rangle$) asymptotic states.

The axiomatic formulation of QFT in Minkowski spacetime is based on the Wightman axioms (Streater and Wightman, 1989). Those axioms make heavy use of Poincaré invariance of flat spacetime and the existence of a preferred vacuum state. None of these statements holds for a general spacetime.[22]

It seems that the most promising approach to define QFT in curved spacetimes is through the algebraic formulation of QFT. This formulation was first developed by Haag and Kastler (1964) for flat spacetimes. Wald (1995) discussed its application to curved spacetimes. It turns out that all Wightman axioms, except one, could be generalized in a relative straightforward manner

[22]For a detailed discussion of the difficulties encountered when trying to extend Wightman axioms to curved spacetimes see Wald (2009).

to curved spacetimes in the algebraic formulation. The remaining axiom states the existence of a unique Poincaré invariant vacuum state. Hollands and Wald (2010) proposed to replace this axiom by the existence of an Operator Product Expansion (OPE) whose coefficients satisfy some properties. OPE's have been shown to hold order by order in perturbation theory in the presence of renormalizable interactions in curved spacetimes (Hollands, 2007). Furthermore, several results have been proved within the algebraic formulation, for instance that renormalized perturbation theory can be constructed in curved spacetimes (Hollands and Wald, 2001, 2002, 2003), including Yang-Mills fields (Hollands, 2008).

This is still an open area of research. We refer to Wald (2006) for further details and references about the topic.

Canonical formulation

In contrast to the algebraic formulation, the canonical formulation of QFT in curved spacetimes (Birrell and Davies, 1984; Ford, 1997) is a straightforward way to generalize the theory from flat to curved spacetimes. This formulation is useful from a physical point of view when the spacetime has a symmetry or at least an approximate symmetry that enables us to decompose the field into positive and negative frequency parts for a physically relevant observer. In cosmological scenarios the spacetime metric is well described by (flat) FRW spacetimes which in fact do possess a conformal Killing vector field that singles out a preferred vacuum state (Bunch-Davies vacuum).

In the following we introduce very briefly this formulation for a scalar field. Assuming no coupling between the field and curvature, the classical action for real scalar field ϕ with potential $V(\phi)$ in arbitrary $(D+1)$-dimensional curved spacetime is given by

$$S[\phi, g_{\mu\nu}] \;=\; \int \mathrm{d}^{D+1}x\, \sqrt{g}\left(\frac{1}{2}\, g^{\mu\nu}\, \partial_\mu\phi\, \partial_\nu\phi \;-\; V(\phi)\right) \tag{8}$$

where $g_{\mu\nu}$ is the spacetime metric. The equations of motion derived from the previous action are

$$\Box\,\phi \;+\; V'(\phi) \;=\; 0\,. \tag{9}$$

In order to implement the canonical quantization for the field ϕ, a complete set of mode solutions $\{\phi_k\}$ for eq. (9) has to be found. However, solutions of the field equations are not a covariant concept and therefore a preferred frame of reference, a particular coordinate system $(\eta, \mathbf{x})$, is selected from the beginning. The solutions have to be orthonormal, i.e.

$$(\phi_k, \phi_{k'}) \;=\; \delta^D(\mathbf{k} - \mathbf{k}')\,, \tag{10}$$

with respect to the standard scalar product in curved spacetime

$$(\phi_k, \phi_{k'}) \;=\; i \int_\Sigma \left[\phi^*_{k'}\left(\partial_\mu\phi_k\right) - \left(\partial_\mu\phi^*_{k'}\right)\phi_k\,\right] \sqrt{g_\Sigma}\,\mathrm{d}\Sigma^\mu, \tag{11}$$

where $d\Sigma^\mu = n^\mu d\Sigma$, n^μ is a unit timelike vector directed to the future and orthogonal to the spatial hypersurface Σ, whereas $\sqrt{g_\Sigma}$ is the determinant of the metric on Σ. This scalar product is independent of the choice of the spatial hypersurface Σ.

In terms of the orthonormal modes, the scalar field ϕ can be expanded as

$$\phi(\eta, \mathbf{x}) = \int d^D\mathbf{k} \left[c_\mathbf{k}\, \phi_k(\eta, \mathbf{x}) + c^\dagger_\mathbf{k}\, \phi^*_k(\eta, \mathbf{x}) \right]. \tag{12}$$

Next, the quantum field is promoted to a quantum operator by identifying the c-numbers $c^\dagger_{\mathbf{k}'}$ and $c_\mathbf{k}$ with the creation $a^\dagger_{\mathbf{k}'}$ and annihilation $a_\mathbf{k}$ operators that satisfy the standard commutation relations

$$[a_\mathbf{k}, a^\dagger_{\mathbf{k}'}] = \delta^D(\mathbf{k} - \mathbf{k}')\,. \tag{13}$$

The vacuum state associated to the (quantum) modes $\{\phi_k\}$ is defined by

$$a_\mathbf{k}|0\rangle = 0 \quad \forall \mathbf{k}\,, \tag{14}$$

from which the whole Fock space is constructed by applying $\{a^\dagger_{\mathbf{k}'}\}$ operators.

In spite of the simplicity of equation (14) in defining the vacuum state, it is important to highlight that the vacuum state depends on the mode solutions $\{\phi_k\}$ and consequently on the frame of reference $(\eta, \mathbf{x})$ chosen at the beginning in order to solve the Klein-Gordon equation. In flat spacetime, it is natural to consider inertial observers in order to pick up a vacuum, that can be shown to be equivalent for every inertial observer.[23] In cosmological spacetimes, comoving observers are also relevant observers from a physical point of view. However, in a general spacetime there is no well motivated election of a vacuum state. This problem, as recognized long ago, cannot be overcome because states are not covariant objects to start with, which implies that the concept of particles is ambiguous and observer dependent.[24]

Another important issue is that, in general, it is not possible to obtain explicit expressions for set of solutions $\{\phi_k\}$, which is mandatory in order to quantize the theory. However, there are perturbative methods (Zeldovich and Starobinsky, 1972; Birrell and Davies, 1980). For instance, a WKB ansatz

$$\phi_k(\eta, \mathbf{x}) = f_k(\eta, \mathbf{x})\, e^{i\theta_k(\eta, \mathbf{x})}\,, \tag{15}$$

where $f_k(\eta, \mathbf{x})$ is assumed to evolve slowly in space and time, provides a good starting point. This enables us to simplify the equation of motion. Such an adiabatic ansatz works whenever the Compton wavelength of the field is much smaller than the typical astrophysical or cosmological

[23] In inertial coordinates, the mode solutions of the Klein-Gordon equation are given by plane waves which are indeed covariant under Lorentz transformations, i.e. plane waves are solutions in any inertial frame. Therefore, the vacuum state defined by pane waves is the same for any inertial observer.

[24] This phenomenon is well illustrated by the Unruh effect (see Crispino et al., 2008, for a recent review).

scales involved.

Despite the problems encountered when trying to formulate QFT in curved spacetimes, this formulation of the theory is enough to obtain some non-trivial results. For example, estimations of the amount of particle creation produced by gravitational fields[25] in expanding universes could be obtained in a fairly straightforward way (Parker, 1969, 1971). In this regard, Bogolubov coefficients play an important role (Bogolyubov, 1947). These coefficients express the creation and annihilation operators defined by a particular set of solutions in terms of the corresponding operators defined by another set of solutions.

Another far-reaching theoretical result is the Hawking radiation (Hawking, 1974, 1975). This result together with the subject of black hole thermodynamics introduced by Bekenstein (1973) have led to the developments of new areas of research like Holography (Bousso, 2002).

Green functions

Large efforts have been devoted to the study of Green functions in curved spacetimes. General properties of vacuum states could be studied within this approach. The most important advantage is that it is a covariant way to deal with quantum fields in curved spacetime. Important results as the DeWitt-Schwinger and Hadamard representations for a Green function in curved spacetimes are also worthwhile to mention. We follow Albareti (2014) in part of this section.

Green functions are vacuum expectations values of products of free field operators in a particular vacuum state. The simplest ones are

$$G^{+}(x,x') = \langle 0|\phi(x)\phi(x')|0\rangle \quad \text{Positive frequency function} \tag{16}$$
$$G^{-}(x,x') = \langle 0|\phi(x')\phi(x)|0\rangle \quad \text{Negative frequency function}, \tag{17}$$

which are known as Wightman functions. Two important ones because of their symmetry properties are

$$i\,G(x,x') = \langle 0|\left[\phi(x),\phi(x')\right]|0\rangle \quad \text{Pauli-Jordan or Schwinger function} \tag{18}$$
$$G^{(1)}(x,x') = \langle 0|\left\{\phi(x),\phi(x')\right\}|0\rangle \quad \text{Hadamard's elementary function}, \tag{19}$$

which are antisymmetric and symmetric in their arguments respectively.[26] The most important because of its role in flat QFT is the Feynman propagator

$$i\,G_F(x,x') = \langle 0|T\left(\phi(x)\phi(x')\right)|0\rangle, \tag{22}$$

[25] This idea was first suggested by Schrodinger (1939).

[26] They can be written in terms of the Wightman functions as

$$i\,G(x,x') = G^{+}(x,x') - G^{-}(x,x') \tag{20}$$
$$G^{(1)}(x,x') = G^{+}(x,x') + G^{-}(x,x'). \tag{21}$$

where the T operator stands for the time ordered product of the fields.

One of the main reason for considering Green function is that the ultraviolet divergences of QFT are related with the short distance properties of vacuum expectation values of field operators (Ford, 1997). It is reasonable to expect on physical grounds that the high frequency behavior of the field is independent of the global structure of spacetime and of the particular quantum state, which indeed is globally defined. Instead, it should only depends on the local geometry. This is a quite important requirement for applying regularization and renormalization procedures. These considerations also apply to Green functions. The importance of this short-distance behavior was pointed out by DeWitt (1964) at the classical and quantum levels. DeWitt introduced the so-called DeWitt-Schwinger and Hadamard representation of the Feynman propagator based on previous considerations found in the work of Schwinger (1951) and Hadamard (1923).

In the following a short revision of both representations is presented.

Hadamard representation

The Hadamard representation is built from a set of two-point coefficients which are defined by recursive relations derived from the Klein-Gordon equation. In this sense, it is similar to DeWitt-Schwinger representation, however it is more general since it can also encode additional physical information about the field such as the effect of boundary conditions and the dependence on the quantum state.

The Hadamard expansion is given by

$$G_F^{\mathrm{H}}(x,x') = \frac{i}{8\pi^2}\left[\frac{U(x,x')}{-\sigma_{x,x'}+i\epsilon} + V(x,x')\ln\left[-\sigma_{x,x'}+i\epsilon\right] + W(x,x')\right], \tag{23}$$

where $U(x,x')$, $V(x,x')$ and $W(x,x')$ are symmetric in x,x' and regular as $x' \to x$, and $\sigma_{p,q}$ is the Synge's world function (or geodetic distance) defined as

$$\sigma_{p,q} = \begin{cases} \frac{1}{2}(\Delta\tau)^2_{p,q} & p \text{ and } q \text{ timelike related} \\ -\frac{1}{2}(\Delta s)^2_{p,q} & p \text{ and } q \text{ spacelike related} \\ 0 & p \text{ and } q \text{ nulllike related} \end{cases} \tag{24}$$

where $(\Delta\tau)_{p,q}$ and $(\Delta s)_{p,q}$ are the proper time and proper length respectively between the points p and q. $V(x,x')$ and $W(x,x')$ could be expanded as follows

$$V(x,x') = \sum_{n=0}^{\infty} V_n(x,x')\,\sigma^n_{x,x'} \tag{25}$$

$$W(x,x') = \sum_{n=0}^{\infty} W_n(x,x')\,\sigma^n_{x,x'}\,. \tag{26}$$

The coefficients $V_n(x,x')$ and $W_n(x,x')$ are determined by recursive relations derived from the Klein-Gordon equation. However, the term $W_0(x,x')$ is undetermined by the recursive relations and it may encode additional information about the field.

The divergent structure of (23) is known as the Hadamard behaviour and the vacuum state derived from it is called a Hadamard state (Carroll, 2004). This expansion is more useful to study the divergent structure of the Green function. In particular, we can compare in a straightforward way if a specific Green function behaves as expected from the Minkowski case.

However, we should comment that it is not completely obvious that we must recover the Minkowski behaviour in curved spacetimes at high frequencies. For instance, if the field is non-minimally coupled to gravity there may exist non-trivial differences with the flat case. An example is given by the stress-energy tensor of a scalar field with a conformal coupling to curvature which differs from the stress-energy tensor of the minimally coupled field even when the curvature vanishes (Tagirov, 2005).

DeWitt-Schwinger representation

This representation also known as the heat kernel expansion of the Feynman Green function in general curved spacetimes has a great number of applications. It is of fundamental importance in Mathematics in order to study the relation between the spectral decomposition of a differential operator and the properties of the underlying manifold. We refer the reader to the extensive treatment Vassilevich (2003) for more details. For us, this expansion is useful to study the short-distance behaviour $x \to x'$.

We follow Birrell and Davies (1984) in its derivation. Let us consider normal coordinates with origin at x' in a d-dimensional spacetime. Then, for x (x^α) in the neighbourhood of x'

$$g_{\mu\nu}(x) \;=\; \eta_{\mu\nu} \;+\; \frac{1}{3}R_{\mu\alpha\nu\beta}\,x^\alpha\,x^\beta \;-\; \frac{1}{6}R_{\mu\alpha\nu\beta\,\gamma}\,x^\alpha\,x^\beta\,x^\gamma \;+\; \ldots \tag{27}$$

where $\eta_{\mu\nu}$ is Minkowski metric, and $R_{\mu\alpha\nu\beta}$ is the Riemann tensor. Then, the geodetic distance is given by

$$\sigma_{x,x'} \;=\; -\frac{1}{2}\eta_{\mu\nu}\,x^\mu\,x^\nu \tag{28}$$

at leading order. Next, we define

$$\mathcal{G}_F(x,x') \;=\; (-g(x))^{1/4}\,G_F(x,x'), \tag{29}$$

where $g(x) = |\det g_{\mu\nu}|$ and its Fourier transform as

$$\mathcal{G}_F(x,x') \;=\; \frac{1}{(2\pi)^d}\int \mathrm{d}k^d\,e^{ik\cdot x}\,\mathcal{G}_F(k), \tag{30}$$

where $k \cdot x = \eta_{\mu\nu} k^\mu x^\nu$. Then, using the expansion of the metric around x' in normal coordinates it is possible to solve the Klein-Gordon equation by iteration in momentum space to any adiabatic order, i.e. derivatives of the metric. By returning to coordinate space, the following expression is obtained[27]

$$\mathcal{G}_F(x,x') = \frac{1}{(4\pi)^{d/2}} \int_0^\infty \frac{1}{(is)^{d/2}} \exp\left(-im^2 s + \frac{\sigma_{x,x'}}{2is}\right) F(x,x';is), \tag{32}$$

where $F(x,x';is)$ can be expanded as

$$F(x,x';is) = \sum_{j=0}^{\infty} a_j(x,x')\,(is)^j\,. \tag{33}$$

The functions $a_j(x,x')$ are called the heat-kernel coefficients and they are computed using recursive relations derived from the Klein-Gordon equation. Finally, it is possible to show that the DeWitt-Schwinger representation reads

$$G_F^{\rm DS}(x,x') = \frac{\Delta^{1/2}(x,x')}{(4\pi)^{d/2}} \int_0^\infty \frac{1}{(is)^{d/2}} \exp\left(-im^2 s + \frac{\sigma_{x,x'}}{2is}\right) F(x,x';is), \tag{34}$$

where Δ is the Van Vleck determinant

$$\Delta(x,x') = -\frac{\det\left[\partial_\mu \partial_\nu \sigma_{x,x'}\right]}{\sqrt{g(x)g(x')}} \tag{35}$$

which coincides with $(-g(x))^{-1/2}$ in normal coordinates. If the expansion (33) is replaced in (34) the integral in s can be performed and we get the adiabatic expansion of the DeWitt-Schwinger representation

$$G_F^{\rm DS}(x,x') = \frac{-i\pi\,\Delta^{1/2}(x,x')}{(4\pi i)^{d/2}} \sum_{j=0}^{\infty} a_j(x,x') \left(-\frac{\partial}{\partial m^2}\right)^j \left(\frac{2m^2}{-\sigma_{x,x'}+i\epsilon}\right)^{(d-2)/4} \times H^{(2)}_{(d-2)/2}\left((2m^2(\sigma_{x,x'}-i\epsilon))^{1/2}\right), \tag{36}$$

where the $-i\epsilon$ prescription ensures that the Green function represents the expectation value of a time ordered product of fields in some set of states. The first term of eq. (36) is the same as the

[27] The integral representation

$$\frac{1}{k^2-m^2+i\epsilon} = -i\int_0^\infty e^{is(k^2-m^2+i\epsilon)} \tag{31}$$

have been used to obtain equation (32) in going from momentum to coordinate space. In this way, the integration in k and s can be interchanged and a closed expression in coordinate space is obtained.

Feynman propagator in flat spacetime. The heat-kernel coefficients $a_j(x,x')$ cannot be determined exactly and they are computed by expanding them in terms of $\sigma_{x,x'}$ and its covariant derivatives. This is a formidable task. It is important to note that they are purely geometrical two-points objects formally independent of the spacetime dimension. They are also important in connection with spectral geometry, topology of manifolds and the Atiyah-Singer index theorem (Gilkey, 1984).

With the asymptotic expansion given by eq. (34), one can obtain an expression for the one-loop effective Lagrangian, given by[28]

$$L_{\rm eff} \;=\; \frac{i}{2}\lim_{x'\to x}\int_{m^2}^{\infty} {\rm d}m^2\, G_F^{\rm DS}(x,x')\,, \tag{37}$$

as

$$L_{\rm eff} \;=\; \lim_{x'\to x} -i\frac{\Delta^{1/2}(x,x')}{2(4\pi)^{d/2}}\sum_{j=0}^{\infty} a_j(x,x')\int_0^{\infty}\frac{(is)^{j-1}}{(is)^{d/2}}\exp\left(-im^2 s+\frac{\sigma_{x,x'}}{2is}\right)\,. \tag{38}$$

Let us notice that the first $d/2+1$ terms in the previous expression are divergent as $\sigma_{x,x'}\to 0$. By performing an analytical continuation over the complex plane of the dimension d, the coincidence limit $x'\to x$ can be computed to get

$$\begin{aligned} L_{\rm eff} \;&=\; \frac{1}{2(4\pi)^{d/2}}\sum_{j=0}^{\infty} a_j(x)\,(m^2)^{d/2-j}\,\Gamma(j-d/2) \\ &=\; \frac{1}{2(4\pi)^{d/2}}\left(\frac{m}{\mu}\right)^{d-4}\sum_{j=0}^{\infty} a_j(x)\,m^{4-2j}\,\Gamma(j-d/2)\,, \end{aligned} \tag{39}$$

where $a_j(x)\equiv a_j(x,x)$ and μ is an arbitrary mass scale. In $d=4$ dimensions, the first three terms of eq. (39) are divergent because of the poles of the Gamma functions. Expanding around the poles, the effective Lagrangian reads

$$L_{\rm eff} \;=\; -\frac{1}{(4\pi)^{d/4}}\left[\frac{1}{d-4}+\frac{\gamma}{2}+\frac{1}{2}\ln\left(\frac{m^2}{\mu^2}\right)\right]\left(\frac{4m^4}{d(d-2)}\,a_0-\frac{2m^2}{d-2}\,a_1+a_2\right)\,. \tag{40}$$

The first three $a_j(x)$ coefficients are given by

$$a_0(x) \;=\; 1 \tag{41}$$

$$a_1(x) \;=\; \left(\frac{1}{6}-\xi\right)R \tag{42}$$

$$a_2(x) \;=\; \frac{1}{180}\left(R_{\alpha\beta\gamma\delta}R^{\alpha\beta\gamma\delta}-R_{\alpha\beta}R^{\alpha\beta}\right)-\frac{1}{6}\left(\frac{1}{5}-\xi\right)\Box R+\frac{1}{2}\left(\frac{1}{6}-\xi\right)^2 R^2\,, \tag{43}$$

[28] In Paper II, we provide a derivation of this expression.

where $R_{\mu\nu} = R^{\alpha}{}_{\mu\alpha\nu}$ is the Ricci tensor, $R = g^{\mu\nu}R_{\mu\nu}$ is the Ricci scalar and ξ is the coupling of the field ϕ with the Ricci scalar.[29]

The result of eq. (40) can be renormalized by absorbing the divergences into the gravitational Lagrangian or into the matter Lagrangian. In any case, the renormalized parameters eventually depend on the curvature, for instance through the coefficient $a_1(x)$. The relative size of the curvature corrections is given by $\sim R/m^2$. This effect is currently negligible for any of the fields of the Standard Model. In the case of neutrinos and depending on their mass, this effect could be relevant after the electroweak phase transition. Concerning the Higgs field, the contribution due to $a_1(x)$ results in a correction to its effective potential proportional to $m^2(\phi)\,R$ that would produce a spacetime dependence of the Higgs vacuum expectation value. However, this effect is negligible after the electroweak transition.

DeWitt-Schwinger vs Hadamard

Both representation could be used in connection with the regularization and renormalization of the stress-energy tensor and the calculation of the renormalized effective action of a quantum field on a curved spacetime. The DeWitt-Schwinger expansion was used jointly with the point-splitting prescription to obtain important results concerning the renormalization of the stress-energy tensor (Christensen, 1976, 1978; Bunch and Davies, 1978a,b). This method has been modified using the Hadamard representation resulting in a more general and efficient method (see Décanini and Folacci (2006) and references therein). It is also more rigorous because of its axiomatic foundation.

Let us notice that it is possible to relate both representations through expressing the Hadamard coefficients $U_n(x,x')$ and $V_n(x,x')$ in terms of the adiabatic coefficients $a_j(x,x')$ of the DeWitt-Schwinger expression. For instance, $U_n(x,x')$ and $V_n(x,x')$ are expressed as a function of the first n and $n+1$ adiabatic coefficients $a_j(x,x')$, respectively. However, this does not fix completely the Hadamard representation of the Feynman propagator since we still have the freedom to choose $W_0(x,x')$. It can be proved that the DeWitt-Schwinger expansion is recovered from the Hadamard form when a specific $W_0(x,x')$ is chosen.

The more general character of the Hadamard representation highlights the fact that the DeWitt-Schwinger representation is a local expansion which depends on curvature alone and it is independent of the vacuum state. But, the effective action is in general a non-local functional which can depend on the particular choice of vacuum and the global properties of the spacetime.

In this respect, the effect of curvature on the expectation values of fields in curved backgrounds predicted by the DeWitt-Schwinger expansion may not be the only or even the dominant effect due to the structure of spacetime. There could be effects due to the properties of the vacuum state and the topological structure of spacetime. It is important to note that these effect may not be expressed in a covariant way, for instance in terms of the curvature, because of the non-covariant nature of

[29] The equation of motion for a field with a non-minimal coupling to gravity ($\xi \neq 0$) is given by

$$\Box\phi + V'(\phi) + \xi R\phi = 0\,.$$

the vacuum state itself. Therefore, these contributions may not be suppressed as the curvature terms given by the local expansion. They may be expressed directly in terms of the components of the metric $g_{\mu\nu}$. This lead us to compute, in this thesis, these effects on particular spacetimes and quantum states with a different approach in order to take into account the properties of particular vacuum states.

Paper II

"Gravitational perturbations of the Higgs field"

Physical Review D, Volume 95, 044030.

Authors: Franco D. Albareti, Antonio L. Maroto and Francisco Prada.

Motivation

The discovery at the Large Hadron Collider of the Higgs boson in 2012 is one of the greatest success of Particle Physics in recent years. According to the Standard Model prediction, its existence also implies the presence of a classical scalar field that permeates all of space and generates the masses of quarks, leptons and gauge bosons. The effects of classical gravitational fields on its evolution, which eventually impacts on the masses of elementary particles, are believed to be dependent on curvature and therefore to be negligible at macroscopic scales. However, although local contributions do depend on curvature alone and are independent of the vacuum state, the effective action is in general a non-local functional which can depend on the particular choice of vacuum and the global properties of the space-time. In this work, we present a formalism based on mode summation which allows to compute the complete one-loop effective potential of self-interacting scalar fields in perturbed Robertson-Walker spacetimes using adiabatic approximation.

PHYSICAL REVIEW D **95,** 044030 (2017)

Gravitational perturbations of the Higgs field

Franco D. Albareti,[1,2,*] Antonio L. Maroto,[3,†] and Francisco Prada[1,2,4,‡]

[1]*Instituto de Física Teórica UAM/CSIC, Universidad Autónoma de Madrid, Cantoblanco, E-28049 Madrid, Spain*

[2]*Campus of International Excellence UAM+CSIC, Cantoblanco, E-28049 Madrid, Spain*

[3]*Departamento de Física Teórica, Universidad Complutense de Madrid, 28040 Madrid, Spain*

[4]*Instituto de Astrofísica de Andalucía (CSIC), Glorieta de la Astronomía, E-18080 Granada, Spain*

(Received 19 February 2016; revised manuscript received 15 December 2016; published 21 February 2017)

We study the possible effects of classical gravitational backgrounds on the Higgs field through the modifications induced in the one-loop effective potential and the vacuum expectation value of the energy-momentum tensor. We concentrate our study on the Higgs self-interaction contribution in a perturbed FRW metric. For weak and slowly varying gravitational fields, a complete set of mode solutions for the Klein-Gordon equation is obtained to leading order in the adiabatic approximation. Dimensional regularization has been used in the integral evaluation, and a detailed study of the integration of nonrational functions in this formalism has been presented. As expected, the regularized effective potential contains the same divergences as in flat spacetime, which can be renormalized without the need of additional counterterms. We find that, in contrast with other regularization methods, even though metric perturbations affect the mode solutions, they do not contribute to the leading adiabatic order of the potential. We also obtain explicit expressions of the complete energy-momentum tensor for general nonminimal coupling in terms of the perturbed modes. The corresponding leading adiabatic contributions are also obtained.

DOI: 10.1103/PhysRevD.95.044030

I. INTRODUCTION

There are two equally fundamental aspects of the Higgs mechanism for electroweak symmetry breaking which have received remarkably different attention in the last years. On one hand, we have the prediction that a new scalar boson should be present in the spectrum of the theory. Such a new particle has been recently discovered by the ATLAS and CMS experiments at the LHC [1,2]. The most precise measurement to date of its mass comes from a combination of data from both experiments and is given by $m_H = 125.09 \pm 0.21(\text{stat}) \pm 0.11(\text{syst})$ GeV [3]. A large deal of experimental effort is being devoted to the study of the properties of the Higgs boson. Apart from improving the precision in the determination of its mass, measurements of its production and decay channels, self-coupling and couplings to other particles are being performed. So far, all of them are in excellent agreement with the predictions of the Standard Model (SM) [4–6].

On the other hand, the mechanism also predicts the existence of a Higgs field, i.e., a constant classical field $\hat{\phi} = v$ with v the Higgs vacuum expectation value (VEV).[1] given by $v = 246.221 \pm 0.002$ GeV [7]. It is precisely the interaction with the Higgs field what generates the masses of quarks, leptons and gauge bosons. The presence of this nonvanishing field which permeates all of space is a distinctive feature with respect to the rest of SM fields which have vanishing VEVs. Moreover, together with the homogeneous gravitational field created by the cosmological energy density, the Higgs field is the only SM field which is present today in the Universe on its largest scales. This fact opens the interesting possibility of probing the Higgs field not only by exciting its quanta in colliders, but by directly perturbing its VEV. Thus, for example, the fact that the Higgs field is a dynamical field sourced by massive particles suggests that the presence of a heavy particle could induce shifts in the masses of neighboring ones [8]. This effect does not need the production of on-shell Higgs particles, but because of the short range of the corresponding Yukawa interaction, it is negligible at distances beyond the Compton wavelength of the Higgs boson. Existing data does not seem to contain enough kinematic information in order to confirm or exclude it. A similar approach has been proposed in [9] in order to probe the Higgs couplings to electrons and light quarks. The idea of generating peculiar Higgs shifts was also considered in a different context in [10]. In that work a nonminimal coupling of the Higgs field to the spacetime curvature was considered. The nonminimal coupling modifies the effective potential inducing shifts of the VEV in high-curvature regions such as those near neutron stars or black holes [11].

In this work, we explore further the effects of classical gravitational fields on the Higgs VEV. We consider the

*'la Caixa'-Severo Ochoa Scholar, franco.albareti@csic.es

†maroto@ucm.es

‡f.prada@csic.es

[1]In the SM, the Higgs VEV is related to the Fermi coupling constant by $v = (\sqrt{2}G_F)^{-1/2}$. The value of this constant is known since the original works of Fermi in the early 30's.

SM Higgs minimally coupled to gravity. The Higgs VEV corresponds to the constant field configuration that minimizes the effective potential. This potential contains not only the classical (tree-level) contribution, but also loop corrections introduced by quantum effects of all the particles that couple to the Higgs, including the Higgs self-interactions [12]. More relevant from the point of view of the present paper is the fact that these quantum corrections are sensitive to the spacetime geometry. The aim of this work is precisely to start the study of the Higgs one-loop effective potential in weak and slowly varying gravitational backgrounds. For simplicity and as a first step, we limit ourselves to the contributions of the Higgs self-interactions. The fact that we assume weak gravitational backgrounds, i.e., whose curvature scale is much smaller than the Higgs mass, allows us to use an adiabatic approximation and avoid the problems generated by mode mixing and particle production typical of quantum field theory in curved spacetime. For the same reason, we can still define an effective quasi-potential [13,14] instead of using the full effective action since all the kinetic terms are suppressed with respect to the potential ones.

Our work deals with the calculation of vacuum expectation values of quadratic operators in curved spacetime [15,16]. These are divergent objects whose renormalization requires the introduction of additional counterterms depending on the curvature tensors. Different techniques have been used in the literature to work out these divergences which, because of the fact that they are determined by the short-distance physics, depend locally on the geometry of spacetime [17–26]. But, apart from the local divergent contributions, there are also finite nonlocal terms which are sensitive to the large-scale structure of the manifold and, in general, depend on the quantum state on which the expectation value is evaluated. In some particular simple geometries, such as conformally flat metrics, these finite contributions can be exactly computed in some cases from the knowledge of the trace anomaly, but in general only brute force methods, such as mode summation, are available to evaluate them [27–30]. This is precisely the approach we follow in this work. In particular, we extend the analysis performed in [31] to arbitrary dimension in order to calculate the integrals over the quantum modes using dimensional regularization. Several errors in [31] are also corrected in the present paper.

The work is organized as follows: in Sec. II, the effective action formalism is briefly reviewed. The field quantization in arbitrary $D+1$ dimensions in the adiabatic approximation is discussed in Sec. III. Section IV contains the full mode solutions to first order in metric perturbations. The general results for the Higgs effective potential and the method used to obtain them are described in Sec. V. The vacuum expectation value of the energy-momentum tensor is calculated in Sec. VI. The paper ends in Sec. VII with some discussions and conclusions.

II. ONE-LOOP EFFECTIVE ACTION

The classical action for a minimally coupled real scalar field with potential $V(\phi)$ in arbitrary $(D+1)$-dimensional curved spacetime reads

$$S[\phi, g_{\mu\nu}] = \int \mathrm{d}^{D+1}x\sqrt{g}\left(\frac{1}{2}g^{\mu\nu}\partial_\mu\phi\partial_\nu\phi - V(\phi)\right). \quad (1)$$

In the case of the real Higgs field, the classical potential is given by

$$V(\phi) = V_0 + \frac{1}{2}M^2\phi^2 + \frac{\lambda}{4}\phi^4 \quad (2)$$

with $M^2 < 0$. The minimum corresponds to $\phi = v$ with $v^2 = -M^2/\lambda$. The mass of the Higgs boson at tree-level is given by $m_H^2 = V''(v) = -2M^2$ and from the recently measured value of m_H at the LHC, the Higgs self-coupling is $\lambda \simeq 1/8$.

The action is minimized by the solutions $\phi = \hat{\phi}$ of the classical equation of motion:

$$\Box\hat{\phi} + V'(\hat{\phi}) = 0. \quad (3)$$

The quantum fluctuations around the classical solution $\delta\phi = \phi - \hat{\phi}$ satisfy the equation of motion

$$(\Box + m^2(\hat{\phi}))\delta\phi = 0 \quad (4)$$

with

$$m^2(\hat{\phi}) = V''(\hat{\phi}) = M^2 + 3\lambda\hat{\phi}^2. \quad (5)$$

The effective action which takes into account the effect of quantum fluctuations on the dynamics of the classical field can be written as

$$W[\hat{\phi}, g_{\mu\nu}] = \int \mathrm{d}^{D+1}x\sqrt{g}L_{\mathrm{eff}} \quad (6)$$

which can be expanded up to one-loop order as

$$W[\hat{\phi}, g_{\mu\nu}] = S[\hat{\phi}, g_{\mu\nu}] + W^{(1)}[\hat{\phi}, g_{\mu\nu}]. \quad (7)$$

The one-loop correction $W^{(1)}$ can be written as [21]

$$W^{(1)}[\hat{\phi}, g_{\mu\nu}] = \frac{i}{2}\ln\det(-K) = \frac{i}{2}\mathrm{Tr}\ln(-K) \quad (8)$$

where Tr denotes the functional trace and K is the quadratic operator associated to the quantum fluctuations

$$K(x,y) = (\Box_x + m^2(\hat{\phi}))\frac{\delta^{D+1}(x,y)}{\sqrt{g}}. \quad (9)$$

The corresponding Feynman's Green function

$$iG_F(x,y) = \langle 0|T(\delta\phi(x)\delta\phi(y))|0\rangle \quad (10)$$

satisfies

$$K(x,y)G_F(y,z) = -\frac{\delta^{D+1}(x,z)}{\sqrt{g}} \tag{11}$$

where the de Witt repeated indices rule has been assumed.

Following [32,33], let us consider the derivative of the one-loop effective action with respect to the mass parameter m^2, so that from (11) we can write

$$\frac{\mathrm{d}W^{(1)}}{\mathrm{d}m^2} = -\frac{i}{2}\mathrm{Tr}G_F \tag{12}$$

or writing the trace explicitly

$$\begin{aligned}\frac{\mathrm{d}W^{(1)}}{\mathrm{d}m^2} &= -\frac{1}{2}\int \mathrm{d}^{D+1}x\sqrt{g}iG_F(x,x) \\ &= -\frac{1}{2}\int \mathrm{d}^{D+1}x\sqrt{g}\langle 0|\delta\phi^2(x)|0\rangle. \end{aligned}\tag{13}$$

Thus, we can finally get a formal expression for the one-loop contribution to the effective Lagrangian as

$$L^{(1)}_{\mathrm{eff}}(x) = -\frac{1}{2}\int_0^{m^2(\hat{\phi})} \mathrm{d}m^2\langle 0|\delta\phi^2(x)|0\rangle. \tag{14}$$

In general, in a static homogeneous spacetime, $\hat{\phi}$ is a constant field and the effective Lagrangian defines the effective potential $V_1(\hat{\phi}) = -L^{(1)}_{\mathrm{eff}}(\hat{\phi})$. In time-dependent or inhomogeneous spacetimes, $\hat{\phi}$ changes in time or space and the effective potential is ill defined. In this case, the effective Lagrangian is a function of the classical fields; i.e., it will, in general, depend on $\hat{\phi}$ and $g_{\mu\nu}$ and arbitrary order derivatives,

$$L_{\mathrm{eff}} = L_{\mathrm{eff}}[\hat{\phi}, g_{\mu\nu}, \partial\hat{\phi}, \partial^2\hat{\phi}, \partial g_{\mu\nu}, \partial^2 g_{\mu\nu}, \ldots]. \tag{15}$$

However, in the case in which the background fields $(\hat{\phi}, g_{\mu\nu})$ evolve very slowly in space and time compared to the evolution of the fluctuations, the derivative terms in the effective Lagrangian are negligible, and the effective Lagrangian can be considered as an effective quasipotential [13,14]. As we will explicitly show in the next section, this is indeed the case for Higgs fluctuations in weak gravitational backgrounds so that we can still define the one-loop effective potential as

$$V_{\mathrm{eff}}(\hat{\phi}) = V(\hat{\phi}) + V_1(\hat{\phi}), \tag{16}$$

where

$$V_1(\hat{\phi}) = -L^{(1)}_{\mathrm{eff}}(\hat{\phi}) = \frac{1}{2}\int_0^{m^2(\hat{\phi})} \mathrm{d}m^2\langle 0|\delta\phi^2|0\rangle. \tag{17}$$

The equation of motion for the classical field, thus, reduces to

$$V'_{\mathrm{eff}}(\hat{\phi}) \simeq 0; \tag{18}$$

i.e., the effective (quasi)potential correctly determines the VEV for a slowly varying background metric.

The central object in this calculation is the vacuum expectation value of a quadratic operator (14). The standard Schwinger–de Witt representation [15,16] allows us to obtain a local expansion of G_F in curvatures over the mass parameter m^2. However, as mentioned before, this representation does not provide the full nonlocal finite contributions of the effective action in which we are interested in this work. Thus we will follow [15] and evaluate the expectation value from the explicit mode expansion of the quantum fields.

III. QUANTIZATION AND ADIABATIC APPROXIMATION

We will consider quantum fluctuations of the Higgs field in a $(D+1)$-dimensional spacetime metric which can be written as a scalar perturbation around a flat Robertson-Walker background

$$\mathrm{d}s^2 = a^2(\eta)\{[1+2\Phi(\eta,\mathbf{x})]\mathrm{d}\eta^2 - [1-2\Psi(\eta,\mathbf{x})]\mathrm{d}\mathbf{x}^2\}, \tag{19}$$

where η is the conformal time, $a(\eta)$ the scale factor, and Φ and Ψ are the scalar perturbations in the longitudinal gauge. This metric describes the spacetime geometry in cosmological contexts with density perturbations, but also, in the $a(\eta) = 1$ case, it provides a good description of weak gravitational fields generated by slowly rotating astrophysical objects like the Sun.

Up to first order in metric perturbations, Eq. (4) for the fluctuation field $\delta\phi$ reads

$$\begin{aligned}&\delta\phi'' + [(D-1)\mathcal{H} - \Phi' - D\Psi']\delta\phi' - [1+2(\Phi+\Psi)]\nabla^2\delta\phi \\ &\quad - \boldsymbol{\nabla}\delta\phi\cdot\boldsymbol{\nabla}[\Phi - (D-2)\Psi] + a^2(1+2\Phi)m^2(\hat{\phi})\delta\phi = 0,\end{aligned} \tag{20}$$

where $\mathcal{H} = a'/a$ is the comoving Hubble parameter.

In order to evaluate $V_1(\hat{\phi})$, we need to quantize the fluctuation field. Because of the inhomogeneities of the metric tensor, exact solutions for the perturbed Eq. (20) are not expected to be found. Nevertheless, a perturbative expansion of the solution in powers of metric perturbations can be obtained. Moreover, when the mode frequency ω is larger than the typical temporal or spatial frequency of the background metric, i.e., $\omega^2 \gg \mathcal{H}^2$ and $\omega^2 \gg \{\nabla^2\Phi, \nabla^2\Psi\}$, one can consider an adiabatic approximation in order to quantize the field fluctuations $\delta\phi$. Since $\omega \geq m_H$, the

adiabatic approximation is extremely good during the whole matter and acceleration eras until present, and also during most of the radiation era, for all cosmological and astrophysical scales of interest.

Let us start with the canonical quantization procedure for the field perturbations $\delta\phi$. Thus, following [34,35], we build a complete set of mode solutions for (20), which are orthonormal with respect to the standard scalar product in curved spacetime [15],

$$(\delta\phi_k, \delta\phi_{k'}) = i\int_\Sigma [\delta\phi^*_{k'}(\partial_\mu\delta\phi_k) - (\partial_\mu\delta\phi^*_{k'})\delta\phi_k]\sqrt{g_\Sigma}\mathrm{d}\Sigma^\mu, \tag{21}$$

with $\mathrm{d}\Sigma^\mu = n^\mu \mathrm{d}\Sigma$. Here n^μ is a unit timelike vector directed to the future and orthogonal to the $\eta =$ const hypersurface Σ, i.e.,

$$\mathrm{d}\Sigma^\mu = \mathrm{d}^D\mathbf{x}\left(\frac{1-\Phi}{a}, \mathbf{0}\right), \tag{22}$$

whereas the determinant of the metric on the spatial hypersurface reads to first order in metric perturbations

$$\sqrt{g_\Sigma} = a^D(1 - D\Psi). \tag{23}$$

With this definition, the scalar product is independent on the choice of spatial hypersurface Σ.

In terms of orthonormal modes,

$$(\delta\phi_k, \delta\phi_{k'}) = \delta^D(\mathbf{k} - \mathbf{k}'), \tag{24}$$

the fluctuation field $\delta\phi$ can be expanded as

$$\delta\phi(\eta, \mathbf{x}) = \int \mathrm{d}^D\mathbf{k}[a_\mathbf{k}\delta\phi_k(\eta, \mathbf{x}) + a^\dagger_\mathbf{k}\delta\phi^*_k(\eta, \mathbf{x})]. \tag{25}$$

The corresponding creation and annihilation operators satisfy the standard commutation relations

$$[a_\mathbf{k}, a^\dagger_{\mathbf{k}'}] = \delta^D(\mathbf{k} - \mathbf{k}') \tag{26}$$

and the vacuum state associated to the quantum modes $\{\delta\phi_k\}$ is defined as usual by $a_\mathbf{k}|0\rangle = 0\ \forall\mathbf{k}$.

In order to construct the orthonormal set, we use a WKB ansatz,

$$\delta\phi_k(\eta, \mathbf{x}) = f_k(\eta, \mathbf{x})e^{i\theta_k(\eta,\mathbf{x})}, \tag{27}$$

and assume that $f_k(\eta, \mathbf{x})$ evolves slowly in space and time, whereas the evolution of $\theta_k(\eta, \mathbf{x})$ is rapid. In general, as mentioned above, such an adiabatic ansatz works whenever the Compton wavelength of the field perturbation is much smaller than the typical astrophysical or cosmological scales involved. In particular, in the adiabatic expansion we assume $\partial\theta \sim ma$ and $\partial f \sim \mathcal{H}f$.

Substituting (27) in (20), we obtain to the leading adiabatic order $\mathcal{O}((\partial\theta)^2)$

$$-\theta'^2_k + [1 + 2(\Phi + \Psi)](\boldsymbol{\nabla}\theta_k)^2 + m^2a^2(1 + 2\Phi) = 0 \tag{28}$$

and to the next-to-leading order $\mathcal{O}(\partial\theta)$

$$\begin{aligned} &f_k\theta''_k + 2f'_k\theta'_k + [(D-1)\mathcal{H} - \Phi' - D\Psi']f_k\theta'_k \\ &\quad - f_k\nabla^2\theta_k - 2\boldsymbol{\nabla}f_k\cdot\boldsymbol{\nabla}\theta_k \\ &\quad - f_k\boldsymbol{\nabla}\theta_k\cdot\boldsymbol{\nabla}[\Phi - (D-2)\Psi] = 0. \end{aligned} \tag{29}$$

Notice that $\partial^2\theta \sim \mathcal{H}\partial\theta$ and that, in the adiabatic expansion, $\mathcal{H} \sim \partial\Phi$.

IV. PERTURBATIVE EXPANSION AND MODE SOLUTIONS

To solve these two equations, (28) and (29), we look for a perturbative expansion in the metric potentials. To obtain the lowest-order solution; i.e., in the absence of metric perturbations, we write (20) in the limit $\Phi = \Psi = 0$ and get

$$\delta\phi^{(0)\prime\prime} + (D-1)\mathcal{H}\delta\phi^{(0)\prime} - \nabla^2\delta\phi^{(0)} + a^2m^2(\hat{\phi})\delta\phi^{(0)} = 0, \tag{30}$$

where $a^2m^2(\hat{\phi})$ only depends on time. Fourier transforming the spatial coordinates, the following positive frequency solution with momentum $\mathbf{k}$ is obtained

$$\delta\phi^{(0)}_k(\eta, \mathbf{x}) = F_k(\eta)e^{i\mathbf{k}\cdot\mathbf{x} - i\int^\eta \omega_k(\eta')\mathrm{d}\eta'} \tag{31}$$

with

$$\omega^2_k = k^2 + m^2a^2 \tag{32}$$

and

$$F_k(\eta) = \frac{1}{(2\pi)^{D/2}}\frac{1}{a^{(D-1)/2}\sqrt{2\omega_k}}, \tag{33}$$

which is fixed by the normalization condition (24).

Once the unperturbed solution is known, we can look for the first-order corrections. Thus, the amplitude and phase of (27) are expanded in metric perturbations as follows

$$\begin{aligned} f_k(\eta, \mathbf{x}) &= F_k(\eta) + \delta f_k(\eta, \mathbf{x}) \\ \theta_k(\eta, \mathbf{x}) &= \mathbf{k}\cdot\mathbf{x} - \int^\eta \omega_k(\eta')\mathrm{d}\eta' + \delta\theta_k(\eta, \mathbf{x}) \end{aligned} \tag{34}$$

where δf_k and $\delta\theta_k$ are first order in perturbations. Substituting (35) in the leading equation (28), we obtain

(32) to the lowest order as expected, and to first order we get

$$\omega_k \delta\theta_k' + \mathbf{k}\cdot\boldsymbol{\nabla}\delta\theta_k + k^2(\Phi+\Psi) + m^2a^2\Phi = 0. \quad (35)$$

On the other hand, by substituting in the next-to-leading equation (30), we recover (33) to the lowest perturbative order, whereas to first order we get

$$\begin{aligned} &F_k\delta\theta_k'' + 2F_k'\delta\theta_k' + (D-1)\mathcal{H}F_k\delta\theta_k' - F_k\nabla^2\delta\theta_k \\ &\quad - 2\omega_k\delta f_k' - 2\mathbf{k}\cdot\boldsymbol{\nabla}\delta f_k - (D-1)\omega_k\mathcal{H}\delta f_k - \omega_k'\delta f_k \\ &\quad + \omega_k F_k\Phi' + D\omega_k F_k\Psi' - F_k\mathbf{k}\cdot\boldsymbol{\nabla}[\Phi - (D-2)\Psi] = 0. \end{aligned} \quad (36)$$

The two new equations (35) and (36) can also be solved by performing an additional Fourier transformation in the spatial coordinates since the equations coefficients only depend on time.

A. Phase solution $\delta\theta_k$

Equation (35) in Fourier space reads

$$\delta\theta_k'(\eta,\mathbf{p}) + i\frac{\mathbf{k}\cdot\mathbf{p}}{\omega_k}\delta\theta_k(\eta,\mathbf{p}) = -\omega_k\left[\Phi(\eta,\mathbf{p}) + \frac{k^2}{\omega_k^2}\Psi(\eta,\mathbf{p})\right], \quad (37)$$

where

$$\delta\theta_k(\eta,\mathbf{p}) = \frac{1}{(2\pi)^{3/2}}\int \mathrm{d}^3\mathbf{x}\,\delta\theta_k(\eta,\mathbf{x})e^{-i\mathbf{p}\cdot\mathbf{x}} \quad (38)$$

and analogous definitions apply for $\Phi(\eta,\mathbf{p})$, $\Psi(\eta,\mathbf{p})$ and $\delta f_k(\eta,\mathbf{p})$.[2] Defining

$$\begin{aligned} \beta_k(\eta_f,\eta_i) &= \int_{\eta_i}^{\eta_f}\frac{\mathrm{d}\eta'}{\omega_k(\eta')} \\ G_k(\eta,\mathbf{p}) &= -\omega_k\left[\Phi(\eta,\mathbf{p}) + \frac{k^2}{\omega_k^2}\Psi(\eta,\mathbf{p})\right], \end{aligned} \quad (39)$$

the solution of (37) is

$$\delta\theta_k(\eta,\mathbf{p}) = \int_0^\eta e^{-i\mathbf{k}\cdot\mathbf{p}\beta_k(\eta,\eta')}G_k(\eta',\mathbf{p})\mathrm{d}\eta' + e^{-i\mathbf{k}\cdot\mathbf{p}\beta_k(\eta,0)}\delta\theta_k(0,\mathbf{p}). \quad (40)$$

The term $\delta\theta_k(0,\mathbf{p})$ stands for the initial boundary condition of the modes or, equivalently, the phase difference of the modes at the initial time. In principle, $\delta\theta_k(0,\mathbf{p})$ is not completely arbitrary since the orthonormalization condition of the modes (24) may constrain its functional dependence. We discuss this point at the end of this section.

[2]In the following, the wave vector of the quantum modes is denoted by $\mathbf{k}$, and $\mathbf{p}$ is used for that of metric perturbations.

B. Amplitude solution δf_k

Let us write

$$\delta f_k(\eta,\mathbf{p}) = F_k(\eta)P_k(\eta,\mathbf{p}) \quad (41)$$

and following a similar procedure with the next-to-leading-order equation (36), it can be rewritten in Fourier space as

$$P_k'(\eta,\mathbf{p}) + i\frac{\mathbf{k}\cdot\mathbf{p}}{\omega_k}P_k(\eta,\mathbf{p}) = \frac{H_k(\eta,\mathbf{p})}{2\omega_k}, \quad (42)$$

where

$$H_k(\eta,\mathbf{p}) = \omega_k Q_k'(\eta,\mathbf{p}) + T_k(\eta,\mathbf{p}) \quad (43)$$

with

$$Q_k(\eta,\mathbf{p}) = -i\frac{\mathbf{k}\cdot\mathbf{p}}{\omega_k^2}\delta\theta_k(\eta,\mathbf{p}) + \left[D - \frac{k^2}{\omega_k^2}\right]\Psi(\eta,\mathbf{p}) \quad (44)$$

and

$$\begin{aligned} T_k(\eta,\mathbf{p}) &= p^2\delta\theta_k(\eta,\mathbf{p}) \\ &\quad - i\mathbf{k}\cdot\mathbf{p}[\Phi(\eta,\mathbf{p}) - (D-2)\Psi(\eta,\mathbf{p})]. \end{aligned} \quad (45)$$

The corresponding solution is given by

$$P_k(\eta,\mathbf{p}) = \int_0^\eta e^{-i\mathbf{k}\cdot\mathbf{p}\beta_k(\eta,\eta')}\frac{H_k(\eta',\mathbf{p})}{2\omega_k(\eta')}\mathrm{d}\eta' + e^{-i\mathbf{k}\cdot\mathbf{p}\beta_k(\eta,0)}P_k(0,\mathbf{p}). \quad (46)$$

The integration constant $P_k(0,\mathbf{p})$ is fixed by the normalization condition (24).

1. Time-independent gravitational potentials

For simplicity, in the rest of the work we focus on time-independent gravitational potentials. This case encompasses super-Hubble modes in both matter and radiation era, and also sub-Hubble modes in the matter era. This is also a good approximation to describe the gravitational potentials in the Solar System. In such a case, the constants $P_k(0,\mathbf{p})$ are given by

$$P_k(0,\mathbf{p}) = \frac{1}{2}\left(D - \frac{k^2}{\omega_k(0)^2}\right)\Psi(\mathbf{p}). \quad (47)$$

Integrating by parts in (46), the integration constant can be eliminated and the following expression is obtained:

$$P_k(\eta,\mathbf{p}) = \frac{1}{2}Q_k(\eta,\mathbf{p}) - i\int_0^\eta \left\{\frac{\mathbf{k}\cdot\mathbf{p}}{2\omega_k(\eta')}e^{-i\mathbf{k}\cdot\mathbf{p}\beta_k(\eta,\eta')} \times \left[Q_k(\eta',\mathbf{p}) + \frac{T_k(\eta',\mathbf{p})}{\mathbf{k}\cdot\mathbf{p}}\right]\right\}\mathrm{d}\eta'. \quad (48)$$

There are three types of contributions to P_k, depending on the number of time integrals involved. Thus, we can write

$$P_k(\eta,\mathbf{p}) = P_k^{(0)}(\eta,\mathbf{p}) + P_k^{(1)}(\eta,\mathbf{p}) + P_k^{(2)}(\eta,\mathbf{p}) \quad (49)$$

where

$$P_k^{(0)}(\eta,\mathbf{p}) = \frac{1}{2}\left(D - \frac{k^2}{\omega_k(\eta)^2}\right)\Psi(\mathbf{p}) \quad (50)$$

$$P_k^{(1)}(\eta,\mathbf{p}) = \int_0^\eta e^{-i\mathbf{k}\cdot\mathbf{p}\beta_k(\eta,\eta')}N_k^{(1)}(\eta,\eta',\mathbf{p})\mathrm{d}\eta' \quad (51)$$

$$P_k^{(2)}(\eta,\mathbf{p}) = \int_0^\eta\int_0^{\eta'} e^{-i\mathbf{k}\cdot\mathbf{p}\beta_k(\eta,\eta'')}N_k^{(2)}(\eta',\eta'',\mathbf{p})\mathrm{d}\eta''\mathrm{d}\eta' \quad (52)$$

with

$$N_k^{(1)}(\eta,\eta',\mathbf{p}) = \frac{i\mathbf{k}\cdot\mathbf{p}}{2\omega_k^2(\eta)\omega_k(\eta')}\left\{[\omega_k^2(\eta')-\omega_k^2(\eta)]\Phi(\mathbf{p}) + \left[k^2+\omega_k^2(\eta)\left(\frac{k^2}{\omega_k^2(\eta')}-2\right)\right]\Psi(\mathbf{p})\right\} \quad (53)$$

$$N_k^{(2)}(\eta',\eta'',\mathbf{p}) = \frac{(\mathbf{k}\cdot\mathbf{p})^2 - p^2\omega_k^2(\eta')}{2\omega_k^3(\eta')\omega_k(\eta'')} \times [\omega_k^2(\eta'')\Phi(\mathbf{p}) + k^2\Psi(\mathbf{p})] \quad (54)$$

where $p = |\mathbf{p}|$.

C. Orthonormalization condition

In order to quantize the field canonically, we must check that the modes $\delta\phi_k$ used to define the creation and annihilation operators are orthonormal (24). This may restrict the functional dependence of the initial conditions of our solution, i.e., $P_k(0,\mathbf{p})$ and $\delta\theta_k(0,\mathbf{p})$.[3] We already fixed $P_k(0,\mathbf{p})$ when imposing the correct normalization of the modes; hence, we can only play with $\delta\theta_k(0,\mathbf{p})$ to have orthogonal modes. The scalar product (21) can be computed using (27), (35), (40), and (46) to get

$$(\delta\phi_k,\delta\phi_{k'}) = \delta^D(\mathbf{k}-\mathbf{k}') + \tau_\Psi(\mathbf{k},\mathbf{k}') + \tau_{\delta\theta}(\mathbf{k},\mathbf{k}'), \quad (55)$$

where $\tau_{\Psi,\delta\theta}$ are first order in metric perturbation. The explicit expressions for $\tau_{\Psi,\delta\theta}$ are given in Appendix A. In this appendix it is shown that they are zero for $\forall\mathbf{k},\mathbf{k}'$ up to corrections beyond the leading adiabatic order for slowly varying gravitational fields. This result does not impose any restriction on the functional dependence of $\delta\theta_k(0,\mathbf{p})$.

Different initial conditions $\delta\theta_k(0,\mathbf{p})$ amount to different definitions of the vacuum. The discussion above guarantees that the modes given by (27), (35), (40), (46), are orthonormal for any choice of the vacuum. In the following we take $\delta\theta_k(0,\mathbf{p}) = 0$ as the initial condition for the modes.

V. HIGGS EFFECTIVE POTENTIAL

Once we have the expressions for the mode solutions of the perturbative equations, namely (40) and (41) [together with (46)]; we can proceed to calculate the one-loop contribution to the effective potential (17).

Let us first calculate $\langle 0|\delta\phi^2(\eta,\mathbf{x})|0\rangle$ to first order in metric perturbations. Because of the inhomogeneity of the background, this quantity depends on $(\eta,\mathbf{x})$ as follows

$$\langle 0|\delta\phi^2(\eta,\mathbf{x})|0\rangle = \langle\delta\phi^2\rangle_{\mathrm{h}}(\eta) + \langle\delta\phi^2\rangle_{\mathrm{i}}(\eta,\mathbf{x}) \quad (56)$$

where

$$\langle\delta\phi^2\rangle_{\mathrm{h}}(\eta) = \int \mathrm{d}^D\mathbf{k}F_k^2(\eta) \quad (57)$$

and

$$\langle\delta\phi^2\rangle_{\mathrm{i}}(\eta,\mathbf{x}) = 2\int \mathrm{d}^D\mathbf{k}F_k^2(\eta)[\mathrm{Re}P_k(\eta,\mathbf{x}) - \mathrm{Im}\delta\theta_k(\eta,\mathbf{x})]. \quad (58)$$

A. Homogeneous contribution $\langle\delta\phi^2\rangle_{\mathrm{h}}$

The homogeneous contribution $\langle\delta\phi^2\rangle_{\mathrm{h}}$ reads

$$\langle\delta\phi^2\rangle_{\mathrm{h}}(\eta) = \frac{1}{2(2\pi)^D a^{D-1}(\eta)}\int\frac{\mathrm{d}^D\mathbf{k}}{\sqrt{k^2+m^2a^2(\eta)}} = \frac{1}{2(2\pi)^D a^{D-1}(\eta)}\frac{2\pi^{D/2}}{\Gamma(D/2)}\int_0^\infty\frac{\mathrm{d}k k^{D-1}}{\sqrt{k^2+m^2a^2(\eta)}} \quad (59)$$

which is analogous to the Minkowskian result, except for the scale-factor dependence.

B. Nonhomogeneous contribution $\langle\delta\phi^2\rangle_{\mathrm{i}}$

The inhomogeneous component $\langle\delta\phi^2\rangle_{\mathrm{i}}$ can be dealt with more easily in momentum space. The only angular dependence of the quantum fluctuation wave vector $\mathbf{k}$

[3] $P_k(0,\mathbf{x})$ and $\delta\theta_k(0,\mathbf{x})$ are assumed to be real. If this were not the case, the phase of $P_k(0,\mathbf{x})$ could be absorbed into $\delta\theta_k(0,\mathbf{x})$ and the imaginary part of $\delta\theta_k(0,\mathbf{x})$ could also be absorbed into $P_k(0,\mathbf{x})$ in a trivial way.

enters as $\mathbf{k}\cdot\mathbf{p} = kp\hat{x}$ with $\hat{x} = \cos\theta$, where we have taken the k_z direction along $\mathbf{p}$. On the other hand, the contribution from $\delta\theta$ in (58) vanishes after integrating in $\hat{x}$. Then, we have

$$\langle\delta\phi^2\rangle_{\rm i}(\eta,\mathbf{p}) = \frac{1}{(2\pi)^D a^{D-1}(\eta)}\int \mathrm{d}^D\mathbf{k}\,\frac{P_k(\eta,\mathbf{p})}{\sqrt{k^2+m^2a^2(\eta)}}. \tag{60}$$

Since the integration on $\hat{x}$ can be performed in a straightforward way, let us define

$$\hat{P}_k(\eta,\mathbf{p}) = \int_{-1}^{1}\mathrm{d}\hat{x}(1-\hat{x}^2)^{(D-3)/2}P_k(\eta,\mathbf{p}), \tag{61}$$

where we have included the general integration measure in D dimensions. Hence, we can write (see Appendix B)

$$\langle\delta\phi^2\rangle_{\rm i}(\eta,\mathbf{p}) = \frac{1}{(2\pi)^D a^{D-1}(\eta)}\frac{2\pi^{(D-1)/2}}{\Gamma((D-1)/2)} \times\int_0^\infty \mathrm{d}k\,\frac{k^{D-1}\hat{P}_k(\eta,\mathbf{p})}{\sqrt{k^2+m^2a^2(\eta)}}. \tag{62}$$

Both integrals (60) and (62) are divergent in $D=3$ dimensions, and they should be regularized as discussed in the next section.

C. Regularization

Let us now discuss the regularization procedure based on standard dimensional regularization techniques.

1. Regularized homogeneous contribution $\langle\delta\phi^2\rangle_{\rm h}(\eta)$

The momentum integral in $\langle\delta\phi^2\rangle_{\rm h}$ (60) can be done using (B3) of Appendix B. After expanding for small ϵ with $D = 3-\epsilon$ dimensions, the final result is

$$\langle\delta\phi^2\rangle_{\rm h}(\eta) = \frac{m^2(\hat{\phi})}{16\pi^2}\left[\ln\left(\frac{m^2(\hat{\phi})}{\mu^2}\right) - N_\epsilon - \frac{3}{2}\right], \tag{63}$$

where μ is the renormalization scale and

$$N_\epsilon = \frac{2}{\epsilon} + \log 4\pi - \gamma \tag{64}$$

with γ the Euler-Mascheroni constant.

2. Regularized nonhomogeneous contribution $\langle\delta\phi^2\rangle_{\rm i}(\eta,\mathbf{x})$

Let us now consider the inhomogeneous contribution (62). We cannot apply directly standard dimensional regularization formulas because of the nontrivial k dependence of $\hat{P}_k(\eta,\mathbf{p})$. Thus, additional work is necessary.

First, it should be noticed that the dependence of $\hat{P}_k(\eta,\mathbf{p})$ on the direction of $\mathbf{p}$ only enters through the potentials, $\Phi(\mathbf{p})$ and $\Psi(\mathbf{p})$. Therefore, it can be expanded in the following way:

$$\hat{P}_k(\eta,\mathbf{p}) = \left[\sum_{l=0}^{\infty}P^{\Phi}_{k,l}(\eta)p^{2l}\right]\Phi(\mathbf{p}) + \left[\sum_{l=0}^{\infty}P^{\Psi}_{k,l}(\eta)p^{2l}\right]\Psi(\mathbf{p}). \tag{65}$$

The coefficients $P^{\{\Phi,\Psi\}}_{k,l}(\eta)$ are given in Appendix C. The $l=0$ terms only get contributions from the $P^{(0)}_k(\eta,\mathbf{p})$ term given in (50), and its integral vanishes in dimensional regularization. The $l>0$ terms involve time integrals of the form

$$\int_0^\eta \mathrm{d}\eta'\left(\prod_{i=1}^{2l-1}\int_{\eta'}^{\eta}\frac{\mathrm{d}\eta_i}{\omega_k(\eta_i)}\right)\frac{k^{2\alpha}}{\omega_k(\eta)^a\omega_k(\eta')^b} \tag{66}$$

for the contributions coming from $P^{(1)}_k(\eta,\mathbf{p})$ in (51), and

$$\int_0^\eta \mathrm{d}\eta'\int_0^{\eta'}\mathrm{d}\eta''\left(\prod_{i=1}^{2l-2}\int_{\eta''}^{\eta}\frac{\mathrm{d}\eta_i}{\omega_k(\eta_i)}\right)\frac{k^{2\alpha}}{\omega_k(\eta)^a\omega_k(\eta')^b\omega_k(\eta'')^c} \tag{67}$$

for those coming from $P^{(2)}_k(\eta,\mathbf{p})$ in (52), with α, a, b, $c\in\mathbb{Z}$. In order to simplify the functional dependence on k, we apply the generalized Feynman trick,

$$\frac{1}{A_1^{d_1}\cdots A_n^{d_n}} = \frac{\Gamma(d_1+\cdots+d_n)}{\Gamma(d_1)\cdots\Gamma(d_n)} \times\int_0^1\mathrm{d}x_1\cdots\int_0^1\mathrm{d}x_n\times\delta(x_1+\ldots+x_n-1) \times\frac{x_1^{d_1-1}\cdots x_n^{d_n-1}}{(x_1A_1+\cdots+x_nA_n)^{d_1+\cdots+d_n}}. \tag{68}$$

Then, let the parameters of the Feynman formula be defined by

$$n = 2l+1 \tag{69}$$

$$A_j = \begin{cases}\omega_k^2(\eta) & \text{if } j=1\\ \omega_k^2(\eta') & \text{if } j=2\\ \omega_k^2(\eta_{j-2}) & \text{if } 3\le j\le 2l+1\end{cases} \tag{70}$$

$$d_j = \begin{cases}a/2 & \text{if } j=1\\ b/2 & \text{if } j=2\\ 1/2 & \text{if } 3\le j\le 2l+1\end{cases} \tag{71}$$

for the case (66) [with a trivial modification for the expression (67)]. In this way, the k dependence only

appears in $\sum_{i=1}^{2l+1} x_i \omega_{k,i}^2$ which can be simplified in the following way,

$$\sum_{i=1}^{2l+1} x_i \omega_{k,i}^2 = \sum_{i=1}^{2l+1} x_i (k^2 + m^2 a_i^2) = k^2 + m^2 \sum_{i=1}^{2l+1} x_i a_i^2, \tag{72}$$

where we have used $\sum_{i=1}^{2l+1} x_i = 1$. Now, the k dependence is simple enough to use standard dimensional regularization formulas (Appendix B). The integration over the $\{x_i\}$ and the time integrals can be performed analytically (Appendix D).

As we did with $\hat{P}_k(\eta, \mathbf{p})$, we now decompose $\langle \delta\phi^2 \rangle_{\rm i}(\eta, \mathbf{p})$ into two terms proportional to $\Phi(\mathbf{p})$ and $\Psi(\mathbf{p})$, respectively,

$$\langle \delta\phi^2 \rangle_{\rm i}(\eta, \mathbf{p}) = \langle \delta\phi^2 \rangle_{\rm i}^{\Phi}(\eta, \mathbf{p}) \Phi(\mathbf{p}) + \langle \delta\phi^2 \rangle_{\rm i}^{\Psi}(\eta, \mathbf{p}) \Psi(\mathbf{p}). \tag{73}$$

Then, integrating in dimensional regularization, we see that the $\mathcal{O}(1/\epsilon)$ terms cancel out, and the results are finite,

$$\langle \delta\phi^2 \rangle_{\rm i}^{\{\Phi,\Psi\}}(\eta, \mathbf{p}) = \frac{m^2}{4\pi^2 a^2(\eta)} \left[\sum_{l=1}^{\infty} R_l^{\{\Phi,\Psi\}}(\eta) p^{2l} \right], \tag{74}$$

where $R_l^{\{\Phi,\Psi\}}$ are the already regularized integrals in k of $P_{k,l}^{\{\Phi,\Psi\}}$ divided by m^2 for convenience. The coefficients $R_l^{\{\Phi,\Psi\}}$ can be written as

$$R_l^{\{\Phi,\Psi\}}(\eta) = R_{l,\rm pol}^{\{\Phi,\Psi\}}(\eta) + R_{l,\log}^{\{\Phi,\Psi\}}(\eta), \tag{75}$$

where, as shown in Appendix D, $R_{l,\rm pol}^{\{\Phi,\Psi\}}$ are polynomials in η, and $R_{l,\log}^{\{\Phi,\Psi\}}$ involve a logarithmic dependence on η.

The most important aspect of (74) is that all the divergent parts have canceled out. In particular, the divergent terms coming from $P_k^{(1)}(\eta, \mathbf{p})$ cancel exactly the ones from $P_k^{(2)}(\eta, \mathbf{p})$ order by order in p. This means that the UV behavior is the same as in an unperturbed FRW background and the inhomogeneous contributions are finite to the leading adiabatic order.

D. Nonhomogeneous contribution: Particular cases

1. Nonexpanding spacetimes

Let us consider weak gravitational fields generated by static sources. For the corresponding spacetime metric, we can take (19) with $a(\eta) = 1$ and static potentials $\Phi(\mathbf{x})$ and $\Psi(\mathbf{x})$ which allow us to use the previous results. This simplifies the calculations in several of the steps discussed above. For instance, all the time integrals can be done in a straightforward way, there is no need to apply the Feynamn trick since the ω's are all the same, and the coefficients $R_{l,\log}^{\{\Phi,\Psi\}}$ are zero (see Appendix D).

The results for a nonexpanding geometry read

$$R_l^{\Phi}(\eta) = R_{l,\rm pol}^{\Phi}(\eta) = 0 \tag{76}$$

$$R_l^{\Psi}(\eta) = R_{l,\rm pol}^{\Psi}(\eta) = 0, \tag{77}$$

which imply

$$\langle \delta\phi^2 \rangle_{\rm i}^{\Phi}(\eta, \mathbf{p}) = 0 \tag{78}$$

$$\langle \delta\phi^2 \rangle_{\rm i}^{\Psi}(\eta, \mathbf{p}) = 0 \tag{79}$$

and

$$\langle \delta\phi^2 \rangle_{\rm i}(\eta, \mathbf{p}) = 0. \tag{80}$$

Thus, to the leading adiabatic order, the metric perturbations do not contribute to the Higgs effective potential in dimensional regularization. This is in contrast with previous results [31] using cutoff regularization, in which nonvanishing inhomogeneous contributions were obtained.

Although we have considered a particular coordinate choice in (19), corresponding to the longitudinal gauge, since in the absence of metric perturbations $V_{\rm eff}^{\rm h}(\hat{\phi})$ is a constant, the Stewart-Walker lemma [36] guarantees that the obtained effective potential is gauge invariant.

2. Expanding spacetimes: Cosmology

Now we consider the case of a perturbed expanding universe with scale factor $a(\eta)$ and constant metric perturbations $\Phi(\mathbf{x})$ and $\Psi(\mathbf{x})$. In particular, we will concentrate in the matter-dominated era, in which the metric perturbations are constant both for sub-Hubble and super-Hubble modes. In addition, we will also provide results for super-Hubble modes in the radiation era for which the metric perturbations are also constant.

For the Ψ contribution, we get for the matter and radiation eras with $a \propto \eta^2$ and $a \propto \eta$, respectively,

$$R_{l,\rm pol}^{\Psi}(\eta) = 0; \qquad R_{l,\log}^{\Psi}(\eta) = 0. \tag{81}$$

The Φ terms are harder to compute since the $R_{l,\log}^{\Phi}$ contribution is not zero, and the integration over the Feynman parameters $\{x_i\}$ and the time integrals has to be performed by Taylor expanding the logarithm (see Appendix D). An exact analytical expression can be obtained for each order of the logarithm expansion given in terms of finite sums, which can be computed numerically for practical purposes. We have checked that the relative difference between $R_{l,\rm pol}^{\Phi}$ and $R_{l,\log}^{\Phi}$ terms is $\sim 10^{-4}$ for $l = 1, 2, 3$ and $\sim 10^{-2}$ for $l = 4, 5$. Then,

$$\frac{R^{\Phi}_{l,\mathrm{pol}}(\eta)+R^{\Phi}_{l,\log}(\eta)}{R^{\Phi}_{l,\mathrm{pol}}(\eta)} \leq 10^{-2} \quad \text{for } l=1,2,3,4,5.$$

This suggests that the exact Φ contribution also may be zero, as for the Ψ terms, so that for expanding geometries as well, static perturbations do not contribute to the Higgs effective potential to the leading adiabatic order.

E. Higgs effective potential

Taking into account (17), the one-loop contribution to the effective potential can be expressed as

$$V_1(\eta,\mathbf{x}) = V_1^{\mathrm{h}}(\eta) + V_1^{\mathrm{i}}(\eta,\mathbf{x}). \tag{82}$$

Given the fact that, to the leading order, the nonhomogeneous contribution vanishes, the potential reads

$$V_1 = V_1^{\mathrm{h}}(\eta) = \frac{1}{2}\int_0^{m^2(\hat{\phi})} \mathrm{d}m^2 \langle \delta\phi^2 \rangle_{\mathrm{h}}(\eta), \tag{83}$$

and substituting (63), we get

$$V_1(\hat{\phi}) = \frac{m^4(\hat{\phi})}{64\pi^2}\left[\ln\left(\frac{m^2(\hat{\phi})}{\mu^2}\right) - N_\epsilon - \frac{3}{2}\right]. \tag{84}$$

As expected from previous works [17–26], the homogeneous contribution is constant even though the geometry is expanding. The N_ϵ term is proportional to $m^4(\hat{\phi})$, so that we have three kinds of divergences: constant, quadratic in $\hat{\phi}$ and quartic, which can be reabsorbed in the renormalization of the tree-level potential parameters V_0, M^2 and λ. This means that at the leading adiabatic order we obtain exactly the same divergences as in flat spacetime and we do not need additional counterterms to renormalize the effective potential.

Following the minimal subtraction scheme $\overline{\mathrm{MS}}$, we remove the terms proportional to N_ϵ. Thus, we are left with the complete renormalized homogeneous effective potential,

$$V_{\mathrm{eff}}(\hat{\phi}) = V_0 + \frac{1}{2}M^2\hat{\phi}^2 + \frac{\lambda}{4}\hat{\phi}^4 + \frac{m^4(\hat{\phi})}{64\pi^2}\left[\ln\left(\frac{m^2(\hat{\phi})}{\mu^2}\right) - \frac{3}{2}\right], \tag{85}$$

which agrees with the standard result in flat spacetime. Here, the physical mass M and coupling constant λ are defined at a given physical scale μ. Since the renormalized effective potential is independent of the renormalization scale μ, M^2 and the coupling constant should depend on μ according to the renormalization group equations

$$\beta(\lambda) \equiv \frac{\mathrm{d}\lambda}{\mathrm{d}(\log\mu)} = \frac{18\lambda^2}{(4\pi)^2}$$
$$\gamma_M(\lambda) \equiv \frac{\mathrm{d}(\log M^2)}{\mathrm{d}(\log\mu)} = \frac{6\lambda}{(4\pi)^2}. \tag{86}$$

VI. ENERGY-MOMENTUM TENSOR

In the previous sections, we have considered the one-loop correction to the effective potential. The complete set of perturbed modes obtained also allows us to evaluate the vacuum expectation value of the energy-momentum tensor. For the sake of completeness we will include also a possible nonminimal coupling to curvature, so that the equation for an arbitrary massive scalar field now reads

$$(\Box + m^2 + \xi R)\varphi = 0, \tag{87}$$

Notice that, to the leading adiabatic order, the curvature term is not going to modify the mode solutions found in Sec. IV; however, the energy-momentum tensor acquires new contributions. Thus,

$$\begin{aligned} T^{\mu}_{\nu} = &-\delta^{\mu}_{\nu}\left(\frac{1}{2}-2\xi\right)(g^{\rho\sigma}\partial_\rho\varphi\partial_\sigma\varphi - m^2\varphi^2) \\ &+ (1-2\xi)g^{\mu\rho}\partial_\rho\varphi\partial_\nu\varphi - 2\xi\varphi\nabla^{\mu}\nabla_\nu\varphi \\ &+ \frac{2}{D+1}\xi g^{\mu}_{\nu}(\varphi\Box\varphi + m^2\varphi^2) \\ &- \xi\left(R^{\mu}_{\nu} - \frac{1}{2}Rg^{\mu}_{\nu} + \frac{2D}{D+1}\xi R g^{\mu}_{\nu}\right)\varphi^2. \end{aligned} \tag{88}$$

Considering perturbations over a flat Robertson-Walker background (19), the vacuum expectation value of this tensor, $\langle T^{\mu}_{\nu}\rangle$, can be explicitly written to the leading adiabatic order in Fourier space as a mode sum in terms of the expansion (35) as

$$\langle T^0_0(\eta,\mathbf{p})\rangle = \rho(\eta,\mathbf{p}) = \frac{1}{(2\pi)^D}\frac{1}{a^{D+1}}\int \mathrm{d}^D\mathbf{k}\,\frac{\omega_k}{2}\left[1 + 2\frac{k^2}{\omega_k^2}\Psi(\mathbf{p}) + 2P_k(\eta,\mathbf{p}) + 2i\frac{\mathbf{k}\cdot\mathbf{p}}{\omega_k^2}\delta\theta_k(\eta,\mathbf{p}) - \frac{2\xi}{\omega_k^2}P_k''(\eta,\mathbf{p})\right] \tag{89}$$

$$\langle T^i_i(\eta,\mathbf{p})\rangle = -\,p_i(\eta,\mathbf{p}) = -\frac{1}{(2\pi)^D}\frac{1}{a^{D+1}}\int \mathrm{d}^D\mathbf{k}\left[\frac{k_i^2}{2\omega_k}(1 + 2\Psi(\mathbf{p}) + 2P_k(\eta,\mathbf{p})) + 2i\frac{k_i p_i}{2\omega_k}\delta\theta_k(\eta,\mathbf{p}) + \xi\frac{p_i^2}{\omega_k}P_k(\eta,\mathbf{p})\right] \tag{90}$$

$$\langle T^i_0(\eta,\mathbf{p})\rangle = \frac{1}{(2\pi)^D}\frac{1}{a^{D+1}}\int \mathrm{d}^D\mathbf{k}\left[\frac{k_i}{2}\left(1 + 2P_k(\eta,\mathbf{p}) + 2i\frac{\mathbf{k}\cdot\mathbf{p}}{2\omega_k^2}\delta\theta_k(\eta,\mathbf{p})\right) + \frac{i}{2}p_i\delta\theta_k(\eta,\mathbf{p}) + \xi\frac{ip_i}{\omega_k}P_k'(\eta,\mathbf{p})\right] \tag{91}$$

$$\langle T^i_j(\eta,\mathbf{p})\rangle = -\frac{1}{(2\pi)^D}\frac{1}{a^{D+1}}\int \mathrm{d}^D\mathbf{k}\left[\frac{k_i k_j}{2\omega_k}(1+2\Psi(\mathbf{p})+2P_k(\eta,\mathbf{p}))+i\frac{k_i p_j+k_j p_i}{2\omega_k}\delta\theta_k(\eta,\mathbf{p})+\xi\frac{p_i p_j}{\omega_k}P_k(\eta,\mathbf{p})\right] \tag{92}$$

$$\langle T^\mu_\mu(\eta,\mathbf{p})\rangle = \frac{1}{(2\pi)^D}\frac{1}{a^{D+1}}\int \mathrm{d}^D\mathbf{k}\left[\frac{m^2}{2\omega_k}(1+2P_k(\eta,\mathbf{p}))-\frac{\xi}{\omega_k}(P_k''(\eta,\mathbf{p})+p^2P_k(\eta,\mathbf{p}))\right]. \tag{93}$$

The integration over the quantum modes can be performed using the same methods applied above and some tricks to reduce the integrals involving the components of $\mathbf{k}$, k_i or k_ik_j, to integrals of scalar character in $\mathbf{k}$ (Appendix B). After doing that, the homogeneous part is found to be diagonal, and the energy ρ and pressure p are given in the minimal substraction scheme $\overline{\mathrm{MS}}$ by

$$\rho = -p = \frac{m^4}{64\pi^2}\left[\log\left(\frac{m^2}{\mu^2}\right)-\frac{3}{2}\right], \tag{94}$$

where μ is the renormalization physical scale.

On the other hand, much as for the effective potential, the nonhomogeneous part of the energy-momentum tensor vanishes to this order.

While classical and weak gravitational fields are not able to change the UV behavior of quantum effects, it is expected that gravity should modify the IR parts of all quantum corrections. The result presented in this work shows that, within the dimensional regularization scheme, there are no gravitational corrections arising from a perturbed FRW metric up to first order in perturbations, and to the leading order in the adiabatic expansion, to the vacuum expectation value of the energy-momentum tensor of a scalar field. Then, gravitational corrections may appear beyond the leading adiabatic order, or through nonlinear terms.

In the considered regime, namely the one in which the Hubble scale is much smaller than the mass of the quantum field, corrections beyond the zero adiabatic order are negligible and they are unlikely to belong to the experimental realm in the near future.

On the other hand, although nonlinear contributions are expected to be smaller than the linear ones, they will be more important than the contribution from the first adiabatic order. Nevertheless, the computation of the second-order corrections to the energy-momentum tensor is a formidable task which is well beyond the scope of this work.

VII. DISCUSSION AND CONCLUSIONS

In this work, we have computed the one-loop corrections to the effective potential due to the self-interactions of the Higgs field and the vacuum expectation value of its energy-momentum tensor in a perturbed FRW background. Unlike previous results based on the Schwinger–de Witt approximation, we have calculated explicitly a complete orthonormal set of modes of the perturbed Klein-Gordon equation and the dimensional regularization procedure was used for the mode summation to the leading adiabatic order. The integrals containing metric perturbations involved nonrational functions of the momenta so that standard formulas in dimensional regularization were not suitable to evaluate them. New expressions have been developed for those cases which applied both to static and expanding backgrounds.

We have checked that the homogeneous contribution agrees with the Minkowski result as expected. On the other hand, we have found that to the leading adiabatic order, and to first order in metric perturbations, no additional contributions appear either in the regularized effective potential nor in the energy-momentum tensor. This is in contrast with previous results obtained with a cutoff regularization [31], in which quartic and quadratic inhomogeneous divergences appear in the calculation. Thus, we see that dimensional regularization ensures that the theory can be renormalized just absorbing the divergences in the tree-level parameters (at the leading adiabatic order).

We expect additional contributions from the metric perturbations at the next-to-leading adiabatic orders. Unlike the Schwinger–de Witt method which provides a local expansion of the effective action. The mode summation method used in this work could allow to determine the corresponding finite nonlocal contributions. In this sense, the explicit mode calculation obtained here together with the method developed to perform the integrals in dimensional regularization of nonrational functions of the momenta are a fundamental first step in this program. The results presented in this work would also allow to calculate the temperature effects on the Higgs effective potential using the explicit mode summation and, in general, the complete expressions of other expectations values in perturbed metric backgrounds. Work is in progress in these directions.

ACKNOWLEDGMENTS

This work has been supported by the Spanish MICINNs Consolider-Ingenio 2010 Programme under MultiDark Grant No. CSD2009-00064, MINECO Centro de Excelencia Severo Ochoa Programme under Grant No. SEV-2012-0249, and MINECO Grants No. FIS2014-52837-P, AYA-2012-31101 and AYA2014-60641-C2-1-P. FDA acknowledges financial support from 'la Caixa'-Severo Ochoa doctoral fellowship.

APPENDIX A: ORTHONORMALIZATION CONDITION: $\tau_\Psi(\mathbf{k},\mathbf{k}')$ AND $\tau_{\delta\theta}(\mathbf{k},\mathbf{k}')$

In this appendix, we show that $\tau_\Psi(\mathbf{k},\mathbf{k}')$ and $\tau_{\delta\theta}(\mathbf{k},\mathbf{k}')$ appearing in (55) are zero to the leading adiabatic order. This implies that the modes given by (27), (35), (40), (41), (46) are orthonormal and, therefore, the scalar field $\delta\phi$ can be quantized within the canonical formalism.

The explicit expressions for $\tau_\Psi(\mathbf{k},\mathbf{k}')$ and $\tau_{\delta\theta}(\mathbf{k},\mathbf{k}')$ are

$$\tau_\Psi(\mathbf{k},\mathbf{k}') = \int \mathrm{d}^D\mathbf{x}\,\frac{(\omega_k-\omega_{k'})(k^2\omega_{k'}^2-k'^2\omega_k^2)}{4(\omega_k\omega_{k'})^{5/2}}\Psi(\mathbf{x})\frac{e^{i(\mathbf{k}-\mathbf{k}')\cdot\mathbf{x}}}{(2\pi)^D} \tag{A1}$$

$$\tau_{\delta\theta}(\mathbf{k},\mathbf{k}') = \int \mathrm{d}^D\mathbf{x}\,\frac{(\omega_k-\omega_{k'})(\omega_{k'}^2\mathbf{k}\cdot\nabla\delta\theta_k(0,\mathbf{x})-\omega_k^2\mathbf{k}'\cdot\nabla\delta\theta_{k'}(0,\mathbf{x}))}{4(\omega_k\omega_{k'})^{5/2}}\frac{e^{i(\mathbf{k}-\mathbf{k}')\cdot\mathbf{x}}}{(2\pi)^D}. \tag{A2}$$

First, let us focus on τ_Ψ in Fourier space:

$$\begin{aligned}\tau_\Psi(\mathbf{k},\mathbf{k}') &= \int \mathrm{d}^D\mathbf{x}\int\frac{\mathrm{d}^D\mathbf{p}}{(2\pi)^{D/2}}\frac{(\omega_k-\omega_{k'})(k^2\omega_{k'}^2-k'^2\omega_k^2)}{4(\omega_k\omega_{k'})^{5/2}}\Psi(\mathbf{p})\frac{e^{i(\mathbf{k}-\mathbf{k}'+\mathbf{p})\cdot\mathbf{x}}}{(2\pi)^D}\\ &= \int\frac{\mathrm{d}^D\mathbf{p}}{(2\pi)^{D/2}}\frac{(\omega_k-\omega_{k'})(k^2\omega_{k'}^2-k'^2\omega_k^2)}{4(\omega_k\omega_{k'})^{5/2}}\Psi(\mathbf{p})\delta^D(\mathbf{k}-\mathbf{k}'+\mathbf{p})\\ &= \frac{1}{(2\pi)^{D/2}}\frac{(\omega_k-\omega_{k'})(k^2\omega_{k'}^2-k'^2\omega_k^2)}{4(\omega_k\omega_{k'})^{5/2}}\Psi(\mathbf{k}-\mathbf{k}').\end{aligned} \tag{A3}$$

Since Ψ varies over macroscopic scales, we can a assume an exponential damping for Ψ when $|\mathbf{k}-\mathbf{k}'|\gg|\nabla\Psi|\sim\mathcal{H}$; therefore, $\tau_\Psi(\mathbf{k},\mathbf{k}')\approx 0$ in this case. For $|\mathbf{k}-\mathbf{k}'|\sim\mathcal{H}$, we can Taylor expand the coefficient in front of $\Psi(\mathbf{k}-\mathbf{k}')$ in $\mathcal{H}/\omega_k$ to get

$$\tau_\Psi(\mathbf{k},\mathbf{k}')\approx\frac{1}{(2\pi)^{D/2}}\frac{m^2k^2}{2\omega_k^4}\left(\frac{\mathcal{H}}{\omega_k}\right)^2\Psi(\mathbf{k}-\mathbf{k}'), \tag{A4}$$

which is beyond the leading adiabatic order.

The same procedure works for $\tau_{\delta\theta}$, for instance,

$$\begin{aligned}\tau_{\delta\theta}(\mathbf{k},\mathbf{k}') &= \int \mathrm{d}^D\mathbf{x}\int\frac{\mathrm{d}^D\mathbf{p}}{(2\pi)^{D/2}}\frac{(\omega_k-\omega_{k'})i\mathbf{p}\cdot(\omega_{k'}^2\mathbf{k}\delta\theta_k(0,\mathbf{p})-\omega_k^2\mathbf{k}'\delta\theta_{k'}(0,\mathbf{p}))}{4(\omega_k\omega_{k'})^{5/2}}\frac{e^{i(\mathbf{k}-\mathbf{k}'+\mathbf{p})\cdot\mathbf{x}}}{(2\pi)^D}\\ &= \int\frac{\mathrm{d}^D\mathbf{p}}{(2\pi)^{D/2}}\frac{(\omega_k-\omega_{k'})i\mathbf{p}\cdot(\omega_{k'}^2\mathbf{k}\delta\theta_k(0,\mathbf{p})-\omega_k^2\mathbf{k}'\delta\theta_{k'}(0,\mathbf{p}))}{4(\omega_k\omega_{k'})^{5/2}}\delta^D(\mathbf{k}-\mathbf{k}'+\mathbf{p})\\ &= \frac{1}{(2\pi)^{D/2}}\frac{(\omega_k-\omega_{k'})i(\mathbf{k}-\mathbf{k}')\cdot(\omega_{k'}^2\mathbf{k}\delta\theta_k(0,\mathbf{k}-\mathbf{k}')-\omega_k^2\mathbf{k}'\delta\theta_{k'}(0,\mathbf{k}-\mathbf{k}'))}{4(\omega_k\omega_{k'})^{5/2}}.\end{aligned} \tag{A5}$$

The initial condition is supposed to not introduce power at small scales; therefore, $\delta\theta_k(0,\mathbf{k}-\mathbf{k}')$ is also exponentially damped for modes $|\mathbf{k}-\mathbf{k}'|\gg\mathcal{H}$. For $|\mathbf{k}-\mathbf{k}'|\sim\mathcal{H}$, we can Taylor expand in $\mathcal{H}/\omega_k$ to get

$$\begin{aligned}\tau_{\delta\theta}(\mathbf{k},\mathbf{k}')\approx{}&\frac{i}{(2\pi)^{D/2}}\frac{1}{4\omega_k^3}\mathbf{k}\cdot\frac{\mathbf{k}-\mathbf{k}'}{|\mathbf{k}-\mathbf{k}'|}\left(\frac{\mathcal{H}}{\omega_k}\right)^3\\ &\times((m^2-k^2)\delta\theta_k(0,\mathbf{k}-\mathbf{k}')\\ &+\omega_k^2\mathbf{k}\cdot\nabla\delta\theta_k(0,\mathbf{k}-\mathbf{k}')).\end{aligned} \tag{A6}$$

Thus, for $|\mathbf{k}-\mathbf{k}'|\sim\mathcal{H}$, $\tau_{\delta\theta}$ is also beyond the leading adiabatic order. Note that the nabla operator in (A6) is to be understood as acting over the index variable k, not over the argument $\mathbf{k}-\mathbf{k}'$.

APPENDIX B: DIMENSIONAL REGULARIZATION FORMULAS

The fundamental formula used in dimensional regularization in Euclidean space is [37,38]

$$\int \frac{\mathrm{d}^D\mathbf{k}}{(2\pi)^D}\frac{k^{2\alpha}}{(k^2+m^2)^\beta} = m^{2(\alpha-\beta)}\left(\frac{m^2}{4\pi}\right)^{D/2} \times \frac{\Gamma(D/2+\alpha)\Gamma(\beta-\alpha-D/2)}{\Gamma(\beta)\Gamma(D/2)}. \tag{B1}$$

This expression has been used to compute $\langle\delta\phi^2\rangle_{\mathrm{h}}$ in (60) in $D = 3-\epsilon$. The left-hand side of the equation can be written as

$$\int \frac{\mathrm{d}^D\mathbf{k}}{(2\pi)^D}\frac{k^{2\alpha}}{(k^2+m^2)^\beta} = \frac{1}{(2\pi)^D}\frac{2\pi^{D/2}}{\Gamma(D/2)}\int_0^\infty \mathrm{d}k\,\frac{k^{D-1}k^{2\alpha}}{(k^2+m^2)^\beta}, \tag{B2}$$

then

$$\int_0^\infty \mathrm{d}k\,\frac{k^{D-1}k^{2\alpha}}{(k^2+m^2)^\beta} = \left[\frac{1}{(2\pi)^D}\frac{2\pi^{D/2}}{\Gamma(D/2)}\right]^{-1} m^{2(\alpha-\beta)}\left(\frac{m^2}{4\pi}\right)^{D/2} \times \frac{\Gamma(D/2+\alpha)\Gamma(\beta-\alpha-D/2)}{\Gamma(\beta)\Gamma(D/2)}. \tag{B3}$$

On the other hand, for the $\langle\delta\phi^2\rangle_{\mathrm{i}}$ term in (60), we have to deal with integrals of the following form,

$$\int \frac{\mathrm{d}^D\mathbf{k}}{(2\pi)^D}\frac{f(\mathbf{k}\cdot\mathbf{p})}{(k^2+m^2)^\beta}, \tag{B4}$$

where $f(\mathbf{k}\cdot\mathbf{p})$ is an analytical function. Taking the k_z direction along $\mathbf{p}$, we have $f(\mathbf{k}\cdot\mathbf{p}) = f(kp\hat{x})$ with $k = |\mathbf{k}|$, $p = |\mathbf{p}|$ and $\hat{x} = \cos(\theta_{D-2})$, θ_{D-2} being the angle between $\mathbf{k}$ and $\mathbf{p}$. When using spherical coordinates in D dimensions $\{\phi, \theta, \theta_2, \ldots, \theta_{D-2}\}$, the volume element can be expressed as

$$\mathrm{d}^D\mathbf{k} = k^{D-1}\sin^{D-2}(\theta_{D-2})\sin^{D-3}(\theta_{D-3})\ldots \times \sin(\theta)\mathrm{d}k\mathrm{d}\phi\mathrm{d}\theta\ldots\mathrm{d}\theta_{D-2}. \tag{B5}$$

The integrand of (B4) depends on $\cos(\theta_{D-2})$, so we can integrate in all the angular variables but θ_{D-2}. With that purpose, notice that the area of a sphere in a D-dimensional space is

$$\overbrace{\int_0^\pi\cdots\int_0^\pi}^{D-2}\int_0^{2\pi}\sin^{D-2}(\theta_{D-2})\sin^{D-3}(\theta_{D-3})\ldots \times \sin^2(\theta_2)\sin(\theta)\mathrm{d}\phi\mathrm{d}\theta\mathrm{d}\theta_2\ldots\mathrm{d}\theta_{D-2} = \frac{2\pi^{D/2}}{\Gamma(D/2)}. \tag{B6}$$

Since all the integrals involved can be factorized, the integration over all the angular variables but θ_{D-2} is simply given by the area of a sphere in $(D-1)$-dimensional space, i.e., $\frac{2\pi^{(D-1)/2}}{\Gamma((D-1)/2)}$. Therefore, Eq. (B4) can be expressed as

$$\int \frac{\mathrm{d}^D\mathbf{k}}{(2\pi)^D}\frac{f(\mathbf{k}\cdot\mathbf{p})}{(k^2+m^2)^\beta} = \frac{1}{(2\pi)^D}\frac{2\pi^{(D-1)/2}}{\Gamma((D-1)/2)}\int_0^\infty \mathrm{d}k \times \frac{k^{D-1}}{(k^2+m^2)^\beta}\hat{f}(kp), \tag{B7}$$

where $\hat{f}(kp) = \int_{-1}^1 \mathrm{d}\hat{x}(1-\hat{x}^2)^{(D-3)/2}f(kp\hat{x})$. Finally, Taylor expanding $\hat{f}(kp)$, the expression can be regularized order by order using Eq. (B3).

To regularize physical quantities like $\langle\delta\phi^2\rangle_{\mathrm{h}}$ and $\langle\delta\phi^2\rangle_{\mathrm{i}}$, two important aspects should be taken into consideration. First of all, the full physical expression should be computed in D dimensions, so that when taking $D = 3-\epsilon$, all the terms are expanded in ϵ. Moreover, a physical scale μ^ϵ should be introduced to compensate the physical dimensions.

1. Integrals involving k_i or k_ik_j

Finally, we explain how to compute the integrals involving the components of $\mathbf{k}$, k_i, and k_ik_j, appearing in the expression of the energy-momentum tensor in Sec. VI. For these cases, the other vector quantity, namely the wave vector of the metric perturbations $\mathbf{p}$, can be used to produce scalar quantities that can be easily computed in terms of the expressions given above. For instance

$$\int \mathrm{d}^D\mathbf{k}\,g(k,\mathbf{k}\cdot\mathbf{p})k_i = Ap_i, \tag{B8}$$

taking the scalar product with $\mathbf{p}$ in each member we get that

$$A = \int \mathrm{d}^D\mathbf{k}\,g(k,\mathbf{k}\cdot\mathbf{p})\frac{\mathbf{k}\cdot\mathbf{p}}{p^2} \tag{B9}$$

which can be integrated using the expression (B7). For the remaining case, we have

$$\int \mathrm{d}^D\mathbf{k}\,g(k,\mathbf{k}\cdot\mathbf{p})k_ik_j = B\delta_{ij} + Cp_ip_j, \tag{B10}$$

where B and C can be computed solving the system obtained by taking the trace and contracting with p^ip^j. The results are

$$B = \frac{1}{(D-1)}\int \mathrm{d}^D\mathbf{k}\,g(k,\mathbf{k}\cdot\mathbf{p})\frac{(kp)^2-(\mathbf{k}\cdot\mathbf{p})^2}{p^2} \tag{B11}$$

$$C = \frac{1}{(D-1)}\int \mathrm{d}^D\mathbf{k}\,g(k,\mathbf{k}\cdot\mathbf{p})\frac{D(\mathbf{k}\cdot\mathbf{p})^2-(kp)^2}{p^4}. \tag{B12}$$

APPENDIX C: $P_{k,l}^{\{\Phi,\Psi\}}$

In this appendix, the exact expressions for the $P_{k,l}^{\{\Phi,\Psi\}}(\eta)$ coefficients of Eq. (65) are given. First, let us separate these coefficients as

$$P_{k,l}^{\Phi}(\eta) = P_{k,l}^{\Phi,(0)}(\eta) + P_{k,l}^{\Phi,(1)}(\eta) + P_{k,l}^{\Phi,(2)}(\eta), \quad \text{(C1)}$$

where the indices (0), (1), (2) stand for the contribution coming from $P_k^{(0)}$ in (50), $P_k^{(1)}$ in (51), and $P_k^{(2)}$ in (52), respectively. The same definition applies for the terms $P_{k,l}^{\Psi}$.

The $l = 0$ coefficients are given by

$$P_{k,0}^{\Phi}(\eta) = 0 \quad \text{(C2)}$$

$$P_{k,0}^{\Psi}(\eta) = P_{k,0}^{\Psi,(0)}(\eta) = \frac{1}{2}\frac{\sqrt{\pi}\Gamma((D-1)/2)}{\Gamma(D/2)}\left(D - \frac{k^2}{\omega_k^2(\eta)}\right). \quad \text{(C3)}$$

For $l > 0$, we have

$$P_{k,l}^{\Phi}(\eta) = P_{k,l}^{\Phi,(1)}(\eta) + P_{k,l}^{\Phi,(2)}(\eta) \quad \text{(C4)}$$

$$P_{k,l}^{\Psi}(\eta) = P_{k,l}^{\Psi,(1)}(\eta) + P_{k,l}^{\Psi,(2)}(\eta) \quad \text{(C5)}$$

with

$$P_{k,l}^{\Phi,(1)}(\eta) = \frac{(-1)^l}{2^{2l}}\frac{\sqrt{\pi}\Gamma((D-1)/2)}{(l-1)!\Gamma(D/2+l)}k^{2l}\int_0^{\eta} d\eta'\left(\prod_{i=1}^{2l-1}\int_{\eta'}^{\eta}\frac{d\eta_i}{\omega_k(\eta_i)}\right)\left[\frac{1}{\omega_k(\eta')} - \frac{\omega_k(\eta')}{\omega_k^2(\eta)}\right] \quad \text{(C6)}$$

$$P_{k,l}^{\Psi,(1)}(\eta) = \frac{(-1)^l}{2^{2l}}\frac{\sqrt{\pi}\Gamma((D-1)/2)}{(l-1)!\Gamma(D/2+l)}k^{2l}\int_0^{\eta} d\eta'\left(\prod_{i=1}^{2l-1}\int_{\eta'}^{\eta}\frac{d\eta_i}{\omega_k(\eta_i)}\right)\left[\frac{2}{\omega_k(\eta')} - \frac{k^2}{\omega_k^2(\eta)\omega_k(\eta')} - \frac{k^2}{\omega_k^3(\eta')}\right] \quad \text{(C7)}$$

$$P_{k,l}^{\Phi,(2)}(\eta) = \frac{(-1)^l}{2^{2l-1}}\frac{\sqrt{\pi}\Gamma((D-1)/2)}{(l-1)!\Gamma(D/2+l-1)}k^{2l}\int_0^{\eta} d\eta'\int_0^{\eta'} d\eta''\left(\prod_{i=1}^{2l-2}\int_{\eta''}^{\eta}\frac{d\eta_i}{\omega_k(\eta_i)}\right)\left[\frac{\omega_k(\eta'')}{k^2\omega_k(\eta')} - \frac{(2l-1)\omega_k(\eta'')}{(D-2l-2)\omega_k^3(\eta')}\right] \quad \text{(C8)}$$

$$P_{k,l}^{\Psi,(2)}(\eta) = \frac{(-1)^l}{2^{2l-1}}\frac{\sqrt{\pi}\Gamma((D-1)/2)}{(l-1)!\Gamma(D/2+l-1)}k^{2l}\int_0^{\eta} d\eta'\int_0^{\eta'} d\eta''\left(\prod_{i=1}^{2l-2}\int_{\eta''}^{\eta}\frac{d\eta_i}{\omega_k(\eta_i)}\right)\left[\frac{1}{\omega_k(\eta')\omega_k(\eta'')} - \frac{(2l-1)k^2}{(D-2l-2)\omega_k^3(\eta')\omega_k(\eta'')}\right]. \quad \text{(C9)}$$

The integral over k of all these terms can be regularized with the expressions given in Appendix B after applying the generalized Feynman trick discussed in Sec. V. After regularization, we are left with two terms: one polynomic in η, the other one logarithmic in η. The integration over the Feynman parameters $\{x_i\}$ and the time integrals can be done following the procedure discussed in Appendix D.

APPENDIX D: INTEGRATION OVER $\{x_i\}$ AND $\{\eta_i\}$

This appendix shows how to compute the integrals over $\{x_i\}$ and $\{\eta_i\}$ appearing in the $R_l^{\{\Phi,\Psi\}}$ coefficients in (74). These terms have the general form

$$\overbrace{\int d\eta_1 \cdots \int d\eta_{2N}}^{2N}\overbrace{\int_0^1 \frac{dx_1}{\sqrt{x_1}} \cdots \int_0^1 \frac{dx_{2N+1}}{\sqrt{x_{2N+1}}}}^{2N+1}\delta\left(\sum_{k=1}^{2N+1} x_k - 1\right)\left\{\mathrm{Pol}_1(\{x_i\},\{\eta_i\}) + \log\left[\sum_{k=1}^{2N+1} x_k a^2(\eta_k)\right]\mathrm{Pol}_2(\{x_i\},\{\eta_i\})\right\}, \quad \text{(D1)}$$

where the logarithmic contribution is included in the $R_{l,\log}^{\{\Phi,\Psi\}}$ part of (75), whereas the pure polynomic one coming from Pol_1 is included in $R_{l,\mathrm{pol}}^{\{\Phi,\Psi\}}$. Notice that we have redefined $2l$ appearing in expression (74), namely the power of p, to be $2N$ in (D1) in order to highlight its importance in the following discussion. Since the polynomials only introduce trivial modifications of the following formulas, let us focus on the expression

$$\overbrace{\int d\eta_1 \cdots \int d\eta_{2N}}^{2N}\overbrace{\int_0^1 \frac{dx_1}{\sqrt{x_1}} \cdots \int_0^1 \frac{dx_{2N+1}}{\sqrt{x_{2N+1}}}}^{2N+1}\delta\left(\sum_{k=1}^{2N+1} x_k - 1\right)\log\left[\sum_{k=1}^{2N+1} x_k a^2(\eta_k)\right]. \quad \text{(D2)}$$

There are $2N+1$ variables x_i from the Feynman trick and all of them are integrated from 0 to 1. There are also $2N+1$ time variables η_i, but only $2N$ of them are integrated. In particular, η_{2N+1} is not integrated. In order to recover the expressions given in the text, we have renamed η as η_{2N+1}, η' as η_{2N} and η'' as η_{2N-1}. From the general expression (D2), it is straightforward to prove that for $a(\eta)=1$, the logarithm vanishes since $\sum_{k=1}^{2N+1} x_k = 1$. Therefore, $R^{\{\Phi,\Psi\}}_{l,\log}=0$ in nonexpanding spacetimes.

First, we deal with the integration over the $\{x_i\}$. Defining new variables $y_i^2 = x_i$ for $i=1,\ldots,2N+1$, this integration can be written over the $2N$ sphere

$$\int_0^1 \frac{\mathrm{d}x_1}{\sqrt{x_1}}\cdots\int_0^1 \frac{\mathrm{d}x_{2N+1}}{\sqrt{x_{2N+1}}}\delta\left(\sum_{k=1}^{2N+1} x_k - 1\right) = 2^{2N}\int_{S^{2N}} \mathrm{d}^{2N}\Omega. \tag{D3}$$

Then, the logarithm can be expressed as

$$\log\left[\sum_{k=1}^{2N+1} y_k^2 a^2(\eta_k)\right] = \log\left[a^2(\eta_{2N+1})\right] + \log\left[1+\sum_{k=1}^{2N} y_k^2\left(\frac{a^2(\eta_k)}{a^2(\eta_{2N+1})}-1\right)\right], \tag{D4}$$

where we have used that $y_{2N+1}^2 = 1-\sum_{k=1}^{2N} y_k^2$. The first logarithm on the right-hand side is the usual logarithm of the scale factor which appears in dimensional regularization in a FRW metric and it cancels out at the end. On the other hand, since η_{2N+1} is an upper limit in all the time integrations (see next subsection), we have $\eta_k \le \eta_{2N+1}$ for $k=1,\ldots,2N$. Thus, considering expanding universes, the argument of the logarithm is of the form $1+x$ with $-1<x\le 1$. Hence, it can be Taylor expanded as

$$\log\left[1+\sum_{k=1}^{2N} y_k^2\left(\frac{a^2(\eta_k)}{a^2(\eta_{2N+1})}-1\right)\right] = \sum_{j=1}^{\infty}\frac{(-1)^{j+1}}{j}\left[\sum_{k=1}^{2N} y_k^2\left(\frac{a^2(\eta_k)}{a^2(\eta_{2N+1})}-1\right)\right]^j, \tag{D5}$$

where the last factor on the right-hand side can also be expanded using the multinomial theorem

$$\left[\sum_{k=1}^{2N} y_k^2\left(\frac{a^2(\eta_k)}{a^2(\eta_{2N+1})}-1\right)\right]^j = \sum_{\substack{l_1,l_2,\ldots,l_{2N}=0 \\ \sum_{i=1}^{2N} l_i = j}}^{j} \frac{j!}{l_1!l_2!\cdots l_{2N}!}\prod_{m=1}^{2N}\left[y_m^2\left(\frac{a^2(\eta_m)}{a^2(\eta_{2N+1})}-1\right)\right]^{l_m}. \tag{D6}$$

Therefore, the integration over the $2N$-sphere reduces to an integration of this kind:

$$\int_{S^{2N}} \mathrm{d}^{2N}\Omega\, y_1^{2l_1} y_2^{2l_2}\cdots y_{2N}^{2l_{2N}} = \frac{\sqrt{\pi}\prod_{i=1}^{2N}\Gamma(\frac{1}{2}+l_i)}{2^{2N}\Gamma(N+\frac{1}{2}+\sum_{i=1}^{2N} l_i)} \equiv \frac{1}{2^{2N}}\Gamma[\{l_i\},2N]. \tag{D7}$$

Then,

$$2^{2N}\int_{S^{2N}} \mathrm{d}^{2N}\Omega \log\left[1+\sum_{k=1}^{2N} y_k^2\left(\frac{a^2(\eta_k)}{a^2(\eta_{2N+1})}-1\right)\right] = \sum_{j=1}^{\infty}\frac{(-1)^{j+1}}{j}\sum_{\substack{l_1,l_2,\ldots,l_{2N}=0 \\ \sum_{i=1}^{2N} l_i = j}}^{j}\frac{j!}{l_1!l_2!\cdots l_{2N}!}\Gamma[\{l_i\},2N]\prod_{m=1}^{2N}\left(\frac{a^2(\eta_m)}{a^2(\eta_{2N+1})}-1\right)^{l_m}. \tag{D8}$$

Applying the binomial theorem to the last factors,

$$\left(\frac{a^2(\eta_m)}{a^2(\eta_{2N+1})}-1\right)^{l_m} = \sum_{i_m=0}^{l_m}(-1)^{l_m-i_m}\binom{l_m}{i_m}\left[\frac{a^2(\eta_m)}{a^2(\eta_{2N+1})}\right]^{i_m}, \tag{D9}$$

and gathering all the results, we get

$$2^{2N}\int_{S^{2N}} \mathrm{d}^{2N}\Omega \log\left[1+\sum_{k=1}^{2N} y_k^2\left(\frac{a^2(\eta_k)}{a^2(\eta_{2N+1})}-1\right)\right] = -\sum_{j=1}^{\infty}\sum_{\substack{l_1,l_2,\ldots,l_{2N}=0 \\ \sum_{i=1}^{2N} l_i = j}}^{j}\frac{(j-1)!}{l_1!l_2!\cdots l_{2N}!}\Gamma[\{l_i\},2N]\sum_{i_1,i_2,\ldots,i_{2N}=0}^{l_1,l_2,\ldots,l_{2N}}(-1)^{\sum_{m=1}^{2N} i_m}\prod_{m=1}^{2N}\binom{l_m}{i_m}\left[\frac{a^2(\eta_m)}{a^2(\eta_{2N+1})}\right]^{i_m}. \tag{D10}$$

Finally, the time integrations can be done in a straightforward way since the dependence on η_m of the scale factor is polynomial for the cosmologies considered in this work.

1. $R^{\Psi}_{l,\log} = 0$ for all cosmologies

In Sec. V D, it is mentioned that the $R^{\Psi}_{l,\log}$ coefficients are all zero for all the cases considered. In fact, these expressions vanish not because of the integration over $\{x_i\}$ but because the polynomial $\mathrm{Pol}_2(\{x_i\},\{\eta_i\})$ in (D1) is zero for the Ψ contribution. This can be shown by summing the already regularized expression for (C5). Although the limits of integration are apparently different in each of the terms (C7), (C9), the region of integration is the same. For instance, the first integral can be written as

$$\int_0^\eta d\eta' \left(\prod_{i=1}^{2l-1}\int_{\eta'}^{\eta} d\eta_i\right) = \int_0^\eta d\eta' \left(\prod_{i=1}^{2l-1}\int_{0}^{\eta} d\eta_i \theta(\eta_i-\eta')\right), \tag{D11}$$

where θ is the step function, while

$$\int_0^\eta d\eta' \int_0^{\eta'} d\eta'' \left(\prod_{i=1}^{2l-2}\int_{\eta''}^{\eta} d\eta_i\right) = \int_0^\eta d\eta' \int_0^{\eta} d\eta'' \theta(\eta'-\eta'') \left(\prod_{i=1}^{2l-2}\int_{0}^{\eta} d\eta_i \theta(\eta_i-\eta'')\right). \tag{D12}$$

Then, redefining in the last integral η' as η_{2l-1} and η'' as η', both integrals have the same form

$$\overbrace{\int_0^\eta d\eta_1 \cdots \int_0^\eta d\eta_{2N}}^{2N} \prod_{i=1}^{2N-1} \theta(\eta_i-\eta_{2N}). \tag{D13}$$

[1] G. Aad *et al.* (ATLAS Collaboration), Phys. Lett. B **716**, 1 (2012).
[2] S. Chatrchyan *et al.* (CMS Collaboration), Phys. Lett. B **716**, 30 (2012).
[3] G. Aad *et al.* (ATLAS and CMS Collaborations), Phys. Rev. Lett. **114**, 191803 (2015).
[4] G. Belanger, B. Dumont, U. Ellwanger, J. F. Gunion, and S. Kraml, Phys. Rev. D **88**, 075008 (2013).
[5] M. V. Marono (CMS Collaboration), arXiv:1409.1711.
[6] The Third Annual Large Hadron Collider Physics Conference, http://lhcp2015.com/; Higgs boson coupling measurements, https://indico.cern.ch/event/389531/contributions/929540/.
[7] J. F. Donoghue, E. Golowich, and B. R. Holstein, *Dynamics of the Standard Model* (Cambridge University, Cambridge, England, 1992).
[8] S. Reucroft, Y. N. Srivastava, J. Swain, and A. Widom, Eur. Phys. J. C **48**, 781 (2006).
[9] C. Delaunay, R. Ozeri, G. Perez, and Y. Soreq, arXiv:1601.05087.
[10] R. Onofrio, Phys. Rev. D **82**, 065008 (2010).
[11] G. A. Wegner and R. Onofrio, Eur. Phys. J. C **75**, 307 (2015).
[12] S. R. Coleman and E. J. Weinberg, Phys. Rev. D **7**, 1888 (1973).
[13] B. L. Hu, Phys. Lett. **123B**, 189 (1983); B. L. Hu and D. J. O' Connor, Phys. Rev. D **30**, 743 (1984); L. F. Chen and B. L. Hu, Phys. Lett. **160B**, 36 (1985).
[14] S. Sinha and B. L. Hu, Phys. Rev. D **38**, 2423 (1988).
[15] N. D. Birrell and P. C. W. Davies, *Quantum Fields in Curved Space* (Cambridge University, Cambridge, England, 1982).
[16] L. Parker and D. Toms, *Quantum Field Theory in Curved Spacetime* (Cambridge University, Cambride, England, 2009).
[17] J. S. Schwinger, Phys. Rev. **82**, 914 (1951).
[18] B. S. DeWitt, Phys. Rep. **19**, 295 (1975).
[19] P. C. W. Davies, S. A. Fulling, S. M. Christensen, and T. S. Bunch, Ann. Phys. (N.Y.) **109**, 108 (1977).
[20] T. S. Bunch and P. C. W. Davies, J. Phys. A **11**, 1315 (1978).
[21] I. L. Buchbinder, S. D. Odintsov, and I. L. Shapiro, *Effective Action in Quantum Gravity* (Tomsk Pedagogical Institute, Tomsk, Russia, 1992).
[22] L. Parker and S. A. Fulling, Phys. Rev. D **9**, 341 (1974).
[23] S. A. Fulling and L. Parker, Ann. Phys. (N.Y.) **87**, 176 (1974).
[24] A. Ringwald, Ann. Phys. (N.Y.) **177**, 129 (1987).
[25] E. Elizalde and S. D. Odintsov, Phys. Lett. B **303**, 240 (1993); Russ. Phys. J. **37**, 25 (1994).
[26] E. Elizalde and S. D. Odintsov, Phys. Lett. B **321**, 199 (1994).
[27] W. H. Huang, Classical Quantum Gravity **10**, 2021 (1993).
[28] W. H. Huang, Classical Quantum Gravity **8**, 83 (1991).
[29] W. H. Huang, Phys. Rev. D **48**, 3914 (1993).
[30] P. O. Kazinski, Phys. Rev. D **80**, 124020 (2009).
[31] A. L. Maroto and F. Prada, Phys. Rev. D **90**, 123541 (2014).
[32] A. I. Vainshtein, V. I. Zakharov, V. A. Novikov, and M. A. Shifman, Sov. J. Nucl. Phys. **39**, 77 (1984); Yad. Fiz. **39**, 124 (1984).
[33] J. A. Zuk, Phys. Rev. D **32**, 2653 (1985).
[34] F. D. Albareti, J. A. R. Cembranos, and A. L. Maroto, Phys. Rev. D **90**, 123509 (2014).
[35] F. D. Albareti, J. A. R. Cembranos, and A. L. Maroto, Int. J. Mod. Phys. D **23** 1442019 (2014).
[36] J. Stewart, *Advanced General Relativity* (Cambridge University, Cambridge, England, 1991).
[37] P. Pascual and R. Tarrach, *QCD: Renormalization for the Practitioner* (Springer-Verlag, Berlin, 1984).
[38] H. Kleinert and V. Schulte-Frohlinde, *Critical Properties of Φ^4-Theories* (World Scientific, Singapore, 2001).

Paper III

"Finite-temperature corrections to the energy-momentum tensor at one loop in static spacetimes"

Physical Review D, Volume 97, 125017.

Authors: Franco D. Albareti, Antonio L. Maroto and Francisco Prada.

Motivation

Following the line of research developed in Paper II, we continue the study of quantum corrections to the dynamics of scalar fields arising in non-trivial geometries. In this paper, we consider the one-loop effective potential and expectation value of the energy-momentum tensor in a thermal state in a perturbed static background. We derive analytical expressions in the high and low temperature regimes and study the effects of the gravitational potentials on the expectation value of a self-interacting scalar field.

Finite-temperature corrections to the energy-momentum tensor at one loop in static spacetimes

Franco D. Albareti,[1,2,*] Antonio L. Maroto,[3,†] and Francisco Prada[1,2,4,‡]
[1]*Instituto de Física Teórica UAM/CSIC, Universidad Autónoma de Madrid, Cantoblanco, E-28049 Madrid, Spain*
[2]*Campus of International Excellence UAM+CSIC, Cantoblanco, E-28049 Madrid, Spain*
[3]*Departamento de Física Teórica and UPARCOS, Universidad Complutense de Madrid, 28040 Madrid, Spain*
[4]*Instituto de Astrofísica de Andalucía (CSIC), Glorieta de la Astronomía, E-18080 Granada, Spain*

(Received 18 May 2018; published 21 June 2018)

Finite-temperature corrections to the effective potential and the energy-momentum tensor of a scalar field are computed in a perturbed Minkoswki spacetime. We consider the explicit mode decomposition of the field in the perturbed geometry and obtain analytical expressions in the nonrelativistic and ultrarelativistic limits to first order in scalar metric perturbations. In the static case, our results are in agreement with previous calculations based on the Schwinger-DeWitt expansion which indicate that thermal effects in a curved spacetime can be encoded in the local Tolman temperature at leading order in perturbations and in the adiabatic expansion. We also study the shift of the effective potential minima produced by thermal corrections in the presence of static gravitational fields. Finally, we discuss the dependence on the initial conditions set for the mode solutions.

DOI: 10.1103/PhysRevD.97.125017

I. INTRODUCTION

Finite-temperature corrections to the effective potential in quantum field theory play a fundamental role in the description of phase transitions in the early Universe. In particular, symmetry restoration at high temperatures is an essential ingredient of the Higgs mechanism for electroweak symmetry breaking. In flat spacetime, such thermal corrections were computed for the first time in the seminal papers of Dolan and Jackiw [1] and Weinberg [2] using thermal Green functions methods. The possibility of extending those methods to more realistic scenarios incorporating spacetime curvature meets certain difficulties since finite-temperature field theory is only well defined provided the geometry possesses a global timelike Killing field. Thus, for example, for static or stationary spacetimes, the thermal Green functions method has been applied for homogeneous and isotropic Einstein static spaces in [3]. These methods were extended to conformally static Robertson-Walker backgrounds in [4]. The conditions for the construction of a thermal field theory in more general expanding universes (not strictly static) were discussed in [5,6], where the adiabatic techniques were introduced.

An alternative approach to the adiabatic expansion for thermal field theory in general curved spacetime is the so-called Schwinger-DeWitt [7,8] expansion of the effective action. Both approaches are known to agree in the results for the ultraviolet divergences in zero-temperature field theory. The Schwinger-DeWitt expansion, being a local curvature expansion, is manifestly covariant, but it is not sensitive to the global properties of the spacetime such as the presence of boundaries and does not contain information about the nonlocal part of the effective action. Going beyond the Schwinger-DeWitt approximation requires brute force methods based on explicit mode summation [9]. Thus, for example, in [10], phase transitions in homogeneous but anisotropic Bianchi I and Kasner cosmologies were studied using explicit modes sum. In recent works [11,12], we started this program in the case of weak inhomogeneous gravitational fields by studying the one-loop corrections to the vacuum expectation value (VEV) of the energy-momentum tensor and the effective potential of a massive scalar field. Thus, in [11], using a regularization procedure based on a simple comoving cutoff, a nonvanishing contribution of metric perturbations to the effective potential was obtained. However, the renormalization procedure required the use of noncovariant counterterms. In contrast, dimensional regularization was used in

*franco.albareti@csic.es
†maroto@ucm.es
‡f.prada@csic.es

[12] to isolate the divergences, applying techniques developed specifically to deal with nonrational integrands. In this case, the renormalized effective potential, being explicitly covariant, did not contain contributions from the inhomogeneous gravitational fields at the leading order in metric perturbation and in the adiabatic expansion in both static and cosmological spacetimes.

In this work, we extend these methods to include finite-temperature effects. The inclusion of the Bose-Einstein factor, accounting for the statistical distribution of the energy states, produces a smooth behavior of all quantities involved at large energies, making it unnecessary to apply any regularization technique (once the vacuum contribution is renormalized). As mentioned above, in order to compute the aforementioned contribution, we apply the "brute force" method described in [11,12], i.e., performing a summation over the perturbed modes of the quantum field obtained as solutions of the Klein-Gordon equation. We are able to get analytical expressions for the effective potential and the energy-momentum tensor in the nonrelativistic and the ultrarelativistic limits. In the static limit, we find that local gravitational effects can be taken into account through the Tolman temperature [13]. This is in accordance with computations of the energy-momentum tensor of a scalar field at finite temperature in a static spacetime using the Schwinger-DeWitt approach, [14,15]. However, we also obtain the explicit time dependence of the expectation values for finite times, which shows that the Tolman temperature can only be defined in the asymptotic time regions.

The work is organized as follows. Section II describes the general approach to compute an expectation value over a thermal state in a perturbed FRW metric. The particular expressions to be computed in the case of static spacetimes are presented in Sec. III. Sections IV and V explain the approximations applied to obtain the final result in the nonrelativitic and ultrarelativistic limits, respectively. Shifts in the minimum of the effective potential produced by thermal correction are discussed in Sec. VI. Our conclusions are presented in Sec. VII.

II. FINITE-TEMPERATURE CORRECTIONS

Given a scalar field ϕ, with potential $V(\phi)$, its classical action in a $(D+1)$-dimensional spacetime with metric tensor $g_{\mu\nu}$ can be written as

$$S[\phi, g_{\mu\nu}] = \int \mathrm{d}^{D+1}x\sqrt{g}\left(\frac{1}{2}g^{\mu\nu}\partial_\mu\phi\partial_\nu\phi - V(\phi)\right). \quad (1)$$

As is well known, the solutions $\phi = \hat{\phi}$ of the classical equation of motion,

$$\Box\hat{\phi} + V'(\hat{\phi}) = 0, \quad (2)$$

are those that minimize the action. On the other hand, quantum fluctuations around the classical solution $\delta\phi = \phi - \hat{\phi}$ satisfy the equation of motion,

$$(\Box + m^2(\hat{\phi}))\delta\phi = 0, \quad (3)$$

with

$$m^2(\hat{\phi}) = V''(\hat{\phi}). \quad (4)$$

Let us consider a metric which can be written as a scalar perturbation around a flat Robertson-Walker background,

$$\mathrm{d}s^2 = a^2(\eta)\{[1+2\Phi(\eta,\mathbf{x})]\mathrm{d}\eta^2 - [1-2\Psi(\eta,\mathbf{x})]\mathrm{d}\mathbf{x}^2\}, \quad (5)$$

where η is the conformal time, $a(\eta)$ the scale factor, and Φ and Ψ are the scalar perturbations in the longitudinal gauge. Given this geometry, the mode solutions $\delta\phi_k$ to (3) can be found using a WKB approximation to first order in metric perturbations and to the leading adiabatic order as [12]

$$\delta\phi_k(\eta,\mathbf{x}) = \delta\phi_k^{(0)}(\eta,\mathbf{x})(1 + P_k(\eta,\mathbf{x}) + i\delta\theta_k(\eta,\mathbf{x})), \quad (6)$$

where

$$\delta\phi_k^{(0)}(\eta,\mathbf{x}) = \frac{1}{(2\pi)^{D/2}}\frac{1}{a(\eta)^{(D-1)/2}\sqrt{2\omega_k}}e^{i\mathbf{k}\cdot\mathbf{x} - i\int^\eta \omega_k(\eta')\mathrm{d}\eta'} \quad (7)$$

are the unperturbed mode solutions with

$$\omega_k^2(\eta) = k^2 + m^2a^2(\eta). \quad (8)$$

The explicit expressions for $P_k(\eta,\mathbf{x})$ and $\delta\theta_k(\eta,\mathbf{x})$ in Fourier space are shown in Appendix A.

The effects of quantum fluctuations on the classical field configuration can be taken into account using the one-loop effective potential [12,16]

$$V_{\mathrm{eff}}(\hat{\phi}) = V(\hat{\phi}) + \frac{1}{2}\int_0^{m^2(\hat{\phi})}\mathrm{d}m^2\langle\delta\phi^2\rangle, \quad (9)$$

where $V(\hat{\phi})$ is the tree-level potential and the expectation value of the operator $\langle\delta\phi^2\rangle$ is taken over a particular quantum state of the field. Taking into account (6) and (7) and assuming that the quantum state has a fixed number of particles per mode n_k, the one-loop contribution to the effective potential reads

$$\frac{1}{2}\int_0^{m^2(\hat{\phi})} \mathrm{d}m^2 \langle \delta\phi^2 \rangle = \frac{1}{(2\pi)^D a^{D-1}(\eta)} \frac{1}{2} \int_0^{m^2(\hat{\phi})} \mathrm{d}m^2 \int \mathrm{d}^D\mathbf{k} \left(\frac{1}{2} + n_k\right) \frac{1 + 2P_k(\eta, \mathbf{p})}{\sqrt{k^2 + m^2 a^2(\eta)}}$$
$$= \frac{2}{(2\pi)^D a^{D-1}(\eta)} \frac{2\pi^{(D-1)/2}}{\Gamma((D-1)/2)} \frac{1}{2} \int_0^{m^2(\hat{\phi})} \mathrm{d}m^2 \int_0^{\infty} \mathrm{d}k k^{D-1} \left(\frac{1}{2} + n_k\right) \frac{1 + \hat{P}_k(\eta, \mathbf{p})}{\sqrt{k^2 + m^2 a^2(\eta)}} \quad (10)$$

where we have defined

$$\hat{P}_k(\eta, \mathbf{p}) = \int_{-1}^{1} \mathrm{d}\hat{x} (1 - \hat{x}^2)^{(D-3)/2} P_k(\eta, \mathbf{p}), \quad (11)$$

where $\hat{x} = \mathbf{k} \cdot \mathbf{p}/(kp)$ and including the general integration measure in D dimensions.

From now on, we consider a thermal quantum state. Then, the number of particles per mode is given by the Bose-Einstein distribution,

$$n_k^T = \frac{1}{e^{\omega_k/T} - 1}, \quad (12)$$

where T is the temperature of the state, for the moment understood as a parameter of the Bose-Einstein distribution (see next section).

Let us define $V_1(\hat{\phi})$ as the one-loop quantum vacuum contribution, i.e.,

$$V_1(\hat{\phi}) = \frac{1}{(2\pi)^D a^{D-1}(\eta)} \frac{2\pi^{(D-1)/2}}{\Gamma((D-1)/2)} \int_0^{m^2(\hat{\phi})} \mathrm{d}m^2 \times \int_0^{\infty} \mathrm{d}k k^{D-1} \frac{1}{2} \frac{1 + \hat{P}_k(\eta, \mathbf{p})}{\sqrt{k^2 + m^2 a^2(\eta)}}, \quad (13)$$

and $V_T(\hat{\phi})$ as the term that includes finite-temperature corrections,

$$V_T(\hat{\phi}) = \frac{1}{(2\pi)^D a^{D-1}(\eta)} \frac{2\pi^{(D-1)/2}}{\Gamma((D-1)/2)} \int_0^{m^2(\hat{\phi})} \mathrm{d}m^2 \times \int_0^{\infty} \mathrm{d}k k^{D-1} n_k^T \frac{1 + \hat{P}_k(\eta, \mathbf{p})}{\sqrt{k^2 + m^2 a^2(\eta)}}, \quad (14)$$

so that we can write the one-loop effective potential at finite temperature as

$$V_{\mathrm{eff}}(\hat{\phi}) = V(\hat{\phi}) + V_1(\hat{\phi}) + V_T(\hat{\phi}). \quad (15)$$

It is important to notice that both the vacuum and the thermal contributions have a homogeneous term, corresponding to the background geometry, and an inhomogeneous one, proportional to the perturbations. Then,

$$V_1(\hat{\phi}) = V_1^{\mathrm{h}}(\hat{\phi}) + V_1^{\mathrm{i}}(\hat{\phi}), \quad (16)$$

$$V_T(\hat{\phi}) = V_T^{\mathrm{h}}(\hat{\phi}) + V_T^{\mathrm{i}}(\hat{\phi}). \quad (17)$$

The homogeneous part due to vacuum effects $V_1^{\mathrm{h}}(\hat{\phi})$, after applying the minimal substraction scheme $\overline{\mathrm{MS}}$ in dimensional regularization with $D = 3 + \epsilon$, is given by [12]

$$V_1^{\mathrm{h}}(\hat{\phi}) = \frac{m^4(\hat{\phi})}{64\pi^2} \left[\ln\left(\frac{m^2(\hat{\phi})}{\mu^2}\right) - \frac{3}{2}\right]. \quad (18)$$

A detailed analysis of the inhomogeneous part of the vacuum $V_1^{\mathrm{i}}(\hat{\phi})$ was performed in [11] with a cutoff regularization and in [12] using dimensional regularization. When a cutoff Λ is used, the result turns out to be proportional to $m^2(\hat{\phi})\Lambda^2\Phi$ in the static case; i.e., only the quadratic divergence appears. In dimensional regularization, we find to first order in perturbations and to the leading adiabatic order that

$$V_1^{\mathrm{i}}(\hat{\phi}) = 0 \quad (19)$$

in agreement with the absence of logarithmic divergences in the cutoff case.

In this work, we focus on the thermal contribution $V_T(\hat{\phi})$. The corresponding inhomogeneous contribution can, in turn, be split in the terms proportional to Φ and Ψ as

$$V_T(\hat{\phi}) = V_T^{\mathrm{h}}(\hat{\phi}) + V_T^{\Phi}(\hat{\phi}) + V_T^{\Psi}(\hat{\phi}) \quad (20)$$

It is important to note that expression (9) defines the potential except for the addition of an arbitrary function which could depend on the spacetime coordinates and the temperature. This function does not modify the dynamics of the field (2) since it does not introduce any dependence on $m(\hat{\phi})$.

In the same fashion, the thermal contribution to the components of the energy-momentum tensor can be obtained from the expressions given in Ref. [12] including the number of particles per mode n_k^T, thus,

$$\langle T^0{}_0(\eta, \mathbf{p}) \rangle = \rho(\eta, \mathbf{p}) = \frac{1}{(2\pi)^D} \frac{1}{a^{D+1}} \int \mathrm{d}^D\mathbf{k} \left(\frac{1}{2} + n_k^T\right) \omega_k \left[1 + 2\frac{k^2}{\omega_k^2}\Psi(\mathbf{p}) + 2P_k(\eta, \mathbf{p}) + 2i\frac{\mathbf{k} \cdot p}{\omega_k^2}\delta\theta_k(\eta, \mathbf{p})\right] \quad (21)$$

$$\langle T^i{}_i(\eta,\mathbf{p})\rangle = -\,p_i(\eta,\mathbf{p}) = -\frac{1}{(2\pi)^D}\frac{1}{a^{D+1}}\int \mathrm{d}^D\mathbf{k}\left(\frac{1}{2}+n_k^T\right)\left[\frac{k_i^2}{\omega_k}(1+2\Psi(\mathbf{p})+2P_k(\eta,\mathbf{p}))+2i\frac{k_i p_i}{\omega_k}\delta\theta_k(\eta,\mathbf{p})\right] \tag{22}$$

$$\langle T^i{}_0(\eta,\mathbf{p})\rangle = \frac{1}{(2\pi)^D}\frac{1}{a^{D+1}}\int \mathrm{d}^D\mathbf{k}\left(\frac{1}{2}+n_k^T\right)\left[k_i\left(1+2P_k(\eta,\mathbf{p})+2i\frac{\mathbf{k}\cdot\mathbf{p}}{\omega_k^2}\delta\theta_k(\eta,\mathbf{p})\right)+ip_i\delta\theta_k(\eta,\mathbf{p})\right] \tag{23}$$

$$\langle T^i{}_j(\eta,\mathbf{p})\rangle = -\frac{1}{(2\pi)^D}\frac{1}{a^{D+1}}\int \mathrm{d}^D\mathbf{k}\left(\frac{1}{2}+n_k^T\right)\left[\frac{k_i k_j}{\omega_k}(1+2\Psi(\mathbf{p})+2P_k(\eta,\mathbf{p}))+i\frac{k_i p_j+k_j p_i}{\omega_k}\delta\theta_k(\eta,\mathbf{p})\right] \tag{24}$$

$$\langle T^\mu{}_\mu(\eta,\mathbf{p})\rangle = \frac{1}{(2\pi)^D}\frac{1}{a^{D+1}}\int \mathrm{d}^D\mathbf{k}\left(\frac{1}{2}+n_k^T\right)\left[\frac{m^2}{\omega_k}(1+2P_k(\eta,\mathbf{p}))\right]. \tag{25}$$

Let us divide the energy-momentum tensor, in the same way as for the potential case, in a vacuum contribution, which does not depend on the number of particles per mode n_k^T, and a thermal contribution.

$$\langle T^\mu{}_\nu(\eta,\mathbf{p})\rangle = \langle T^\mu{}_\nu(\eta,\mathbf{p})\rangle_{\mathrm{vac}} + \langle T^\mu{}_\nu(\eta,\mathbf{p})\rangle_T. \tag{26}$$

each one having a homogeneous and an inhomogeneous part. It can be shown [12] that the energy-momentum tensor of the vacuum is given by $\langle T^\mu{}_\nu(\eta,\mathbf{p})\rangle_{\mathrm{vac}} = \rho_{\mathrm{vac}}\delta^\mu{}_\nu$, where the energy density ρ_{vac} and pressure p_{vac} are given in the $\bar{\mathrm{M}}$S renormalization scheme with $D = 3+\epsilon$ by

$$\rho_{\mathrm{vac}} = -p_{\mathrm{vac}} = \frac{m^4}{64\pi^2}\left[\log\left(\frac{m^2}{\mu^2}\right)-\frac{3}{2}\right]. \tag{27}$$

This implies that the inhomogeneous part of the vacuum contribution is zero when dimensional regularization is used, therefore metric perturbations do not contribute to the leading adiabatic order. In this paper, we compute the homogeneous and inhomogeneous parts of $\langle T^\mu{}_\nu(\eta,\mathbf{p})\rangle_T$.

III. STATIC SPACETIMES

Although the expressions for the perturbed solutions given in Appendix A are valid for general perturbed FRW spacetimes, in this work we focus on static spacetimes; i.e., we will take $a = 1$ and $\Phi = \Phi(\mathbf{x})$, $\Psi = \Psi(\mathbf{x})$. The general case is of great interest for cosmological scenarios, nevertheless the time dependence of the scale factor increases the complexity of the computations, making extremely difficult to obtain analytical expressions. In addition, in order to define a thermodynamic temperature, there must be a timelike Killing vector field; namely, the spacetime must be static or stationary.

In order to compute $V_T(\hat{\phi})$ and the energy-momentum tensor $\langle T^\mu{}_\nu(\eta,\mathbf{p})\rangle_T$ thermal contributions, our first step will be to expand the $P_k(\eta,\mathbf{p})$ and $\delta\theta_k(\eta,\mathbf{p})$ functions in powers of $p\eta$ (Appendix B). These expansions allow us to find a common structure of the integrals involved.

A. Effective potential

Taking into account (B1) and (10), it is clear that we have to deal with the following kind of integrals,

$$\frac{1}{2}\int_0^{m^2(\hat{\phi})}\mathrm{d}m^2\int_0^\infty \mathrm{d}k k^{D-1}\frac{1}{e^{\omega_k/T}-1}\frac{1}{\omega_k}\left(\frac{k}{\omega_k}\right)^{2\alpha}\left(\frac{m}{\omega_k}\right)^{2n}$$
$$\alpha = 0,1,2,\ldots \qquad n = 0,1,2, \tag{28}$$

to compute the finite-temperature correction to the effective potential.

It is convenient to use the dimensionless variables $u = \omega_k/T$ and $x = m/T$ instead of k and m, respectively. In terms of these new variables, the integral reduces to (extracting a global factor T^{D+1})

$$I^X_{\alpha,n} \equiv \int_0^X \mathrm{d}x\int_x^\infty \mathrm{d}u\frac{1}{e^u-1}\frac{x^{1+2n}}{u^{2\alpha+2n}}(u^2-x^2)^{D/2+\alpha-1}, \tag{29}$$

where $X \equiv m(\hat{\phi})/T$.

It is also useful to interchange the order of integration of this integral and divide it in the following way,

$$I^X_{\alpha,n} = \left(\int_0^X \mathrm{d}u\int_0^u \mathrm{d}x + \int_X^\infty \mathrm{d}u\int_0^X \mathrm{d}x\right)\times\left(\frac{1}{e^u-1}\frac{x^{1+2n}}{u^{2\alpha+2n}}(u^2-x^2)^{D/2+\alpha-1}\right), \tag{30}$$

where the first part takes into account the contribution from modes with energies below the mass of the field, while the second part includes the contribution from modes with energies above the mass of the field.

B. Energy-momentum tensor

To compute the energy-momentum tensor, the following integrals appear:

$$\int_0^\infty \mathrm{d}k k^{D-1} \frac{1}{e^{\omega_k/T}-1} \omega_k \left(\frac{k}{\omega_k}\right)^{2\alpha} \left(\frac{m}{\omega_k}\right)^{2n}$$
$$\alpha = 0, 1, 2, \ldots \quad n = 0, 1, 2. \tag{31}$$

Using the same dimensionless variables u and x, we get (also extracting a global factor T^{D+1})

$$J^X_{\alpha,n} \equiv \int_X^\infty \mathrm{d}u \frac{1}{e^u - 1} \frac{X^{2n}}{u^{2\alpha+2n-2}} (u^2 - X^2)^{D/2+\alpha-1}. \tag{32}$$

Only modes with energies above the mass of the field contribute to the energy-momentum tensor.

In the following, we compute the integrals $I^X_{\alpha,n}$ (30) and $J^X_{\alpha,n}$ (32) in the nonrelativistic and the ultrarelativistic limits.

IV. NONRELATIVISTIC LIMIT

A. Effective potential

In the nonrelativistic limit $m(\hat{\phi})/T \to \infty$ (or $X \to \infty$), the contribution from modes with energies above the mass of the field is exponentially damped because of the Bose-Einstein factor; hence, the leading contribution in the nonrelativistic limit is given by the first part of (30) when taking $X = \infty$,

$$I^\infty_{\alpha,n} = \int_0^\infty \mathrm{d}u \int_0^u \mathrm{d}x \frac{1}{e^u - 1} \frac{x^{1+2n}}{u^{2\alpha+2n}} (u^2 - x^2)^{D/2+\alpha-1}$$
$$= \frac{\Gamma(D/2+\alpha) n!}{2\Gamma(D/2+\alpha+n+1)} D! \zeta(D+1), \tag{33}$$

where $\zeta(x)$ is the Riemann Zeta function.

Therefore, using expression (10) together with the result for the integral (33) and the expansion of $\hat{P}_k(\eta, \mathbf{p})$ (B1), we obtain (assuming $D = 3$) for the leading contributions after resummation of the series in $p\eta$

$$V^h_{T(L)}(\hat{\phi}) = \frac{\pi^2}{90} T^4 \tag{34}$$

$$V^\Phi_{T(L)}(\hat{\phi}) = \frac{\pi^2}{90} T^4 \Phi(\mathbf{p}) \times 4 \left[3 \frac{\sin(p\eta)}{(p\eta)^3} - 3 \frac{\cos(p\eta)}{(p\eta)^2} - 1\right] \tag{35}$$

$$V^\Psi_{T(L)}(\hat{\phi}) = \frac{\pi^2}{90} T^4 \Psi(\mathbf{p}) \times 12 \left[\left(\frac{6}{(p\eta)^4} - \frac{1}{(p\eta)^2}\right) \cos(p\eta) + \left(\frac{3}{(p\eta)^3} - \frac{6}{(p\eta)^5}\right) \sin(p\eta)\right]. \tag{36}$$

Note that there is no dependence on the field (which may appear through mass terms). Therefore, these expressions do not affect the field dynamics and they can be neglected. On the other hand, even though we are considering static backgrounds, there is an explicit time dependence of the result. This can be traced back to the particular mode choice in (A1) and (A2). In particular, taking the $\eta \to \infty$ limit, which corresponds to setting initial conditions for the modes in the remote past, we recover static results for the effective potential.

In the static limit $\eta \to \infty$, the following expression is obtained:

$$V_{T(L)}(\hat{\phi}) = \frac{\pi^2}{90} T^4 (1 - 4\Phi(\mathbf{p})). \tag{37}$$

It can be shown that the leading inhomogeneous effect in the static limit only depends on the Φ potential and, in fact, it can be obtained from the homogeneous result replacing the temperature by the local Tolman temperature [13],

$$T_{\mathrm{Tolman}} = \frac{T}{\sqrt{g_{00}}} \simeq T(1 - \Phi(\mathbf{p})). \tag{38}$$

Notice, however, that in the results for finite time given in (35) and (36), the explicit time dependence of the effective potential prevents the introduction of a Tolman temperature.

The next-to-leading correction, $V^{(NL)}_T$, including terms $\mathcal{O}(T/m(\hat{\phi}))$, can be obtained by applying a modified version of the Laplace method to the following integral,[1]

$$I^X_{\alpha,n} - I^\infty_{\alpha,n} \simeq -\int_X^\infty \mathrm{d}u \int_X^u \mathrm{d}x e^{-u} \frac{x^{1+2n}}{u^{2\alpha+2n}} (u^2 - x^2)^{D/2+\alpha-1}$$
$$= \int_X^\infty \mathrm{d}u \frac{1}{2} e^{-u} u^D \left[B_{X^2/u^2}(1+n, D/2+\alpha) - \frac{\Gamma(1+n)\Gamma(D/2+\alpha)}{\Gamma(D/2+\alpha+n+1)}\right], \tag{39}$$

where we have replaced the Bose-Einstein factor by the Boltzmann factor. $B_z(a, b)$ is the incomplete Beta function. When $u/X \gg 1$, the integrand is exponentially damped as $e^{-u/X}$. Then, we Taylor expand the expression inside the brackets around $X^2/u^2 = 1$ to obtain

$$I^X_{\alpha,n} - I^\infty_{\alpha,n} \sim -\int_X^\infty \mathrm{d}u \frac{1}{D+2\alpha} e^{-u} u^D \left(1 - \frac{X^2}{u^2}\right)^{D/2+\alpha}$$
$$= -\int_X^\infty \mathrm{d}u \frac{1}{D+2\alpha} \exp\left[-u + D\log(u) + \left(\frac{D}{2}+\alpha\right) \log\left(1 - \frac{X^2}{u^2}\right)\right]. \tag{40}$$

[1]The symbol $\simeq$ stands for an approximation in the Taylor sense, while $\sim$ stands for an asymptotic approximation, namely the quotient between both results equals 1 in the appropriate limit.

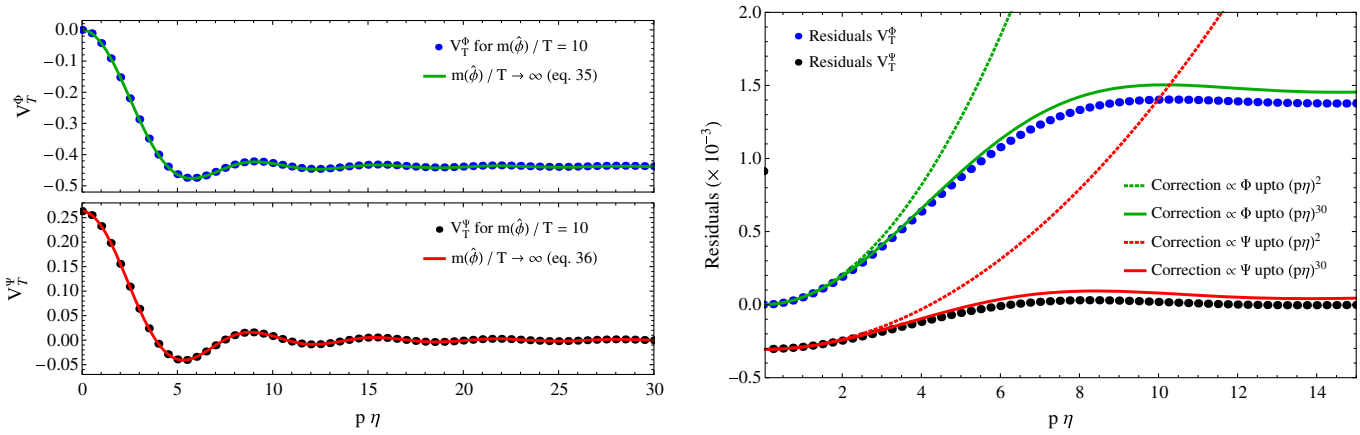

FIG. 1. Left panel: Points correspond to the numerical value of the thermal contributions to the potential proportional to Φ and Ψ taking $m(\hat{\phi})/T = 10$, whereas the solid lines represent the leading approximations (35) and (36). Right panel: Points are the difference between the numerical values of the potential and the approximations (35) (blue points) and (36) (black points) for $m(\hat{\phi})/T = 10$. The next-to-leading correction for $m(\hat{\phi})/T = 10$ up to $(p\eta)^2$ (dashed lines) and $(p\eta)^{30}$ (solid lines) is shown for comparison.

The expression inside the exponential has a maximum at $u \sim X$ when $X \to \infty$.[2] Taylor expanding the argument of the exponential around $u = X$ up to order $O(u)$ (including the logarithmic divergence), the integration in u can be performed to get the following result,

$$I^X_{\alpha,n} - I^\infty_{\alpha,n} \sim -2^{3(D/2+\alpha)+1}\Gamma(D/2+\alpha)e^{-X} \times \frac{X^{D+1}}{(4X - D + 6\alpha)^{D/2+\alpha+1}} \sim -2^{D/2+\alpha-1}\Gamma(D/2+\alpha)e^{-X}X^{D/2-\alpha}, \quad (41)$$

which does not depend on n. Because of the factor $X^{D/2-\alpha}$ in the last expression, the expansion in $p\eta$ mixes with the expansion in $X(= m(\hat{\phi})/T)$.

Finally, the next-to-leading contribution to the potential for $p\eta \ll 1$ is given by

$$V_{T(NL)}(\hat{\phi}) = -\frac{T^4}{2\sqrt{2}\pi^{3/2}} e^{-m(\hat{\phi})/T}\left(\frac{m(\hat{\phi})}{T}\right)^{3/2} \times \left(1 + 3\Psi(\mathbf{p}) - \frac{(p\eta)^2}{2}\Phi(\mathbf{p})\right). \quad (42)$$

A better approximation for smaller values of X is obtained if we do not drop α in the denominator in (41). This improved approximation is shown in Fig. 1 (right panel). It is important to note that each order in $(p\eta)$ is suppressed by a factor $[T/m(\hat{\phi})]$ with respect to the previous order, because of the mixing discussed above. For instance, the correction proportional to Ψ does not depend on $(p\eta)$ to leading order in $[T/m(\hat{\phi})]$ [see Eq. (42)], then the dependence on $(p\eta)^2$ proportional to Ψ is suppressed by a factor $[T/m(\hat{\phi})]$ with respect to the $(p\eta)^2$ correction proportional to Φ, as shown in Fig. 1 (right panel).

Because of the mixing between the expansion in $X(= m(\hat{\phi})/T)$ and $p\eta$ we cannot obtain a result valid for arbitrary scales p and times η. However, it is possible to obtain the static result by taking the limit $\eta \to \infty$ directly on (10). According to this procedure, we get

$$V_{T(NL)}(\hat{\phi}) = -\frac{T^4}{2\sqrt{2}\pi^{3/2}} e^{-m(\hat{\phi})/T}\left(\frac{m(\hat{\phi})}{T}\right)^{3/2} \times \left(1 - \frac{35}{8}\Phi(\mathbf{p}) - \left(\frac{m(\hat{\phi})}{T}\right)\Phi(\mathbf{p})\right). \quad (43)$$

As can be checked in a straightforward way from (43), also for the next to leading contribution in the static limit, the inhomogeneous correction can be obtained from the homogeneous result by replacing the temperature with the Tolman temperature [13].

B. Energy-momentum tensor

The leading order of the energy-momentum tensor is already exponentially damped, since only modes with energies above the mass of the field contribute. We write the integral (32) as

$$J^X_{\alpha,n} \simeq \int_X^\infty du e^{-u}\frac{X^{2n}}{u^{2\alpha+2n-2}}(u^2 - X^2)^{D/2+\alpha-1} \quad (44)$$

[2]Here we are dropping a term linear in α in the expression for the maximum. This means that we cannot allow $\alpha \to \infty$. Since α is related with the order of the expansion in $p\eta$, the results are only valid if the series appearing in (B1) is truncated at some order such that $\alpha \ll X$. Although it could be done for arbitrary α, it would not be very useful if the expression cannot be resummed. Nevertheless, it will be shown that the l-term is suppressed by a factor $1/X^l$, thus only the first terms are relevant in this limit $(X \to \infty)$.

where the Bose-Einstein factor has been replaced by the Boltzmann factor. Applying the Laplace's method again we get

$$\begin{aligned} J^X_{\alpha,n} &\simeq X^{2n}\int_X^\infty \mathrm{d}u \exp\left[-u-2(\alpha+n-1)\log(u)+\left(\frac{D}{2}+\alpha-1\right)\log\left(u^2-X^2\right)\right] \\ &\sim 2^{3(D/2+\alpha)-1}\Gamma(D/2+\alpha)e^{-X}\frac{X^{D+1}}{(4X-D+6\alpha+8n-6)^{D/2+\alpha}} \\ &\sim 2^{D/2+\alpha-1}\Gamma(D/2+\alpha)e^{-X}X^{D/2-\alpha+1} \end{aligned} \tag{45}$$

Then, taking into account the expressions given in Sec. II and the result (45), the energy-momentum tensor for $p\eta \ll 1$ is given by

$$\begin{aligned} \rho_T &\equiv \langle T^0{}_0(\eta,\mathbf{p})\rangle_T \\ &\sim \frac{T^4}{2\sqrt{2}\pi^{3/2}}e^{-m(\hat{\phi})/T}\left(\frac{m(\hat{\phi})}{T}\right)^{5/2} \\ &\quad\times\left(1+3\Psi(\mathbf{p})-\frac{(p\eta)^2}{2}\Phi(\mathbf{p})\right) \end{aligned} \tag{46}$$

$$\begin{aligned} -p_T &\equiv \langle T^i{}_i(\eta,\mathbf{p})\rangle_T \\ &\sim -\frac{T^4}{2\sqrt{2}\pi^{3/2}}e^{-m(\hat{\phi})/T}\left(\frac{m(\hat{\phi})}{T}\right)^{3/2} \\ &\quad\times\left(1+5\Psi(\mathbf{p})-\frac{5(p\eta)^2}{6}\Phi(\mathbf{p})\right) \end{aligned} \tag{47}$$

$$\langle T^i{}_0(\eta,\mathbf{p})\rangle_T \sim -\frac{T^4}{2\sqrt{2}\pi^{3/2}}e^{-m(\hat{\phi})/T}\left(\frac{m(\hat{\phi})}{T}\right)^{5/2}(ip_i)\eta\Phi(\mathbf{p}) \tag{48}$$

$$\begin{aligned} \langle T^i{}_j(\eta,\mathbf{p})\rangle_T \sim &-\frac{T^4}{2\sqrt{2}\pi^{3/2}}e^{-m(\hat{\phi})/T}\left(\frac{m(\hat{\phi})}{T}\right)^{3/2} \\ &\times(i^2p_ip_j)\eta^2\Phi(\mathbf{p}) \quad i\neq j \end{aligned} \tag{49}$$

where ρ_T and p_T are the energy density and pressure produced by the thermal corrections. We have only retained the leading order in $m(\hat{\phi})/T$. Further corrections $\mathcal{O}((p\eta)^{2l})$ are suppressed by a factor $(m(\hat{\phi})/T)^l$.

In the nonrelativistic case, it is not possible to take the static limit in the final expressions since we only have the results for $p\eta \ll 1$ as discussed before. However, the static expression can be obtained by taking the static limit in the original expressions (25)

$$\rho_T \equiv \langle T^0{}_0(\eta,\mathbf{p})\rangle_T \sim \frac{T^4}{2\sqrt{2}\pi^{3/2}}e^{-m(\hat{\phi})/T}\left(\frac{m(\hat{\phi})}{T}\right)^{5/2}\left(1-\frac{39}{8}\Phi(\mathbf{p})-\left(\frac{m(\hat{\phi})}{T}\right)\Phi(\mathbf{p})\right) \tag{50}$$

$$-p_T \equiv \langle T^i{}_i(\eta,\mathbf{p})\rangle_T \sim -\frac{T^4}{2\sqrt{2}\pi^{3/2}}e^{-m(\hat{\phi})/T}\left(\frac{m(\hat{\phi})}{T}\right)^{3/2}\left(1-\frac{35}{8}\Phi(\mathbf{p})-\left(\frac{m(\hat{\phi})}{T}\right)\Phi(\mathbf{p})\right). \tag{51}$$

Once again, in the static limit, the inhomogeneous corrections, depending only on the Φ potential and can be obtained from the homogenous one by introducing the Tolman temperature.

V. ULTRARELATIVISTIC LIMIT

A. Effective potential

In the ultrarelativistic limit, $m(\hat{\phi})/T \to 0$ (or $X \to 0$), the dominant contribution comes from modes with energies higher than the mass of the field. Therefore, the second part of (30) gives

$$\begin{aligned} I^X_{\alpha,n} &\simeq \int_X^\infty \mathrm{d}u\int_0^X \mathrm{d}x\frac{1}{e^u-1}\frac{x^{1+2n}}{u^{2\alpha+2n}}(u^2-x^2)^{D/2+\alpha-1} \\ &= \int_X^\infty \mathrm{d}u\frac{1}{2}\frac{u^D}{e^u-1}B_{X^2/u^2}(1+n,D/2+\alpha) \\ &\simeq \int_X^\infty \mathrm{d}u\frac{1}{2}\frac{u^{D-2n-2}}{e^u-1}\frac{X^{2+2n}}{1+n} \end{aligned} \tag{52}$$

where we have expanded the incomplete Beta function $B_z(a,b)$ for $X \ll 1$ in the last line. The leading contribution comes from $n=0$. Replacing the lower limit of integration by 0 we get in that limit

$$I^X_{\alpha,0} \simeq \int_0^\infty \mathrm{d}u \frac{1}{2}\frac{u^{D-2}}{e^u-1}X^2 = \frac{1}{2}\Gamma(D-1)\mathrm{Li}_{D-1}(1)X^2 \tag{53}$$

where $\mathrm{Li}_n(z)$ is the polylogarithm function.

Therefore, from (30) and using the expansion of $\hat{P}_k(\eta,\mathbf{p})$ in (B1) and the result (53), we can resum this contribution to get the leading contribution

$$V^h_{T(L)}(\hat{\phi}) = \frac{T^4}{24}\left(\frac{m(\hat{\phi})}{T}\right)^2 \tag{54}$$

$$V^\Phi_{T(L)}(\hat{\phi}) = \frac{T^4}{12}\left(\frac{m(\hat{\phi})}{T}\right)^2 \Phi(\mathbf{p}) \times \left(\frac{\sin(p\eta)}{p\eta} - 1\right) \tag{55}$$

$$V^\Psi_{T(L)}(\hat{\phi}) = \frac{T^4}{12}\left(\frac{m(\hat{\phi})}{T}\right)^2 \Psi(\mathbf{p}) \times \left(\frac{\sin(p\eta)}{p\eta}\right) \tag{56}$$

The explicit time dependence of the general results obtained in a static metric can be traced back to the initial conditions of the modes. Taking the limit $\eta \to \infty$ in (55) and (56), the initial conditions are washed out and the remaining correction in Fourier space is

$$V_{T(L)}(\hat{\phi}) = \frac{T^4}{24}\left(\frac{m(\hat{\phi})}{T}\right)^2 (1 - 2\Phi(\mathbf{p})). \tag{57}$$

In this case we can also obtain the inhomogeneous result by replacing the temperature by the local Tolman temperature [13] in the homogeneous result.

To get the real space result in the static limit, one has to compute the Fourier transform of the complete expression and then take the static limit, $\eta \to \infty$. Following this procedure, it is possible to get the real space result for arbitrary perturbation (see Appendix C) which reads

$$V_{T(L)}(\hat{\phi}) = \frac{T^4}{24}\left(\frac{m(\hat{\phi})}{T}\right)^2 (1 - 2\Phi(\mathbf{r})). \tag{58}$$

Therefore, as expected, the static limit and the Fourier transform commute [compare (57) and (58)]. This is a general conclusion for the functions in Fourier space appearing in this paper due to the results of Appendix C.

In real space, the corrections due to Newtonian perturbations $\Phi_N(\mathbf{p})$ and $\Psi_N(\mathbf{p})$ given by

$$\Phi_N(\mathbf{p}) = \Psi_N(\mathbf{p}) = -4\pi\frac{GM}{p^2} \tag{59}$$

$$\Phi_N(\mathbf{r}) = \Psi_N(\mathbf{r}) = -\frac{GM}{r}, \tag{60}$$

inside the light cone ($r < |\eta|$) are

$$V^{\Phi_N}_{T(L)}(\hat{\phi}) = \frac{T^4}{12}\left(\frac{m(\hat{\phi})}{T}\right)^2 \Phi_N(\mathbf{r}) \times \left(\frac{r}{|\eta|} - 1\right) \tag{61}$$

$$V^{\Psi_N}_{T(L)}(\hat{\phi}) = \frac{T^4}{12}\left(\frac{m(\hat{\phi})}{T}\right)^2 \Psi_N(\mathbf{r}) \times \left(\frac{r}{|\eta|}\right) \tag{62}$$

while on and outside the light cone ($r \geq |\eta|$) are

$$V^{\Phi_N}_{T(L)}(\hat{\phi}) = 0 \tag{63}$$

$$V^{\Psi_N}_{T(L)}(\hat{\phi}) = \frac{T^4}{12}\left(\frac{m(\hat{\phi})}{T}\right)^2 \Psi_N(\mathbf{r}). \tag{64}$$

The next-to-leading order corrections can be obtained by computing the first part of Eq. (30) plus next-to-leading terms coming from Eq. (52) (see Appendix D). Finally, after resummation of the series expansion (B1) we get for $V_{T(NL)}$, [up to $O((m/T)^5)$]

$$V^h_{T(NL)}(\hat{\phi}) = T^4\left(\frac{m(\hat{\phi})}{T}\right)^3\left[-\frac{1}{12\pi} + \frac{1}{32\pi^2}\left(\frac{m(\hat{\phi})}{T}\right)\left(\log\left(\frac{T}{M}\right) + \frac{3}{4} - \gamma + \log(4\pi)\right)\right] \tag{65}$$

$$V^\Phi_{T(NL)}(\hat{\phi}) = T^4\left(\frac{m(\hat{\phi})}{T}\right)^3 \Phi(\mathbf{p})\left[-\frac{1}{12\pi}(J_0(p\eta) - 1) + \frac{1}{32\pi^2}\left(\frac{m(\hat{\phi})}{T}\right)(\cos(p\eta) - 1) + \frac{1}{720\pi}\left(\frac{m(\hat{\phi})}{T}\right)^2 p\eta J_1(p\eta)\right] \tag{66}$$

$$V^\Psi_{T(NL)}(\hat{\phi}) = T^4\left(\frac{m(\hat{\phi})}{T}\right)^3 \Psi(\mathbf{p})\left[-\frac{1}{12\pi}\left(J_0(p\eta) + \frac{J_1(p\eta)}{p\eta}\right) + \frac{1}{32\pi^2}\left(\frac{m(\hat{\phi})}{T}\right)\left(\cos(p\eta) + \frac{2\sin p\eta}{p\eta}\right) + \frac{1}{720\pi}\left(\frac{m(\hat{\phi})}{T}\right)^2 (p\eta J_1(p\eta) - 3J_0(p\eta))\right] \tag{67}$$

where γ is Euler's constant and $J_n(x)$ Bessel functions. The leading and next-to-leading inhomogeneous thermal corrections of V_T are shown in Fig. 2.

Considering Newtonian perturbations Φ_N and Ψ_N, in real space we get for the region inside the light cone ($r < |\eta|$)

$$V^{\Phi_N}_{T(NL)}(\hat{\phi}) = T^4\left(\frac{m(\hat{\phi})}{T}\right)^3 \Phi_N(\mathbf{r}) \times \left[\frac{1}{12\pi} - \frac{1}{6\pi^2}\arcsin\left(\frac{r}{|\eta|}\right)\right] \tag{68}$$

$$V^{\Psi_N}_{T(NL)}(\hat{\phi}) = T^4\left(\frac{m(\hat{\phi})}{T}\right)^3 \Psi_N(\mathbf{r}) \times \left[-\frac{1}{12\pi^2}\frac{r}{\eta}\sqrt{1-\frac{r^2}{\eta^2}} - \frac{1}{4\pi^2}\arcsin\left(\frac{r}{|\eta|}\right)\right], \tag{69}$$

and outside and on the light cone ($r \geq |\eta|$)

$$V^{\Phi_N}_{T(NL)}(\hat{\phi}) = 0 \tag{70}$$

$$V^{\Psi_N}_{T(NL)}(\hat{\phi}) = T^4\left(\frac{m(\hat{\phi})}{T}\right)^3 \Psi_N(\mathbf{r}) \times \left[-\frac{1}{8\pi}\right]. \tag{71}$$

Here for simplicity we have only shown the $\mathcal{O}(m/T)^3$ contributions.

In the static limit $\eta \to \infty$ one gets

$$V_{T(NL)}(\hat{\phi}) = -\frac{T^4}{12\pi}\left(\frac{m(\hat{\phi})}{T}\right)^3 (1 - \Phi(\mathbf{p})), \tag{72}$$

which is also valid in real space replacing $\Phi(\mathbf{p})$ by $\Phi(\mathbf{r})$ (see Appendix C). Here again we find that the inhomogeneous result can be obtained by replacing the temperature in the homogeneous contribution by the local Tolman temperature.

B. Energy-momentum tensor

The leading contribution is given by the integral (32) when $n = 0$

$$\begin{aligned} J^X_{\alpha,0} &= \int_X^\infty \mathrm{d}u \frac{1}{e^u - 1}\frac{1}{u^{2\alpha-2}}(u^2 - X^2)^{D/2+\alpha-1} \\ &\simeq \int_0^\infty \mathrm{d}u \frac{u^{D-2}}{e^u - 1}(u^2 + (1 - D/2 - \alpha)X^2) \\ &= \Gamma(D-1)[(D-1)D\zeta(D+1) \\ &\quad + (1 - D/2 - \alpha)\zeta(D-1)X^2] \end{aligned} \tag{73}$$

where we have replaced the lower limit of integration by 0 and expanded the integrand around $X = 0$ in the second line. Therefore, we get for the energy-momentum tensor

$$\frac{\rho_T}{T^4} = \frac{\langle T^0{}_0(\eta,\mathbf{p})\rangle_T}{T^4} \simeq \frac{\pi^2}{30}\left(1 - 4\Phi(\mathbf{p}) + \frac{4\sin(p\eta)}{p\eta}(\Phi(\mathbf{p}) + \Psi(\mathbf{p}))\right) - \frac{1}{24}\left(\frac{m(\hat{\phi})}{T}\right)^2\left[1 + \left(2\cos(p\eta) + \frac{4\sin(p\eta)}{p\eta}\right)\Psi(\mathbf{p}) + (2\cos(p\eta) - 2)\Phi(\mathbf{p})\right] \tag{74}$$

$$\frac{p_T}{T^4} = -\frac{\langle T^i{}_i(\eta,\mathbf{p})\rangle_T}{T^4} \simeq \frac{\pi^2}{90}\left(1 - 4\Phi(\mathbf{p}) + \frac{4\sin(p\eta)}{p\eta}(\Phi(\mathbf{p}) + \Psi(\mathbf{p}))\right) - \frac{1}{24}\left(\frac{m(\hat{\phi})}{T}\right)^2\left[1 + \left(\frac{2}{3}\cos(p\eta) + \frac{8\sin(p\eta)}{3p\eta}\right)\Psi(\mathbf{p}) + \left(\frac{2}{3}\cos(p\eta) + \frac{4\sin(p\eta)}{3p\eta} - 2\right)\Phi(\mathbf{p})\right] \tag{75}$$

$$\frac{\langle T^i{}_0(\eta,\mathbf{p})\rangle_T}{T^4} \simeq \left(i\frac{p_i}{p}\right)\frac{2\pi^2}{15}\left(\frac{\cos(p\eta)}{p\eta} - \frac{\sin(p\eta)}{(p\eta)^2}\right)(\Phi(\mathbf{p}) + \Psi(\mathbf{p})) + \left(i\frac{p_i}{p}\right)\frac{1}{12}\left(\frac{m(\hat{\phi})}{T}\right)^2\left[\sin(p\eta)\Phi(\mathbf{p}) + \left(\sin(p\eta) + 2\frac{\sin(p\eta)}{(p\eta)^2} - 2\frac{\cos(p\eta)}{p\eta}\right)\Psi(\mathbf{p})\right] \tag{76}$$

$$\frac{\langle T^i{}_j(\eta,\mathbf{p})\rangle_T}{T^4} \simeq \left(i^2\frac{p_i p_j}{p^2}\right)\frac{2\pi^2}{15}\left(\frac{\sin(p\eta)}{p\eta} + 3\frac{\cos(p\eta)}{(p\eta)^2} - 3\frac{\sin(p\eta)}{(p\eta)^3}\right)(\Phi(\mathbf{p}) + \Psi(\mathbf{p})) + \left(i^2\frac{p_i p_j}{p^2}\right)\frac{1}{12}\left(\frac{m(\hat{\phi})}{T}\right)^2 \times \left[\left(\frac{\sin(p\eta)}{p\eta} - \cos(p\eta)\right)\Phi(\mathbf{p}) + \left(6\frac{\sin(p\eta)}{(p\eta)^3} - \frac{\sin(p\eta)}{p\eta} - 6\frac{\cos(p\eta)}{(p\eta)^2} - \cos(p\eta)\right)\Psi(\mathbf{p})\right] \quad i \neq j \tag{77}$$

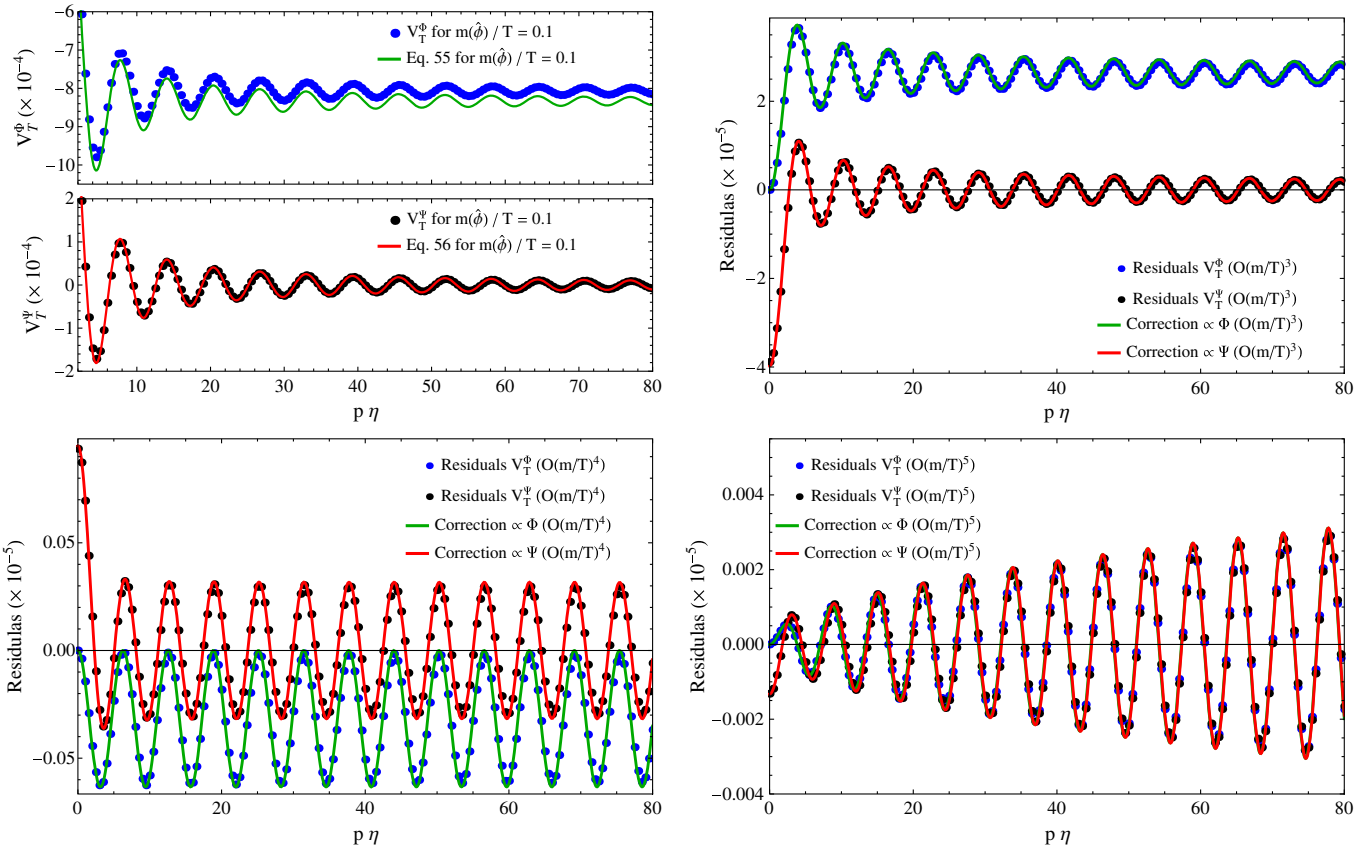

FIG. 2. Left upper panel: Points show the numerical value of the thermal contribution to the potential taking $m(\hat{\phi})/T = 0.1$ and the continuous line corresponds to the approximations in (55) and (56). Right upper panel: Difference between the numerical value of the potential for $m(\hat{\phi})/T = 0.1$ and the approximations (55) (blue points) or (56) (black points). The next-to-leading corrections $[O((m/T)^3)]$ given by (66) (green solid line) and (67) (red solid line) for $m(\hat{\phi})/T = 0.1$. Left bottom panel: Difference between the numerical value and the $O((m/T)^3)$ approximation (blue and black points). The $O((m/T)^4)$ correction is plotted as a solid line. Right bottom panel: Difference between the numerical value and the $O((m/T)^4)$ approximation (blue and black points). The $O((m/T)^5)$ correction is plotted as a solid line.

$$\frac{\langle T^\mu{}_\mu(\eta,\mathbf{p})\rangle_T}{T^4} \simeq \frac{1}{12}\left(\frac{m(\hat{\phi})}{T}\right)^2\left[1+\left(\frac{2\sin(p\eta)}{p\eta}-2\right)\Phi(\mathbf{p})+\frac{2\sin(p\eta)}{p\eta}\Psi(\mathbf{p})\right], \tag{78}$$

which does not correspond to a perfect fluid.[3]

In real space, we have for Newtonian perturbations inside the light cone ($r < |\eta|$)

$$\frac{\rho_T}{T^4} = \frac{\langle T^0{}_0(\eta,\mathbf{r})\rangle_T}{T^4} \simeq \frac{\pi^2}{30}\left\{1-4\left[\left(1-\frac{r}{|\eta|}\right)\Phi_N(\mathbf{r})-\frac{r}{|\eta|}\Psi_N(\mathbf{r})\right]\right\}-\frac{1}{24}\left(\frac{m(\hat{\phi})}{T}\right)^2\left[1-2\Phi_N(\mathbf{r})+4\frac{r}{|\eta|}\Psi_N(\mathbf{r})\right] \tag{79}$$

$$\frac{p_T}{T^4} = -\frac{\langle T^i{}_i(\eta,\mathbf{r})\rangle_T}{T^4} \simeq \frac{\pi^2}{90}\left\{1-4\left[\left(1-\frac{r}{|\eta|}\right)\Phi_N(\mathbf{r})-\frac{r}{|\eta|}\Psi_N(\mathbf{r})\right]\right\}-\frac{1}{24}\left(\frac{m(\hat{\phi})}{T}\right)^2\left[1-2\left(1-\frac{2}{3}\frac{r}{|\eta|}\right)\Phi_N(\mathbf{r})+\frac{8}{3}\frac{r}{|\eta|}\Psi_N(\mathbf{r}))\right] \tag{80}$$

$$\frac{\langle T^i{}_0(\eta,\mathbf{r})\rangle_T}{T^4} \simeq \frac{\pi^2}{45\eta^2}\partial_i[r^3(\Phi_N(\mathbf{r})+\Psi_N(\mathbf{r}))]-\frac{1}{36\eta^2}\left(\frac{m(\hat{\phi})}{T}\right)^2\partial_i(r^3\Psi_N(\mathbf{r})) \tag{81}$$

[3]The energy-momentum tensor given by Eqs. (74)–(77) is conserved.

$$\frac{\langle T^{i}{}_{j}(\eta,\mathbf{r})\rangle_T}{T^4} \simeq -\frac{\pi^2}{300|\eta|^3}\partial_i\partial_j[r^5(\Phi_N(\mathbf{r})+\Psi_N(\mathbf{r}))] + \frac{1}{240|\eta|^3}\left(\frac{m(\hat{\phi})}{T}\right)^2\partial_i\partial_j(r^5\Psi_N(\mathbf{r})) \quad i\neq j \tag{82}$$

$$\frac{\langle T^{\mu}{}_{\mu}(\eta,\mathbf{r})\rangle_T}{T^4} \simeq \frac{1}{12}\left(\frac{m(\hat{\phi})}{T}\right)^2\left[1-2\left(1-\frac{r}{|\eta|}\right)\Phi_N(\mathbf{r}) + 2\frac{r}{|\eta|}\Psi_N(\mathbf{r})\right]. \tag{83}$$

Outside the light cone ($r > |\eta|$), we get

$$\frac{\rho_T}{T^4} = \frac{\langle T^{0}{}_{0}(\eta,\mathbf{r})\rangle_T}{T^4} \simeq \frac{\pi^2}{30}(1+4\Psi_N(\mathbf{r})) - \frac{1}{24}\left(\frac{m(\hat{\phi})}{T}\right)^2[1+6\Psi_N(\mathbf{r})] \tag{84}$$

$$\frac{p_T}{T^4} = -\frac{\langle T^{i}{}_{i}(\eta,\mathbf{r})\rangle_T}{T^4} \simeq \frac{\pi^2}{90}(1+4\Psi_N(\mathbf{r})) - \frac{1}{24}\left(\frac{m(\hat{\phi})}{T}\right)^2\left[1+\frac{10}{3}\Psi_N(\mathbf{r}))\right] \tag{85}$$

$$\frac{\langle T^{i}{}_{0}(\eta,\mathbf{r})\rangle_T}{T^4} \simeq -\frac{2\pi^2\eta}{45}\partial_i(\Phi_N(\mathbf{r})+\Psi_N(\mathbf{r})) + \frac{\eta}{12}\left(\frac{m(\hat{\phi})}{T}\right)^2\partial_i\left(\Phi_N(\mathbf{r})+\frac{5}{3}\Psi_N(\mathbf{r})\right) \tag{86}$$

$$\frac{\langle T^{i}{}_{j}(\eta,\mathbf{r})\rangle_T}{T^4} \simeq -\frac{2\pi^2\eta^2}{225}\partial_i\partial_j(\Phi_N(\mathbf{r})+\Psi_N(\mathbf{r})) + \frac{\eta^2}{36}\left(\frac{m(\hat{\phi})}{T}\right)^2\partial_i\partial_j\left(\Phi_N(\mathbf{r})+\frac{7}{5}\Psi_N(\mathbf{r})\right) \quad i\neq j \tag{87}$$

$$\frac{\langle T^{\mu}{}_{\mu}(\eta,\mathbf{r})\rangle_T}{T^4} \simeq \frac{1}{12}\left(\frac{m(\hat{\phi})}{T}\right)^2[1+2\Psi_N(\mathbf{r})], \tag{88}$$

and on the light cone ($r = |\eta|$), the results are

$$\frac{\rho_T}{T^4} = \frac{\langle T^{0}{}_{0}(\eta,\mathbf{r})\rangle_T}{T^4} \simeq \frac{\pi^2}{30}(1+4\Psi_N(\mathbf{r})) - \frac{1}{24}\left(\frac{m(\hat{\phi})}{T}\right)^2[1-\Phi_N(\mathbf{r})+5\Psi_N(\mathbf{r})] \tag{89}$$

$$\frac{p_T}{T^4} = -\frac{\langle T^{i}{}_{i}(\eta,\mathbf{r})\rangle_T}{T^4} \simeq \frac{\pi^2}{90}(1+4\Psi_N(\mathbf{r})) - \frac{1}{24}\left(\frac{m(\hat{\phi})}{T}\right)^2\left[1-\frac{1}{3}\Phi_N(\mathbf{r})+3\Psi_N(\mathbf{r})\right] \tag{90}$$

$$\frac{\langle T^{i}{}_{0}(\eta,\mathbf{r})\rangle_T}{T^4} \simeq -\frac{2\pi^2\eta}{45}\partial_i(\Phi_N(\mathbf{r})+\Psi_N(\mathbf{r})) + \frac{\eta}{12}\left(\frac{m(\hat{\phi})}{T}\right)^2\partial_i\left(\Phi_N(\mathbf{r})+\frac{5}{3}\Psi_N(\mathbf{r})\right) \tag{91}$$

$$\frac{\langle T^{i}{}_{j}(\eta,\mathbf{r})\rangle_T}{T^4} \simeq -\frac{2\pi^2\eta^2}{225}\partial_i\partial_j(\Phi_N(\mathbf{r})+\Psi_N(\mathbf{r})) + \frac{\eta^2}{36}\left(\frac{m(\hat{\phi})}{T}\right)^2\partial_i\partial_j\left(\Phi_N(\mathbf{r})+\frac{7}{5}\Psi_N(\mathbf{r})\right) \quad i\neq j \tag{92}$$

$$\frac{\langle T^{\mu}{}_{\mu}(\eta,\mathbf{r})\rangle_T}{T^4} \simeq \frac{1}{12}\left(\frac{m(\hat{\phi})}{T}\right)^2[1+2\Psi_N(\mathbf{r})]. \tag{93}$$

In the static limit, the energy density and pressure are

$$\frac{\rho_T}{T^4} = \frac{\langle T^{0}{}_{0}(\eta,\mathbf{p})\rangle_T}{T^4} \simeq \frac{\pi^2}{30}(1-4\Phi(\mathbf{p})) - \frac{1}{24}\left(\frac{m(\hat{\phi})}{T}\right)^2(1-2\Phi(\mathbf{p})) \tag{94}$$

$$\frac{p_T}{T^4} = -\frac{\langle T^{i}{}_{i}(\eta,\mathbf{p})\rangle_T}{T^4} \simeq \frac{\pi^2}{90}(1-4\Phi(\mathbf{p})) - \frac{1}{24}\left(\frac{m(\hat{\phi})}{T}\right)^2(1-2\Phi(\mathbf{p})) \tag{95}$$

$$\frac{\langle T^{\mu}{}_{\mu}(\eta,\mathbf{p})\rangle_T}{T^4} \simeq \frac{1}{12}\left(\frac{m(\hat{\phi})}{T}\right)^2(1-2\Phi(\mathbf{p})), \tag{96}$$

the nondiagonal terms being zero. Once again, these results can be interpreted as being the corresponding energy density and pressure for a classical gas at the local Tolman temperature [13] in agreement with [14,15]. The same expressions for the static limit apply in real space (see Appendix C).

VI. THERMAL SHIFT OF THE EFFECTIVE POTENTIAL MINIMA

Once the effective potential is obtained, the value of the field for which

$$V_{\text{eff}}{}'(\hat{\phi}) = 0 \tag{97}$$

determines the value attained by the classical field $\hat{\phi}$. The inhomogeneous contributions to the effective potential will now induce a spatial dependence on $\hat{\phi}$ which can be written as

$$\hat{\phi}(\eta, \mathbf{x}) = \hat{\phi}_0 + \Delta\hat{\phi}(\eta, \mathbf{x}), \tag{98}$$

where $\hat{\phi}_0$ is the minimum of the potential in the absence of metric perturbations, but including the one-loop corrections, i.e.,

$$V_{\rm eff}^{\rm h}{}'(\hat{\phi}_0) = V'(\hat{\phi}_0) + V_1^{\rm h\prime}(\hat{\phi}_0) + V_T^{\rm h}{}'(\hat{\phi}_0) = 0, \tag{99}$$

then to first order in metric perturbations and taking into account that $V_1^i = 0$ in dimensional regularization, we get

$$\Delta\hat{\phi} = -\frac{V_T^{\rm i}{}'(\hat{\phi}_0)}{V_{\rm eff}^{\rm h}{}''(\hat{\phi}_0)} = -\frac{1}{V_{\rm eff}^{\rm h}{}''(\hat{\phi}_0)} \frac{{\rm d}m^2}{{\rm d}\hat{\phi}}\bigg|_{\hat{\phi}=\hat{\phi}_0} \frac{{\rm d}V_T^{\rm i}}{{\rm d}m^2}\bigg|_{\hat{\phi}=\hat{\phi}_0}. \tag{100}$$

Thus, the relative classical field variation is given by the temperature correction

$$\Delta\hat{\phi} = -\frac{V'''(\hat{\phi}_0)}{V_{\rm eff}^{\rm h}{}''(\hat{\phi}_0)} \frac{{\rm d}V_T^{\rm i}}{{\rm d}m^2}\bigg|_{\hat{\phi}=\hat{\phi}_0}. \tag{101}$$

The perturbation is therefore proportional to the third derivative of the tree-level potential, so that variations in the field expectation value are only generated in theories with self-interactions.

In the nonrelativistic limit and in the static limit we get in Fourier space

$$\Delta\hat{\phi}_T(\eta, \mathbf{p}) = \frac{e^{-m(\hat{\phi})/T}}{4\sqrt{2}\pi^{3/2}} \left(\frac{m(\hat{\phi})}{T}\right)^{3/2} \times V'''(\hat{\phi}_0)\left(\frac{T^2}{V_{\rm eff}^{\rm h}{}''(\hat{\phi}_0)}\right)\Phi(\mathbf{p}). \tag{102}$$

In the ultrarelativistic limit, we obtain for arbitrary η

$$\Delta\hat{\phi}(\eta, \mathbf{p}) = -\frac{V'''(\hat{\phi}_0)}{12}\left(\frac{T^2}{V_{\rm eff}^{\rm h}{}''(\hat{\phi}_0)}\right)\left[\left(\frac{\sin(p\eta)}{p\eta} - 1\right)\Phi(\mathbf{p}) + \left(\frac{\sin(p\eta)}{p\eta}\right)\Psi(\mathbf{p})\right]. \tag{103}$$

which in the static limit reduces to

$$\Delta\hat{\phi}(\mathbf{p}) = \frac{V'''(\hat{\phi}_0)}{12}\left(\frac{T^2}{V_{\rm eff}^{\rm h}{}''(\hat{\phi}_0)}\right)\Phi(\mathbf{p}), \tag{104}$$

valid also in real space replacing $\Phi(\mathbf{p})$ by $\Phi(\mathbf{r})$. In particular, in real space, we get for Newtonian potentials inside the light cone ($r < |\eta|$)

$$\Delta\hat{\phi}(\eta, r) = -\frac{V'''(\hat{\phi}_0)}{12}\left(\frac{T^2}{V_{\rm eff}^{\rm h}{}''(\hat{\phi}_0)}\right) \times \left[\left(\frac{r}{|\eta|} - 1\right)\Phi_N(\mathbf{r}) + \frac{r}{|\eta|}\Psi_N(\mathbf{r})\right], \tag{105}$$

while outside and on the light cone ($r \geq |\eta|$)

$$\Delta\hat{\phi}(\eta, r) = -\frac{V'''(\hat{\phi}_0)}{12}\left(\frac{T^2}{V_{\rm eff}^{\rm h}{}''(\hat{\phi}_0)}\right)\Psi_N(\mathbf{r}). \tag{106}$$

Thus, we see that outside and on the light cone ($r \geq |\eta|$), the result reduces to minus the static limit result (104). Inside the light cone ($r < |\eta|$), the thermal shift depends on time and approaches asymptotically the static case.

From these results we see that there is a negligible shift in the classical field $\hat{\phi}$ at low temperature because of the exponential suppression, however, depending on the form of the tree-level potential, the shift generated by metric perturbations in the ultrarelativistic limit could be relevant in certain cases.

Now, let us focus on the critical temperature of the phase transition $T_{\rm c}$ defined by [16]

$$V_{\rm eff}(\hat{\phi}_0 + \Delta\hat{\phi}) = V_{\rm eff}(0) \tag{107}$$

where $V_{\rm eff}$, $\hat{\phi}_0$ and $\Delta\hat{\phi}$ depend on the temperature T. Expanding Eq. (107) around the critical temperature in the absence of metric perturbations $T_{\rm c}^0$, we get for the leading order

$$V_{\rm eff}^{\rm h}(\hat{\phi}_0) = V_{\rm eff}^{\rm h}(0) \tag{108}$$

which is the definition of $T_{\rm c}^0$. Considering the next to leading order and solving for $\delta T_{\rm c} = T_{\rm c} - T_{\rm c}^0$, we obtain the following expression for the shift in the critical temperature produced by metric perturbations[4]

$$\delta T_{\rm c} = -\frac{V_{\rm eff}^{\rm i}(\hat{\phi}_0)}{\frac{\rm d}{{\rm d}T}(V_{\rm eff}^{\rm h}(\hat{\phi}_0))}\bigg|_{T=T_{\rm c}^0}. \tag{109}$$

It can be shown (see Appendix E) that in the static limit

[4]To get this expression we have redefined the effective potential by adding a function of the temperature in such a way that $V_{\rm eff}^{\rm h}(0) = 0$ and $\frac{\rm d}{{\rm d}T}V_{\rm eff}^{\rm h}(0) = 0$ for every T. This does not change the dynamics of the field since the aforementioned function of the temperature does not depend on the field ϕ

$$\frac{V^{\rm i}_{\rm eff}(\hat{\phi}_0)}{\frac{\rm d}{{\rm d}T}(V^{\rm h}_{\rm eff}(\hat{\phi}_0))} = -T\Phi(\mathbf{p}) \tag{110}$$

therefore, in that case, the shift in the critical temperature is given by

$$\frac{\delta T_{\rm c}}{T^0_{\rm c}} = \Phi(\mathbf{p}). \tag{111}$$

i.e., once again the curvature perturbation Ψ does not contribute to the shift.

VII. CONCLUSIONS

Considering a scalar field at finite temperature in an inhomogeneous static spacetime, we have computed the one-loop corrections to the effective potential and to the energy-momentum tensor induced by static scalar metric perturbations around a Minkowski background to first order in metric perturbations. To this aim, we have applied the formalism developed in [11,12]. In particular we have used the explicit expressions for the perturbed field modes together with the assumptions of adiabatic evolution of the field. In order to obtain analytical expressions, the nonrelativistic and ultrarelativistic limits have been considered.

In the nonrelativistic limit, we obtained the corresponding expressions in the static limit and also the limits for large-scale perturbations (small p) or times close to the initial time. In the ultrarelativistic limit, we obtain the complete results for arbitrary p and η up to $\mathcal{O}(m/T)^5$. In the static limit, our results agree with those in [14,15] which were obtained by means of the Schwinger-DeWitt expansion. The energy density and pressure in the static limit are consistent with a local thermal distributions at the local Tolman temperature. Besides, our results are sensitive to the initial conditions set at the initial time for the mode solutions.

We have also discussed the space-dependent shift in the classical field induced by the metric perturbations. As expected, in the nonrelativistic limit the shift is Boltzmann suppressed. However, in the ultrarelativistic case and depending on the shape of the potential, the shift could be non-negligible.

The results of the paper have shown that mode summation is a useful technique to obtain explicit expressions for one-loop quantities at zero and finite temperature. Unlike the more standard Schwinger-DeWitt expansion, this method allows to calculate not only the local contributions to the effective action, but also the finite nonlocal ones which will appear at second order in the perturbative expansion. Future work along this line will allow to explore this possibility.

ACKNOWLEDGMENTS

This work has been supported by the Spanish MICINNs Consolider-Ingenio 2010 Programme under Grant MultiDark CSD2009-00064, by the Spanish Research Agency (Agencia Estatal de Investigación) through Grant IFT Centro de Excelencia Severo Ochoa SEV-2016-0597 and MINECO Grants No. FIS2014-52837-P, No. FIS2016-78859-P(AEI/FEDER, UE), No. AYA-2012-31101 and No. AYA2014-60641-C2-1-P. F. D. A. acknowledges financial support from "la Caixa"-Severo Ochoa doctoral fellowship.

APPENDIX A: PERTURBED MODE SOLUTION

The expression for $P_k(\eta,\mathbf{p})$ and $\delta\theta_k(\eta,\mathbf{p})$ is given by [12] (see also [17,18]),

$$P_k(\eta,\mathbf{p}) = \int_0^\eta e^{-i\mathbf{k}\cdot\mathbf{p}\beta_k(\eta,\eta')}\frac{H_k(\eta',\mathbf{p})}{2\omega_k(\eta')}{\rm d}\eta' + e^{-i\mathbf{k}\cdot\mathbf{p}\beta_k(\eta,0)}P_k(0,\mathbf{p}), \tag{A1}$$

$$\delta\theta_k(\eta,\mathbf{p}) = \int_0^\eta e^{-i\mathbf{k}\cdot\mathbf{p}\beta_k(\eta,\eta')}G_k(\eta',\mathbf{p}){\rm d}\eta' + e^{-i\mathbf{k}\cdot\mathbf{p}\beta_k(\eta,0)}\delta\theta_k(0,\mathbf{p}), \tag{A2}$$

where $P_k(0,\mathbf{p})$, $\delta\theta_k(0,\mathbf{p})$ are the initial conditions, and

$$\beta_k(\eta_f,\eta_i) = \int_{\eta_i}^{\eta_f}\frac{{\rm d}\eta'}{\omega_k(\eta')} \tag{A3}$$

$$H_k(\eta,\mathbf{p}) = \omega_k Q'_k(\eta,\mathbf{p}) + T_k(\eta,\mathbf{p}) \tag{A4}$$

$$Q_k(\eta,\mathbf{p}) = -i\frac{\mathbf{k}\cdot\mathbf{p}}{\omega_k^2}\delta\theta_k(\eta,\mathbf{p}) + \left[D - \frac{k^2}{\omega_k^2}\right]\Psi(\eta,\mathbf{p}) \tag{A5}$$

$$T_k(\eta,\mathbf{p}) = p^2\delta\theta_k(\eta,\mathbf{p}) - i\mathbf{k}\cdot\mathbf{p}[\Phi(\eta,\mathbf{p}) - (D-2)\Psi(\eta,\mathbf{p})] \tag{A6}$$

$$G_k(\eta,\mathbf{p}) = -\omega_k\left[\Phi(\eta,\mathbf{p}) + \frac{k^2}{\omega_k^2}\Psi(\eta,\mathbf{p})\right]. \tag{A7}$$

$P_k(0,\mathbf{p})$ is fixed by the orthonormalization condition of the modes while $\delta\theta_k(0,\mathbf{p})$ remains arbitrary. The arbitrariness in $\delta\theta_k(0,\mathbf{p})$ can also be absorbed in a change of the lower integration limit in (A2). As we will see, only setting the time origin to $\eta_0 \to -\infty$, which is equivalent to taking $\eta \to \infty$, corresponds to the exact static limit.

Full details about the solutions (A1) and (A2), and about the orthonormalization condition, are given in [12].

APPENDIX B: EXPANSION IN $p\eta$ FOR STATIC SPACETIMES

The following expansions have been used for the computation of the potential and the energy-momentum tensor,

$$\hat{P}_k(\eta,\mathbf{p}) = \left(3-\frac{k^2}{\omega_k^2}\right)\Psi(\mathbf{p}) + \sum_{l=1}^{\infty}\frac{(-1)^l}{(2l+1)!}(p\eta)^{2l}\left(\frac{k}{\omega_k}\right)^{2l}\frac{1}{k^2\omega_k^2} \times [(2k^4+(3+2l)k^2m^2)(\Phi(\mathbf{p})+\Psi(\mathbf{p})) + (1+2l)m^4\Phi(\mathbf{p})]. \tag{B1}$$

$$\int_{-1}^{1}\mathrm{d}\hat{x}\left(\frac{ikp\hat{x}}{\omega_k^2}\right)P_k(\eta,\mathbf{p}) = i\sum_{l=1}^{\infty}\frac{(-1)^l}{(2l-1)!}(p\eta)^{2l}\left(\frac{k}{\omega_k}\right)^{2l} \times\left[\frac{1}{(2l+1)k^2\omega_k\eta}((2l+1)m^4\Phi(\mathbf{p})+3k^4(\Phi(\mathbf{p})+\Psi(\mathbf{p}))+k^2m^2((2l+3)\Psi(\mathbf{p})+2(l+2)\Phi(\mathbf{p}))) - \frac{\omega_k}{(2l-1)k^2\eta}(m^2\Phi(\mathbf{p})+k^2(\Phi(\mathbf{p})+\Psi(\mathbf{p})))\right] \tag{B2}$$

$$\delta\theta_k(\eta,\mathbf{p}) = \sum_{l=0}^{\infty}\frac{(-1)^{l+1}}{(l+1)!}\eta^{l+1}\left(\frac{i\mathbf{k}\cdot\mathbf{p}}{\omega_k}\right)^l\frac{1}{\omega_k}[m^2\Phi(\mathbf{p})+k^2(\Phi(\mathbf{p})+\Psi(\mathbf{p}))] \tag{B3}$$

$$\delta\hat{\theta}_k(\eta,\mathbf{p}) = -2\sum_{l=0}^{\infty}\frac{(-1)^l}{(2l+1)!}(p\eta)^{2l}\left(\frac{k}{\omega_k}\right)^{2l}\frac{\omega_k\eta}{2l+1}\left[\left(\frac{m}{\omega_k}\right)^2\Phi(\mathbf{p})+\left(\frac{k}{\omega_k}\right)^2(\Phi(\mathbf{p})+\Psi(\mathbf{p}))\right] \tag{B4}$$

$$\int_{-1}^{1}\mathrm{d}\hat{x}\left(\frac{ikp\hat{x}}{\omega_k^2}\right)\delta\theta_k(\eta,\mathbf{p}) = 2\sum_{l=1}^{\infty}\frac{(-1)^l}{(2l+1)!}(p\eta)^{2l}\left(\frac{k}{\omega_k}\right)^{2l}\left[\left(\frac{m}{\omega_k}\right)^2\Phi(\mathbf{p})+\left(\frac{k}{\omega_k}\right)^2(\Phi(\mathbf{p})+\Psi(\mathbf{p}))\right]. \tag{B5}$$

$$\int_{-1}^{1}\mathrm{d}\hat{x}\left(\frac{ikp\hat{x}}{\omega_k^2}\right)^2\delta\theta_k(\eta,\mathbf{p}) = -4\sum_{l=1}^{\infty}\frac{(-1)^l}{(2l+1)!}(p\eta)^{2l}\left(\frac{k}{\omega_k}\right)^{2l}\frac{l}{\omega_k\eta}\left[\left(\frac{m}{\omega_k}\right)^2\Phi(\mathbf{p})+\left(\frac{k}{\omega_k}\right)^2(\Phi(\mathbf{p})+\Psi(\mathbf{p}))\right]. \tag{B6}$$

Both $\hat{P}_k(\eta,\mathbf{p})$ and $\int_{-1}^{1}\mathrm{d}\hat{x}(\frac{ikp\hat{x}}{\omega_k^2})\delta\theta_k(\eta,\mathbf{p})$ are the main terms appearing in the computation, while the remaining ones can be obtained from these expressions.

APPENDIX C: MULTIPOLE EXPANSION AND FOURIER TRANSFORM

1. Fourier transform in three dimensions

In this discussion we follow [19]. The Fourier transform of a function $f(\mathbf{r})$ is defined as[5]

$$f(\mathbf{p}) = \int \mathrm{d}^3\mathbf{r} f(\mathbf{r})e^{-i\mathbf{p}\cdot\mathbf{r}} \tag{C1}$$

Then, the inverse transform is given by

$$f(\mathbf{r}) = \int \frac{\mathrm{d}^3\mathbf{p}}{(2\pi)^3}f(\mathbf{p})e^{i\mathbf{p}\cdot\mathbf{r}} \tag{C2}$$

[5]With the usual abuse of notation for using the same label for the function and for its Fourier transform. Note the nonunitary convention (the factor $1/(2\pi)^3$ is introduced when going from Fourier space to real space).

We are interested in the following integrals,

$$I_{lm}(\mathbf{p}) = \int \mathrm{d}^3\mathbf{r} f(r)Y_{lm}(\hat{\mathbf{r}})e^{-i\mathbf{p}\cdot\mathbf{r}} \tag{C3}$$

$$I_{lm}(\mathbf{r}) = \int \frac{\mathrm{d}^3\mathbf{p}}{(2\pi)^3}f(p)Y_{lm}(\hat{\mathbf{p}})e^{i\mathbf{p}\cdot\mathbf{r}}, \tag{C4}$$

where $Y_{lm}(\hat{\mathbf{x}})$ are the usual spherical harmonics. Using the Rayleigh expansion,

$$e^{i\mathbf{p}\cdot\mathbf{r}} = \sum_{l=0}^{\infty}(2l+1)i^l j_l(pr)P_l(\hat{\mathbf{p}}\cdot\hat{\mathbf{r}}), \tag{C5}$$

where $j_l(x)$ are spherical Bessel functions and $P_l(x)$ are the Legendre polynomials, the addition theorem for spherical harmonics,

$$P_l(\hat{\mathbf{p}}\cdot\hat{\mathbf{r}}) = \frac{4\pi}{2l+1}\sum_{m=-l}^{l}Y_{lm}(\hat{\mathbf{r}})Y^*_{lm}(\hat{\mathbf{p}}), \tag{C6}$$

and the orthonormalization of the spherical harmonics,

$$\int \mathrm{d}\Omega_p Y^*_{lm}(\hat{\mathbf{p}})Y_{l'm'}(\hat{\mathbf{p}}) = \delta_{ll'}\delta_{mm'}, \tag{C7}$$

$I_{lm}(\mathbf{p})$ and $I_{lm}(\mathbf{r})$ can be written as

$$I_{lm}(\mathbf{p}) = 4\pi(-i)^l Y_{lm}(\hat{\mathbf{p}}) \int_0^\infty \mathrm{d}r r^2 f(r) j_l(pr) \tag{C8}$$

$$I_{lm}(\mathbf{r}) = \frac{i^l}{2\pi^2} Y_{lm}(\hat{\mathbf{r}}) \int_0^\infty \mathrm{d}p p^2 f(p) j_l(pr). \tag{C9}$$

2. Multipole expansion in Fourier space

An arbitrary potential generated by a finite static matter distribution $\rho(\mathbf{x})$ can be written as a multipole expansion in spherical coordinates in the region outside the matter distribution as

$$\Phi(\mathbf{r}) = -\frac{1}{r}\sum_{l=0}^{\infty}\sum_{m=-l}^{l} \frac{Q_{lm}}{r^l}\sqrt{\frac{4\pi}{2l+1}} Y_{lm}(\hat{\mathbf{r}}) \tag{C10}$$

where Q_{lm} are the spherical multipole moments of the mass distribution given by

$$Q_{lm} = \int \rho(\mathbf{r}') r'^l \sqrt{\frac{4\pi}{2l+1}} Y^*_{lm}(\hat{r'}) \mathrm{d}^3\mathbf{r}' \tag{C11}$$

The Fourier transform of the potential is

$$\Phi(\mathbf{p}) = -\frac{4\pi}{p^2}\sum_{l=0}^{\infty}\frac{(-i)^l}{(2l-1)!!}\sum_{m=-l}^{l} Q_{lm} p^l \sqrt{\frac{4\pi}{2l+1}} Y_{lm}(\hat{\mathbf{p}}). \tag{C12}$$

where we have used the following result,

$$\lim_{\lambda\to 0^+}\int_0^\infty \mathrm{d}r r^2 \frac{e^{-\lambda r}}{r^{(l+1)}} j_l(pr) = \frac{p^{l-2}}{(2l-1)!!}, \tag{C13}$$

where we have introduced a regularizing factor $e^{-\lambda r}$ [which in fact it is only necessary for $l = 0$, the remaining cases being convergent].

To get the results for potential and energy-momentum tensor in real space we have to compute the following integrals:

$$\frac{1}{(2\pi)^3}\int \Phi(\mathbf{p})\frac{\sin(p\eta)}{(p\eta)^{2k+1}} e^{i\mathbf{p}\cdot\mathbf{r}}\mathrm{d}^3\mathbf{p} \overset{p'=p\eta}{=} \frac{1}{\eta^3}\frac{1}{(2\pi)^3}\int \Phi(\mathbf{p}'/\eta)\frac{\sin(p')}{(p')^{2k+1}} e^{i\mathbf{p}'\cdot\mathbf{r}/\eta}\mathrm{d}^3\mathbf{p}'. \tag{C14}$$

Taking into account the multipole expansion of the potential in Fourier space (C12), it can be shown for each multipole that the integral will be proportional to

$$\frac{1}{\eta^{l+1}}\int_0^\infty \mathrm{d}p' e^{-\lambda p} p'^2 p'^{l-2}\frac{\sin(p')}{(p')^{2k+1}} j_l(p'r/\eta), \tag{C15}$$

where we have introduced a regularizing factor $e^{-\lambda p}$. Since the spherical Bessel functions of the first kind are finite, in particular at the origin, we get that in the static limit $\eta \to \infty$, the integral goes to zero. The same argument applies for the integrals involving cosine functions.

APPENDIX D: NEXT-TO-LEADING TERMS IN THE ULTRARELATAVISTIC LIMIT

Next to leading-order corrections can be obtained by expanding the Bose-Einstein factor and performing the integration term by term. For instance, the integrals we are interested in are of the following form,

$$X^4\int_1^\infty \frac{f(\tilde{u})}{e^{X\tilde{u}}-1}\mathrm{d}\tilde{u}, \tag{D1}$$

where $\tilde{u} = u/X$ and $X = m(\hat{\phi})/T$. Using the Taylor expansion of the Bose-Einstein factor,

$$\frac{1}{e^{X\tilde{u}}-1} = \sum_{k=0}^{\infty}\frac{B_k}{k!}\frac{\tilde{u}^k}{\tilde{u}}X^{k-1}, \tag{D2}$$

the next-to-leading corrections in X can be obtained as far as the integrals are convergent. B_k are the Bernoulli numbers. The function $f(\tilde{u})$ appearing in the calculations behaves as $\sim\frac{1}{\tilde{u}^3}$ in the limit $\tilde{u}\to\infty$; therefore, the integrals can be performed up to $k = 2$.

APPENDIX E: EXPRESSION FOR $V^{\mathrm{i}}_{\mathrm{eff}}$ AND $\frac{\mathrm{d}}{\mathrm{d}T}V^{\mathrm{i}}_{\mathrm{eff}}$ IN THE STATIC LIMIT

Let us define (following [16])

$$J^\nu(x) = \int_x^\infty \frac{2(u^2-x^2)^{\nu/2}}{e^u-1}\mathrm{d}u \tag{E1}$$

$$F^{(\nu)}(X) = \int_0^X x^{2-\nu}J^\nu(x)\mathrm{d}x. \tag{E2}$$

Then, in the static limit we have

$$V^{\mathrm{h}}_{\mathrm{eff}} = \frac{T^4}{4\pi^2}F^{(1)}\left(\frac{m(\hat{\phi})}{T}\right) \tag{E3}$$

and

$$V^{\mathrm{i}}_{\mathrm{eff}} = -\frac{T^4}{4\pi^2}\left[2F^{(1)}\left(\frac{m(\hat{\phi})}{T}\right)+F^{(-1)}\left(\frac{m(\hat{\phi})}{T}\right)\right]\Phi(\mathbf{p}), \tag{E4}$$

which can be read from Eq. (10). The derivative with respect to the temperature of the homogeneous effective potential is given by

$$\frac{\mathrm{d}}{\mathrm{d}T}(V_{\mathrm{eff}}^{\mathrm{h}}(\hat{\phi}_0)) = \frac{T^3}{4\pi^2}\left[4F^{(1)}\left(\frac{m(\hat{\phi})}{T}\right) - \left(\frac{m(\hat{\phi})}{T}\right)^2 J^{(1)}\left(\frac{m(\hat{\phi})}{T}\right)\right]. \quad \text{(E5)}$$

The second term in the right-hand side of the last equation can be written as

$$\left(\frac{m(\hat{\phi})}{T}\right)^2 J^{(1)}\left(\frac{m(\hat{\phi})}{T}\right) = \int_0^{m(\hat{\phi})/T} \frac{\mathrm{d}}{\mathrm{d}x}(x^2 J^{(1)}(x))\mathrm{d}x = 2F^{(1)}\left(\frac{m(\hat{\phi})}{T}\right) - F^{(-1)}\left(\frac{m(\hat{\phi})}{T}\right), \quad \text{(E6)}$$

where we have used the following property of $J^{(\nu)}(x)$

$$\frac{\partial J^{(\nu)}(x)}{\partial x} = -\nu x J^{(\nu-2)}(x). \quad \text{(E7)}$$

Therefore, Eqs. (E5) and (E6) give us

$$\frac{V_{\mathrm{eff}}^{\mathrm{i}}(\hat{\phi}_0)}{\frac{\mathrm{d}}{\mathrm{d}T}(V_{\mathrm{eff}}^{\mathrm{h}}(\hat{\phi}_0))} = -T\Phi(\mathbf{p}). \quad \text{(E8)}$$

[1] L. Dolan and R. Jackiw, Phys. Rev. D **9**, 3320 (1974).
[2] S. Weinberg, Phys. Rev. D **9**, 3357 (1974).
[3] J. S. Dowker and R. Critchley, Phys. Rev. D **15**, 1484 (1977).
[4] I. T. Drummond, Nucl. Phys. **B190**, 93 (1981).
[5] L. Parker and S. A. Fulling, Phys. Rev. D **9**, 341 (1974).
[6] B. L. Hu, Phys. Lett. **108B**, 19 (1982).
[7] J. S. Schwinger, Phys. Rev. **82**, 914 (1951).
[8] B. S. DeWitt, Phys. Rep. **19**, 295 (1975).
[9] N. D. Birrell and P. C. W. Davies, *Quantum Fields in Curved Space* (Cambridge University Press, Cambridge, England, 1982).
[10] W. H. Huang, Classical Quantum Gravity **10**, 2021 (1993).
[11] A. L. Maroto and F. Prada, Phys. Rev. D **90**, 123541 (2014).
[12] F. D. Albareti, A. L. Maroto, and F. Prada, Phys. Rev. D **95**, 044030 (2017).
[13] R. C. Tolman and P. Ehrenfest, Phys. Rev. **36**, 1791 (1930).
[14] N. Nakazawa and T. Fukuyama, Nucl. Phys. **B252**, 621 (1985).
[15] B. R. Holstein, Physica A **158**, 387 (1989).
[16] V. Mukhanov, *Physical Foundations of Cosmology* (Cambridge University Press, Cambridge, England, 2005).
[17] F. D. Albareti, J. A. R. Cembranos, and A. L. Maroto, Phys. Rev. D **90**, 123509 (2014).
[18] F. D. Albareti, J. A. R. Cembranos, and A. L. Maroto, Int. J. Mod. Phys. D **23**, 1442019 (2014).
[19] G. S. Adkins, arXiv:1302.1830.

Conclusions

The variation of fundamental constants of Nature has become a wide area of research during the last two decades. From the observational side, high precision constraints are being set in a continuous way thanks to the observational efforts that are currently in progress. These constraints involve quite different physics and a huge range of scales. From atomic clocks, laboratory spectroscopy and meteorite dating; passing through stellar physics, high resolution quasar spectra, the 21 cm hydrogen line and, in general, observations of astrophysical sources in the full electromagnetic spectrum; to CMB map and Big Bang nucleosynthesis. A necessarily incomplete enumeration that may give the reader a picture of the diverse physical scenarios that are being considered in this search.

From the theoretical side, most of the extensions of our current theoretical models, including modified gravity theories and string theory, can accommodate a variation of fundamental constants due to the presence of extra fields or dimensions. Furthermore, an experimental confirmation will entangle the violation of the Equivalence Principle, an historical piece of Physics in which General Relativity is rooted.

In this thesis, we intended to provide a contribution on both sides, observations and theory. Concerning observations, we have set a constraint for the variation of the fine-structure constant of $\Delta\alpha/\alpha = (0.9 \pm 1.8) \times 10^{-5}$ at redshift $z < 1$ from a sample of quasar spectra observed by the SDSS-III/BOSS and SDSS-II surveys. This bound represents the most accurate result obtained with [O III] emission lines. Our sample is built by applying well defined selected criteria to 45 802 objects at $z < 1$ classified as quasars and collected from the SDSS-III/BOSS DR12 quasar catalogue. After that, we get a sample of 10 363 quasars which where combined with 2 853 previously studied SDSS-II/DR7 quasars, to finally obtain a final sample of 13 175 quasars after eliminating 41 re-observed objects.

We also performed a very detailed study of the impact produced by several parameters of the analysis and the developed code, and also by properties of quasars and the [O III] doublet. For instance, redshift and location on the sky of the quasars; width, amplitude, S/N and R^2 coefficient derived from the fitting profiles of the [O III] lines; polynomial order for the continuum subtraction and the method to determine the line position (e.g. Gaussian/Voigt profiles). The results were shown to be quite robust, and they are consistent with no variation of the fine-structure constant. The precision of the emission-line method in our study is dominated by the sky subtraction algorithm employed on the SDSS spectra. This is supported by the correlation between the standard deviation of the results as a function of redshift and the sky emission lines.

In order to improve the precision with emission lines, high-resolution spectroscopy is mandatory.

However, the analysis of galaxy spectra taken from the DEEP2 survey carried out in our article showed that on-going large galaxy surveys like DESI could also provide quite stringent constraint for $\Delta\alpha/\alpha$ at low redshift. This is due to the presence of narrower emission lines in galaxies than in quasars.

On the theoretical side, we explored the large-scale effects of spacetime over quantum corrections to scalar fields. These quantum corrections can be expressed in terms of expectation values over quantum states. The DeWitt-Schwinger approximation can be used to compute these expectations values in general spacetimes as a local expansion in curvature. However, this approximation is not able to reproduce the nonlocal effect due to the large scale properties of the spacetime. In order to overcome this drawback, we computed the complete corrections using brute force methods. This means that: a) a complete orthonormal set of modes of the Klein-Gordon equation in a perturbed FRW background was obtained at the leading adiabatic order; b) the expectation values was computed as a mode summation; c) dimensional regularization techniques were employed to obtain the finite one-loop corrections to the effective potential and energy-momentum tensor of the scalar field.

We showed that for vacuum states the homogeneous contribution agrees with the Minkowski case as expected, and that there are no additional contributions appearing either in the regularized effective potential or in the energy-momentum tensor. Therefore, the theory can be renormalized just absorbing the divergences in the tree-level parameters (at the leading adiabatic order) using dimensional regularization. In particular, this result applies to the Higgs field when considering only its self-interactions.

Furthermore, we also computed the expectations values over thermal quantum states in an inhomogeneous static space-time, i.e. a Minkowski background with scalar metric perturbations. In the static limit, our results agree with previous calculations that were obtained by means of the DeWitt-Schwinger expansion. The energy density and pressure in the static limit are consistent with a local thermal distributions at the Tolman temperature. Besides, we also obtained the full dependence of the expectation value on the initial conditions for the mode solutions.

An important effect in thermal states is that a space-dependent shift in the classical value of the field is induced by the metric perturbations. In the non relativistic limit, i.e. low temperature compared to the mass of the scalar field, the shift is Boltzmann suppressed. However, in the ultra-relativistic case and depending on the particular shape of the potential, the shift could be non-negligible.

As a final conclusion on this part of the thesis, we proved that mode summation is a useful technique to obtain explicit expressions for expectation values over vacuum and thermal states at the leading adiabatic order. Unlike the more standard DeWitt-Schwinger expansion, this method allows to calculate not only the local contributions, but also the finite non-local ones. Additional contributions from the metric perturbations at the next-to-leading adiabatic orders are also expected.

Conclusiones

El estudio de la variación de las constantes fundamentales de la Naturaleza ha adquirido gran relevancia durante las últimas dos décadas. Desde el punto de vista experimental, se establecen restricciones muy precisas continuamente gracias a los esfuerzos observacionales actualmente en curso. Diversas ramas de la física y un amplio rango de escalas están involucradas en la obtención de estas restricciones. Desde relojes atómicos, espectroscopía en el laboratorio y datación de meteoritos; pasando por la física estelar, espectros de cuásares de alta resolución, la línea de 21 cm del hidrógeno y, en general, observaciones de fuentes astrofísicas en todo el espectro electromagnético; hasta el mapa del CMB y la nucleosíntesis del Big Bang. Esta enumeración da una idea de los diferentes sistemas físicos que se están estudiando en esta investigación.

En el aspecto teórico, la mayoría de las extensiones de los modelos actuales, incluyendo teorías de gravedad modificada y la teoría de cuerdas, predicen una variación de las constantes fundamentales producida por la presencia de campos adicionales o de dimensiones extra. Por otro lado, una confirmación experimental implicaría la violación del Principio de Equivalencia, una parte clave de la física que forma la base de Relatividad General.

En esta tesis, hemos intentado hacer una contribución en ambas partes, observación y teoría. Con respecto a las observaciones, hemos establecido una restricción para la variación de la constante de estructura fina de $\Delta\alpha/\alpha = (0.9 \pm 1.8) \times 10^{-5}$ hasta desplazamientos al rojo de $z < 1$. Esta medida se obtuvo a partir de una muestra de espectros de cuásares tomados por los cartografiados SDSS-III/BOSS y SDSS-II. Es el resultado más preciso obtenido hasta el momento a partir de las líneas de emisión del doblete de [O III]. La muestra se construyó aplicando criterios bien definidos a 45 802 objetos a $z < 1$ clasificados como cuásares y recopilados en el catálogo de cuásares del SDSS-III/BOSS DR12. De esta forma, obtuvimos una muestra de 10 363 objetos que, combinados con otros 2 853 cuásares previamente observados por el SDSS-II/DR7, dieron lugar a la muestra final que contiene 13 175 cuásares después de eliminar 41 objetos repetidos.

También realizamos un análisis muy detallado del impacto producido por varios parámetros del análisis y del código utilizado así como debido a las características del los cuásares y del doblete del [O III]. Estudiamos, por ejemplo, el desplazamiento al rojo y la ubicación en la esfera celeste de los cuásares; el ancho, la amplitud, la S/N y el coeficiente R^2 derivado de los ajustes de las líneas del [O III]; el grado del polinomio usado para la sustracción del contínuo y el método para determinar la posición de las líneas (por ejemplo, adoptando perfiles gaussianos o de Voigt). Se concluyó que los resultados son bastante robustos y que son consistentes con una variación nula de la constante de estructura fina. La precisión del método que utilizamos en nuestro estudio, basado en líneas

de emisión, está limitada por el algoritmo de sustracción del cielo empleado en los espectros del SDSS. Esta afirmación se fundamenta en la correlación existente entre la desviación estándar de las medidas como función del desplazamiento al rojo y las líneas de emisión del cielo.

Para mejorar la precisión alcanzada con líneas de emisión es necesario utilizar espectroscopía de mayor resolución espectral. Sin embargo, el análisis de los espectros de galaxias tomados por DEEP2 mostró que los cartografiados de galaxias actualmente en curso como DESI podrían proporcionar restricciónes bastante precisas para $\Delta\alpha/\alpha$ a bajos desplazamientos al rojo. Esto se debe a que las líneas de emisión son más estrechas en los espectros de galaxias que en cuásares.

Desde el punto de vista teórico, hemos explorado efectos del espacio-tiempo que se manifiestan en correcciones cuánticas a campos escalares. Estas correcciones pueden expresarse en términos de valores esperados sobre estados cuánticos. La aproximación de DeWitt-Schwinger permite calcular estos valores esperados en espacio-tiempos generales como una expansión local en la curvatura. Sin embargo, no puede reproducir efectos no locales debido a la estructura a gran escala del espacio-tiempo. Por lo tanto, hemos empleado métodos de fuerza bruta para calcular las correcciones completas, incluidas las contribuciones no locales. Para ello: a) obtuvimos un conjunto completo de modos ortonormales de la ecuación de Klein-Gordon hasta el primer orden adiabático en un espacio-tiempo FRW con perturbaciones escalares; b) calculamos los valores esperados como una suma de modos; c) empleamos técnicas de regularización dimensional para obtener las correcciones finitas a un loop al potencial efectivo y al tensor de energía-momento del campo escalar.

Para los estados de vacío, la contribución homogénea coincide con el resultado de Minkowski como era de esperar. Además, no hay contribuciones adicionales, ya sea en el potencial efectivo regularizado o en el tensor de energía-momento. Por lo tanto, la teoría se puede renormalizar simplemente absorbiendo las divergencias en los parámetros a nivel árbol (en el orden adiabático dominante) utilizando regularización dimensional. En particular, este resultado es aplicable al campo de Higgs cuando sólo se consideran sus auto-interacciones.

Por otro parte, también calculamos los valores esperados en estados cuánticos térmicos en un espacio-tiempo estático no homogéneo. En el límite estático, nuestros resultados concuerdan con cálculos anteriores obtenidos mediante la expansión de DeWitt-Schwinger. La densidad de energía y la presión en el límite estático son consistentes con distribuciones térmicas locales caracterizadas por la temperatura de Tolman. Además, también obtuvimos la dependencia del valor esperado con las condiciones iniciales de los modos.

Un efecto importante en los estados térmicos es que las perturbaciones métricas inducen una variación espacial en el valor del campo clásico. En el límite no relativista, es decir, a baja temperatura en comparación con la masa del campo escalar, este efecto está suprimido por el factor de Boltzmann. Sin embargo, en el caso ultra-relativista y dependiendo de la forma particular del potencial, el efecto podría no ser despreciable.

Como conclusión final de esta parte de la tesis, hemos visto que la suma de modos es una técnica útil para obtener expresiones explícitas para valores esperados en el vacío y en estados térmicos. A diferencia de la expansión de DeWitt-Schwinger, el método utilizado en esta tesis permite calcular las contribuciones finitas no locales. Es de esperar que se encuentren contribuciones debidas a las perturbaciones métricas en los siguientes órdenes adiabáticos.

Bibliography

Abbott, T. M. C., Abdalla, F. B., Alarcon, A., Aleksić, J., Allam, S., Allen, S., et al. (2018). Dark energy survey year 1 results: Cosmological constraints from galaxy clustering and weak lensing. Phys. Rev. D, 98:043526.

Alam, S., Albareti, F. D., Allende Prieto, C., Anders, F., Anderson, S. F., Anderton, T., et al. (2015). The Eleventh and Twelfth Data Releases of the Sloan Digital Sky Survey: Final Data from SDSS-III. ApJS, 219:12.

Albareti, F. D. (2014). Vacuum state defnitions in a de sitter spacetime through green functions. Master's thesis, Universidad Autónoma de Madrid.

Albareti, F. D., Allende Prieto, C., Almeida, A., Anders, F., Anderson, S., Andrews, B. H., et al. (2017a). The 13th Data Release of the Sloan Digital Sky Survey: First Spectroscopic Data from the SDSS-IV Survey Mapping Nearby Galaxies at Apache Point Observatory. ApJS, 233:25.

Albareti, F. D., Comparat, J., Gutiérrez, C. M., Prada, F., Pâris, I., Schlegel, D., et al. (2015). Constraint on the time variation of the fine-structure constant with the SDSS-III/BOSS DR12 quasar sample. MNRAS, 452:4153–4168.

Albareti, F. D., Maroto, A. L., and Prada, F. (2017b). Gravitational perturbations of the Higgs field. Phys. Rev. C, 95(4):044030.

Albareti, F. D., Maroto, A. L., and Prada, F. (2018). Finite-temperature corrections to the energy-momentum tensor at one loop in static spacetimes. Phys. Rev. C, 97(12):125017.

Bahcall, J. N. and Salpeter, E. E. (1965). On the Interaction of Radiation from Distant Sources with the Intervening Medium. ApJ, 142:1677–1680.

Bahcall, J. N., Sargent, W. L. W., and Schmidt, M. (1967). An Analysis of the Absorption Spectrum of 3c 191. ApJL, 149:L11.

Bahcall, J. N. and Schmidt, M. (1967). Does the Fine-Structure Constant Vary with Cosmic Time? Phys. Rev. Lett., 19:1294–1295.

Bahcall, J. N., Steinhardt, C. L., and Schlegel, D. (2004). Does the Fine-Structure Constant Vary with Cosmological Epoch? ApJ, 600:520–543.

Barrow, J. (2005). Varying constants. Philosophical Transactions of the Royal Society of London Series A, 363:2139–2153.

Barrow, J. D. and Magueijo, J. (1998). Varying-α theories and solutions to the cosmological problems. Physics Letters B, 443:104–110.

Bekenstein, J. D. (1973). Black holes and entropy. Phys. Rev. D, 7:2333–2346.

Berengut, J. C., Dzuba, V. A., Flambaum, V. V., King, J. A., Kozlov, M. G., Murphy, M. T., et al. (2011). Atomic Transition Frequencies, Isotope Shifts, and Sensitivity to Variation of the Fine Structure Constant for Studies of Quasar Absorption Spectra. Astrophysics and Space Science Proceedings, 22:9.

Birrell, N. D. and Davies, P. C. W. (1980). Massive particle production in anisotropic space-times. Journal of Physics A: Mathematical and General, 13(6):2109.

Birrell, N. D. and Davies, P. C. W. (1984). Quantum Fields in Curved Space. Cambridge Monographs on Mathematical Physics. Cambridge Univ. Press, Cambridge, UK.

Blanton, M. R., Bershady, M. A., Abolfathi, B., Albareti, F. D., Allende Prieto, C., Almeida, A., et al. (2017). Sloan Digital Sky Survey IV: Mapping the Milky Way, Nearby Galaxies, and the Distant Universe. AJ, 154:28.

Bogolyubov, N. N. (1947). On the theory of superfluidity. J. Phys.(USSR), 11:23–32. [Izv. Akad. Nauk Ser. Fiz.11,77(1947)].

Bousso, R. (2002). The holographic principle. Rev. Mod. Phys., 74:825–874.

Brans, C. and Dicke, R. H. (1961). Mach's principle and a relativistic theory of gravitation. Phys. Rev., 124:925–935.

Buckingham, E. (1914). On physically similar systems; illustrations of the use of dimensional equations. Phys. Rev., 4:345–376.

Bunch, T. S. and Davies, P. C. W. (1978a). Non-conformal renormalised stress tensors in robertson-walker space-times. Journal of Physics A: Mathematical and General, 11(7):1315.

Bunch, T. S. and Davies, P. C. W. (1978b). Quantum field theory in de sitter space: Renormalization by point-splitting. Proceedings of the Royal Society of London. Series A, Mathematical and Physical Sciences, 360(1700):117–134.

Carroll, S. M. (2004). Spacetime and geometry. An introduction to general relativity. Addison Wesley.

Carter, B. (1974). Large number coincidences and the anthropic principle in cosmology. volume 63 of *IAU Symposium*, pages 291–298.

Carter, B. (1983). The anthropic principle and its implications for biological evolution. Philosophical Transactions of the Royal Society of London A: Mathematical, Physical and Engineering Sciences, 310(1512):347–363.

Chand, H., Petitjean, P., Srianand, R., and Aracil, B. (2005). Probing the time-variation of the fine-structure constant: Results based on Si IV doublets from a UVES sample. A&A, 430:47–58.

Chand, H., Srianand, R., Petitjean, P., and Aracil, B. (2004). Probing the cosmological variation of the fine-structure constant: Results based on VLT-UVES sample. A&A, 417:853–871.

Chand, H., Srianand, R., Petitjean, P., Aracil, B., Quast, R., and Reimers, D. (2006). Variation of the fine-structure constant: very high resolution spectrum of QSO HE 0515-4414. A&A, 451:45–56.

Christensen, S. M. (1976). Vacuum expectation value of the stress tensor in an arbitrary curved background: The covariant point-separation method. Phys. Rev. D, 14:2490–2501.

Christensen, S. M. (1978). Regularization, renormalization, and covariant geodesic point separation. Phys. Rev. D, 17:946–963.

Clifton, T., Ferreira, P. G., Padilla, A., and Skordis, C. (2012). Modified gravity and cosmology. Phys. Rep., 513:1–189.

Crispino, L. C. B., Higuchi, A., and Matsas, G. E. A. (2008). The unruh effect and its applications. Rev. Mod. Phys., 80:787–838.

Dawson, K. S., Kneib, J.-P., Percival, W. J., Alam, S., Albareti, F. D., Anderson, S. F., et al. (2016). The SDSS-IV Extended Baryon Oscillation Spectroscopic Survey: Overview and Early Data. AJ, 151:44.

Décanini, Y. and Folacci, A. (2006). Off-diagonal coefficients of the DeWitt-Schwinger and Hadamard representations of the Feynman propagator. Phys. Rev. C, 73(4):044027.

DeWitt, B. S. (1964). Dynamical theory of groups and fields. Conf. Proc., C630701:585–820. [Les Houches Lect. Notes13,585(1964)].

Dicke, R. H. (1957). Gravitation without a principle of equivalence. Rev. Mod. Phys., 29:363–376.

Dicke, R. H. (1961). Dirac's Cosmology and Mach's Principle. Nature, 192:440.

Dirac, P. A. M. (1937). The Cosmological Constants. Nature, 139:323.

Dirac, P. A. M. (1938). A new basis for cosmology. Proceedings of the Royal Society of London A: Mathematical, Physical and Engineering Sciences, 165(921):199–208.

Dirac, P. A. M. (1974). Cosmological models and the large numbers hypothesis. Proceedings of the Royal Society of London A: Mathematical, Physical and Engineering Sciences, 338(1615):439–446.

Duff, M. J. (2015). How fundamental are fundamental constants? Contemporary Physics, 56:35–47.

Duff, M. J., Okun, L. B., and Veneziano, G. (2002). Trialogue on the number of fundamental constants. JHEP, 2002(03):023.

Dzuba, V. A., Flambaum, V. V., and Kozlov, M. G. (1996). Combination of the many-body perturbation theory with the configuration-interaction method. Phys. Rev. A, 54:3948–3959.

Dzuba, V. A., Flambaum, V. V., and Webb, J. K. (1999a). Calculations of the relativistic effects in many-electron atoms and space-time variation of fundamental constants. Phys. Rev. A, 59:230–237.

Dzuba, V. A., Flambaum, V. V., and Webb, J. K. (1999b). Calculations of the relativistic effects in many-electron atoms and space-time variation of fundamental constants. Phys. Rev. A, 59:230–237.

Dzuba, V. A., Flambaum, V. V., and Webb, J. K. (1999c). Space-time variation of physical constants and relativistic corrections in atoms. Phys. Rev. Lett., 82:888–891.

Ellis, G. F. R. (2007). Note on Varying Speed of Light Cosmologies. Gen. Rel. Grav., 39:511–520.

Ellis, G. F. R. and Uzan, J.-P. (2005). c is the speed of light, isn't it? American Journal of Physics, 73:240–247.

Evans, T. M., Murphy, M. T., Whitmore, J. B., Misawa, T., Centurion, M., D'Odorico, S., et al. (2014). The UVES Large Program for testing fundamental physics - III. Constraints on the fine-structure constant from three telescopes. MNRAS, 445:128–150.

Faraoni, V. (2004). Cosmology in scalar tensor gravity. Springer Netherlands.

Fierz, M. (1956). On the physical interpretation of P.Jordan's extended theory of gravitation. Helv. Phys. Acta, 29:128–134.

Ford, L. H. (1997). Quantum field theory in curved space-time. pages 345–388. (arXiv:gr-qc/9707062).

Fourier, J. B. J. (2009). The Analytical Theory of Heat. Cambridge Library Collection - Mathematics. Cambridge University Press.

García-Berro, E., Isern, J., and Kubyshin, Y. A. (2007). Astronomical measurements and constraints on the variability of fundamental constants. The Astronomy and Astrophysics Review, 14(2):113–170.

Gilkey, P. B. (1984). Invariance theory, the heat equation and the Atiyah-Singer index theorem. Publish or Perish.

Grupe, D., Pradhan, A. K., and Frank, S. (2005). Studying the Variation of the Fine-Structure Constant Using Emission-Line Multiplets. AJ, 130:355–366.

Gutiérrez, C. M. and López-Corredoira, M. (2010). The Value of the Fine Structure Constant over Cosmological Times. ApJ, 713:46–51.

Haag, R. and Kastler, D. (1964). An algebraic approach to quantum field theory. Journal of Mathematical Physics, 5(7):848–861.

Hadamard, J. (1923). Lectures on the Cauchy Problem in Linear Partial Differential Equations. Yale University Press, New Haven.

Halzen, F. and Martin, A. D. (1984). Quarks and Leptons: An Introductory Course in Modern Particle Physics. John Wiley and Sons.

Hawking, S. W. (1974). Black hole explosions? Nature, 248:30–31.

Hawking, S. W. (1975). Particle creation by black holes. Communications in Mathematical Physics, 43(3):199–220.

Hogan, C. J. (2000). Why the universe is just so. Rev. Mod. Phys., 72:1149–1161.

Hollands, S. (2007). The Operator Product Expansion for Perturbative Quantum Field Theory in Curved Spacetime. Communications in Mathematical Physics, 273:1–36.

Hollands, S. (2008). Renormalized Quantum Yang-Mills Fields in Curved Spacetime. Reviews in Mathematical Physics, 20:1033–1172.

Hollands, S. and Wald, R. M. (2001). Local Wick Polynomials and Time Ordered Products of Quantum Fields in Curved Spacetime. Communications in Mathematical Physics, 223:289–326.

Hollands, S. and Wald, R. M. (2002). Existence of Local Covariant Time Ordered Products of Quantum Fields in Curved Spacetime. Communications in Mathematical Physics, 231:309–345.

Hollands, S. and Wald, R. M. (2003). On the Renormalization Group in Curved Spacetime. Communications in Mathematical Physics, 237:123–160.

Hollands, S. and Wald, R. M. (2010). Axiomatic Quantum Field Theory in Curved Spacetime. Communications in Mathematical Physics, 293:85–125.

Itzykson, C. and Zuber, J. (2012). Quantum Field Theory. Dover Books on Physics. Dover Publications.

Jordan, P. (1937). Die physikalischen Weltkonstanten. Naturwissenschaften, 25:513–517.

Köhler, R. (2010). The International Vocabulary of Metrology, 3rd Edition: Basic and General Concepts and Associated Terms. Why? How?, pages 233–238. Wiley-Blackwell, (https://onlinelibrary.wiley.com/doi/pdf/10.1002/9780470611371.ch21).

King, J. A., Webb, J. K., Murphy, M. T., Flambaum, V. V., Carswell, R. F., Bainbridge, M. B., et al. (2012). Spatial variation in the fine-structure constant - new results from VLT/UVES. MNRAS, 422:3370–3414.

Klypin, A., Prada, F., Betancort-Rijo, J., and Albareti, F. D. (2018). Density distribution of the cosmological matter field. MNRAS, 481:4588–4601.

Kotuš, S. M., Murphy, M. T., and Carswell, R. F. (2017). High-precision limit on variation in the fine-structure constant from a single quasar absorption system. MNRAS, 464:3679–3703.

Levshakov, S. A., Centurión, M., Molaro, P., and D'Odorico, S. (2005). VLT/UVES constraints on the cosmological variability of the fine- structure constant. A&A, 434:827–838.

Levshakov, S. A., Centurión, M., Molaro, P., D'Odorico, S., Reimers, D., Quast, R., et al. (2006). Most precise single redshift bound to $\Delta\alpha/\alpha$. A&A, 449:879–889.

Levshakov, S. A., Molaro, P., Lopez, S., D'Odorico, S., Centurión, M., Bonifacio, P., et al. (2007). A new measure of $\Delta\alpha/\alpha$ at redshift z = 1.84 from very high resolution spectra of <ASTROBJ>Q 1101-264</ASTROBJ>. A&A, 466:1077–1082.

Levy-Leblond, J. M. (1977). The Importance of Being (a) Constant.

Maeda, K.-I. (1988). On Time Variation of Fundamental Constants in Superstring Theories. Modern Physics Letters A, 3:243–249.

Magueijo, J. (2003). New varying speed of light theories. Rept. Prog. Phys., 66:2025.

Magueijo, J., Barrow, J. D., and Sandvik, H. B. (2002). Is it e or is it c? Experimental tests of varying alpha. Phys. Lett., B549:284–289.

Martínez Fiorenzano, A. F., Vladilo, G., and Bonifacio, P. (2003). Search for alpha variation in UVES spectra: Analysis of C IV and Si IV doublets towards QSO 1101-264. Memorie della Societa Astronomica Italiana Supplementi, 3:252.

Martins, C. J. A. P. (2017). The status of varying constants: a review of the physics, searches and implications. Reports on Progress in Physics, 80(12):126902.

Murphy, M. T. and Cooksey, K. L. (2017). Subaru Telescope limits on cosmological variations in the fine-structure constant. MNRAS, 471:4930–4945.

Murphy, M. T., Malec, A. L., and Prochaska, J. X. (2016). Precise limits on cosmological variability of the fine-structure constant with zinc and chromium quasar absorption lines. MNRAS, 461:2461–2479.

Murphy, M. T., Webb, J. K., and Flambaum, V. V. (2003). Further evidence for a variable fine-structure constant from Keck/HIRES QSO absorption spectra. MNRAS, 345:609–638.

Murphy, M. T., Webb, J. K., Flambaum, V. V., Dzuba, V. A., Churchill, C. W., Prochaska, J. X., et al. (2001a). Possible evidence for a variable fine-structure constant from QSO absorption lines: motivations, analysis and results. MNRAS, 327:1208–1222.

Murphy, M. T., Webb, J. K., Flambaum, V. V., Prochaska, J. X., and Wolfe, A. M. (2001b). Further constraints on variation of the fine-structure constant from alkali-doublet QSO absorption lines. MNRAS, 327:1237–1243.

Newton, I., Motte, A., and Machin, J. (1729). The Mathematical Principles of Natural Philosophy. Number v. 1 in The Mathematical Principles of Natural Philosophy. B. Motte.

Oberhummer, H., Csótó, A., and Schlattl, H. (2000). Stellar Production Rates of Carbon and Its Abundance in the Universe. Science, 289:88–90.

Okun, L. B. (1991). The fundamental constants of physics. Soviet Physics Uspekhi, 34(9):818.

Pâris, I., Petitjean, P., Ross, N. P., Myers, A. D., Aubourg, É., Streblyanska, A., et al. (2017). The Sloan Digital Sky Survey Quasar Catalog: Twelfth data release. A&A, 597:A79.

Parker, L. (1969). Quantized fields and particle creation in expanding universes. i. Phys. Rev., 183:1057–1068.

Parker, L. (1971). Quantized fields and particle creation in expanding universes. ii. Phys. Rev. D, 3:346–356.

Planck Collaboration, Ade, P. A. R., Aghanim, N., Arnaud, M., Ashdown, M., Aumont, J., et al. (2016). Planck 2015 results. XIV. Dark energy and modified gravity. A&A, 594:A14.

Potekhin, A. Y. and Varshalovich, D. A. (1994). Non-variability of the fine-structure constant over cosmological time scales. A&AS, 104:89–98.

Rahmani, H., Maheshwari, N., and Srianand, R. (2014). Constraining the variation in the fine-structure constant using SDSS DR7 quasi-stellar object spectra. MNRAS, 439:L70–L74.

Rozental, I. L. and Estrin, J. (1988). Big Bang Big Bounce. Springer-Verlag Berlin Heidelberg.

Savedoff, M. P. (1956). Physical Constants in Extra-Galactic Nebulæ. Nature, 178:688–689.

Schrodinger, E. (1939). The proper vibrations of the expanding universe. Physica, 6:899–912.

Schwinger, J. (1951). On gauge invariance and vacuum polarization. Phys. Rev., 82:664–679.

Srianand, R., Chand, H., Petitjean, P., and Aracil, B. (2004). Limits on the time variation of the electromagnetic fine-structure constant in the low energy limit from absorption lines in the spectra of distant quasars. Phys. Rev. Lett., 92:121302.

Streater, R. F. and Wightman, A. S. (1989). PCT, Spin and Statistics, and All That. Princeton University Press.

Tagirov, E. A. (2005). A mystery of conformal coupling. ArXiv General Relativity and Quantum Cosmology e-prints.

Tegmark, M. (1998). Is "the Theory of Everything" Merely the Ultimate Ensemble Theory? Annals of Physics, 270:1–51.

Teller, E. (1948). On the change of physical constants. Phys. Rev., 73:801–802.

Tisza, L. (1963). The conceptual structure of physics. Rev. Mod. Phys., 35:151–184.

Uzan, J.-P. (2003). The fundamental constants and their variation: observational and theoretical status. Rev. Mod. Phys., 75:403–455.

Uzan, J.-P. (2011). Varying Constants, Gravitation and Cosmology. Living Reviews in Relativity, 14:2.

Vassilevich, D. V. (2003). Heat kernel expansion: user's manual. Phys. Rep., 388:279–360.

Wald, R. M. (1984). General relativity. Chicago Univ. Press, Chicago, IL.

Wald, R. M. (1995). Quantum Field Theory in Curved Space-Time and Black Hole Thermodynamics. Chicago Lectures in Physics. University of Chicago Press, Chicago, IL.

Wald, R. M. (2006). The History and Present Status of Quantum Field Theory in Curved Spacetime. ArXiv General Relativity and Quantum Cosmology e-prints.

Wald, R. M. (2009). The Formulation of Quantum Field Theory in Curved Spacetime. preprint, (arXiv:0907.0416).

Webb, J. K., Flambaum, V. V., Churchill, C. W., Drinkwater, M. J., and Barrow, J. D. (1999). Search for time variation of the fine structure constant. Phys. Rev. Lett., 82:884–887.

Webb, J. K., King, J. A., Murphy, M. T., Flambaum, V. V., Carswell, R. F., and Bainbridge, M. B. (2011). Indications of a spatial variation of the fine structure constant. Phys. Rev. Lett., 107:191101.

Webb, J. K., Murphy, M. T., Flambaum, V. V., Dzuba, V. A., Barrow, J. D., Churchill, C. W., et al. (2001). Further evidence for cosmological evolution of the fine structure constant. Phys. Rev. Lett., 87:091301.

Weinberg, S. (1983). Overview of theoretical prospects for understanding the values of fundamental constants. Philosophical Transactions of the Royal Society of London A: Mathematical, Physical and Engineering Sciences, 310(1512):249–252.

Whitmore, J. B. and Murphy, M. T. (2015). Impact of instrumental systematic errors on fine-structure constant measurements with quasar spectra. MNRAS, 447:446–462.

York, D. G., Adelman, J., Anderson, Jr., J. E., Anderson, S. F., Annis, J., Bahcall, N. A., et al. (2000). The Sloan Digital Sky Survey: Technical Summary. AJ, 120:1579–1587.

Zeldovich, Ya. B. and Starobinsky, A. A. (1972). Particle production and vacuum polarization in an anisotropic gravitational field. Sov. Phys. JETP, 34:1159–1166. [Zh. Eksp. Teor. Fiz.61,2161(1971)].